Environmental stimuli shape adaptive immunity by enhancing T helper cell differentiation and the germinal centre response

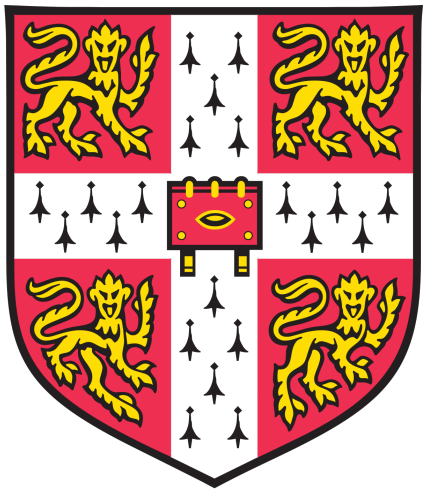

Marisa Stebegg

Darwin College

The Babraham Institute

University of Cambridge

This dissertation is submitted for the degree of Doctor of Philosophy

March 2019

Declaration

This dissertation is the result of my own work and includes nothing which is the outcome of work done in collaboration except as declared in the Preface and specified in the text.

It is not substantially the same as any that I have submitted, or, is being concurrently submitted for a degree or diploma or other qualification at the University of Cambridge or any other University or similar institution except as declared in the Preface and specified in the text. I further state that no substantial part of my dissertation has already been submitted, or, is being concurrently submitted for any such degree, diploma or other qualification at the University of Cambridge or any other University or similar institution except as declared in the Preface and specified in the text

The research in this thesis was carried out under the supervision of Dr Michelle Linterman in the Department of Lymphocyte Signalling at the Babraham Institute, Cambridge between April 2016 and end of March 2019.

It does not exceed the prescribed word limit of 60,000 words.

Marisa Stebegg

March 2019

Summary

THESIS TITLE:
Environmental stimuli shape adaptive immunity by enhancing T helper cell differentiation and the germinal centre response

NAME: Marisa Stebegg

Immune cells have evolved to respond to external danger signals and to incorporate information about environmental cues to adapt their differentiation and effector function. Because of this, it is important that immune cells are studied in the context of their surroundings. In this thesis, I investigated the roles of environmental endoplasmic reticulum (ER) stress, the gut microbiome and ageing on adaptive immunity. Immune cells have been shown to integrate inflammatory signalling with the ER stress response pathway. This response is triggered by a variety of environmental stresses such as low nutrient availability, hypoxia and mechanical stress. I found that the ER stress response acts as a potent driver of T helper 17 (Th17) cell differentiation resulting in Th17 cells with a pathogenic gene expression signature. This suggests a link between ER stress-inducing conditions such as low nutrient availability, and the pathology of Th17 cell-mediated autoimmune diseases. Another physiological scenario in which the immune microenvironment changes is during ageing. Ageing-related changes of the gut microbiome have recently been linked to increased frailty and systemic inflammation. This change in microbial composition with age occurs in parallel with a decline in function of the gut immune system, however it is not clear if there is a causal link between the two. Here, I establish that the defective germinal centre (GC) reaction in Peyer's patches in the small intestine of aged mice can be rescued by co-housing of adult and aged mice, and *via* faecal transfers from adult into aged mice. This demonstrates that the poor GC reaction in aged animals is not irreversible, and that it is possible to improve immune responses in older individuals by replenishing the gut microbiome. To determine whether GC responses can also be improved in peripheral lymph nodes, we investigated the role of defective helper T cell priming in aged mice. We observed that the age-associated defect in the GC reaction is partly due to impaired T cell priming by dendritic cells (DCs). By boosting type I interferon signalling in DCs at the time of immunisation, I was able to improve T cell priming and GC formation in aged mice. This demonstrates that not only the gut microbiome, but also DCs are exciting targets to improve GC responses in ageing and highlights the importance of environmental stimuli in shaping adaptive immunity.

Table of acknowledgement of assistance received during course of this thesis

1) Initial training in techniques and laboratory practice and subsequent mentoring:

Marc Veldhoen: mentoring for Th17 cell project, training in *in vitro* Th17 cell cultures, mouse dissections and EAE

Michelle Linterman: mentoring for ageing projects, training in mouse dissections and NP-1W1K conjugation

Cristina Ferreira: training in flow cytometry

Danika Hill: mentoring for ageing projects, training in flow cytometry/FACS and FlowJo data analysis

Alice Denton: training in dissections of Peyer's patches

Ine Vanderleyden / Alyssa Silva-Cayetano: training in confocal imaging and ELISAs

Laura Peachey: training in DNA isolation from faecal bacteria

Timothy Jenkins: training in 16S rDNA sequencing analysis using QIIME2 and Calypso

Wim Pierson: training in how to use Qubit

Alexandre Bignon: training in dendritic cell preparations and adoptive cell transfers

Qiagen Aarhus team: training in RNA sequencing analysis using Qiagen's BmWB

Home Office personal licence training: training in animal handling

Babraham flow cytometry courses: training in flow cytometry

Babraham bioinformatics courses: training in GraphPad Prism and Inkscape

2) Data obtained from a technical service provider

Transnetyx: genotyping of mice

BSU Breeding Unit: breeding and day-to-day maintenance of C57BL/6 and BALB/c mice

BSU Transgenics Unit: breeding and day-to-day maintenance of transgenic mice

BSU Experimental Unit: intraperitoneal, intravenous and subcutaneous (s.c.) injections as well as oral gavages, faecal pellet collections and exchanges of dirty bedding

BSU Import Unit: EAE experiments

Flow Cytometry Facility: day-to-day maintenance of Fortessas, FACS sorting

Babraham Institute Sequencing facility: RNA sequencing, QC using Agilent Chips

BGI: 16S rDNA library preparation and sequencing of samples from young and aged mice

Eurofins: 16S rDNA library preparation, sequencing of samples from *Bcl6*$^{fl/fl}$*Cd4*$^{cre/+}$ mice

Babraham Chemistry Facility: synthesis of NP-SA

Cambridge Research Biochemicals: synthesis of 1W1K-biotin

NIH Tetramer Core Facility: synthesis of 1W1K-PE tetramers

3) Data produced jointly (*e.g.* where it was necessary to have two pairs of hands)

Silvia Innocentin: helped with dissections, cell preparations and cell counts for all experiments in Chapter 4 and most experiments in Chapter 5, helped with faecal collections and the preparation of NP-CTx for Chapter 4, performed many subcutaneous immunisations for Chapter 5, performed RNA isolations and RT-qPCRs for Figure 5.5G-H

Michelle Linterman: conjugated NP-1W1K and performed subcutaneous immunisations for some experiments in Chapter 5

Alice Denton: performed subcutaneous immunisations for some experiments in Chapter 5

4) Data/materials provided by someone else

Alyssa Silva-Cayetano: created Figures 1.2 and 1.8 shown in the introduction

Verena Brucklacher-Waldert: conducted the EAE experiments shown in Figure 3.7

Marc Veldhoen: performed adoptive-transfer EAE experiments shown in Figure 3.8

Alexandre Bignon: started the project presented in Chapter 5 – generated the data presented in Figures 5.1, 5.2, 5.3, 5.4, 5.6A-C

Ine Vanderleyden: generated confocal images of young and aged LNs in Figure 5.2C

Wim Pierson: prepared Eα-GFP for all experiments

Danika Hill: preformed cDNA synthesis and library preparation for DC RNA sequencing

Edward Carr: performed some analysis of DC RNA sequencing data

Christel Krueger: performed some analysis and the pathway enrichment analysis of DC RNA sequencing data shown in Figure 5.6A-C

Michelle Linterman: performed some analysis for DC RNA sequencing data, phenotyped DCs in H2$^{+/-}$ mice and performed adoptive transfers into these mice as shown in Figure 5.5A-C, drafted the figures for Chapter 5

Adrian Liston, James Dooley and Oliver Burton: hosted the H2$^{+/-}$ mouse experiments in Belgium

Alice Denton: created mouse artwork shown in Figure 5.10A and 5.11A

Acknowledgements

Even though the title page of this thesis only lists my name, it would not have come true without the support of a large number of people who I want to acknowledge here.

First of all Marc, who made this all possible when he offered me this PhD position three years ago as part of the ENLIGHT-TEN programme and who supervised me during the first year of my PhD, and Michelle, who adopted me into her lab when Marc moved to Lisbon. I will always be grateful for her supervision, her mentoring and detailed feedback on this thesis. She is - and always will be - a true role-model for me.

I also owe a lot to every other member of the Linterman lab: Silvia who crawled out of bed to help me with experiments on so many occasions, who proofread large parts of this thesis and is generally a good soul in the lab, keeping stocks in order and us on track. Alyssa and Ine, who became true friends and shared the ups and downs of this PhD experience with me. I had lots of fun and helpful discussions with Sigrid, Alyssa and Ine in the office. Danika, who gave me a lot of valuable scientific advice, proofread part of this thesis and is a caring mentor and friend. Louise, who is an amazing resource of scientific knowledge, bakes delicious sweets and also proofread one of the thesis chapters. Alice, who shared all her knowledge about laboratory techniques with me and taught me how to dissect Peyer's patches. Ed, who patiently helped me with my bioinformatics questions. Thanks also to all the past members of the Linterman lab, especially Wim who showed me around the lab and Alex who entrusted me with his dendritic cell project. Similarly, I wish to acknowledge all the help of past Veldhoen lab members, especially from Joana, Verena, Jörg and Cristina. I also truly appreciated Tim's help and advice on how to do 16S rDNA sequencing and Laura for showing me how to isolate bacterial DNA. Not to forget, thanks to all the other ENLIGHTEN-TEN students for becoming great friends, the great times at our biannual meetings, and to Rebecca, who has been an amazing PhD programme coordinator and was a great help throughout my PhD. I also want to acknowledge everyone from outside the institute who shared their mice, reagents and expertise with us, as well as the funding I have received from the EU-funded Horizon 2020 ENLIGHT-TEN project No. 675395 and additional consumables funding provided by Marc and Michelle.

I truly appreciate the help I received from Babraham Institute facilities over the years: Thanks to the BSU for taking such good care of my mice and for performing so many *in vivo* procedures on my mice; the Flow facility for looking after the Fortessas, where I spent a lot of time during my PhD, and Arthur and Attila for running several long FACS sorts for me; Simon and Hanneke in the Imaging facility for showing me how to use the Zeiss confocal microscope and Cristina in the

Sequencing facility for performing all the RNA sequencing for us. I am also indebted to the past and current members of the other labs in the Lymphocyte Signalling Department, who, on many occasions, saved my experiments by sharing their reagents and expertise. Thanks also to Rebecca Ludwig, Jochen Hühn, Martin Turner, Peter Evans, Geoff Butcher, and Duncan Needham for their support with my move from the Veldhoen to the Linterman lab.

I am unbelievably lucky to have amazing friends both here in Cambridge and abroad, who always lend me a sympathetic ear and make me laugh: Chiara, who has shared this Cambridge experience with me from the very start and has found a place for me in her big heart. Joana who is my close friend, mentor and role-model from the Veldhoen lab. Anja who boldly approached me at the HO course and has since been one of my best friends (and housemates) in Cambridge. Thanks also to Constantin, Ben, Bea, Sophia, Mariana, Nathan, Esther, Charlie and Dan for lots of fun times. Luka and Kati back in Austria, for being my oldest friends who know me by heart and - like Ulli, Anna, Martina and Lisa - are always there for me despite the distance. Lisa, David, Alice, Marietta, Philipp and Carina, who are my university and PhD buddies abroad, for being a great scientific resource and amazing friends. Sabrina, Anne and Helen for always staying in touch. And last but not least, my heartfelt thanks to Andi, my love and my best friend, who always makes me laugh and has taught me so much. I am also eternally grateful to my parents who love me unconditionally and support me wherever I go.

At times I didn't know where this PhD would take me, but thanks to the support of everyone named above and many more, this has been one of the most interesting and instructive times of my life.

List of Publications

Restoration of type I interferon signalling in dendritic cells rescues defective T follicular helper cell differentiation in ageing
Bignon A*, Stebegg M*, Hill D, Vanderleyden I, Innocentin S, Krueger C, Boon L, Silva-Cayetano A, Pierson W, Carr E, Webb L, Liston A, Linterman MA
(manuscript in preparation)
*…shared first authors

Heterochronic faecal transplantation boosts gut germinal centres in aged mice
Stebegg M, Silva-Cayetano A, Innocentin S, Jenkins TJ, Cantacessi C, Gilbert C, Linterman MA
Nat Commun. 2019 June 4;10(1),2443

Regulation of the Germinal Centre Response
Stebegg M*, Kumar S*, Silva-Cayetano A*, Fonseca VR, Linterman MA#, and Graca L#.
Front Immunol. 2018 Oct 25;9:2469.
*…shared first authors, #...shared last authors

Cellular Stress in the Context of an Inflammatory Environment Supports TGF-β-Independent T Helper-17 Differentiation.
Brucklacher-Waldert V, Ferreira C, Stebegg M, Fesneau O, Innocentin S, Marie JC, Veldhoen M.
Cell Rep. 2017 Jun 13;19(11):2357-2370.

List of Tables

Table 1.1: Overview of dendritic cell (DC) subsets……14

Table 2.1: List of mouse strains.……..……38

Table 2.2: Cytokines, ER stress modulators and blocking antibodies used for cell culture……43

Table 2.3: Antibodies and conjugated probes used for flow cytometry and FACS……47

Table 2.4: Overview of the RT-qPCR programmes……51

Table 2.5: Overview of TaqMan Gene Expression Assays used for RT-qPCR……..52

Table 2.6: Metadata table of RNA sequencing libraries used for sequencing……54

Table 2.7: Subsets of differentially-expressed genes uploaded to IPA……55

Table 3.1: Top differentially-expressed genes between c-Th17 and e-Th17 cells……..69

Table 3.2: The top canonical IPA pathways are linked with ER stress or T cell differentiation and activation.……72

Table 4.1: Age-related changes on the species level in the gut microbiome of BALB/c and C57BL/6 mice.……91

Table 4.2: Co-housing leads to species-level changes in the gut microbiome of BALB/c and C57BL/6 mice.……..…95

List of Figures

Figure 1.1: Schematic representation of immune cell development…….. 2

Figure 1.2: Schematic depiction of the specialised secondary lymphoid organ (SLO) architecture of lymph nodes (LNs)……. 5

Figure 1.3: Schematic representation of somatic TCRβ chain rearrangements……... 12

Figure 1.4: Schematic representation of dendritic cell (DC) differentiation…….....15

Figure 1.5: Schematic illustration of the T cell receptor (TCR) signalling network……16

Figure 1.6: Schematic depiction of B cell development……18

Figure 1.7: Schematic illustration of V(D)J rearrangements and class switch recombination (CSR) of the heavy chain of the B cell receptor (BCR)……20

Figure 1.8: Schematic representation of the germinal centre (GC) response…….……...23

Figure 1.9: Depiction of Peyer's patches (PPs) and their role in producing commensal-specific IgA antibodies…….…….. 26

Figure 1.10: Schematic overview of age-associated changes in the germinal centre (GC) response……31

Figure 1.11: Schematic overview of the ER stress response……...…....34

Figure 3.1: ER stress enhances the differentiation efficiency of Th17 cells, but not Th1 or Treg cells……..……. 62

Figure 3.2: CPA enhances Th17 cell differentiation……...…….. 64

Figure 3.3: Gating strategy for sorting FP^+ and FP^- T cells from IL-$17A^{FP}$ reporter mice..……..65

Figure 3.4: ER stress induces the expression of Th17 cell-associated genes in the absence of TGFβ. ……... 66

Figure 3.5: CPA treatment induces global gene expression changes in Th17 cells…….…. 68

Figure 3.6: Distinct Th17 and Th1 cell type-specific mRNA expression by e-Th17 cells…..…. 70

Figure 3.7: CPA treatment affects T cell differentiation……...……..……... 73

Figure 3.8: CPA treatment affects T cell activation. ……...……..…….. 74

Figure 3.9: Blockade of the ER stress response ameliorates EAE disease severity…….…… 75

Figure 3.10: e-Th17 cells induce atypical symptoms in adoptive-transfer EAE experiments…… 76

Figure 4.1: Gating strategy for Tfh, Tfr, germinal centre (GC) B and IgA B cells from Peyer's patches or lymph nodes..……... 84

Figure 4.2: Germinal centre B cells are reduced in the Peyer's patches of aged BALB/c and C57BL/6 mice……... 85

Figure 4.3: Germinal centre B cells are not reduced in the mesenteric lymph nodes (LNs) of aged BALB/c and C57BL/6 mice.……86

Figure 4.4: The gut microbiome changes during ageing……...88

Figure 4.5: Age-associated changes of the gut microbiome in female C57BL/6 mice……. 89

Figure 4.6: Age-associated changes in the taxa composition of the gut microbiome in C57BL/6 and BALB/c mice……..90

Figure 4.7: Co-housing boosts the germinal centre response in the Peyer's patches of aged BALB/c mice.……93

Figure 4.8: Co-housing boosts the germinal centre response in the Peyer's patches of aged C57BL/6 mice.……...…... 94

Figure 4.9: Faecal microbiota transplantation (FMT) boosts the germinal centre (GC) response in Peyer's patches irrespective of age…….…….. 97

Figure 4.10: Faecal microbiota transplantation (FMT) boosts the germinal centre (GC) response in the Peyer's patches of aged BALB/c mice……...……98

Figure 4.11: Faecal microbiota transplantation (FMT) between adult mice of different strains does not affect the germinal centre (GC) response in Peyer's patches……..99

Figure 4.12: IgA-coating of faecal bacteria is not affected by ageing or cohousing…….101

Figure 4.13: Faecal microbiota transplantation (FMT) does not affect gut IgA responses…..….102

Figure 4.14: *Bcl6*$^{fl/fl}$*Cd4*$^{cre/+}$ mice have reduced germinal centre (GC) responses, but a near normal gut microbiome……104

Figure 4.15: Tfh cells in Peyer's patches (PPs) are required for antibody responses to foreign antigen. ……... 106

Figure 4.16: Faecal microbiota transplantation (FMT) does not enhance NP-CTx-specific immune responses in the gut……..……... 107

Figure 5.1: Gating strategy for germinal centre (GC) cell populations……...114

Figure 5.2: Germinal centre (GC) responses are impaired in aged mice……..….. 115

Figure 5.3: T cell proliferation is impaired in aged hosts…….…...117

Figure 5.4: cDC2s from aged mice have an impaired activation phenotype……...118

Figure 5.5: T cell priming is abrogated upon blockade of CD80/86 co-stimulation……...121

Figure 5.6: Reduced interferon (IFN) signalling in cDC2s from aged mice……..……122

Figure 5.7: Gating strategy for the quantitation of GFP^+ $CD11b^+$ cDC2s and plasmacytoid dendritic cells (pDCs)……..124

Figure 5.8: Lack of interferon signalling in DCs impairs Tfh cell differentiation……..…… 125

Figure 5.9**:** Numbers of plasmacytoid DCs (pDCs) are reduced in the lymph nodes (LNs) of aged mice.…… 126

Figure 5.10: Imiquimod rejuvenates cDC2 cells in aged mice……..127

Figure 5.11: Imiquimod boosts antigen-specific Tfh cell differentiation in aged mice…… 129

List of Abbreviations and Acronyms

Adar	double-stranded RNA-specific Adenosine Deaminase
AhR	Aryl hydrocarbon Receptor
AID	Activation-Induced cytidine Deaminase
ANOVA	Analysis Of Variance
AP-1	Activator Protein 1
APC	Antigen Presenting Cell
ATF-4/6	Activating Transcription Factor-4/6
Batf	Basic Leucine Zipper (bZIP) Transcription Factor ATF-like
Bcl6	B cell CLL/Lymphoma 6
BCR	B cell Receptor
BER	Base Excision Repair
BiP	Binding immunoglobulin Protein
BmWB	Biomedical Workbench
BSA	Bovine Serum Albumin
c-Th17	conventional Th17 cell
Ccl	Chemokine (C-C motif) ligand
CD	Cluster of Differentiation
CD40L	Cluster of Differentiation 40 Ligand
cDC	conventional Dendritic Cell
cDNA	complementary Deoxyribonucleic Acid
CDR	Complementary-determining Region
CFA	Complete Freund's Adjuvant
CLP	Common Lymphoid Progenitor
CPA	Cyclopiazonic Acid
CRC	CXCL12-expressing Reticular Cell
CSR	Class Switch Recombination
CT	Cholera Toxin
C_T value	Cycle Threshold value
CTLA-4	Cytotoxic T-lymphocyte-Associated protein 4
CXCL	Chemokine (C-X-C motif) Ligand
DAG	Diacylglycerol
DAPI	4',6-Diamidino-2-Phenylindole
DC	Dendritic Cell
DEA	Downstream Effector Analysis
DGE	Differential Gene Expression
DMEM	Dulbecco's Modified Eagle Medium
DNA	Deoxyribonucleic Acid
DSB	DNA Double-strand Breaks
DZ	Dark Zone

e-Th17	ER stress-generated Th17 cell
EAE	Experimentally-induced Autoimmune Encephalitis
EBI2	Epstein-Barr virus-Induced Gene 2
EDTA	Ethylenediaminetetraacetic Acid
EIF2	Eukaryotic Translation-initiation Factor 2
ELISA	Enzyme-Linked Immunosorbent Assay
ER	Endoplasmic Reticulum
FACS	Fluorescence-Activated Cell Sorting
FAE	Follicle-Associated Epithelium
FBS	Foetal Bovine Serum
FC	Fold Change
FcR	Fc Receptors
FDC	Follicular Dendritic Cell
FDR *p*-value	False Discovery Rate *p*-value
Foxp3	Forkhead Box P3
FP	Fluorescent Protein
FRC	Fibroblastic Reticular Cells
GATA3	GATA Binding Protein 3
GC	Germinal Centre
GM-CSF	Granulocyte Macrophage Colony-Stimulating Factor
GxWB	Genomics Workbench
HEL	Hen Egg Lysozyme
HEV	High Endothelial Venule
HIF1a	Hypoxia-Inducible Factor 1 a
HPRT	Hypoxanthine-guanine Phosphoribosyltransferase
ICOS	Inducible T cell Co-Stimulator
ICOSL	Inducible T cell Co-Stimulator Ligand
IFA	Incomplete Freund's Adjuvant
Ifit1	Interferon-Induced protein with Tetratricopeptide repeats 1
IFN	Interferon
IFNAR1/2	Interferon Alpha Receptor subunit 1/2
Ig	Immunoglobulin
IL	Interleukin
IMDM	Iscove's Modified Dulbecco's Medium
IP_3	Inositol Triphosphate
IPA	Ingenuity Pathway Analysis
IRE-1	Inositol Requiring Enzyme 1
IRF4	Interferon Regulatory Factor 4
ISG	Interferon-Stimulated Gene
ITAM	Immunoreceptor Tyrosine-based Activation Motif
iTreg	induced T regulatory cell

KO	Knock-Out
L/D	Live/Dead stain
LN	Lymph Node
LPS	Lipopolysaccharide
LZ	Light Zone
M cell	Microfold cell
MALT	Mucosa-Associated Lymphoid Tissue
MFI	Median Fluorescence Intensity
MGM	Maximum Group Mean
MHC-I/II	Major Histocompatibility Complex class I/II
MMR	Mismatch Repair
MOG	Myelin Oligodendrocyte Glycoprotein
mRNA	messenger RNA
MS	Multiple Sclerosis
MZ	Marginal Zone
NF-κB	Nuclear Factor kappa-light-chain-enhancer of activated B cells
NFAT	Nuclear Factor of Activated T cells
NHEJ	Non-Homologous End-joining
NK cell	Natural Killer cell
NP	4-Hydroxy-3-Nitrophenylacetyl
NP-CT	4-Hydroxy-3-Nitrophenylacetyl-Cholera Toxin
NP-KLH	4-Hydroxy-3-Nitrophenylacetyl-Keyhole Limpet Hemocyanin
OVA	Ovalbumin
PALS	Peri-Arterial Lymphoid Sheath
PAMP	Pathogen-Associated Molecular Pattern
Pax-5	Paired Box 5
PC	Principle Component
PCR	Polymerase Chain Reaction
PD-1	Programmed cell Death protein 1
PdBU	Phorbol 12,13-Dibutyrate
pDC	plasmacytoid Dendritic Cell
PE	Paired-End
PERK	PKR-like ER kinase
PFA	Paraformaldehyde
PIP2	Phosphatidylinositol 4,5-bisphosphate
PKCδ	Protein Kinase C delta
PLCγ1	Protein Kinase C gamma 1
PP	Peyer's Patch
PRR	Pattern Recognition Receptor
RAG	Recombination Activating Gene
RIN	RNA Integrity Number

RNA	Ribonucleic Acid
RORc/a/gt	Retinoic acid receptor-relate
RPKM	Reads Per Kilobase Million
rRNA	ribosomal RNA
RT-qPCR	Quantitative Real-Time Polymerase Chain Reaction
S1P	Sphingosine-1-Phosphate
SAP	Slam-Associated Protein
SCS	Subcapsular Sinus
SD	Standard Deviation
SED	Subepithelial Dome
SEM	Standard Error of the Mean
SERCA	Sarcoplasmic/Endoplasmic Reticulum Calcium-ATPase
SFB	Segmented Filamentous Bacteria
SHM	Somatic Hypermutation
SLO	Secondary Lymphoid Organ
STAT	Signal Transducer and Activator of Transcription
Tbet	T-Cell-Specific T-Box Transcription Factor T-Bet (Tbx21)
TCR	T Cell Receptor
TDT	Terminal Deoxyribonucleotidyl Transferase
Tfh	T follicular helper cell
Tfr	T follicular regulatory cell
TGFβ	Transforming Growth Factor beta
TGFβRi	TGFβ receptor serine kinase inhibitor
Th cell	T helper cell
TMB	3, 3', 5, 5' - Tetramethylbenzidine
TNF	Tumour Necrosis Factor
TNFRS	Tumour Necrosis Factor Receptor Superfamily
Treg cell	T regulatory cell
TUDCA	Tauroursodeoxycholic Acid
UPR	Unfolded Protein Response
UPRE	UPR-Regulated Element
WT	Wildtype = C57BL/6 mouse
Xbp1(s)	X-box binding protein 1
ZAP70	Zeta chain of TCR-associated Protein kinase 70

Table of Contents

1 INTRODUCTION 1
1.1 The immune system 1
1.2 Interactions between the immune system and its microenvironment 2
1.3 Secondary lymphoid organs (SLOs) 3
1.3.1 Lymph nodes (LNs) 4
1.3.2 The spleen 4
1.3.3 Peyer's patches (PPs) 5
1.4 T-dependent immune responses 7
1.4.1 CD4 T cells 8
1.4.2 CD4 T cell development 10
1.4.3 CD4 T cell activation 13
1.5 B cells 17
1.5.1 B cell subsets 17
1.5.2 B cell development 18
1.5.3 B cell activation 20
1.5.4 Class-switch recombination 21
1.6 Germinal centre (GC) responses 22
1.6.1 Tfh cells 23
1.6.2 Tfr cells 25
1.6.3 Specialised GCs in PPs 25
1.6.4 The GC response in ageing 29
1.7 The immune system and the endoplasmic reticulum (ER) stress response pathway 32
1.7.1 The ER stress response 32
1.7.2 The impact of ER stress on immune responses 33
1.8 Aim & Objectives 35
2 MATERIAL AND METHODS 37
2.1 Animal work 37
2.1.1 Co-housing of adult and aged mice 37
2.1.2 Faecal microbiota transplantation (FMT) 38
2.1.3 Oral immunisations 39
2.1.4 Subcutaneous immunisations 39
2.1.5 NP-CTx conjugation and quality control 41
2.1.6 Experimental autoimmune encephalitis (EAE) 41
2.2 T helper cell cultures 42
2.3 Adoptive T cell transfers 43
2.4 Flow cytometry and Fluorescence-activated cell sorting (FACS) 44
2.4.1 Flow cytometry and FACS of *in vitro* differentiated T helper cells 44
2.4.2 Flow cytometry of PPs and LNs 44
2.4.3 Flow cytometry of faecal bacteria 45
2.4.4 Flow cytometry and FACS of dendritic cells 46
2.5 Confocal imaging of germinal centres 48
2.6 Enzyme-linked immunosorbent assay (ELISA) 48
2.6.1 Quantitation of antigen-specific immunoglobulins 48
2.6.2 Quantitation of total free IgA 49
2.7 Real-Time qPCR (RT-qPCR) 50
2.7.1 RNA isolation & cDNA synthesis from *in vitro* differentiated T cells and *ex vivo* cells 50
2.7.2 RNA isolation from lymph nodes 50
2.7.3 RT-qPCR of *in vitro* differentiated T helper cells 50
2.7.4 One-step RT-qPCR of LNs and *ex vivo* isolated cells 51
2.8 RNA sequencing 52
2.8.1 Th17 cells: RNA library preparation and sequencing 52
2.8.2 Th17 cells: RNA sequencing data analysis 53

2.8.3 cDC2 cells: RNA library preparation and sequencing 55
2.8.4 cDC2 cells: RNA sequencing data analysis 56
2.9 16S rDNA sequencing of faecal bacteria 56
2.9.1 DNA isolation 56
2.9.2 16S rDNA sequencing library preparation and sequencing 57
2.9.3 16S rDNA sequencing data analysis 57
2.10 Statistics 58
3 ER STRESS SUPPORTS TGFβ-INDEPENDENT T HELPER 17 DIFFERENTIATION 59
3.1 Abstract 59
3.2 Background 59
3.3 Results 61
3.3.1 ER stress increases Th17 cell differentiation 61
3.3.2 Increased expression of Th1 cell-associated genes in ER stress-generated Th17 cells 67
3.3.3 Potential effects of ER stress on T cell receptor signalling in Th17 cells 71
3.3.4 ER stress promotes EAE pathology 74
3.4 Discussion 77
4 HETEROCHRONIC FAECAL TRANSPLANTATION BOOSTS THE GUT GERMINAL CENTRE REACTION 81
4.1 Abstract 81
4.2 Background 81
4.3 Results 83
4.3.1 The GC reaction is diminished in aged PPs 83
4.3.2 The composition of the gut microbiome changes with age 87
4.3.3 Co-housing rescues the reduced PP GC reaction in aged mice 92
4.3.4 Heterochronic FMT boosts the GC in PPs 96
4.3.5 Cross-strain FMT does not enhance the GC 99
4.3.6 IgA-mediated control of the microbiome is not affected by ageing or FMT 100
4.3.7 Reduction of PP GCs has a minimal impact on the gut microbiome 103
4.3.8 FMT does not enhance PP GC responses to cholera toxin 105
4.4 Discussion 108
5 TYPE I INTERFERON SIGNALLING BOOSTS T FOLLICULAR HELPER CELL DIFFERENTIATION IN AGED MICE 111
5.1 Abstract 111
5.2 Background 111
5.3 Results 113
5.3.1 GC responses are impaired in aged mice 113
5.3.2 Impaired T cell priming in aged animals 116
5.3.3 Interferon signalling is reduced in cDC2 cells from aged mice 119
5.3.4 Lack of type I IFN signalling in DCs is linked with impaired Tfh cell formation 123
5.3.5 Imiquimod-induced type I IFN signalling rejuvenates cDC2s in aged mice 126
5.3.6 Imiquimod enhances Tfh cell priming in aged mice 128
5.4 Discussion 130
6 DISCUSSION 133
6.1 ER stress: a novel driver of Th17 cell pathogenicity? 133
6.2 The GC response in ageing 135
6.2.1 Cross-talk between the gut microbiome and GC responses in the PPs of aged mice 136
6.2.2 T cell priming in aged mice is improved by enhanced type I IFN signalling in cDC2s 140
7 REFERENCES 143

1 INTRODUCTION

1.1 The immune system

The human body is constantly exposed to a wide variety of viruses, bacteria, fungi and parasites, many of which are pathogens that can cause disease, while others are commensals that live in and on us without causing any harm. The host immune system consists of many different cells which have evolved to recognise and control these microorganisms (Chaplin 2010). The different types of immune cells can be broadly subdivided into belonging to one of two main arms of the immune system: the evolutionary-ancient innate immune system and the adaptive immune system, which is only present in vertebrates (Figure 1.1). Innate immune cells encompass dendritic cells (DCs), macrophages, mast cells and granulocytes, all of which are important early responders to infections and help to instruct adaptive immune responses. The adaptive immune system comprises T and B cells, both of which mount highly specific immune responses and can generate immune memory. Innate lymphoid cells, including natural killer (NK) cells, are a specialised immune cell subset at the interface between the innate and adaptive immune system. They can be seen as the innate counterpart to T cells, as they arise from the same progenitor cells as T cells, but do not express adaptive immune receptors.

In order to recognise self from non-self, immune cells rely on two main types of surface receptors. The first type of receptors is found on cells of the innate immune system, whose limited set of germ-line encoded pattern recognition receptors (PRRs) recognises molecular patterns shared between a wide range of microorganisms (Janeway & Medzhitov 2002). These receptors help innate immune cells to act as quick responders to pathogenic infections. The second type of receptors is found on adaptive immune cells. These receptors are assembled from a combination of different gene segments into a huge combinatorial variety of receptors, each of which recognises a unique feature termed antigen (Bonilla & Oettgen 2010). The human body was estimated to contain more than 10^{12} adaptive immune cells, which can carry any one of more than 10^{14} potential different receptors, thus forming a huge antigen receptor repertoire to recognise almost any invading pathogen (Alberts *et al.* 2002a; 2002b). Once antigen receptors on adaptive immune cells bind to their cognate antigens, and receive appropriate co-stimulatory signals, these cells are activated to clonally expand, then differentiate into effector or memory cells (Cantrell 2015). Memory cells persist in the body for long periods of time and mount quick and potent immune responses when they re-encounter the

same antigen. As a result, the adaptive immune system does not only generate specific immune responses, but it also provides long-lasting immune protection against re-infections. This thesis will specifically focus on primary T cell-dependent immune responses.

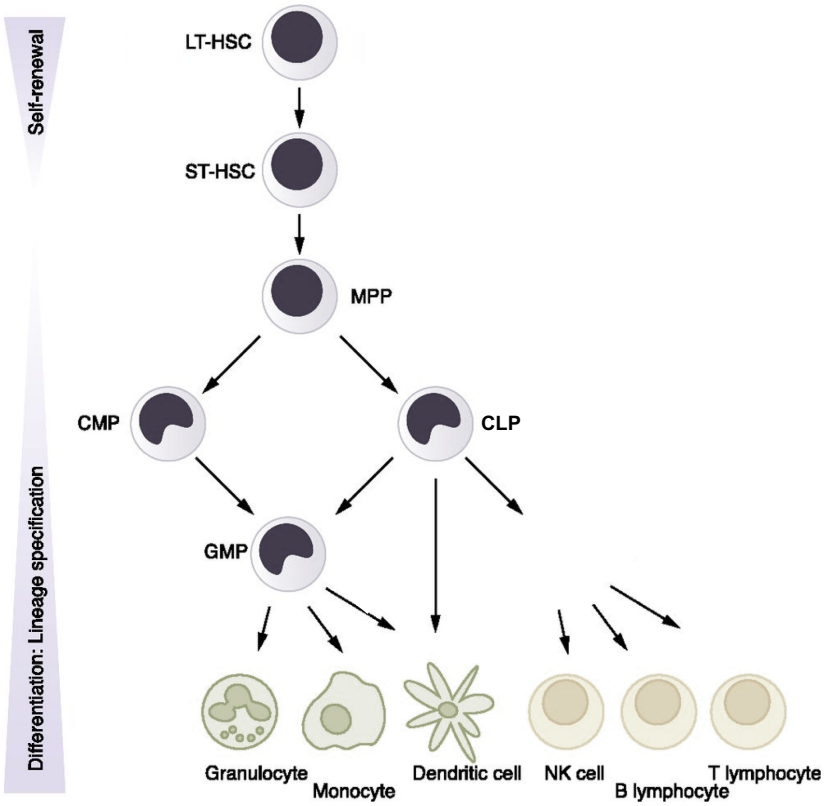

Figure 1.1: Schematic representation of immune cell development. Self-renewing long-term haematopoietic stem cells (LT-HSCs) in the bone marrow give rise to progenitor cells which differentiate to generate all types of immune cells. First, short-term haematopoietic stem cells (ST-HSCs) are formed, which generate multipotent progenitor (MPP) cells. These differentiate into common myeloid progenitors (CMP) or common lymphocyte progenitor (CLP) cells. CMP cells give rise to the innate immune arm by developing into granulocyte-macrophage progenitors (GMP), which differentiate into granulocytes, monocytes and dendritic cells (DCs). CLP cells, on the other hand, give rise to all adaptive immune cells, such as B cells, T cells, natural killer (NK) cells as well as some DC subsets. This image was adapted and republished with the permission of the American Society of Hematology from Blank & Karlsson 2015 (Blank & Karlsson 2015); permission conveyed through Copyright Clearance Center, Inc.

1.2 Interactions between the immune system and its microenvironment

The immune system has evolved to respond to environmental stimuli, to recognise and protect the body from insults and infections. As a result, immune cells are highly responsive to changes in their microenvironment. Adaptive immune cells in particular need to integrate soluble signals from their environment with signals they receive from innate immune cells which act as antigen-presenting cells (APCs) (Mueller & Coles 2014). For their optimal activation, adaptive immune cells need to

bind their cognate antigen while receiving co-stimulatory signals from APCs. Typically, these interactions between innate immune cells and adaptive immune cells are facilitated within secondary lymphoid organs (SLOs).

1.3 Secondary lymphoid organs (SLOs)

SLOs bring immune cells of the innate and adaptive immune system in close proximity, to facilitate the interaction of rare antigen-specific T or B cells with antigen-bearing APCs to trigger the initiation of adaptive immune responses (McComb *et al.* 2013). After their development from haematopoietic stem cells in the bone marrow (Figure 1.1) (Blank & Karlsson 2015), cells of both the innate and adaptive immune system recirculate through the blood, the lymphatic systems and the SLOs, which comprise the spleen, lymph nodes (LNs) and Peyer's patches (PPs). All SLOs develop during embryogenesis, and are characterised by their distinctive physical organisation of immune cells into different zones (Matsuno *et al.* 2010; Ruddle & Akirav 2009). This spatial segregation is achieved by chemokines, soluble signalling molecules which attract cells by binding to chemokine receptors on the cell surface. This induces chemotaxis, the directed migration of cells towards the chemokine source. In the T cell area, T cells co-localise with fibroblastic reticular cells (FRCs), which secrete the C-C motif chemokine ligands CCL19 and CCL21. These attract C-C motif chemokine receptor 7 (CCR7)-expressing T and DCs to the T cell zone. In all SLOs except the spleen, the T cell area also contains high endothelial venules (HEV), specialised capillaries which allow T cells to enter SLOs from the blood stream (Matsuno *et al.* 2010). The B cell follicle is clustered around C-X-C motif chemokine ligand 13 (CXCR13)-expressing follicular dendritic cells (FDCs), a chemokine which is recognised by C-X-C motif chemokine receptor 5 (CXCR5) on the surface of B cells (Chang & Turley 2015). This distinct architecture sets SLOs apart from other less-organised lymphoid tissues, such as mucosa-associated lymphoid tissues (MALT) (Matsuno *et al.* 2010). The main function of SLOs is to collect antigens from the peripheral sites and bring them into contact with recirculating T and B cells. SLOs are highly interconnected with the lymphatic and vascular circulatory systems (Matsuno *et al.* 2010), allowing for the constant entry (and efflux) of T cells, B cells, and antigen-carrying APCs through the blood or lymphatic vessels. Afferent lymphatic vessels also drain free antigen from peripheral tissues (Ruddle & Akirav 2009). This optimises the chances of antigen to come into contact with cells of the adaptive immune system for the generation of antigen-specific immunity.

1.3.1 Lymph nodes (LNs)

LNs are encapsulated SLOs which collect antigens from the peripheral lymphatic system (Figure 1.2) (Stebegg, Kumar, Silva-Cayetano *et al.* 2018). Each LN drains antigens from a specific part of the body (Ruddle & Akirav 2009): inguinal LNs, for instance, drain antigen from the skin in the lower half of the body, while mesenteric LNs are the gut-draining LNs. LNs are covered in a capsule, which surrounds the subcapsular sinus (SCS) (Ruddle & Akirav 2009). Underneath the SCS, the outer cortex contains B cell follicles with FDCs, while the inner para-cortex harbours the T cell zone and FRCs. The medulla in the centre of the LN contains a mix of immune cells, including DCs, macrophages and plasma cells, and serves as exit point from immune cells into the efferent lymphatics (Ruddle & Akirav 2009). For immune cells to exit the lymph node, they need to upregulate their sphingosine-1-phosphate (S1P) receptor (S1PR1). This receptor directs migration towards the chemokine S1P, whose concentration is high in the blood and lymphatics, but low in LNs (Chang & Turley 2015). This allows for the constant efflux and influx of adaptive immune cells into LNs, where they are exposed to antigens imported *via* the lymph. This makes LNs a highly effective induction site for adaptive immune responses against peripheral infections.

1.3.2 The spleen

The spleen drains antigens from the blood, and has three main compartments (Matsuno *et al.* 2010): the white pulp, the red pulp and the in-between marginal zone (MZ). All three compartments are formed around central blood arteries which branch off the trabecular artery. These arteries are embedded into the while pulp, which can be subdivided into the B cell follicle and the peri-arterial lymphoid sheath (PALS), corresponding to the T cell zone. This PALS is encompassed by the MZ, which contains specialised MZ B cells and MZ macrophages (Ruddle & Akirav 2009). The blood empties from the central arteries into the red pulp, which surrounds the MZ and helps to filter damaged cells from the blood, before it re-enters the blood stream *via* the splenic sinuses. Because of this specialised structure, the spleen is the optimal induction site for immune responses against blood-borne antigens.

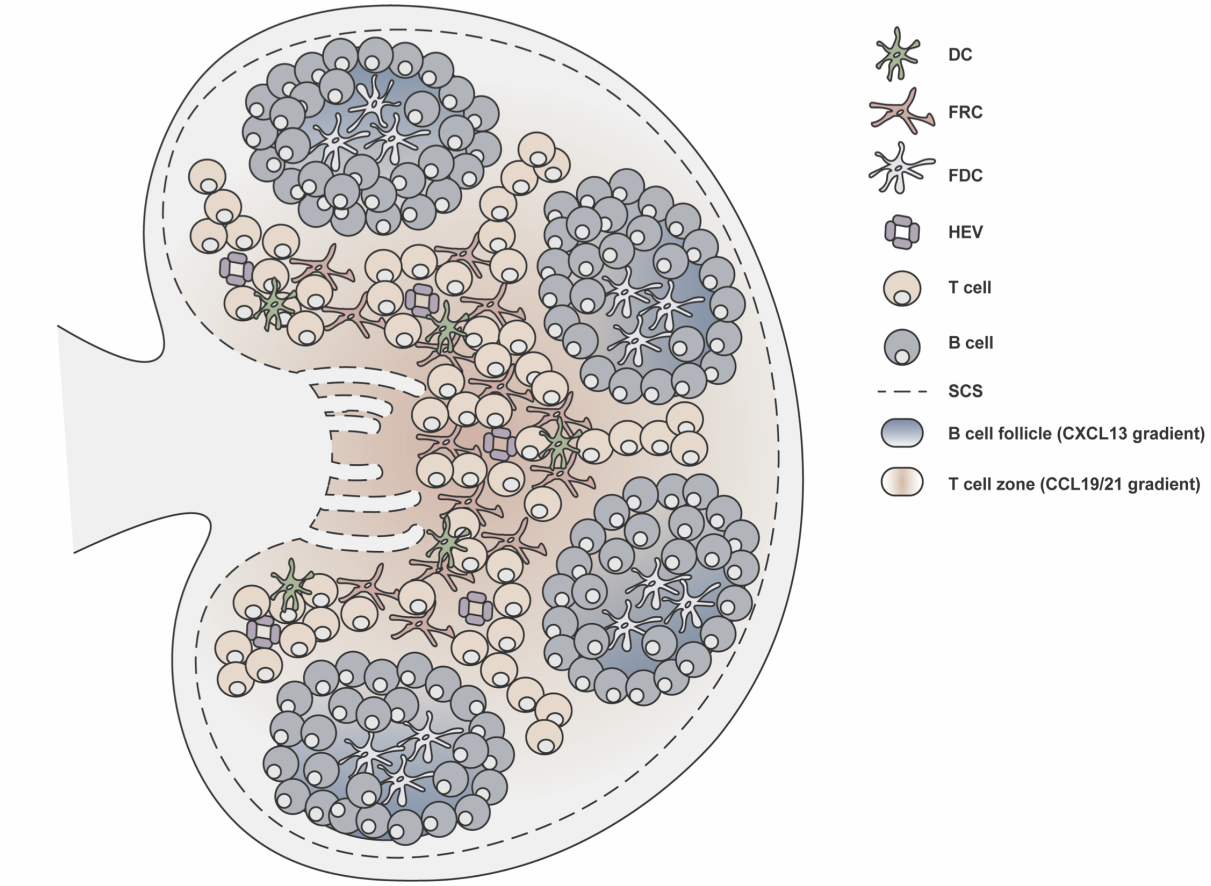

Figure 1.2: Schematic depiction of the specialised secondary lymphoid organ (SLO) architecture of lymph nodes (LNs). LNs can be subdivided into different regions: the T cell zone and B cell follicles. In the T cell zone, fibroblastic reticular cells (FRCs) generate a CCL19 and CCL21 gradient which attracts T cells and dendritic cells (DCs) from the blood stream *via* high endothelial venules (HEVs). Follicular dendritic cells (FDCs) in the B cell zone, in contrast, generate a CXCL13 gradient that attracts and retains B cells. Upon infection or immunisation, antigen drains into the LN *via* afferent lymphatic vessels into the subcapsular sinus (SCS) to trigger the activation of lymphocytes. Immune cells exit the LN *via* the medullary region in the centre of the LN. This image was created and kindly provided by Alyssa Silva-Cayetano (Stebegg, Kumar, Silva-Cayetano *et al*. 2018).

1.3.3 Peyer's patches (PPs)

PPs are non-encapsulated lymphoid tissues associated with the wall of the small intestine (Matsuno *et al.* 2010). This is a single epithelial layer which forms the body's largest mucosal surface. In mice, it covers an area of almost 1.5m^2, which is a hundred times larger than their skin surface (Casteleyn *et al.* 2010). The intestinal epithelium is essential for the digestion and absorption of nutrients as well as the protection against enteric pathogens. It is subdivided into two major segments: the small intestine and the large intestine. The large intestine consists of the colon and terminates in the rectum (Mowat & Agace 2014). While it has little digestive functions, it is crucial for the reabsorption of water and ultimately the excretion of indigestible food components. PPs are

only found in the small intestine, which in mice is subdivided into the duodenum close to the stomach, the jejunum and the ileum leading up to the caecum. Its main functions are the digestion of food and the absorption of nutrients (Mowat & Agace 2014). In mice, 6–12 PPs are interspersed along the whole length of the small intestine, while the human intestine contains 100–200 PPs (Reboldi & Cyster 2016).

PPs are unique SLOs in that they are neither encapsulated nor linked with afferent lymphatics (Reboldi & Cyster 2016). Instead, PPs take up antigens directly from the gut lumen *via* the follicle-associated epithelium (FAE) and its underlying subepithelial dome (SED). PPs consist of varying numbers of B cell follicles intersperse with T cell zones. Immune cells enter PPs *via* HEVs and exit to the gut-draining mesenteric LN *via* efferent lymphatics. Due to their distinct anatomical location close to the intestinal lumen, they are continuously exposed to antigen stimulation from the gut microbiota, a complex mix of bacteria, fungi, viruses and protozoa which populates the whole intestine (Reboldi & Cyster 2016). As a result, PPs differ from LNs and the spleen in their immune functions: they are important to mount antigen-specific immune responses against intestinal pathogens and toxins, and have also been proposed to help control the composition of the gut microbiota (Macpherson *et al.* 2008).

1.3.3.1 Cross-talk of PPs with the gut microbiome

It is estimated that the human body is populated by ~3.8×10^{13} bacterial cells (Sender *et al.* 2016). Of all organs, the intestine contains by far the highest concentration of commensal bacteria. While the concentration of dietary antigens decreases along the small intestine, the amount of commensal microorganisms increases, peaking in the large intestine (Moens & Veldhoen 2012). Studies of gut microbial diversity were long hampered by the lack of culture conditions for many gut bacteria. 16S rDNA sequencing technology now enables the identification of commensal bacterial species composition without the need for prior *in vitro* cultures (Jovel *et al.* 2016). The 16S rDNA gene encodes the RNA-component of the ribosomal 16S subunit, which is characterised by alternating highly-conserved and hypervariable regions. While the conserved regions only differ between high-level phylogenetic taxa, the hypervariable regions can be used to estimate evolutionary relations down to the species level (Rosselli *et al.* 2016). As a result, 16S rDNA sequencing can be used to computationally infer taxonomic identifications of a mix of bacteria. 16S rDNA sequencing revealed that, similar to humans, the murine gut core microbiome consists of two main phyla: *Firmicutes* (especially the *Lachnospiraceae, Ruminococcaceae* and *Lactobacillaceae* families) and *Bacteriodetes* (mainly *Porphyromonadaceae* and *Rikenellaceae*). In addition, *Proteobacteria*, *Actinobacteria, Deferribacteres* and *Verrucomicrobia* are also present in most mouse strains

(Clavel *et al.* 2016; Kostic *et al.* 2013). These commensal bacteria take on many functions: they help with the digestion of certain nutrients (*e.g.* by fermenting complex carbohydrates that the host's digestive enzymes cannot process (Mowat & Agace 2014)), maintain epithelial barrier integrity, influence host metabolism and support the development and priming of the immune system (Moens & Veldhoen 2012). A disruption of these functions, *e.g.* by a change in the composition of the gut microbiota, is termed dysbiosis and has many negative implications for the host (Clavel *et al.* 2016). Therefore, maintenance of balanced cross-talk between the host and its microbiome is crucial to sustain health. PPs play an important part in this cross-talk by providing immune protection against intestinal pathogens and have been suggested to control the composition of the gut microbiota by producing commensal-specific IgA antibodies (Macpherson *et al.* 2008).

1.4 T-dependent immune responses

T cells are crucial for cell-mediated adaptive immunity. They integrate information from their environment, *e.g.* cytokines or antigen presented by other immune cells, to either directly or indirectly fight infections in an antigen-specific manner. T cells can be broadly subdivided into CD4, CD8, γδT and natural killer T (NKT) cells: CD4 T cells and γδT cells secrete large amounts of effector cytokines to instruct immune responses by other immune cells. CD8 T cells can directly remove infected or damaged host cells, and NKT cells can do both (Pennock *et al.* 2013).

For T cell activation, peptide antigens need to be presented to T cells by APCs. In addition to recognising antigen, T cells require co-stimulatory signals to be activated. These are delivered when co-stimulatory receptors on T cells bind co-stimulatory ligands on APCs (Pennock *et al.* 2013). Antigen-mediated stimulation of T cells is achieved by peptide-loaded major histocompatibility complex class I (MHC-I) and class II (MHC-II) molecules on APCs. These peptide-MHC-I and -II complexes interact with the T cell receptor (TCR) and co-receptors on the surface of T cells (Blum *et al.* 2013).

CD8 T cells express cluster of differentiation (CD) 8 co-receptors, which bind to MHC-I molecules. MHC-I classically presents intracellular antigens, which are digested in the cytoplasm and loaded onto MHC-I molecules in the endoplasmic reticulum (ER). MHC-II molecules, on the other hand, are bound by CD4 co-receptors on CD4 T cells and present peptides which are generated from phagocytosed antigens in lysosomes (Blum *et al.* 2013). Correspondingly, CD8 T cells recognise intracellular antigens, *e.g.* virus-derived peptides or tumour-associated antigens, and are specialised on the removal of virus-infected cell as well as damaged or mutated tumour cells (Zhang & Bevan

2011). CD4 T cells, known as helper T (Th) cells, predominantly recognise extracellular antigens and secrete effector cytokines to instruct immune responses.

γδ T cells can express both CD4 and CD8 co-receptors. They are a rare T cell subset which already acquires its effector functions in the thymus (Vantourout & Hayday 2013). This allows γδ T cells to initiate rapid immune responses against non-peptide antigens such as phospholipids and alkylamines at epithelial barrier sites where many γδ T cells reside (Chien *et al.* 2014; Vantourout & Hayday 2013). NKT cells recognise lipid antigens presented on CD1, a MHC-like molecule (Bennstein 2017), in a CD4- and CD8-independent manner. Similar to CD4 T cells, they produce large amounts of cytokines such as IFN-γ, IL-4 and IL-13, and they can additionally act as cytotoxic T cells (Balato *et al.* 2009). This thesis focuses on CD4 T cell-dependent immune responses, especially the role of CD4 T cells as drivers of autoimmune disease and instructors of B cell responses.

1.4.1 CD4 T cells

$CD4^+$ αβ T cells are subdivided into different CD4 T cell subsets, each characterised by the expression of a master transcription factor and subset-specific signature cytokines. These determine the distinct effector functions of each Th cell subset (Gagliani & Huber 2017; Pennock *et al.* 2013). The first Th cells subsets to be described were Th1 and Th2 cells (Mosmann *et al.* 1986), but now also Th9 cells, Th17 cells, regulatory T (Treg) cells, T follicular helper (Tfh) and T follicular regulatory (Tfr) cells are well-established CD4 T cell subsets (Caza & Landas 2015).

1.4.1.1 Th1, Th2 and Th9 cells

Th1 cells form under the influence of IL-12 and are characterised by their expression of the T-box transcription factor T-bet. They are crucial mediators of cellular immunity against intracellular pathogens by secreting IFN-γ (Gagliani & Huber 2017). Th2 cells are essential to control extracellular parasitic infections. GATA Binding Protein 3 (GATA3)-expressing Th2 cells differentiate in response to IL-4 and produce the signature cytokines IL-4, IL-5 and IL-13 (Luckheeram *et al.* 2012). Th9 cells were first described as a subset of Th2 cells, but are now considered to be a distinct Th cell subset. They are generated when exposed to a combination of IL-4 and transforming growth factor (TGF)-β (Veldhoen *et al.* 2008b). This triggers the expression of their master transcription factor interferon regulatory factor (IRF4) and IL-9, the Th9 signature cytokine (Adamu *et al.* 2017; Dardalhon *et al.* 2008; Veldhoen *et al.* 2008b). While Th1, Th2 and Th9 cells mount important immune responses against pathogens, Th1 cells have also been implicated in the pathology of autoimmune disease, while imbalances in Th2 and Th9 cells have

been associated with allergies (Valenta *et al.* 2009). Thus, it is important that Th1, Th2 and Th9 responses are kept in check.

1.4.1.2 Treg cells

Treg cells were first described in 1995 (Sakaguchi *et al.* 1995). They are characterised by expression of the forkhead box protein 3 (Foxp3) and high levels of CD25 on their cell surface (Fontenot *et al.* 2003; Hori *et al.* 2003; Khattri *et al.* 2003). These cells can either arise in the thymus – so-called thymic Treg (tTreg) cells – or be generated *de novo* from naïve CD4 T cells in the periphery under the influence of IL-2 and TGF-β. The latter are termed peripheral Tregs (pTregs) (Gagliani & Huber 2017). Treg cells exert important immunosuppressive functions by producing the anti-inflammatory cytokines IL-10 and TGF-β. They also express co-stimulatory inhibitors, such as cytotoxic T-lymphocyte-associated protein 4 (CTLA-4), which inhibits T cell responses in a cell contact-dependent manner (Gagliani & Huber 2017). Mice and humans lacking Treg cells suffer from a severe autoinflammatory disorder, demonstrating the important role of Treg cells for regulating immune responses (Bennett *et al.* 2001; Brunkow *et al.* 2001; Wildin *et al.* 2001).

1.4.1.3 Th17 cells

Th17 cells are most abundant at epithelial barrier sites where they provide immune protection against extracellular bacteria and fungi (Weaver *et al.* 2013). Th17 cell differentiation is classically driven by the combined actions of IL-6 and TGF-β (Harris *et al.* 2007; Mangan *et al.* 2006; Veldhoen *et al.* 2006a). This induces the Signal transducer and activator of transcription (STAT)3-dependent expression of the Th17 lineage-specific markers RORγt and RORα, transcription factors of the retinoic acid receptor-related orphan receptors (ROR) family (Caza & Landas 2015; McGeachy *et al.* 2007; Veldhoen *et al.* 2006a). Th17 cell differentiation also depends on the aryl hydrocarbon receptor (AhR) and hypoxia-inducible factor 1 alpha (HIF1a) (Dang *et al.* 2011; Veldhoen *et al.* 2008a). Th17 cells produce high levels of the pro-inflammatory cytokines IL-22, IL-17A and IL-17F which attract neutrophils and stimulate a wide range of other immune cells to secrete pro-inflammatory cytokines and chemokines. IL-17A and IL-17F also induce the secretion of antimicrobial peptides at epithelial barrier sites (Korn *et al.* 2009). Thus, Th17 cells provide an important functional link between the adaptive and innate immune system. They have also been suggested to both promote and inhibit cancer growth depending on the type of cancer (Bailey *et al.* 2014; Muranski *et al.* 2008; Wang *et al.* 2009; Wu *et al.* 2009). More importantly, Th17 cells were found to be key mediators of many autoimmune diseases where they are often enriched at sites of inflammation (Maddur *et al.* 2012). Amongst others, they have been directly implicated in the

immunopathology of rheumatoid arthritis, psoriasis, and multiple sclerosis (MS), an autoimmune disorder associated with axon demyelination in the central nervous system and progressive neurological deterioration (Bedoya *et al.* 2013; Jadidi-Niaragh & Mirshafiey 2011). Work from both *in vitro* and *in vivo* experiments revealed that Th17 cell pathogenicity is linked with their propensity to adopt a Th1-like cell phenotype and produce the inflammatory cytokines GM-CSF and IFNγ under the influence of IL-23 (El-Behi *et al.* 2011; Ghoreschi *et al.* 2010; Hirota *et al.* 2011; Jain *et al.* 2016; McGeachy *et al.* 2007). In addition to IL-23-driven Th17 cell pathology, other environmental factors, such as high salt concentrations or the presence of different AhR ligands, have also been shown to influence Th cell differentiation and pathogenicity (Quintana *et al.* 2008; Veldhoen *et al.* 2008a; Wu *et al.* 2013). In this report, a novel role for the endoplasmic reticulum (ER) stress response as a driver of pathogenic Th17 cell differentiation is described, highlighting the strong impact of another environmental stimulus on the generation of Th17 cells with pathogenic *versus* protective properties.

1.4.1.4 Tfh and Tfr cells

Both T follicular helper (Tfh) and T follicular regulatory (Tfr) cells are found in lymphoid structures called germinal centres (GCs). Here Tfh cells provide B cell help *via* direct T-B cell contacts and the production of IL-21 for the generation of highly-specific antibody responses, while Tfr cells have suppressive functions. Both cell types express the master-transcription factors Bcl6 (B cell CLL/Lymphoma 6) as well as high levels of PD-1 (programmed cell death protein 1) and CXCR5. Tfr cells additionally express Foxp3, the master regulator of regulatory T cells (Linterman *et al.* 2011; Vinuesa *et al.* 2016). The role of Tfh and Tfr cells in regulating the GC response will be discussed in more detail in section 1.3.2.4.

1.4.2 CD4 T cell development

CD4 T cells are generated in the thymus from T cell progenitors arising from haematopoietic stem cells in the bone marrow (Koch & Radtke 2011). Bone marrow is the soft tissue in the cavities of bones, which forms an essential survival niche for haematopoietic stem cells (Gurkan & Akkus 2008). The niche is shaped by a stroma formed of reticular cells and mesenchymal stem cells. Here, haematopoietic stem cells differentiate into common lymphoid progenitor (CLP) cells, which, amongst others, give rise to T cell progenitors. These cells leave the bone marrow and migrate towards the thymus (Koch & Radtke 2011). The thymus is a primary lymphoid organ located between the heart and the sternum (Pearse 2006). Its two lobes can be subdivided into an outer lymphocyte-rich cortex and the inner medulla, a tight stromal network of thymic epithelial cells

(Ciofani & Zúñiga-Pflücker 2007). T cell development takes place in both these regions. The generation of T cells is most effective during childhood when the thymus is largest, before thymic atrophy is initiated during puberty (Palmer 2013).

Bone marrow-derived T cell progenitor cells arrive in the thymic cortex, where Notch-1 signalling commits them to the T cell differentiation pathway (Ciofani & Zúñiga-Pflücker 2007). In the subcapsular zone of the cortex, they undergo somatic rearrangements of their TCR genes to generate receptors with a large variety of unique specificities (Koch & Radtke 2011). TCRs are dimers, which can be formed either of a combination of a TCRα and β chain, or γ and δ chains (Krangel 2009). Depending on which TCR chain is successfully recombined first, a small subset of cells commits to the γδ T cell lineage, while the majority of cells will enter the αβ T cell fate *via* a process called β-selection (Koch & Radtke 2011). After recombination of their TCRβ chain, these αβ T cell precursors then enter the double-positive stage by upregulating both their CD4 and CD8 co-receptors and move on to the medulla, where they recombine their TCRα chain. The completed αβ TCR interacts with self-peptide-MHC complexes on thymic stromal cells, *e.g.* thymic epithelial cells and DCs in the medulla (Ciofani & Zúñiga-Pflücker 2007). Double-positive T cells with intermediate affinity for these MHC-self-antigen complexes receive positive survival signals and finally commit to single-positive CD4 or CD8 T cell lineages (Koch & Radtke 2011).

To prevent the generation of self-reactive T cells, cells with high affinity for self-antigens are then eliminated by negative selection. Some of the self-reactive T cells can alternatively develop into tTreg cells by the combined action of TCR and IL-2 signalling (Hsieh *et al.* 2012). All surviving cells, including non-self-reactive and tTreg cells, upregulate S1PR1 which allows them to leave the thymus as mature CD4 or CD8 T cells and seed SLOs and peripheral tissues (Koch & Radtke 2011).

1.4.2.1 Somatic recombination of the TCR

Somatic recombination of the TCR genes during T cell development is crucial for the generation of antigen-specific adaptive immunity. The germline TCR gene locus encodes arrays of V (variable), D (diversity) and J (joining) genes, which need to be spliced together to form one TCR chain in a process called somatic recombination (Figure 1.3) (Krangel 2009). The near-to-random combination of V, D and J segments of each TCR chains can theoretically generate more than 1×10^6 unique TCRs, with varying affinities for different antigens (Bonilla & Oettgen 2010; Glusman *et al.* 2001).

Somatic recombination is driven by the recombinase-activating genes 1 (RAG1) and 2 (RAG2), which are part of the V(D)J recombinase complex (Bonilla & Oettgen 2010). This complex binds

recombination signal sequences at the borders of V, D and J segments. Here it cleaves the DNA, giving rise to hairpin structures. Then Artemis acts as an endonuclease to generate 5' and 3' overhangs at the DNA break sites. The overhangs from one J and one D segment are joined by DNA repair enzymes, before the J-D segment is linked with one of the V segments by a similar process (Bassing *et al.* 2002). This process of non-homologous end-joining is imperfect and can lead to the addition or removal of bases at the ligation site. In addition, the terminal deoxyribonucleotidyl transferase (TDT) enzyme actively adds a random sequence of 1-5 nucleotides to the ligation site, resulting in so-called junctional diversity of the recombined TCR. This further increases the number of receptors theoretically generated from the germline locus to 10^{15} (Davis & Bjorkman 1988), but can also result in the generation of abrogated or non-functional TCRs. Only T cell precursors which express fully-functional TCR proteins on their surface can receive positive survival signals and differentiate into mature T cells (Koch & Radtke 2011).

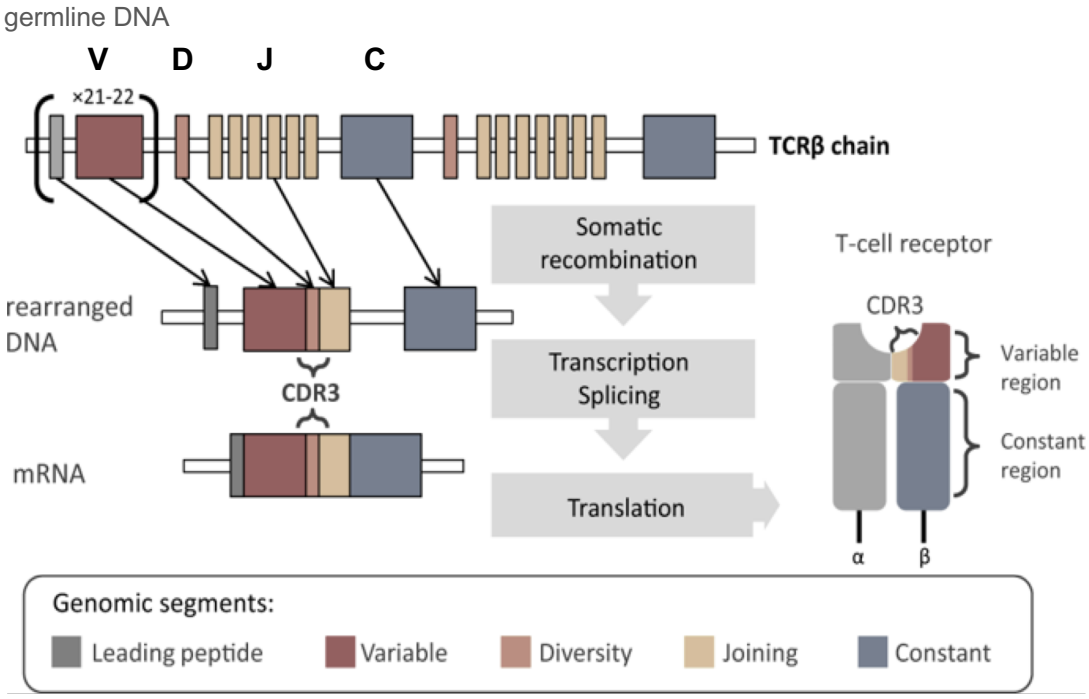

Figure 1.3: Schematic representation of somatic TCRβ chain rearrangements. The TCRβ chain is generated by V(D)J recombination of its germline DNA. First, one J segment is joint with a D segment during DJ-recombination, then this gene segment is linked with a V gene and its leading peptide during V(D)J recombination. The recombined variable region contains complementary-determining regions (CDRs), such as CDR3, which are part of the antigen-binding domains of the TCR. The final TCRβ chain is formed by transcriptional splicing of its mRNA transcript. This image was taken from Migalska *et al*. 2018, licenced under CC BY 4.0 © 2018 (Migalska *et al.* 2018).

1.4.3 CD4 T cell activation

CD4 T cells leave the thymus as naïve cells which recirculate through the body *via* the blood and SLOs. To fulfil their immune functions, these naïve cells need to be activated by professional APCs. As described above, this is dependent on peptide-MHC-mediated triggering of the TCR combined with additional stimulation of the T cell *via* co-stimulatory receptors (Pennock *et al.* 2013). This initiates the clonal expansion of T cells. Cytokines further direct CD4 T cell differentiation into distinct effector phenotypes, by inducing the expression of subset-specific master transcription factors (Bonilla & Oettgen 2010).

1.4.3.1 T cell activation by dendritic cells (DCs)

DCs are the main APC for the initiation of CD4 T cell-dependent immune responses (Segura 2016). Generally, DCs are classified into resident DCs, which reside in SLOs, and migratory DCs which circulate between tissues. These are further subdivided into conventional DCs (cDCs), plasmacytoid DCs (pDCs), Langerhans cells and monocyte-derived DCs based on their functions (Segura 2016) (Table 1.1; Figure 1.4).

Activated DCs provide all three signals required for T cell activation and differentiation: signal one is provided when DCs take up antigen, internalise it and present peptide-MHC-II complexes to CD4 T cells (Webb & Linterman 2017). Upon activation of PPRs on the surface of DCs by PAMPs, DCs also provide signal two by upregulating the expression of co-stimulatory molecules on their surface (Krishnaswamy *et al.* 2018). PAMP-dependent activation also triggers signal three – the production of the cytokines which drive Th cell subset-specific differentiation (Krishnaswamy *et al.* 2018; Webb & Linterman 2017).

Co-stimulation is essential to trigger T cell activation (Pennock *et al.* 2013). Signalling *via* the TCR alone induces T cell anergy, a state of hypo-responsiveness to further TCR stimulation. Only if a T cell receives simultaneous stimulation *via* its TCR and its co-stimulatory receptors, it will become fully activated. As co-stimulatory ligands on DCs are only upregulated in the presence of foreign antigens or inflammation, this helps to prevent activation of the adaptive immune system in the absence of an infection (Pennock *et al.* 2013). The primary co-stimulatory receptor on T cells is CD28 (Harding *et al.* 1992), but other immunoglobulin superfamily and tumour necrosis factor (TNF) receptor superfamily (TNFRSF) members, such as CD40, CD27, OX-40, 41BB, can also act as co-stimulatory receptors. When they interact with their ligands on activated DCs (CD80/CD86, CD40 ligand (CD40L), CD70, OX-40L and 41BBL respectively), these receptors promote T cell survival and proliferation (Chen & Flies 2013).

DC subset	Selected marker genes (by Guilliams et al. 2016)	Origin	Functions
pDC	$B220^{+}PDCA\text{-}1^{+}$	common DC progenitor	Production of type I interferons, *e.g.* during viral infections (Swiecki & Colonna 2015)
cDC1	$Batf3^{+}Xcr1^{+}CD8aa^{+/-}$ $CD103^{+/-}$	common DC progenitor	Cross-presentation of phagocytosed antigen to CD8 T cells *via* MHC-I (Merad *et al.* 2013)
cDC2	$Irf4^{+}CD172\alpha^{+}CD11b^{+/-}$	common DC progenitor	CD4 T cell activation *via* MHC-II (Krishnaswamy *et al.* 2018)
Langerhans cells	$Langerin^{+}CD24^{+}$	embryonic monocytes	Modulation of T cell responses in the skin (Doebel *et al.* 2017)
Monocyte-derived DCs	$Ly6c^{high}CD64^{high}$	generated from monocytes in infected tissue	Diverse functions, including CD4 T cell activation, cross-priming of CD8 T cells and direct anti-microbial activities (Domínguez & Ardavín 2010)

Table 1.1: Overview of dendritic cell (DC) subsets. DCs can be subdivided into several subsets, depending on their origin and functions. Plasmacytoid DCs (pDCs) and classical DCs (cDC) arise from a common DC progenitor, while Langerhans cells and monocyte-derived DCs are generated from embryonic monocytes and monocytes in infected tissue, respectively. Characterisation of the different DC subsets by marker genes is not trivial - this table lists a selection of subset-specific marker genes as used in this report and cited literature.

Upon T cell activation, the TCR and all its co-stimulatory molecules are clustered at the immunological synapse, which is formed at the interface of DC-T cell contact. This clustering facilitates the recruitment of signalling kinases such as Src protein tyrosine kinases to the TCR (Figure 1.5) (Cantrell 2015; Ghosh 2004). These first phosphorylate immunoreceptor tyrosine-based activation motifs (ITAMs) on CD3 proteins, then ZAP-70 (zeta chain of TCR-associated protein kinase 70) is recruited to these ITAM sites and activates a cascade of downstream phosphorylation events. This results in the activation of phospholipase Cγ1 (PLCγ1) which converts phosphatidylinositol 4,5-bisphosphate (PIP_2) into the second messengers diacylglycerol (DAG) and inositol trisphosphate (IP_3) (Matthews & Cantrell 2009). While DAG activates the protein kinase C θ (PKCθ) and the MAPK/Erk pathways to promote NF-κB (nuclear factor 'kappa-light-chain-enhancer' of activated B-cells) signalling, IP_3 triggers the release of Ca^{2+} from the endoplasmic reticulum (ER) which leads to the activation of the transcription factor NFAT (nuclear factor of activated T cells) (Cantrell 2015). Co-stimulatory molecules further enhances these signalling pathways and also activate PI_3 kinase (PI3K), which promotes Akt and PKCθ activities (Chen &

Flies 2013). Combined, these signalling cascades enhance T cell proliferation and survival. This is accompanied by dramatic changes in T cell metabolism, associated with an increase in the uptake of nutrients and switching from oxidative phosphorylation to aerobic glycolysis. This allows activated T cells to generate enough biomass for clonal expansion and to produce large amounts of effector cytokines (Michalek & Rathmell 2010).

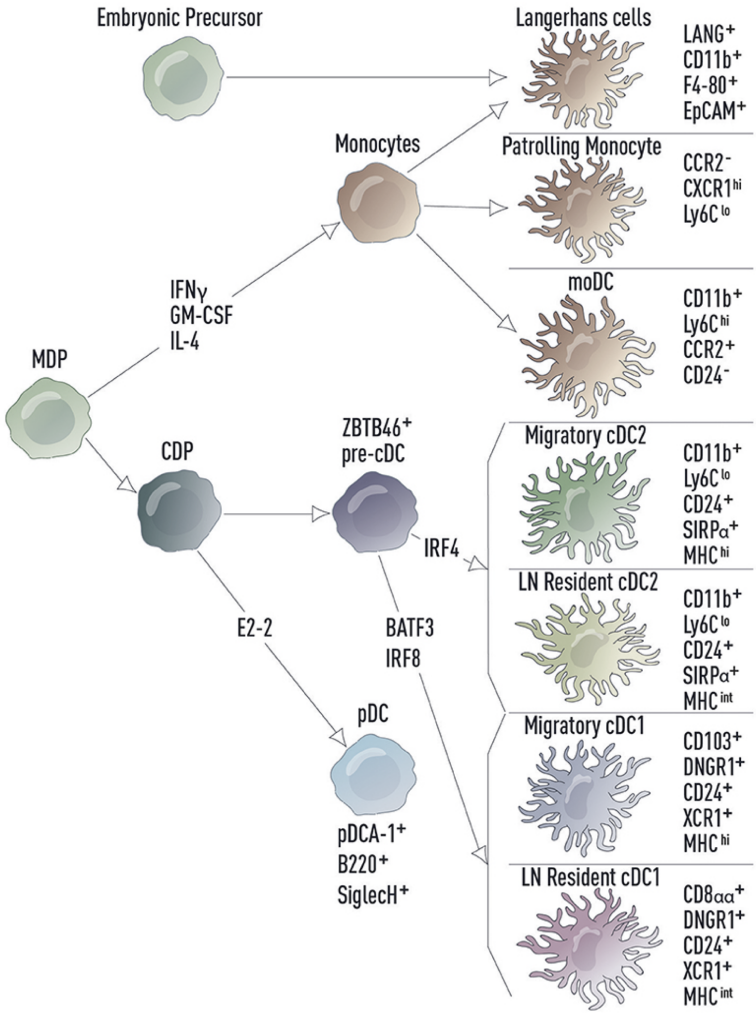

Figure 1.4: Schematic representation of dendritic cell (DC) differentiation. DCs can be subdivided based on their ontogeny and localisation (resident *versus* migratory). Monocyte-macrophage DC progenitors (MDPs) give rise to monocytes and common DC progenitors (CDPs). Monocytes do not only generate macrophages, but also develop into myeloid DCs and Langerhans cells, which also arise from embryonic precursors. CDPs, in turn, differentiate into plasmacytoid DCs (pDCs) and pre-conventional DCs (pre-cDCs). Interferon regulatory factor 4 (IRF4) expression in pre-cDCs drives differentiation into cDC2s, whereas the expression of the basic leucine zipper ATF-like transcription factor 3 (BATF3) leads to the development of cDC1s. On the right, cell surface markers for the identification of the different DC subsets are listed. Image modified from Krishnaswamy *et al*. 2018, licenced under CC BY 4.0 © 2018 (Krishnaswamy *et al.* 2018).

Inhibitory co-receptors prevent T cell activation-induced changes by dampening the signalling pathways downstream of the TCR and co-stimulatory receptors. CTLA-4 and PD-1 are the most prominent inhibitory receptor and restrict T cell activation in several ways (Pennock *et al.* 2013): similar to CD28, CTLA-4 binds to CD80 and CD86, but with higher affinity than CD28, physically preventing CD80/CD86-CD28 interactions. CTLA-4 can also transcytose CD80/CD86, removing them from the surface of DCs and thereby limiting CD28 co-stimulation (Buchbinder & Desai 2016). CTLA-4 and PD-1 can also recruit intracellular phosphatases, which dampen TCR downstream signalling by dephosphorylating and inactivating important signalling nodes, such as PLCγ1 and PKCθ (Chen & Flies 2013).

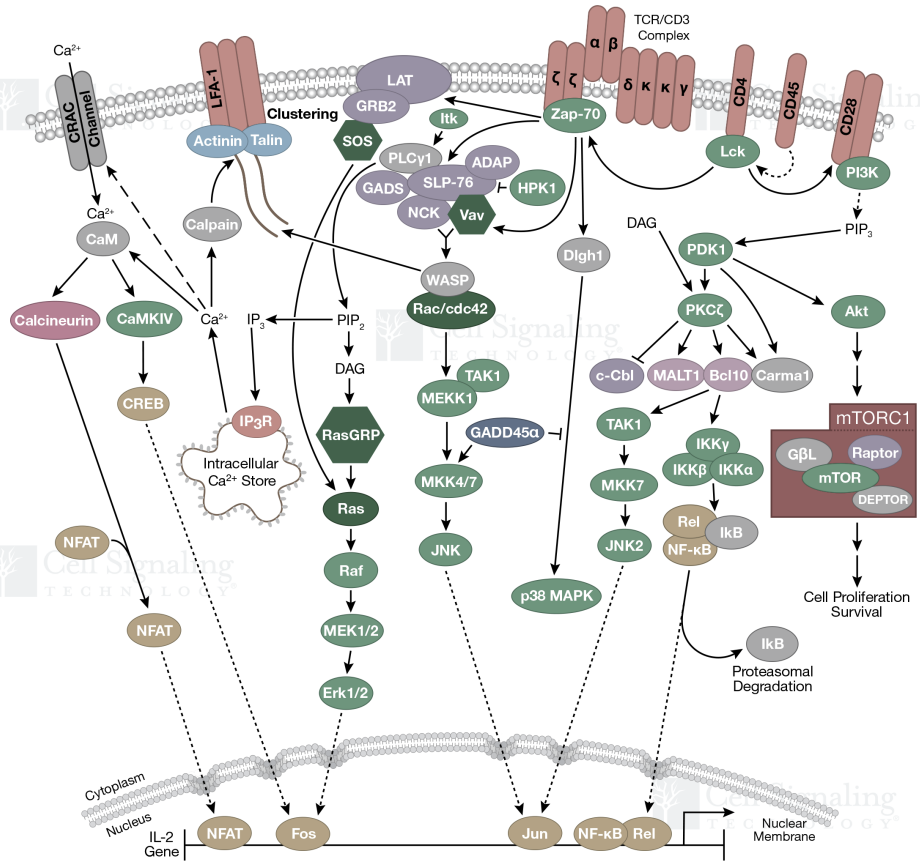

Figure 1.5: Schematic illustration of the T cell receptor (TCR) signalling network. When the TCR on CD4 T cells recognises antigen in the context of CD4 and CD28 co-stimulation, downstream signalling is initiated to mediate T cell activation. During this process, ZAP70 (zeta chain of TCR-associated protein kinase 70) is recruited to the membrane to activate the phospholipase C γ1 (PLCγ1). PLCγ1 converts phosphatidylinositol 4,5-bisphosphate (PIP2) into diacylglycerol (DAG) and inositol trisphosphate (IP3). While DAG activates the protein kinase C delta (PKCθ) and the MAPK/Erk pathways to promote NF-κB signalling, IP3 initiates the release of Ca2+ from the endoplasmic reticulum (ER), resulting in the activation of the transcription factor NFAT (nuclear factor of activated T cells). Illustration reproduced courtesy of Cell Signaling Technology, Inc. (www.cellsignal.com) (Ghosh 2004).

This demonstrates that CD4 T cells have evolved to integrate many signals from their environment to adapt their functions. As described above, they require antigen-presentation and co-stimulation from DCs to be activated. Cytokines produced by these APCs can further drive their differentiation into different effector T cell subsets. In a cell-contact dependent manner and by producing distinct cytokines themselves, they then instruct immune responses by other immune cells to generate context-specific immune responses. While this is crucial to mount antigen-specific immune responses, dysregulated T cell responses have also been associated with chronic inflammatory and autoimmune diseases. Therefore, it is crucial to improve our understanding of how environmental changes impact CD4 T cell-dependent immune responses.

1.5 B cells

Upon activation, B cells can either terminally differentiate into plasma cells, which produce large amounts of antigen-specific antibodies, the secreted form of their antigen receptor - the B cell receptor (BCR) - , or differentiate into IL-10-producing, immunosuppressive B regulatory cells, which are important for immunological tolerance (Lu *et al.* 2017; Rosser & Mauri 2015). This report will mainly focus on B cell-mediated antibody responses which are dependent on plasma cell differentiation initiated by activated CD4 T cells in a process called T cell help, or in a T-independent manner. The resulting antibodies are secreted at mucosal surfaces or circulate the body in the blood stream to provide immune protection by directly neutralising pathogens or marking them for removal by other immune cell types (Lu *et al.* 2017).

1.5.1 B cell subsets

B cells development takes place in the foetal liver and in the bone marrow, giving rise to two B cell subsets: B-1 and B-2 cells (LeBien & Tedder 2008). B-1 cells are solely derived from the foetal liver early during development and are retained in the host thereafter through self-renewal (Baumgarth 2011). These cells are rare in SLOs and mainly populate the peritoneal and pleural cavities as well as mucosal surfaces such as the intestine. They express a restricted BCR repertoire which is polyreactive. Even in the absence of an antigenic stimulus, these are secreted as natural antibodies of the IgM and IgA isotypes to help protect the body from invading bacteria, *e.g.* upon intestinal lesions (Fagarasan *et al.* 2010). Conversely, B-2 cells can be derived from both the foetal liver and the bone marrow. They seed SLOs as naïve follicular B cells or MZ B cells (Figure 1.6) (LeBien & Tedder 2008). MZ B cells are a specialised B cell subset in the spleen. Similar to B-1 cells, they recognise T-independent carbohydrate and phospholipid antigens to produce IgM antibodies early during an immune response, but can also response to protein antigen in a T-

dependent manner (Hoffman *et al.* 2016; Phan *et al.* 2005; Song & Cerny 2003). Naïve B cells reside in B cell follicles and are best characterised for raising T cell-dependent antibody responses. They express both IgM and IgD BCR isotypes on their surface and are constantly replenished from the bone marrow. Upon activation, they expand clonally and can differentiate into either memory B cells or plasma cells that secrete large amounts of antibodies (LeBien & Tedder 2008).

1.5.2 B cell development

In the bone marrow, B-2 cells are generated from CLPs which first give rise to proB cells (Hardy & Hayakawa 2001; LeBien & Tedder 2008; Yam-Puc *et al.* 2018). proB cells are the earliest stage of B cell development. They express the E2A transcription factor, the B cell marker B220 and paired box 5 (Pax-5), a master regulator of B cell development. Upon downregulation of E2A, they differentiate into preB cells, which undergo somatic rearrangements of their antigen receptor (Hardy & Hayakawa 2001). Immature B cells, which have successfully recombined their BCR, can then leave the bone marrow and seed SLOs in the periphery (Figures 1.6 & 1.7) (LeBien & Tedder 2008).

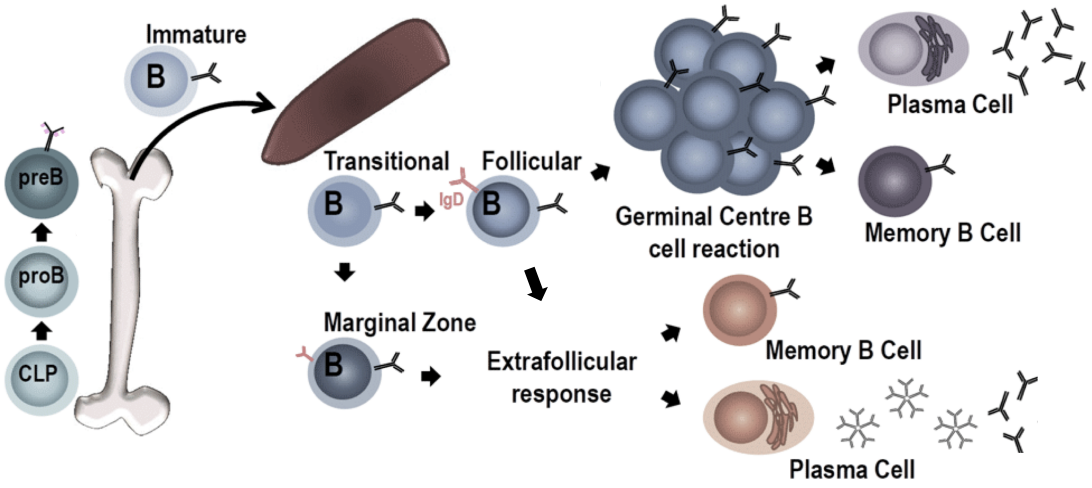

Figure 1.6: Schematic depiction of B cell development. Common lymphoid progenitor (CLP) cells give rise to proB and preB cells in the bone marrow. After successful V(D)J recombination of their B cell receptor (BCR), IgM-expressing immature B cells leave the bone marrow and migrate to secondary lymphoid organs (SLOs) like the spleen. Here, transitional B cells differentiate into marginal zone B cells or follicular B cells, which express both IgM and IgD BCRs on their surface. Upon activation, both B cell subtypes can differentiate into memory B cells and short-lived plasma cells in a germinal centre (GC)-independent fashion. Follicular B cells can migrate to the B cell follicle and seed GCs. During the GC response, GC B cells clonally expand and hypermutate their BCR which, after selection, can lead to enhanced antigen affinity. B cells exiting the GC reaction generate memory B cells and long-lived plasma cells which secrete high-affinity antibodies. Image modified from Yam-Puc *et al.* 2018, licenced by F1000 Research under CC BY © 2018 (Yam-Puc *et al.* 2018).

1.5.2.1 V(D)J recombination of the BCR

B cell development is tightly linked with the rearrangement of their antigen receptor genes. The BCR, also known as immunoglobulin, consists of two heavy and two light chains (Lu *et al.* 2017). Both chains are subdivided into a constant and variable region: the constant region remains constant during B cell development, but can be subject to class switch recombination (CSR) upon B cell activation. The variable region encodes the region of the BCR that binds antigen. The final BCR configuration is generated by rearrangements of various gene segments during B cell development (Lu *et al.* 2017). Immunoglobulin rearrangements are very similar to V(D)J recombination of the TCR in T cells (described in section 1.4.2.1). Each heavy and light chain is encoded by a large gene locus which contains several V, D and J genes (Schroeder & Cavacini 2010). During B cell development, RAG-1 and RAG-2 generate double-strand breaks at the immunoglobulin locus to first join one of the J genes with a D gene. The D-J pair is then recombined with a V gene to form a complete immunoglobulin chain. Somatic rearrangements occur independently for the light and heavy chains, which are then combined to form a functional BCR, resulting in the theoretical combinatorial diversity of almost 2×10^6 different immunoglobulins (Janeway *et al.* 2001; Johnston *et al.* 2006; Schroeder & Cavacini 2010; Ye 2004). In addition, a random number of nucleotides can be lost or gained during the DNA repair process at D-J and V-DJ ligation sites, further increasing BCR diversity by junctional diversification (Janeway *et al.* 2001).

V(D)J recombination of the immunoglobulin heavy chain takes place in proB cells (Figure 1.7) (González *et al.* 2007; LeBien & Tedder 2008). Random mutations during V(D)J recombination can lead to the expression of a truncated or misfolded heavy chain. Only if the recombined heavy chain is functional, it can associate with a so-called surrogate light chain formed of λ5 and VpreB. The resulting complex is termed pre B cell receptor (pre-BCR), which, similar to the BCR, assembles with the accessory proteins Igα and Igβ (Hardy & Hayakawa 2001). Assembly and signalling downstream of the pre-BCR are required to advance B cell development. This is an important safety test, to make sure that only B cells with a functional heavy chain go on to differentiate into preB cells and rearrange their light chain locus. Formation of the pre-BCR stops V(D)J recombination by the downregulation of RAG1 and RAG2 (Schroeder & Cavacini 2010). proB cells then divide a few times, before they turn into preB cells, which reactivate RAG1 and RAG2 to rearrange their BCR light chain (Naradikian *et al.* 2014). B cell development in the bone marrow is completed, when, after successful VJ recombination of the light chain locus, a mature BCR is expressed on the surface of the immature B cell. These cells carry a functional BCR of the IgM isotype on their surface.

75 % of immature bone marrow B cells bind to self-antigens (Wardemann *et al.* 2003), however to limit autoimmunity, cells carrying these BCRs are eliminated from the B cell pool *via* two mechanisms: cell death or receptor editing (Naradikian *et al.* 2014). The latter is dependent on the reactivation of RAG1 and RAG2 expression for another round of light chain rearrangements to modify the antigen-specificity of the BCR. Despite this control mechanism, some self-reactive B cells manage to exit from the bone marrow *via* the blood stream. In the periphery, negative selection of these cells continues by exclusion of these cells from the B cell follicle, anergy, developmental arrest or lack of T cell help (Manjarrez-Orduño *et al.* 2009). Together, these tolerance mechanisms protect the body from auto-reactive B cells, which are generated as a by-product of BCR diversification by V(D)J recombination.

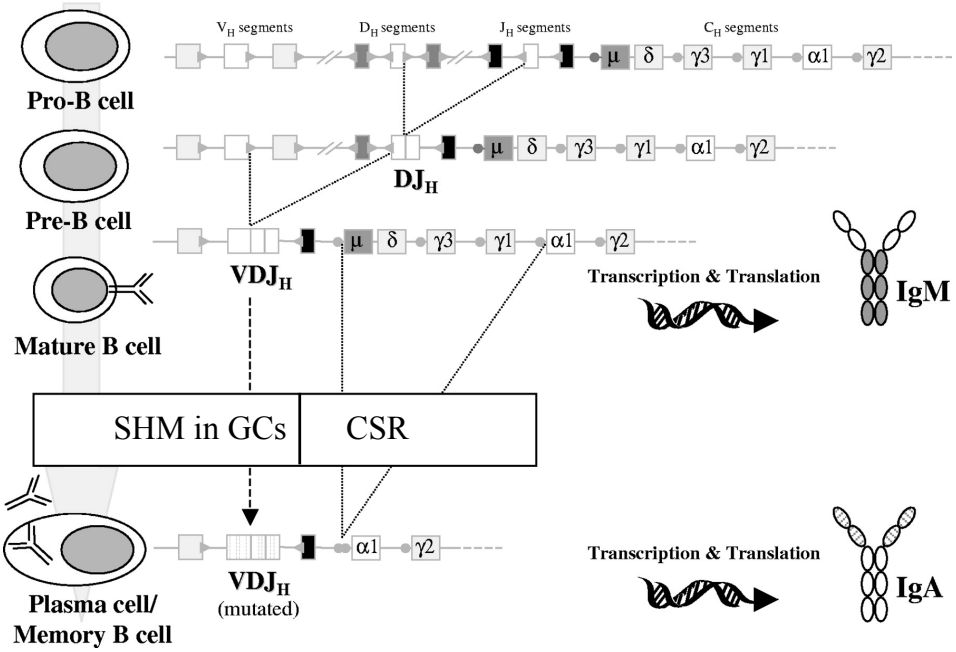

Figure 1.7: Schematic illustration of V(D)J rearrangements and class switch recombination (CSR) of the heavy chain of the B cell receptor (BCR). During B cell development, the BCR germline locus undergoes V(D)J recombination. This gives rise to a mature BCR, which is expressed as IgM on the surface of mature B cells. Upon antigen-dependent activation of B cells CSR can occur, leading to expression of a new immunoglobulin isotype such as IgA. During the germinal centre (GC) response, somatic hypermutation (SHM) of the V(D)J locus can additionally take place. Circles depicted next to constant regions of the heavy chain locus (C_H) represent switch regions. Dotted lines on V, D, and J segments represent hypermutated genes after SHM. This image was modified and republished with the permission of the American Society of Hematology from González *et al.* 2007 (González *et al.* 2007); permission conveyed through Copyright Clearance Center, Inc.

1.5.3 B cell activation

B cells are activated when they recognise their cognate antigen *via* their BCR. BCRs can either bind soluble antigen or antigen presented on the surface of FDCs, macrophages and DCs (Batista &

Harwood 2009). Antigen recognition leads to the upregulation of CCR7 on the surface on B cells, which allows them to migrate from the B cell follicle towards FRC-derived chemokines CCL19 and CCL21 in the T cell zone (Okada *et al.* 2005). At the T-B border between the T cell zone and the B cell follicle, B cells present antigen to T cells. This interaction provides B cells with survival and co-stimulatory signals. T cell-dependent signals induce the expansion of B cells (Chan *et al.* 2009) whose progeny can then either migrate to the B cell follicle and seed the GC response or enter an extrafollicular response. The latter leads to their differentiation into memory B cells or short-lived plasma cells, which secrete the first wave of antibodies essential for the early response against infections while the GC reaction is established (MacLennan *et al.* 2003).

1.5.4 Class-switch recombination

Upon B cell activation, the immunoglobulin heavy chain can undergo somatic recombination of its immunoglobulin constant region in a process called class-switch recombination (CSR) (Figure 1.7) (Schroeder & Cavacini 2010). In the mouse, eight constant regions are found in the heavy chain locus downstream of the V(D)J region (Shimizu *et al.* 1982). Each constant region contains an upstream switch region, which can be recombined with any switch region of the other constant regions during CSR (Schroeder & Cavacini 2010). The class switching process is mediated by activation-induced cytidine deaminase (AID), an enzyme which initiates CSR at switch sites by deaminating cytosines (Stavnezer & Schrader 2014). Enzymes of the base excision repair (BER) and mismatch repair (MMR) pathways are then recruited to the mutated sites, where they induce DNA double-strand breaks (DSBs). These breaks are subsequently recombined by non-homologous end-joining (NHEJ), adding a new constant region to the 3' end of the heavy chain locus (Stavnezer & Schrader 2014). Like this, different isotypes, or antibody classes distinguished only by their C-terminal region, can be generated in addition to the initial IgM and IgD isotypes: IgA, IgE, IgG1, IgG2, IgG3, - and IgG4 in humans only (Schroeder & Cavacini 2010). These constant regions do not interact with antigen, but modulate the effector functions of the secreted antibody: neutralisation of target antigens, activation of immune cells by binding to antibody isotype-specific Fc receptors (FcRs), or activation of the complement system by binding to C1q (Hoffman *et al.* 2016). Antibody isotypes determine the predominant antibody effector function. IgA, for instance, is important to neutralise antigens at mucosal surfaces, while IgE activates mast cells by binding to their IgE-specific FcR (Schroeder & Cavacini 2010). Thus, somatic rearrangements modulate not only antigen specificity of the BCR, but also its effector functions.

1.6 Germinal centre (GC) responses

GCs are where antigen-specific B cells somatically mutate the variable region of their antigen receptor to improve BCR affinity in an antigen-specific manner (Figure 1.8) (Stebegg, Kumar, Silva-Cayetano *et al.* 2018). They then form memory B cells and long-lived plasma cells that secrete antibodies with high antigen-binding affinity (Vinuesa *et al.* 2016). Alternatively, B cells can also form antibody secreting plasma and memory B cells in a GC-independent manner, but these cells usually display lower affinity because of the lack of somatic hypermutation (SHM) at extrafollicular sites (Bortnick & Allman 2013; MacLennan *et al.* 2003).

For a GC reaction to be initiated, B cells need to recognise their cognate antigen *via* their BCR and to interact with antigen-activated T cells at the T-B border (Okada *et al.* 2005). Activated B cells then migrate back into the B cell follicle and form GC B cells (Pereira *et al.* 2009). GC B cells first expand clonally as centroblasts in the dark zone (DZ) of the germinal centre. Centroblasts express the proliferation marker Ki67 and are retained in their niche by expressing CXCR4, which is attracted to the chemokine CXCL12 secreted by CXCL12-expressing reticular cells (CRCs) in the DZ (Allen *et al.* 2004). Here, centroblasts undergo SHM of their antigen receptor gene (Bannard *et al.* 2013). SHM is mediated by AID, the same enzyme that catalyses CSR. During SHM, the repair of AID-induced U:G mismatches results in point mutations of the BCR gene (Peled *et al.* 2008). This can have several outcomes: SHM can disrupt the BCR structure or generate BCRs either with improved antigen affinity or novel antigen-specificity. This can lead to the unintentional emergence of auto-reactive B cell clones with the potential to cause autoimmune diseases if they are not appropriately censored in the GC.

To make sure that SHM in the GC response only gives rise to B cells with improved affinity to foreign antigen, they require, for their survival, positive selection signals from Tfh cells and FDCs in the light zone (LZ) (Mesin *et al.* 2016). To get access to FDCs and T cells, centroblasts need to differentiate into centrocytes which upregulate CXCR5 (Allen *et al.* 2004). CXCR5 is the receptor for CXCL13, a chemokine produced by FDCs in the LZ. Here, centrocytes test their BCR by taking up antigen from the surface of FDCs and presenting it to Tfh cells (Suzuki *et al.* 2009). These cells provide positive selection for B cells with high antigen affinity. B cells with high affinity for antigen take up more antigen from FDCs, and are therefore able to present more peptide-MHC-II complexes to Tfh cells and form longer-lasting T-B cell interactions (Gitlin *et al.* 2014; Shulman *et al.* 2014). As a result, they outcompete lower affinity B cell clones by receiving stronger survival signals. Besides Tfh cells, GCs also contain $Foxp3^+$ Tfr cells, which dampen the GC response and prevent the expansion of auto-reactive B cells (Vanderleyden *et al.* 2014).

Together these selection mechanisms culminate in the generation of long-lived antibody-producing plasma and memory B cells with improved antigen affinity. These cells provide specific immune protection, not only to the primary infection, but also to reinfections for up to several decades (Mesin *et al.* 2016; Takemori *et al.* 2014).

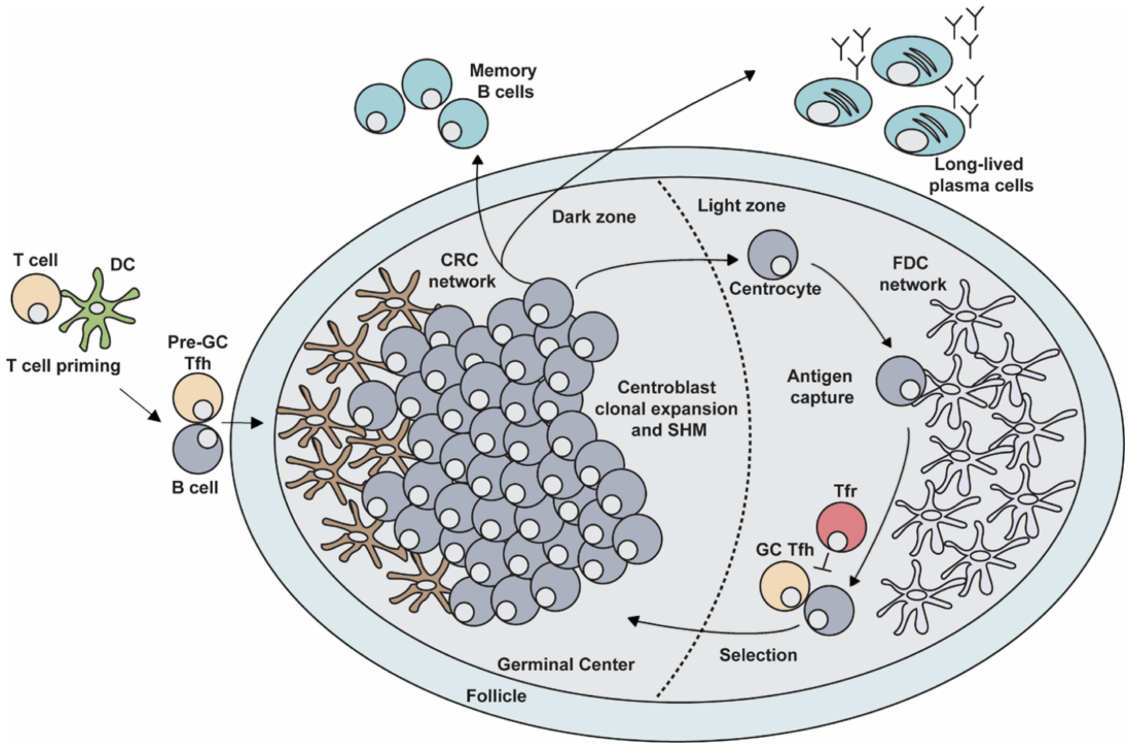

Figure 1.8: Schematic representation of the germinal centre (GC) response. GCs are specialised structures formed in B cell follicles upon infection or immunisation. They consist of two compartments: the dark zone (DZ) and light zone (LZ). The DZ is where B cells form centroblasts which expand clonally and undergo somatic hypermutation (SHM) to enhance their antigen affinity. This compartment is shaped by CXCL12-producing reticular cells (CRCs), which attract and retain the CXCR4-expressing centroblasts. When centroblasts upregulate CXCR5 and differentiate into centrocytes, they migrate towards follicular dendritic cells (FDCs) in the LZ, which express the CXCR5-ligand CXCR13. Here, centrocytes capture antigens from the surface of FDCs and present them to T follicular helper (Tfh) cells for B cell selection. Only centrocytes with high antigen affinity receive vital survival signals from Tfh cells and can exit the GC as long-lived plasma or memory B cells. T follicular regulatory (Tfr) cells dampen the GC response to prevent the emergence of autoreactive B cell clones. This image was created and kindly provided by Alyssa Silva-Cayetano (Stebegg, Kumar, Silva-Cayetano *et al*. 2018).

1.6.1 Tfh cells

Tfh cells are required for the initiation of the GC response, as shown in *Bcl6*$^{fl/fl}$*Cd4*$^{cre/+}$ mice, which lack Tfh cells and cannot form GCs (Hollister *et al.* 2013). Tfh cells are generated when naïve CD4 T cells in SLOs are primed by antigen-presenting DCs. The resulting Tfh cell precursors (pre-Tfh cells) upregulate Bcl6, CXCR5 and Epstein-Barr virus-induced gene 2 (EBI2), while

downregulating CCR7 (Li *et al.* 2016; Webb & Linterman 2017). This leads to the migration of pre-Tfh cells to the T-B border, where concentrations of the CXCR5-ligand CXCL13 are higher. Even if several DC subtypes have been shown to activate T cells and induce their migration to the T-B border, here migratory cDC2s seem to be the dominant Tfh-priming DC subset, especially under conditions of low antigen availability (Krishnaswamy *et al.* 2017; 2018).

As described above, CD4 T cells require three signals to be activated and differentiate into Tfh cells (Krishnaswamy *et al.* 2018): antigen-specific interactions of their TCR with peptide-MHC-II on DCs, co-stimulation and signals from cytokines. Activated cDC2s provide all three signals: signal one is provided when DCs take up antigen, internalise it and present peptide-MHC-II complexes to T cells (Webb & Linterman 2017). Upon activation of PRRs on the surface of DCs by PAMPs, they also provide signal two by upregulating the expression of CD40L, OX40L, the inducible T cell costimulatory ligand (ICOSL), CD80 and CD86, all of which interact with co-stimulatory receptors on the surface of T cells to enhance TCR signalling and boost Tfh differentiation (Krishnaswamy *et al.* 2018). PAMP-dependent activation also triggers signal three – the production of the cytokines such as IL-6, an important driver of Tfh cell differentiation (Eddahri *et al.* 2009; Webb & Linterman 2017). In addition, PAMPs induce the production of type I interferons (IFNs) by DCs. Type I IFN, which comprise several α and β IFNs, is an enhancer of Tfh cell differentiation (Cucak *et al.* 2009). Type I IFNs were proposed to act on Tfh cells by enhancing the DC-dependent production of IL-6 and IL-27 cytokines known to favour Tfh cell differentiation (Batten *et al.* 2010; Cucak *et al.* 2009; Gringhuis *et al.* 2014). IFNAR signalling can also promote the secretion of IL-1β by DCs, which enhances the expression of Bcl6, CXCR5 and the inducible T cell co-stimulator (ICOS) by Tfh cells (Barbet *et al.* 2018). Taken together, this demonstrates that cDC2 cells are potent inducers of Tfh cell differentiation at the T-B border and are therefore crucial to initiate GC responses.

At the T-B border, SLAM-associated protein (SAP)-dependent interactions between antigen-activated T and B cells are further required to enable full Tfh cell differentiation (Qi *et al.* 2008). Mature Tfh cells are characterised by their expression of the transcription factor Bcl6 and the chemokine receptor CXCR5 which facilitates follicular homing (Victora & Nussenzweig 2012). Tfh cells also express high levels of the co-stimulatory molecules CD40L, PD-1 and ICOS (Webb & Linterman 2017). These molecules are important mediators of GC B-Tfh interactions, as GC B cells express their interacting partners CD40 and ICOSL (Vinuesa *et al.* 2016). CD40-CD40L interactions are crucial for GC formation, as CD40L on Tfh cells provide important survival signals to GC B cells (Casamayor-Palleja *et al.* 1996; Foy *et al.* 1993; Takahashi *et al.* 1998). Tfh cells also secrete IL-21 and IL-4 cytokines to regulate GC B cell selection. IL-21 enhances Bcl6 expression in GC B cells (Linterman *et al.* 2010), while IL-4 was shown to support GC B cell selection as well

as CSR (Cunningham *et al.* 2004). Competition of B cells for these factors is crucial to ensure that only B cells with high antigen affinity exit the GC reaction.

The random mutation process during SHM can lead to the emergence of auto-reactive B cell clones with the potential to cause autoimmune diseases. Therefore, the ongoing GC reaction needs to be tightly regulated. An excess number of Tfh cells in the GC leads to impaired B cell selection and the emergence of self-reactive B cell clones which ultimately cause autoimmunity (Linterman *et al.* 2009; Vinuesa *et al.* 2005).

1.6.2 Tfr cells

Tfr cells are negative regulators of the GC response. They have been reported to restrain the production of antibodies, while favouring the emergence of antigen-specific B cell clones (Stebegg, Kumar, Silva-Cayetano *et al.* 2018). Tfr cells derive from $Foxp3^+$ precursors and share phenotypic characteristics of Tfh cells, including expression of Bcl6 and CXCR5 (Aloulou *et al.* 2016). Similar to Tfh cells, Tfr cell differentiation seems to follow a multi-step, Bcl6-dependent differentiation process which relies on both antigen presentation from DCs and interactions with activated B cells (Stebegg, Kumar, Silva-Cayetano *et al.* 2018). Upon immunisation, Tfr cells are recruited into the GC, where they regulate the GC response *via* CTLA4-mediated suppression (Sage *et al.* 2014; Wing *et al.* 2014) and by impairing GC B and Tfh cell metabolism, causing the downregulation of important GC B cell effector molecules such as AID (Sage *et al.* 2016). This negative regulation by Tfr cells is important to control GC size (Linterman *et al.* 2011; Wollenberg *et al.* 2011) and to prevent the emergence of auto-reactive B cells (Fu *et al.* 2018).

1.6.3 Specialised GCs in PPs

In PPs, specialised GC responses give rise to IgA antibodies (Figure 1.9) (Kawamoto *et al.* 2014; Reboldi & Cyster 2016; Stebegg, Kumar, Silva-Cayetano *et al.* 2018). Like other GCs, B cells within PP GCs undergo SHM of the Ig locus, followed by selection of B cells bearing BCRs that bind antigen with high affinity. One key difference to peripheral LNs is that in PPs CSR to the IgA isotype occurs (Craig & Cebra 1971). In AID-deficient animals that lack CSR and SHM, there is aberrant expansion of anaerobic gut commensals and extensive immune hyperplasia (Fagarasan *et al.* 2002; Suzuki *et al.* 2004). Patients with selective IgA deficiency also exhibit changes in their gut microbiome, associated with increased Th17-cell associated inflammation (Fadlallah *et al.* 2018). This demonstrates the key role that IgA antibody responses play in the control of the gut microbiota.

IgA antibodies exist as dimers and are secreted at all mucosal surfaces. In the gut, IgA is secreted into the gut lumen by M cells, specialised epithelial cells above the SED of PPs. Once in the gut, IgAs bind to a wide range of commensal bacteria and alter the composition of the microbiota through a variety of mechanisms (Macpherson *et al.* 2012). These include blocking interactions of bacteria with the host, trapping antigens in the intestinal mucus or interfering with the invasive properties of pathogens (Macpherson *et al.* 2012). In addition, IgA antibodies assist with the controlled intestinal uptake of bacterial antigens to boost local antigen-specific gut immune responses (Pabst 2012; Rey *et al.* 2004).

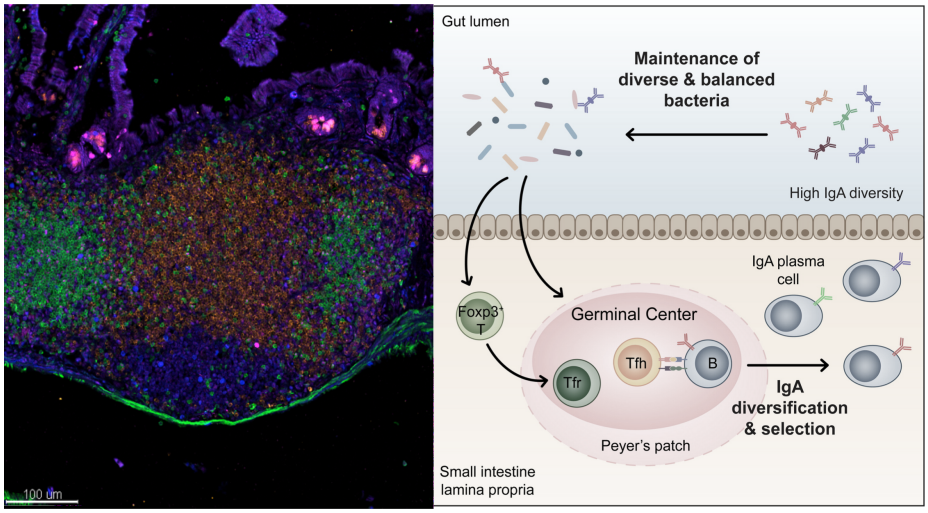

Figure 1.9: Depiction of Peyer's patches (PPs) and their role in producing commensal-specific IgA antibodies. On the left, a confocal immunofluorescence image of a murine PP is shown. Blue Ki67+ GC B cells demarcate the PP germinal centre (GC). CD3+ T cells are shown in green, follicular IgD+ B cells in orange and Foxp3+ cells in pink. On the right, a schematic illustration of a PP is shown. The GC reaction in PPs, which is controlled by T follicular helper (Tfh) and T follicular regulatory (Tfr) cells, generates plasma and memory B cells which secrete somatically hypermutated IgA antibodies. These antibodies are secreted into the intestinal lumen, where they bind to the surface of a wide range of commensal bacteria, helping to control the composition of the gut microbiota. The gut microbiota in turn induces the generation of Foxp3+ T regulatory cells and the production of IgA antibodies by B cells in gut lining. This figure was reprinted from Kawamoto *et al*. 2014 with permission from Elsevier © 2014 Elsevier Inc. (Kawamoto *et al.* 2014).

It is not clear whether this is mediated by IgA antibodies generated in a GC-dependent or -independent fashion. Evidence suggesting that functional IgA antibodies can be generated independently of GCs comes from studies in which mice lack either T-dependent immune responses (CD28-deficient mice and CD40-deficient mice) or Tfh cells ($Bcl6^{fl/fl}Cd4^{cre/+}$). All these animals have high IgA antibody titres, and $Bcl6^{fl/fl}Cd4^{cre/+}$ mice were also shown to have near-to-normal levels of bacterial IgA-coating, and relatively normal composition of the microbiota (Bergqvist *et al.* 2006; Bunker *et al.* 2015; Gärdby *et al.* 2003). However, SHM of IgA antibodies mainly occurs in GCs and analysis of mice that express a variant of AID that can facilitate CSR, but not SHM,

revealed that this strain exhibited aberrant expansion of commensal bacteria and increased bacterial translocation into mesenteric LNs (Wei *et al.* 2011). This suggests that GC responses in the PP play a role in the maintenance of microbial homeostasis.

1.6.3.1 Immune regulation of GCs in PPs by Tfh and Tfr cells

Given the distinct architecture and location of PPs, their regulatory mechanisms are unique from those in other SLOs. Most importantly, Tfh and Tfr cells in PPs are responsive to modulation by the gut microbiota. The ensuing plasticity in T cell regulation allows PP GCs to respond adequately to intestinal infections or changes in the gut microbiota (Stebegg, Kumar, Silva-Cayetano *et al.* 2018).

PPs provide a unique environment for Tfh cell differentiation, where the "rules" established for Tfh cell development are frequently broken. Exclusively in the gut, Tfh cells can derive from RORγt$^+$ Th17 cells (Hirota *et al.* 2013) and Foxp3$^+$ Treg cells (Tsuji *et al.* 2009). The precise mechanism for this is unclear, but it may be driven by stimuli from the microbiota, as microbial sensing plays an important role for Tfh differentiation in the gut. Microbial ATP was shown to control Tfh cell differentiation in PPs *via* interactions with the ATP-gated ionotropic P2X7 receptor (Proietti *et al.* 2014). Moreover, the Th17 cell-promoting segmented filamentous bacteria (SFB) were shown to drive the differentiation of PP Tfh cells (Fei Teng *et al.* 2016). The egress of these "unusual" PP Tfh cells into systemic sites can have dire consequences for health, as they were reported to exacerbate auto-antibody responses in arthritis (Fei Teng *et al.* 2016). This demonstrates the ability of intestinal Tfh cells to integrate multiple signals from the gut microbiota for their development, with implications not only for gut, but also systemic immunity. Therefore, control of Tfh cell development, and their maintained residence in the gut is critical for organismal health (Stebegg, Kumar, Silva-Cayetano *et al.* 2018).

Similar to Tfh cells, PP Tfr cells have gut-specific features. In PP GCs, the Tfh/Tfr ratio is increased compared to peripheral GCs (Kato *et al.* 2014), making PP GCs resemble the early stages of a GC reaction. This has been proposed to enable the expansion of low affinity B cell clones early in the response (Ramiscal & Vinuesa 2013) and is consistent with the proposal of Reboldi *et al.* (Reboldi & Cyster 2016)**,** who suggested that GCs in PPs resemble early GCs in order to favour the quick generation of diverse low-affinity antibodies in response to microbial antigens. Interestingly, gene expression profiling of Tfr cells from PPs and LNs revealed that PP Tfr cells, unlike LN Tfh cells, express the helper cytokine IL-4 (Georgiev *et al.* 2018). This could point to a different, potentially less suppressive, role of Tfr cells within PPs.

As discussed above, Tfr cells are considered to be negative regulators of the GC response, but the data about their functionality in PPs is not clear. STAT3-deficient mice, which lack Tfr cells but have PP Tfh cells, have no observable changes in PP GC size or IgA production in the gut (Wu *et al.* 2016). However, in an adoptive transfer model Kawamoto *et al*. implicated Tfr cells in the regulation of IgA-mediated control of the gut microbiome: the supplementation of T cell-deficient hosts with Treg cells increased IgA production and induced dramatic changes in the composition of the microbiota (Kawamoto *et al.* 2014). This is consistent with the observation that depletion of Treg cells results in a drop in IgA levels (Cong *et al.* 2009). Together, this suggests that both Tfr functionality as well as the Tfh/Tfr ratio in PPs are adjusted to allow for optimal control of the gut microbiota, although further work is required to precisely define the role of Tfr cells in PPs.

1.6.3.2 Immune regulation of GCs in PPs by the gut microbiota

The gut microbiota is a crucial, but often underappreciated, regulator of the GC response in the gut as well as of the systemic immune system (Stebegg, Kumar, Silva-Cayetano *et al.* 2018). Germ-free mice, which lack any form of bacterial colonization, exhibit evident deficits in the maturation of their gut-associated lymphoid tissues, including PPs and mesenteric LNs. Their PPs are small and produce limited amounts of IgA antibodies (Round & Mazmanian 2009). In addition, these mice are more susceptible to enteric infections and their systemic immune response to infections is also stunted (Fagundes *et al.* 2012; Khosravi *et al.* 2014). This demonstrates a strong dependency of the immune system on the microbiota. There is evidence that some bacteria and their products directly affect the GC response in PPs. Transfer of a diverse microbiota into wild-type mice increases GC B cell numbers as well as bacterial IgA-coating (Kawamoto *et al.* 2014). Bacterial products can also directly act on immune cells in the PP: microbial ATP controls Tfh cell differentiation (Proietti *et al.* 2014) and short-chain fatty acids, a diverse group of bacterial metabolites, were shown to boost plasma cell differentiation and intestinal antibody production in PPs (Kim *et al.* 2016; Wu *et al.* 2017). This demonstrates the strong impact of the microbiota on the GC response. Thus, the interplay of the immune system with the microbiota cannot be neglected when studying the regulation of intestinal GCs.

To test if ageing affected this cross-talk, we investigated whether age-associated changes in the composition of the murine gut microbiota were linked with changes in PP GCs of aged mice. Intriguingly, faecal microbiota transplantation from adult into aged mice reversed an ageing-related defects of the GC reaction in PPs. These data confirm that the gut microbiota has a strong impact on GCs in PPs and that an age-associated decline in the GC response can be reversed by changes in its microenvironment.

1.6.4 The GC response in ageing

A very successful medical intervention for the prevention of infectious diseases is vaccination, which generates long-lived humoral immunity by triggering GC responses and extrafollicular responses in the absence of an infection. The efficacy of vaccination is reduced in older people, possibly due to an age-associated impairment of the GC reaction (Aberle *et al.* 2013; Gustafson *et al.* 2018; Linterman 2014). Ageing is a complex process, broadly defined as the age-dependent deterioration of the biological functions of an organism with time. This is associated with a plethora of age-associated defects (López-Otín *et al.* 2013): on a molecular level, there is age-related telomere shortening, the accumulation of genetic mutations, epigenetic changes, accumulation of defective mitochondria and of unfolded proteins due to alterations in the ER stress response (Brown & Naidoo 2012; López-Otín *et al.* 2013). On the cellular level, the communication between cells is affected and there is a reduction in tissue regeneration, associated with the accumulation of senescent cells which secrete large amounts of pro-inflammatory cytokines, a phenotype known as the senescence-associated secretory phenotype (Linterman 2014; López-Otín *et al.* 2013; Tchkonia *et al.* 2013).

Similar to other cells, the functions of immune cells are negatively affected by age both in a cell-intrinsic and -extrinsic manner, but the relative contribution of these effects is still unclear (Nikolich-Žugich 2018). The continued exposure to antigen over time leads to an age-related increase of antigen-experienced memory cells, while the pool of naïve immune cells, which can respond to novel antigen, progressively shrinks with advancing age (Nikolich-Žugich 2018). This is associated with an increased susceptibility to infections, a significant cause of death in old age (Kline & Bowdish 2016).

In mice, advancing age is correlated with a decline in GC size. This is associated with the reduced formation of high-affinity plasma cells, a reduction in SHM and serum antibody levels (Eaton *et al.* 2004; Kosco *et al.* 1989; Kraft *et al.* 1987; Linterman 2014; van Dijk-Härd *et al.* 1997; Yang *et al.* 1996). Interestingly, ageing seems to affect GCs in PPs differently from GCs in the spleen and LNs. Several studies reported on reduced antigen-specific antibody responses in the gut of both BALB/c and C57BL/6 mice (Kato *et al.* 2003; Kawanishi & Kiely 1989; Koga *et al.* 2000), but this was not correlated with a decrease in the overall amount of secreted IgA in the intestine (Senda *et al.* 1988; Thoreux *et al.* 2000). Also, while there is progressive loss of GC B cells in murine PPs during ageing (González-Fernández *et al.* 1994), several paper reported on increasing numbers of somatically mutated antibodies in the PPs of aged mice. This is in contrast to the reduced SHM observed in LNs (Banerjee *et al.* 2002) and is probably due to successive accumulation of mutations

in memory B cells in the gut over the life time of the mouse (Banerjee *et al.* 2002; González-Fernández *et al.* 1994; Rogerson *et al.* 2003).

Age-associated defects in the output of the GC response are linked with changes in T cells, B cells as well as the GC microenvironment (Figure 1.10) (Gustafson *et al.* 2018; Linterman 2014; Nikolich-Žugich 2018). Yang *et al.* used adoptive transfers of aged B cells into young hosts to demonstrate that B cells from aged mice are fully capable of forming GCs in a young environment, but their rate of SHM is reduced (Yang *et al.* 1996). In contrast, adoptive transfers of T cells from aged animals into a young environment, resulted in the formation of smaller GCs with reduced antibody output (Eaton *et al.* 2004). This suggests that, while B cells from aged mice are impaired in SHM, the age-associated decline in the magnitude of the GC response is mainly driven by defects in the T cell compartment. Increasing the naïve T cell output from the thymus, however, is not sufficient to rescue the ageing GC phenotype (Lefebvre *et al.* 2012). What is more, young T cells transferred into aged hosts prior to immunisation form fewer Tfh cells than in young hosts, suggesting that T cell priming by DCs is impaired in old age (Lefebvre *et al.* 2012).

DCs from aged host have a defect in phagocytosis and express lower levels of co-stimulatory molecules (Agrawal *et al.* 2007),(Moretto *et al.* 2008). In addition, Tfh-mediated B cell help was also shown to be impaired in advanced age. Sage *et al*. observed higher numbers of Tfh in aged mice compared to young mice, but these cells seem to be less able to provide B cell help (Sage *et al.* 2015). B cell help from memory Tfh cells during recall responses is also impaired in aged individuals (Yu *et al.* 2012). This is linked with the reduced expression of the important co-stimulatory molecules ICOS and CD40L on the surface of aged T cells, combined with increased levels of co-inhibitory PD-1 (Sage *et al.* 2015). What is more, Sage *et al.* observed a relative increase of suppressive Tfr cells over Tfh cells in the LNs of aged mice (Sage *et al.* 2015). Like Tfh cells, aged Tfr cells expressed increased levels of PD-1 and lower levels of ICOS and Foxp3, but this did not affect their suppressive capacities. Thus, reduced GC responses are linked with reduced B cell help from Tfh cells in the context of increased suppression by Tfr cells (Sage *et al.* 2015).

There are many efforts to enhance GC responses in aged individuals to improve immune responses to infections and vaccinations in the ageing population. Modifications of the vaccine adjuvant (Frech *et al.* 2005) or administration of increased antigen doses (Remarque *et al.* 1993) were shown to improve vaccination responses in older subjects. This suggests that the age-related defect in the GC response is not irreversible, and can be targeted therapeutically to improve immune protection in older individuals.

Our study investigated whether T cell priming by DCs in aged individuals could be improved to enhance GC responses. This led to the discovery of a novel link between reduced co-stimulation by cDC2s in aged mice with defective IFN signalling in the same cells. By enhancing type I IFN signalling at the site of immunisation, we were able to restore CD80 and CD86 expression levels on cDC2s and improved the formation of Tfh cells in aged animals. This confirms that age-associated defects in the GC response are not irreversible and that DCs are a potent target to improve vaccine responses in the ageing population.

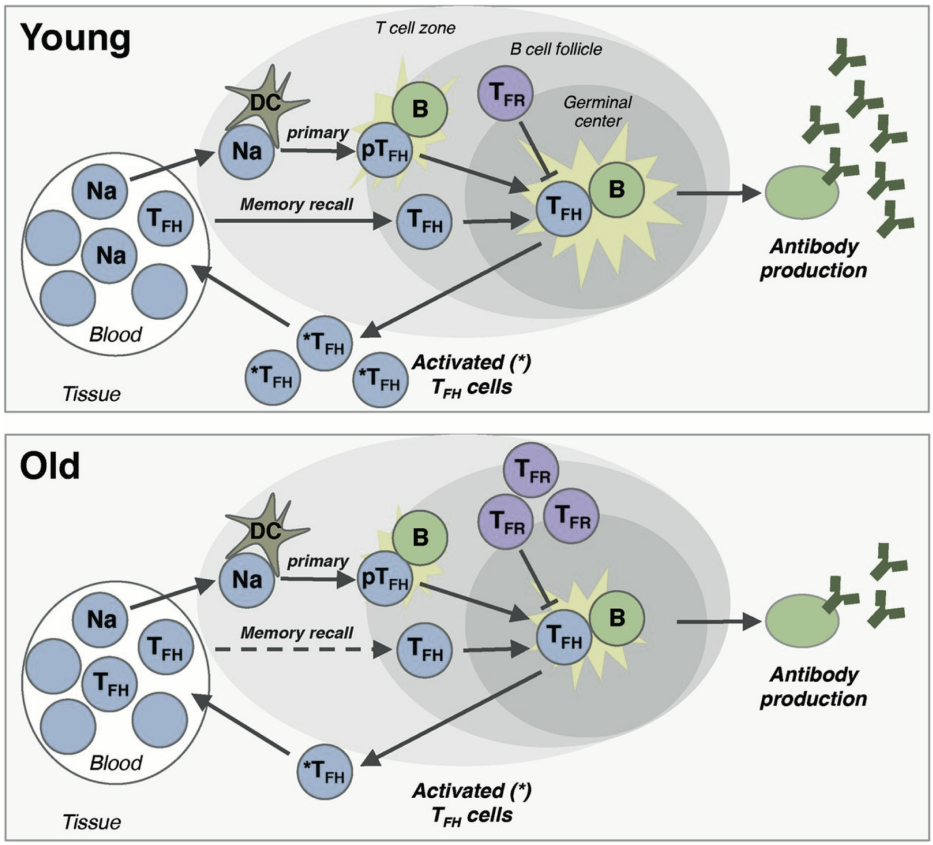

Figure 1.10: Schematic overview of age-associated changes in the germinal centre (GC) response. Upon infection or immunisation, naïve CD4 T cells (Na) are recruited from the blood into secondary lymphoid organs (SLOs), where they interact with antigen-presenting dendritic cells (DCs). Here, DCs prime naïve CD4 T cells to differentiate into pre T follicular helper (Tfh; pT_{FH}) cells which migrate towards the B-cell follicle. These pre-Tfh cells interact with activated B cells to differentiate into mature Tfh (T_{FH}) cells which migrate into the GC. Interactions between Tfh cells and GC B cells during the GC response facilitate the generation of long-lived high affinity antigen-producing plasma cells as well as the release of Tfh cells ($*T_{FH}$) from the SLOs back into the blood. The GC response is negatively controlled by T follicular regulatory (Tfr; T_{FR}) cells. During ageing, the GC response is affected in many ways: firstly, fewer naïve CD4 T cells are available to seed the GC. Secondly, Tfh cell priming by DCs and B cells is impaired and there is a relative increase in inhibitory Tfr cells. Thirdly, Tfh cells recruited from the circulation during recall responses seem to have a reduced capacity for B cells help in aged individuals. Together, this results in the reduced production of antigen-specific antibodies. This image was taken from Gustafson *et al*. 2018, © 2018 (Gustafson *et al.* 2018).

1.7 The immune system and the endoplasmic reticulum (ER) stress response pathway

Immune cell differentiation and effector functions can be influenced by environmental cues such as local metabolite availability (Kominsky *et al.* 2010), salt concentrations (Kleinewietfeld *et al.* 2013; Wu *et al.* 2013) and low oxygen pressure (McNamee *et al.* 2013). All of these conditions are potent inducers of the ER stress response pathway and often occur at sites of active immune responses, *e.g.* sites of inflammation or in GCs. This results in a strong association between immune cell function and the ER stress response (Bettigole & Glimcher 2015).

1.7.1 The ER stress response

The ER is a large organelle integrating many essential cellular functions: this is where lipids and proteins are synthesised and folded and where intracellular Ca^{2+} is stored (Bettigole & Glimcher 2015). These functions are closely interlinked, with perturbations in one adversely affecting the others, triggering a powerful stress response known as the unfolded protein response (UPR) or ER stress response (Bettigole & Glimcher 2015). The ER stress response is initiated upon protein misfolding and intersects with many other stress or inflammatory signalling pathways (Hotamisligil 2010). It consists of three individual branches which act in a coordinated manner and depend on the activation of three different ER transmembrane effector proteins: inositol requiring enzyme 1 (IRE1), PKR-like ER kinase (PERK), and the activating transcription factor-6 (ATF-6) (see Figure 1.11) (So 2018; Todd *et al.* 2008).

Under steady-state conditions, IRE1, PERK and ATF-6 all interact closely with the ER-resident HSP70-type chaperone BiP (also known as Hspa5 or GRP78) which inhibits their activation. BiP has high affinity for unfolded proteins, so when unfolded proteins accumulate in the ER, BiP is titrated away from IRE1, PERK and ATF-6, allowing the full UPR to ensue (Bettigole & Glimcher 2015). The IRE1 signalling axis is the most evolutionary conserved of all ER stress response pathways, leading to the expression of the transcription factor X-box binding protein 1(XBP1), which induces many ER stress-mediated gene expression changes (Bettigole & Glimcher 2015). PERK, when activated, induces phosphorylation of the eukaryotic translation-initiation factor 2 (EIF2). Phosphorylated EIF2 loses its activity as initiator of mRNA translation, thereby arresting most mRNA translation. At the same time, EIF2 phosphorylation results in increased expression levels of the transcription factor ATF-4 which binds to UPR-regulated elements (UPREs) in the promoter-region of ER stress-associated genes (Todd *et al.* 2008). ATF-6 is usually retained in the ER membrane, but upon ER stress, its cytoplasmic ATF-6 fragment is released to act as a

transcription factor (see Figure 1.11). Together, these three pathways induce global changes in gene expression, protein translation, protein folding and degradation.

1.7.2 The impact of ER stress on immune responses

Historically, the UPR has been studied as a stress response to protein misfolding, but it also modulates immune cell development and inflammatory signalling (So 2018). Iwakoshi *et al.* demonstrated that Xbp-1 expression is important for the development and survival of pDCs and cDCs (Iwakoshi *et al.* 2007). In plasma cells, antibody production is dependent on the expression of the ER stress-induced transcription factor Xbp-1 (Shaffer *et al.* 2004). Studies on T cells revealed that antigenic stimulation of the TCR induces ER stress. The ensuing ER stress response is important to shape T cell effector functions, *e.g.* by enhancing Th2 cell differentiation or increasing the production of pro-inflammatory cytokines such as IFN-γ and TNF-α (Kamimura & Bevan 2008; Scheu *et al.* 2006; Thaxton *et al.* 2017; Wheeler *et al.* 2008). Likewise, the ER stress response enhances the secretion of pro-inflammatory cytokines, such as IL-23, IL-6, TNF-α and type I IFNs, by both DCs and macrophages (Bettigole & Glimcher 2015; Hu *et al.* 2011; Martinon *et al.* 2010; Smith *et al.* 2008). This could be mediated by NF-κB signalling, as all 3 UPR branches induce NF-κB activation either by reducing the translation or causing the degradation of the NF-κB repressor IκB (Garg *et al.* 2012). This allows NF-κB to translocate into the nucleus, where it drives the expression of many pro-inflammatory cytokines and other immune-modulatory proteins.

Taken together, this demonstrates that there is a strong bidirectional cross-talk between the immune system and the ER stress response. This allows immune cells to quickly adapt their effector functions to changes in their local microenvironment, such as shifts in nutrient availability or local oxygen levels.

Sites of inflammation in many autoimmune disorders are often characterised by low oxygen and nutrient availability – conditions that trigger ER stress responses (Morito & Nagata 2012; Zhang & Kaufman 2008). These sites also often contain pathogenic Th17 cells (Tesmer *et al.* 2008). This raises the question, whether the ER stress response could be a driver of Th17 cell differentiation and pathogenicity? In this thesis, I demonstrate that ER stress drives the generation of Th17 cells, whose gene expression signature strongly resembles previously-described Th17 cells with a highly pathogenic gene signature (Lee *et al.* 2012).

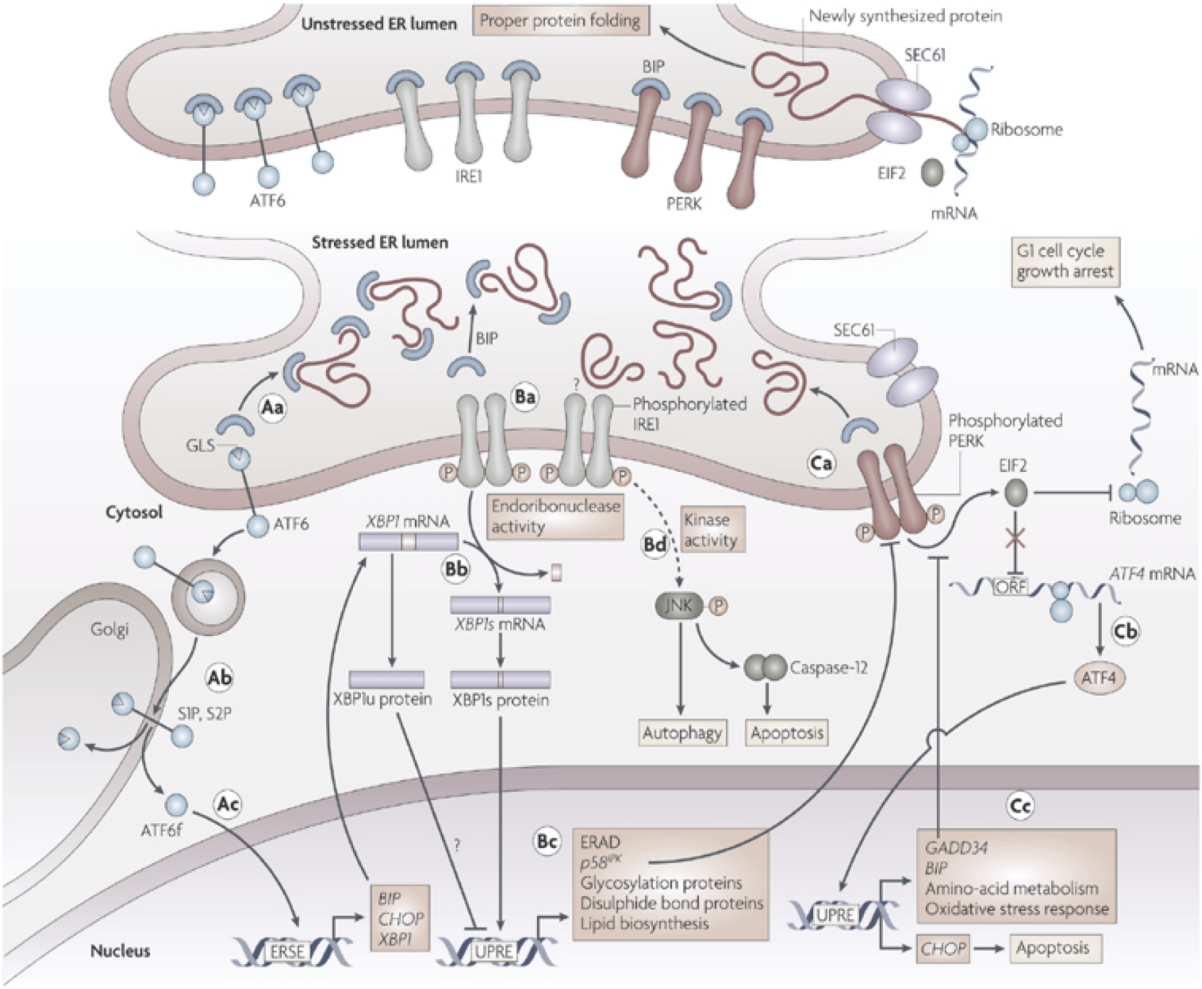

Figure 1.11: Schematic overview of the ER stress response. The ER stress response consists of three individual branches which depend on the activation of three different ER transmembrane proteins: inositol requiring enzyme 1 (IRE1), PKR-like ER kinase (PERK), and the activating transcription factor-6 (ATF-6). Together, these proteins induce global changes in gene expression and protein homeostasis. Under steady-state conditions, the ER-resident chaperone BiP inhibits their activation. When misfolded proteins accumulate in the ER, BiP is titrated away from IRE1, PERK and ATF-6, allowing the unfolded protein response (UPR) to ensue. Activated IRE1 catalyses an unconventional splicing reaction of Xbp1 which yields the highly active transcription factor XBP1S. Activated PERK phosphorylates the eukaryotic translation-initiation factor 2 (EIF2), which consequently loses its activity as initiator of mRNA translation, thereby arresting most mRNA translation. EIF2 phosphorylation also results in increased expression levels of the transcription factor ATF-4 which binds to UPR-regulated elements (UPREs) in the promoter-region of ER stress-associated genes. Once BiP releases ATF-6, this transcription factor translocates into the nucleus, where it activates gene transcription at ER-stress response elements (ERSEs). This image was reprinted from Todd *et al*. 2008 with permission from Springer Nature © 2008 (Todd *et al.* 2008).

1.8 Aim & Objectives

During an ongoing immune response, immune cells incorporate information about their microenvironment to adapt their differentiation pathways and effector functions accordingly. This is achieved by the integration of inflammatory signalling with the ER stress response pathway, which is triggered by a variety of environmental stresses such as low nutrient availability, hypoxia and mechanical stress (Bettigole & Glimcher 2015). The first part of this report focusses on how Th17 cell differentiation and pathogenicity is affected by ER stress. I demonstrate that ER stress drives the generation of Th17 cells with a pathogenic gene signature even in the absence of TGFβ. As a result, these cells cause Th17 cell-associated symptoms in experimental-autoimmune encephalitis (EAE) experiments, a mouse model of multiple sclerosis (MS). This suggests a potential link between ER stress and Th17 cell-mediated autoimmune pathology.

In the second part of this thesis, I investigated whether age-associated defects in the GC response could be linked with changes in its microenvironment. PPs always contain active GCs due to constant stimulation from the gut microbiota. These GCs are an important source of IgA antibodies, which have been suggested to help control the composition of the gut microbiome (Macpherson *et al.* 2012). I observed reduced GC B cells in the PPs of aged mice, which were correlated with distinct age-associated changes in the composition of their gut microbiota. Faecal microbiota transplantation from adult into aged mice was able to reverse these ageing-related defects. These data reveal that the gut microbiota is a potent stimulator of GCs in PPs and that the age-dependent decline in the GC response can be reversed by changes in the microbiota.

Whether the microbiota boosts the GC reactions by acting directly on adaptive immune cells or on other cells in their environment, such as APCs, is not clear. There is strong evidence that the defective GC reaction in peripheral LNs of aged animals is partly due to impaired T cell priming by DCs (Linterman 2014). We observed impaired T cell priming in aged mice, which was correlated with reduced type I interferon signalling in cDC2 cells upon immunisation. By boosting type I interferon signalling in DCs at the time of immunisation, Tfh cell differentiation in peripheral LNs of aged mice was enhanced. This shows that not only the gut microbiota, but also DCs can be targeted to improve GC responses in aged mice and highlights the importance of environmental stimuli in shaping adaptive immunity

2 MATERIAL AND METHODS

2.1 Animal work

All mice listed in Table 2.1 were bred and maintained in the Babraham Institute Biological Support Unit (BSU), where BALB/c and C57BL/6Babr mice were also aged. No primary pathogens or additional agents listed in the FELASA recommendations (FELASA working group *et al.* 2014) were detected during health monitoring surveys of the stock holding rooms. Ambient temperature was ~19-21˚C and relative humidity 52 %. Lighting was provided on a 12 hour light: 12 hour dark cycle including 15 minute 'dawn' and 'dusk' periods of subdued lighting. After weaning, mice were transferred to individually ventilated cages with 1-5 mice per cage. Mice were fed CRM (P) VP diet (Special Diet Services) ad libitum and received seeds (*e.g.* sunflower, millet) at the time of cage-cleaning as part of their environmental enrichment. All mouse experimentation was approved by the Babraham Institute Animal Welfare and Ethical Review Body. Animal husbandry and experimentation complied with existing European Union and United Kingdom Home Office legislation and local standards. Young mice were 6-14 weeks old, and aged C57BL/6 and BALB/c mice 90-105 weeks old at the time of starting an experiment. All experimental mice were housed in the same room. To control for changes in the microbiome due to circadian rhythm, faecal microbiota transplantation (FMT) and faecal pellet collections were always performed at 10am and 3pm, respectively. Due to limited availability of aged male BALB/c mice, all BALB/c experiments were conducted with females. For all other strains, experiments were conducted with both male and female mice.

2.1.1 Co-housing of adult and aged mice

2-3 adult females were consolidated with 2-3 aged females per cage, with a maximum of five mice per cage. After 30-40 days of co-housing, Peyer's patches (PPs), mesenteric lymph nodes (mLNs) and faecal bacteria were harvested for flow cytometric analysis. Blood samples were obtained by cardiac puncture and spun at 13,000 rpm for 15 minutes at room temperature. The serum supernatants were collected and stored at -20˚C for enzyme-linked immunosorbent assays (ELISAs). Faecal supernatants from the contents of the colon and ileum were weighed and incubated for 10 minutes on ice in 12-14 µl sterile-filtered phosphate-buffered saline (PBS) per mg of faeces (70-85 mg/ml faecal input). The samples were then vortexed for 1 minute and spun at 500 g at 4˚C for

5 minutes to pellet bigger particles. 80-100 µl of the supernatant containing faecal bacteria was transferred to a fresh tube, topped up with PBS to reach a total volume of 1 ml and spun at 10,000 g at 4˚C for 5 minutes to pellet bacteria. The supernatants containing free IgA (at a final concentration of 5-8.5 mg/ml faecal input) were harvested and stored at -20˚C, while bacterial pellets were stained for flow cytometry as described below. Faecal pellets were collected from all mice before co-housing and at the end of the experiment and stored at -80˚C for 16S rDNA sequencing.

Name	Strain ID	Source	Ref.
C57BL/6	C57BL/6Babr	JAX/BBU*	
BALB/c	BALB/c	Charles Rivers/BBU*	
Il17a^{cre}	*Il17a$^{tm1.1(icre)Stck}$*	B. Stockinger	(Hirota *et al.* 2011)
Rosa$^{stop\text{-}YFP}$	*Gt(ROSA)26Sor$^{tm1(EYFP)Cos}$*	JAX	(Srinivas *et al.* 2001)
Rosa$^{stop\text{-}tdRFP}$	*Gt(ROSA)26Sor^{tm1Hjf}*	JAX	(Luche *et al.* 2007)
Rag^{cre}	*Rag1$^{tm1(cre)Thr}$*	JAX/ BBU*	(McCormack *et al.* 2003)
Xbp1^{fl}	*Xbp1^{tm2Glm}*	L. Glimcher/A. Kaser	(Hetz *et al.* 2008)
2D2 TCR	*Tg(Tcra2D2)1Kuch*	JAX	(Bettelli *et al.* 2003)
Cd4^{cre}	*Tg(Cd4-cre)1Cwi*	JAX	(Lee *et al.* 2001)
Bcl6^{fl}	*Bcl6tm1.1Dent*	A. Dent	(Hollister *et al.* 2013)
Ifnar1^{ko}	*Ifnar1$^{tm2a(EUCOMM)Wtsi}$*	U. Kalinke	(Skarnes *et al.* 2011)
Ifnar1^{cre}	*Ifnar1^{tm1Uka}*	U. Kalinke	(Le Bon *et al.* 2006)
Cd11c^{cre}	*B6.Cg-Tg(Itgax-cre)1-1Reiz/J*	R. Roychoudhuri	(Caton *et al.* 2007)
OTII TCR	*(TCR)OT2*	K. Okkenhaug	(Barnden *et al.* 1998)
TCR7 TCR	*Tg(TcraBO4H9.1)7Aog*	A. O'Garra	(Neighbors *et al.* 2006)
UbiquitinGFP	*Tg(UBC-GFP)30Scha/J*	M. Turner	(Schaefer *et al.* 2001)
H2$^{+/-}$	B6.129S2-*H2$^{dlAb1\text{-}Ea}$*/J	A. Liston	(Madsen *et al.* 1999)

Table 2.1: List of mouse strains. *BBU=Babraham Breeding Unit

2.1.2 Faecal microbiota transplantation (FMT)

FMT was achieved by oral gavage of faecal slurry. For this, recipient mice were starved for 2 hours prior to FMT. The faecal slurry was obtained by pooling faecal pellets from up to 14 donor mice. The pellets were weighed and resuspended by vortexing at full speed for 1 minute in 1 ml PBS per 300 mg of faeces. After pelleting larger particles by centrifugation at 500 g for 5 minutes, the supernatant was collected as faecal slurry for FMT. Each recipient mouse received 150µl of faecal slurry by oral gavage no more than 1 hour after the initial collection of faecal pellets from donor mice. The remaining slurry was stored at -80ºC for 16S rDNA sequencing. Following FMT, the cages of recipient mice were replenished with dirty bedding and fresh faecal pellets from donor mice once and twice a week respectively. Faecal pellets for 16S rDNA sequencing were collected the day before FMT and at the end of the experiment, and were stored at -80˚C for DNA extraction.

Three weeks after FMT, PPs, mLNs and faecal bacteria were harvested for flow cytometric analysis, while bloods and faecal supernatants from the ileum and colon were collected for ELISAs. Blood samples were obtained by cardiac puncture and spun at 13,000 rpm for 15 minutes at room temperature. The serum supernatants were collected and stored at -20˚C for ELISAs. Faecal supernatants from the contents of the colon and ileum were weighed and incubated for 10 minutes on ice in 12-14 µl sterile-filtered PBS per mg of faeces (70-85 mg/ml faecal input). The samples were then vortexed for 1 minute and spun at 500 g at 4˚C for 5 minutes to pellet bigger particles. 80-100 µl of the supernatant containing faecal bacteria was transferred to a fresh tube, topped up with PBS to reach a total volume of 1 ml and spun at 10,000 g at 4˚C for 5 minutes to pellet bacteria. The supernatant containing free IgA (at a final concentration of 5-8.5 mg/ml faecal input) was harvested and stored at -20˚C, while the bacterial pellet was stained for flow cytometry as described below.

2.1.3 Oral immunisations

For oral immunisations mice were starved for 2 hours prior to administration of antigen. They were then orally gavaged with 200 µl PBS containing 37.5 µg/ml cholera toxin (CTx, Sigma #C8052) plus 37.5 µg/ml NP-CTx or, in the case of $Bcl6^{fl/fl}Cd4^{cre/+}$ mice and their littermate controls, 50 µg/ml CTx plus 5mg/ml ovalbumin (Albumin from chicken egg white, Sigma #SLBQ9036V). NP-CTx was generated in-house as described below. Oral immunisations were performed three times on day 0, 7, and 14. Control groups were gavaged with PBS only. On day 21, PPs, mLNs, blood and faecal contents were harvested. In cases where oral immunisations were combined with FMT, oral immunisations with NP-CTx/CTx were conducted on day 2, day 8 and day 15 after FMT before mice were harvested on day 22. PPs, mLNs and faecal bacteria were harvested for flow cytometric analysis, while bloods and faecal supernatants from the ileum and colon were collected for ELISAs. Blood samples were obtained by cardiac puncture and spun at 13,000 rpm for 15 minutes at room temperature. The serum supernatants were collected and stored at -20˚C for ELISAs. Faecal contents from the colon and ileum were weighed and incubated for 10 minutes on ice in 5 ml sterile-filtered PBS per g of faeces (200 mg/ml faecal input). The samples were then vortexed for 1 minute and spun at 10,000 g at 4˚C for 10 minutes to pellet bacteria and debris. The supernatant containing free IgA was harvested and stored at -20˚C.

2.1.4 Subcutaneous immunisations

Mice were immunized with NP-KLH (4-Hydroxy-3-nitrophenylacetyl-Keyhole Limpet Hemocyanin), NP-1W1K, OVA (ovalbumin) or HEL (Hen Egg Lysozyme) in Alum or Eα-GFP in

Incomplete Freund Adjuvant (IFA). IFA (#F5506) and HEL (Lysozyme from chicken egg white, #62970) and OVA (Albumin from chicken egg white; #A5503) were purchased from Sigma-Aldrich, Imject Alum (#77161) was purchased from Thermo Fisher Scientific and NP-KLH was purchased from Biosearch Technologies (#N-5060-25). Eα-GFP fusion protein was produced in-house by Wim Pierson from XL-1 blue *E.coli* carrying the pTRCHis-Eα-GFP vector as described by Rush and Brewer (Rush & Brewer 2010). NP-1W1K was generated from NP-e-Aminocaproyl-OSu (Biosearch Technologies, #N-1021-100), which was conjugated to Streptavidin by Jonathan Clark from the Babraham Institute Biological Chemistry facility, and biotinylated 1W1K peptide (custom-made by Cambridge Research Biochemicals "biotin-GSGEA-W-GALANKA-V-DKA-acid"). These compounds were conjugated at a 1:6 ratio of NP-SA to 1W1K-biotin in 400 µl PBS for 1 hour at room temperature. Unbound peptide was then removed by two consecutive rounds of dialysis using Centriprep® centrifugal filters with an Ultracel® 10K membrane (Sigma #4304) by spinning at 13,000 rpm for 6 minutes at room temperature. NP-1W1K was freshly conjugated for each experiment. Purified NP-1W1K, NP-KLH, OVA and HEL were first diluted in PBS, then the same volume of Alum was added dropwise to the solution while shaking until a final concentration of 50 µg/ml HEL, 500 µg/ml OVA, 500 µg/ml NP-KLH or 330-500 µg/ml NP-1W1K was reached. After 30 minutes of vortexing, 100 µl of the emulsion were injected subcutaneously (s.c.) into the hind flanks of recipient mice. 1 mg/ml Eα-GFP was emulsified in IFA by trituration through a 20 g needle. 200 µl of this emulsion were injected subcutaneously into the hind flanks of recipient mice. Mice were euthanised at different time points after immunisation, as indicated in the main text or figure legends, when bloods and draining inguinal LNs were collected. Blood samples were obtained by cardiac puncture and spun at 13,000 rpm for 15 minutes at room temperature. The serum supernatants were collected and stored at -20˚C for ELISAs.

In some cases, mice were treated with IFNAR1 blocking antibodies (BioXCell #BE0241), CTLA4-Ig (Orencia® Abatacept) or Aldara cream containing 5 % imiquimod (MEDA Pharma) prior to, or at the time of immunisation. IFNAR1 blocking was achieved by intraperitoneal injection of 0.75 mg of anti-IFNAR1 blocking antibody or the appropriate isotype control (BioXCell #BE0083) in 200 µl PBS 20 hours before immunisation with Eα-GFP. To block CD28 co-stimulation, 500 µg of Abatacept were injected intraperitoneally right before immunisations with HEL in Alum. For Aldara treatment, mice were shaved on their backs 2-3 days before subcutaneous immunisations into their hind flanks. Directly after immunisation, 50-125 mg of Aldara were applied topically to the shaved backs of the anaesthetised animals. The cream was left to absorb for five minutes before the mice were returned to their cages. Aldara-treated and untreated control mice were housed in separate cages to avoid cross-contamination by grooming.

2.1.5 NP-CTx conjugation and quality control

NP-CTx was generated by conjugating NP-e-Aminocaproyl-OSu (Biosearch Technologies #N-1021-100) with CTx (Sigma #C8052) following a protocol adapted from N. Lycke by A. Iseppon and B. Stockinger (Bergqvist *et al.* 2013). First, 2 mg/ml CTx was dialyzed in distilled water for two days at 4˚C in a Slide-A-Lyzer Dialysis Cassette (0.5-3 ml size with a 10K cut-off; Thermo Fisher Scientific #66380) before mixing it with an equal volume of 0.1 M $NaHCO_3$ and 20 equivalents of 10 mg/ml NP-eA-OSu per mole CTx. The mixture was incubated overnight at 4˚C during constant rotation and then transferred into a fresh Slide-A-Lyzer dialysis cassette. The mixture was dialyzed twice against 0.05 M $NaHCO_3$ followed by PBS. The final protein concentration was determined using a BCA assay (Thermo Fisher Scientific #23227). 0.5 mg/ml aliquots of NP-CTx were stored at -80˚C until use.

The NP-CTx conjugation ratio was assessed by ELISA. For this, ELISA plates (Thermo Fisher Scientific 96F Maxisorp #456537) were coated with 2.5 µg/ml NP-CTx or NP conjugated to bovine serum albumin (BSA) in varying conjugation ratios (NP(2)-BSA, NP(7)-BSA and NP(20)-BSA; Biosearch Technologies #N-5050L-H) and incubated at 4˚C overnight. The next day, plates were washed 4 times in 0.05 % Tween 20 (Sigma #P1379) in PBS wash buffer and blocked with 1 % BSA in PBS for 1 hour at room temperature. After an additional wash step, serum from a NP-KLH-immunised mouse was loaded onto the plates at a starting dilution of 1:200 in 1 % BSA/PBS. This initial dilution was titrated down the plate at a 1:4 ratio. The plates were incubated for 2 hours at room temperature and after another wash step, the plates were incubated with 50 µl of polyclonal goat anti-mouse IgG1 HRP-conjugated antibodies (Abcam #ab97240; diluted 1:10,000 in PBS) for 2 hours at room temperature. After a last wash step the plates were developed with 100 µl/well TMB (3, 3', 5, 5' – Tetramethylbenzidine; Biolegend #421101) for up to 20 minutes, when the reaction was stopped with 50 µl/well 0.5 M H_2SO_4. A PHERAstar FS microplate reader (BMG Labtech) was used to measure absorbance at 450 nm. Absorbance values from serially diluted samples were plotted and values which fell into the linear range of the curve were selected to calculate endpoint titres. The NP-CTx conjugation ratio was approximated by comparing its endpoint titre with the endpoint titre of NP-BSA at its different conjugation ratios.

2.1.6 Experimental autoimmune encephalitis (EAE)

Direct EAE experiments were conducted by Marc Veldhoen and Verena Brucklacher-Waldert, who induced direct EAE by subcutaneous immunisations with 250 µl myelin oligodendrocyte glycoprotein (MOG) 35-55 peptide (ProImmune Ltd.) emulsified in Complete Freund's Adjuvant

(CFA; IFA (Sigma # F5506) supplemented with 250 µl mycobacterium tuberculosis extract H37Ra (Difco #231141)). The animals also received intraperitoneal injections with 200 ng pertussis toxin (List Biological Laboratories #181) on days 0 and 2. Tauroursodeoxycholic acid (TUDCA) treatments were started the day prior to MOG/CFA immunisation with a 500 mg/kg dose and were followed with daily intraperitoneal administration at 250 mg/kg. For adoptive-transfer EAE experiments, 2D2 MOG-specific TCR transgenic animals were injected subcutaneously with 250 µg $MOG_{35–55}$ peptide emulsified in CFA. The animals showed no clinical signs of EAE until day 9, when draining lymph nodes and spleens were harvested. Single cell suspensions were re-stimulated over a period of 4 days with 20 µg/ml $MOG_{35–55}$ peptide in complete IMDM (Iscove's Modified Dulbecco's Media (=IMDM, Sigma #I3390) supplemented with 2 mM L-glutamine, 100 U/ml penicillin, 100 µg/ml streptomycin, 200 µM 2-mercaptoethanol, and 5 % foetal bovine serum (FBS)) at 37˚C in a 7 % CO_2 atmosphere. Some cultures were treated with either a combination of 25 ng/ml IL-6, 0.4 ng/ml TGFβ and 4 µg/ml anti–IFN-γ antibodies (conventional "IL6/TGFβ" Th17 condition) or 25 ng/ml IL-6 plus 2 µM cyclopiazonic acid (=CPA in "IL6/CPA" condition). Table 2.2 contains more information about the compounds used. On day 4, cultured cells were collected and washed in PBS. 1.5×10^7 of these MOG-reactivated cells were injected into sub-lethally irradiated C57BL/6 mice (exposed to 450 rad γ-irradiation) by intravenous injection. Classical clinical signs of EAE were assessed blindly and according to the following scores: 0, no signs of disease; 1, flaccid tail; 2, impaired righting reflex and/or gait; 3, partial hind limb paralysis; 4, total hind limb paralysis; and 5, total hind limb paralysis with partial forelimb paralysis. Mice were humanely killed when they started to score 5, lost more than 20 % of their initial weight or displayed symptoms of atypical EAE such as head tilting and ataxia.

2.2 T helper cell cultures

For T cell differentiation *in vitro*, brachial, axial, inguinal and mesenteric LNs as well as spleens were isolated and processed into single cell suspensions by mashing through 70 µm filters. Viable lymphocytes were then separated from the remaining cells in Lympholyte-M Cell Separation medium (Cedarlane #CL5030) during a 15 minute centrifugation step at 1250 g. Naive $CD4^+$ $CD62L^+$ T cells were obtained using Milteny's $CD4^+CD62L^+$ T Cell Isolation Kit II (#130-093-227) following the manufacturer's instructions. Cells were cultured in IMDM (Sigma #I3390) supplemented with 2 mM L-glutamine, 100 U/ml penicillin, 100 µg/ml streptomycin, 200 µM 2-mercaptoethanol, and 5 % FBS. Th17, Th1 and Treg cells were differentiated in 24-well or 96-well plates coated with 2 µg/ml anti-CD3 and 2 or 5 µg/ml anti-CD28.

For conventional Th17 cell differentiation, T cells were cultured in the presence of 25 ng/ml IL-6, 0.4 ng/ml TGFβ and 4 μg/ml anti–IFN-γ antibodies. 3 ng/ml IL-12 was used to drive Th1 cell differentiation. Treg cells were obtained from a combined treatment of 5 ng/ml TGFβ with 5 μg/ml anti–IFN-γ antibodies. To modulate the ER stress response in culture, cells were treated with: 0.5-10 μM CPA, 1-10 μM of the pyruvate analogue BrPA (3-bromopyruvate) or 500 μM of the general ER-stress inhibitor TUDCA. 10 μg/ml anti-TGFβ antibodies were used to block the activity of endogenous TGFβ in FBS in complete cell culture medium. Compounds are listed in Table 2.2.

Cytokines	**Supplier (#Catalogue number)**	**Final concentration**
Recombinant human IL-6	PeproTech #AF-200-06	25 ng/ml
Recombinant murine IL-12	PeproTech #210-12	3 ng/ml
Recombinant human TGFβ1	PeproTech #100-21	0.4 – 5 ng/ml
CPA	Sigma # C1530	0.5 – 10 μM
TUDCA	Sigma #T0266	0.05 – 2 mM
BrPA	Sigma #16490	1.0 – 10 μM
Neutralising antibodies		
anti-IFN-γ	BioXCell Clone XMG1.2	4 – 5 μg/ml
anti-TGFβ	BioXCell Clone 1D11.16.8	10 μg/ml
anti-CD3	BioXCell Clone 145-2C11	2 μg/ml
anti-CD28	BioXCell Clone 37.51	2 – 5 μg/ml

Table 2.2: Cytokines, ER stress modulators and antibodies used for cell culture.

2.3 Adoptive T cell transfers

To perform adoptive HEL- or OVA-specific T cell transfers, total lymphocytes were isolated from the spleen and peripheral LNs (brachial, axial, superficial cervical, inguinal and mesenteric LNs) of TCR7 or OTII transgenic mice, respectively. These mice also expressed ubiquitinGFP$^+$ and/or CD45.1$^+$. All cells were stained with CellTrace™ Violet Cell Proliferation Kit (Invitrogen #C34557; 1:1000 in PBS) for 15 minutes at 37˚C, followed by two washes with PBS containing 2 %FBS at 1800 rpm for 5 minutes at 4˚C. The percentage of TCR-transgenic CD4$^+$ CellTrace$^+$ T cells was determined by flow cytometry, detecting TCR7 T cells using anti-TCRVβ3 antibodies and OTII T cells with anti-TCRVα2 antibodies. An equivalent of 1-5 × 10^6 TCR7$^+$ T cells or 5 × 10^5 OTII T cells was transferred intravenously into C57BL/6, *H2*$^{+/-}$ or *Ifnar1*$^{-/-}$ recipient mice in 100 μl 2 % FBS/PBS. The mice were subsequently immunized subcutaneously into their hind flanks with 100 μl of 5 μg HEL or 50 μg OVA in Alum. Where indicated, mice were pre-treated

intraperitoneally with 500 µg CTLA4-Ig (Orencia® Abatacept) in 100 µl PBS at the time of T cell transfer to block CD86 and CD80 co-stimulation. After 2.5 days, the inguinal LNs of each recipient mouse were harvested and pooled. They were mashed through 70 µm filters to obtain single cells which were then stained for flow cytometry. Antibodies used are listed in Table 2.3.

2.4 Flow cytometry and Fluorescence-activated cell sorting (FACS)

2.4.1 Flow cytometry and FACS of *in vitro* differentiated T helper cells

To assess cytokine production and transcription factor protein levels of *in vitro* differentiated T helper cells, cells were stimulated for 3 hours with 500 g/ml PdBU (Phorbol 12,13-dibutyrate), 500 ng/ml ionomycin and 10 µg/ml brefeldin A (all from Sigma). Cells were stained with anti-CD4 and anti-CD25 antibodies and a fixable viability dye (Molecular Probes' LIVE/DEAD® Fixable Near-IR Dead Cell Stain #L10119), followed by fixation using the eBioscience IC Fixation Buffer (#00-8222-49). T cells were stained with fluorochrome-coupled anti–IL-17A or anti–IFN-γ antibodies. The eBioscience Foxp3/Transcription Factor Staining Buffer set (#00-5323-00) was used for intranuclear Foxp3 stains. Total samples were acquired on a LSRFortessa 5 (BD Biosciences) to determine absolute cell numbers. FACS was used to sort *in vitro*-differentiated Th17 cells obtained from Rosa$^{stop\text{-}tdRFP}$*Il17a*^{Cre} or Rosa$^{stop\text{-}eYFP}$*Il17a*^{Cre} mice. After 3 days of culture in 24-well plates, T cells were washed once with PBS and stained with APC-coupled anti-CD4 antibodies and DAPI (4,6-diamidino-2-phenylindole, Molecular Probes #D1306) as a live/dead stain. $CD4^+$ $DAPI^-$ cells were sorted according to their fluorescent protein (FP) expression levels on a BD FACSAria. FP^- and FP^+ T cells were collected in FBS-coated 15 ml falcon tubes, washed in PBS, pelleted and stored at -80˚C for RT-qPCR. Samples for RNA sequencing were stored in 40 µl RNAlater at -80˚C. Single stained splenocytes served as compensation controls. Data were analysed using FlowJo v10 software (Tree Star). Antibodies are listed in Table 2.3.

2.4.2 Flow cytometry of PPs and LNs

A single cell suspension from dissected PPs and LNs was generated by pressing the tissues through a 70 µm mesh in 2 %FBS in PBS. Cell numbers and viability were determined using a CASY TT Cell Counter (Roche). 1-3 × 10^6 cells were transferred to 96 well plates for subsequent antibody staining. To stain for 1W1K-specific CD4 T cells, cell suspensions were first pre-treated with Dasatinib (BioVision #1568-100, 1:20,000 in DMEM (Dulbecco's modified eagle medium, Gibco

#41965-039) containing 10 % FBS, 100 U/ml penicillin and 100 µg/ml streptomycin) for 10 minutes at 37˚C. Then, a PE-conjugated MHC class II tetramer containing the 1W1K peptide (NIH Tetramer core facility; PE-coupled "I-A(b) EAWGALANKAVDKA") was added to each sample at a final concentration of 1:100 and incubated for 2 hours at room temperature. Cells were stained with LIVE/DEAD® Fixable Blue Dead Cell Stain (Invitrogen #L23105; diluted 1:1000 in PBS) and incubated with FcR block for 15 minutes (anti-mouse CD16/32; eBioscience #14-0161-82). Surface antibody stains and staining for NP-specific B cells with NP(30)-PE (Biosearch Technologies #N-5070-1) were performed for 1 hour at 4˚C in 100 µl Brilliant Stain Buffer (BD Biosciences #563794). For intranuclear staining, cells were fixed with the eBioscience Foxp3/Transcription Factor Staining Buffer (#00-5323-00). Antibody staining with anti-Foxp3, anti-Ki67 and anti-Bcl6 antibodies was performed for 1-2 hours at 4˚C in 1× Permeabilization buffer (eBioscience #00-8333-56). Samples were acquired on a LSRFortessa (BD Biosciences) with stained UltraComp eBeads™ Compensation Beads (Invitrogen #01-2222-41) as compensation controls. Flow cytometry data were analysed using FlowJo v10 software (Tree Star). The antibodies used are listed in Table 2.3.

2.4.3 Flow cytometry of faecal bacteria

To assess IgA-coating of faecal bacteria, we adapted a protocol described previously by Sidonia Fagarasan and Mikako Maruya (Kawamoto *et al.* 2014). Briefly, faecal contents from the ileum and colon were collected and weighed, then incubated for 10 minutes on ice in 12 µl sterile-filtered PBS per mg of faeces. The samples were vortexed at full speed for 1 minute and spun at 500 g at 4˚C for 5 minutes to pellet bigger particles. The supernatant containing faecal bacteria was transferred to a fresh tube, washed in PBS and spun at 10,000 g at 4˚C for 5 minutes to pellet bacteria. Blocking was achieved in 2 % BSA in PBS for 15 minutes, followed by antibody staining of IgA-coated bacteria with anti-IgA and anti-Igκ antibodies in 2 % BSA/PBS for 45 minutes on ice. After a wash step in PBS, bacteria were fixed in 4 % paraformaldehyde (PFA) for 6 hours or overnight at 4˚C. Then, samples were stained with DAPI (Invitrogen #D1306; 1:1000 in a staining buffer containing 0.01 % Tween and 1 mM EDTA) for 30 minutes and AF594-coupled wheat germ agglutinin (=WGA; Invitrogen #W11262; 1:100 in 3M KCl solution) for 5 minutes. The samples were acquired at 5000 events/sec on a LSRFortessa 5 (BD Biosciences) with the side scatter (SSC) threshold set to 200. Single stains served as compensation controls. The antibodies used are listed in Table 2.3.

2.4.4 Flow cytometry and FACS of dendritic cells

For DC analysis, iLNs were harvested and incubated with 10 mg/ml Collagenase D (Roche #11088866001), and 30 U/ml DNase I (Roche #04716728001) in plain RPMI medium (Gibco #11875093) for 15-30 minutes at 37˚C, followed by gentle pipetting to disrupt the tissue. Cells were washed with PBS containing 2 % FBS, before cell numbers were determined using a CASY TT Cell Counter (Roche). All isolated cells were subsequently stained for flow cytometry or FACS. After a wash in PBS, they were stained with LIVE/DEAD® Fixable Blue Dead Cell Stain (Invitrogen #L23105; diluted 1:1000 in PBS) on ice for 10 minutes. After a second wash, they were blocked with FcR block (anti-mouse CD16/32; eBioscience #14-0161-82) for 10-15 minutes at 4˚C. Surface antibody stains were performed for 45-60 minutes at 4˚C in Brilliant Stain Buffer (BD Biosciences #563794). Samples were acquired on a LSRFortessa 5 (BD Biosciences) with stained UltraComp eBeads™ Compensation Beads (Invitrogen #01-2222-41) serving as compensation controls. Flow data were analysed using FlowJo v10 software (Tree Star). The antibodies used are listed in Table 2.3.

FACS was performed with a BD FACSAria (BD Biosciences). For RT-qPCR, 800-4000 GFP^+ $CD11b^+$ cDC2 cells from total draining LNs were sorted into PCR tubes containing 20 µl of RLT lysis buffer supplied with the RNeasy Micro Kit (Qiagen #74004). For RNA sequencing, Danika Hill and Alexandre Bignon sorted 800 cells into PCR tubes containing 8.5 µl of 1× lysis buffer provided with the SMART-Seq v4 Ultra Low Input RNA Kit for Sequencing (Clontech # 634890).

Antibody	Supplier (Clone)	Dilution
AF647-coupled anti-mouse Foxp3	Biolegend (MF-14)	1:250
AF647-coupled anti-mouse IL-17A	Biolegend (TC11-18H10.1)	1:500
PE-coupled anti-mouse IL-4	Biolegend (11B11)	1:200
PB-coupled anti-mouse IFN-γ	Biolegend (XMG1.2)	1:500
APC-coupled anti-mouse CD4	Biolegend (GK1.5)	1:1000
PE-coupled anti-mouse CD25	Biolegend (PC61)	1:200
PE-coupled anti-mouse IL-10	Biolegend (JES5-16E3)	1:200
PE/PE-Cy7-coupled anti-mouse Bcl6	BD Biosciences (K112-91)	1:100
PE-Cy7-coupled anti-mouse CD95	BD Biosciences (Jo2)	1:200
BV605-coupled anti-mouse IgG1	BD Biosciences (A85-1)	1:100
PE-Cy7/BUV395-coupled anti-mouse CD3	BD Biosciences (145-2C11)	1:300
PE-Cy7/BUV395-coupled anti-mouse CD19	BD Biosciences (1D3)	1:200-300
PE-Cy7/BUV395-coupled anti-mouse B220	BD Biosciences (RA3-6B2)	1:300
AF647-coupled anti-mouse CD64	BD Biosciences (X54-5/71)	1:200
PE-Cf594-coupled anti-mouse CD11b	BD Biosciences (M1/70)	1:200
BV786-coupled anti-mouse CD103	BD Biosciences (M290)	1:200
PE/BV510-coupled anti-mouse CD86	BD Biosciences (GL1)	1:300
APC-AF780-coupled anti-mouse PD1	eBioscience (J43)	1:200
APC/Foxp3-coupled anti-mouse Foxp3	eBioscience (FJK-16S)	1:100-1:200
AF488/AF700-coupled anti-mouse Ki67	eBioscience (SolA15)	1:100
Biotin-coupled anti-mouse Gr1	eBioscience (RB6-8C5)	1:200
eF450-coupled anti-mouse CD38	eBioscience (90)	1:400
PerCp-Cy5.5-coupled anti-mouse CD172a	eBioscience (P84)	1:200
eF450-coupled anti-mouse CD24	eBioscience (M1/69)	1:500
APC-AF870-coupled anti-mouse CD11c	eBioscience (N418)	1:200
PE-Cy5/APC-coupled anti-mouse CD80	eBioscience (16-10A1)	1:300
PerCp-Cy5.5-coupled anti-mouse CD45.2	eBioscience (104)	1:200
AF700-coupled anti-mouse MHC-II	eBioscience (M5/114.12.2)	1:400
BV421-coupled anti-mouse CXCR5	Biolegend (L138D7)	1:100
V500/PE/BV605-coupled anti-mouse CD4	Biolegend (RM4-5)	1:400-1:800
BV510/BV785-coupled anti-mouse B220	Biolegend (RA3-6B2)	1:200-1:400
PerCp-Cy5.5-coupled anti-mouse CD44	Biolegend (IM7)	1:200
AF488-coupled anti-mouse GL7	Biolegend (GL7)	1:100
BV605-coupled anti-mouse F4/80	Biolegend (BM8)	1:200
BV650-coupled anti-mouse XCR1 BV650	Biolegend (ZET)	1:200
PE-Cy7-coupled anti-mouse CD40	Biolegend (3/23)	1:300
AF700-coupled anti-mouse CD45.1	Biolegend (A20)	1:200
AF674/FITC-coupled anti-mouse IgA	Southern Biotech (1040-02/-31)	1:100
PerCp-Cy5.5-coupled anti-mouse PDCA-1	Biolegend (927)	1:100
PE/Cy7/APC-Cy-7-coupled anti-mouse Igκ	BD Biosciences (187.1)	1:100
PE-coupled anti-mouse TCR Vβ3	BD Biosciences (KJ25)	1:100
APC-coupled anti-mouse TCR Vα2	eBioscience (B20.1)	1:100
APC/PE/BV421/BV510-coupled Streptavidin	Biolegend, eBioscience	1:600
Biotin-coupled anti-mouse Eα 52-68 peptide	eBioscience (eBioY-Ae)	1:200
NP(30)-PE	Biosearch Tech. (N-5070-1)	1:200
PE-coupled 1W1K-*IA*b tetramer	NIH Tetramer core facility	1:100

Table 2.3: Antibodies and conjugated probes used for flow cytometry and FACS

2.5 Confocal imaging of germinal centres

Draining inguinal LNs or PPs were fixed in periodate-lysine-paraformaldehyde (PLP) containing 1 % (v/v) PFA (Sigma #P6148), 0.075 M L-Lysine (Sigma #L5501), 0.37 M Na_3PO_4 (pH 7.4) (Sigma #342483) and 0.01 M $NaIO_4$ (Sigma #210048), for 4 hours at 4˚C. After fixation, the samples were dehydrated in 30 % sucrose (Sigma #S0389) overnight, embedded in Optimum Cutting Temperature (OCT) medium (VWR #25608-930) on dry ice and stored at -80˚C. The frozen tissues were cut into 10 µm sections using a cryostat (Leica Biosystems) at -20˚C and again stored at -80 °C. For antibody stains, the slides were first air-dried and then hydrated in 0.5 % Tween 20 in PBS (PBS-T). Slides were blocked in 200 µl blocking buffer (PBS containing 2 % BSA and 10 % goat serum), then permeabilised with 200 µl PBS containing 2 % Triton X (Sigma #X100). After three wash steps in PBS-T, the slides were incubated with 200 µl of a primary antibody mix in PBS-T containing 1 % BSA at 4˚C overnight. Sections were stained with eF450-conjugated rat anti-mouse Foxp3 (clone FJK16S, Thermo Fisher Scientific; 1:50), hamster anti-mouse CD3ε (clone 500A2, Thermo Fisher Scientific; 1:200), rabbit anti-mouse Ki67 (#15580, Abcam; 1:100) and AF647-conjugated rat anti-mouse IgD (clone 11-26c.2a, Biolegend; 1:100). The next day, the slides were washed in PBS-T three times, then they were incubated with secondary antibodies in 200 µl PBS-T containing 2 % goat serum for 2 hours at room temperature. The secondary antibodies used were AF568-conjugated goat anti-hamster IgG (#A-21112, Life Technologies; 1:500) and AF488-conjugated goat anti-rabbit (#150077, Abcam; 1:400). Hydromount mounting medium (National diagnostics #HS-106) was used to mount slides and coverslips were gently placed on top of the slides to avoid the formation of air bubbles. Slides were dried overnight for the mounting medium to set. Images were acquired using a Zeiss 780 microscope using 10×, 20× and 40× objectives. Image analysis was performed using ImageJ.

2.6 Enzyme-linked immunosorbent assay (ELISA)

2.6.1 Quantitation of antigen-specific immunoglobulins

ELISA plates (Thermo Fisher Scientific 96F Maxisorp #456537) were coated overnight at 4˚C with 10 µg/ml NP20-BSA (Biosearch Technologies #N-5050H-100), 2.5 µg/ml NP2-BSA (Biosearch Technologies #N-5050L-100) or 1 µg/ml CTx in PBS. The next day, plates were washed 4 times in wash buffer containing 0.05 % Tween 20 in PBS and blocked with 1 % BSA in PBS for 1 hour at room temperature. After an additional wash step, sera or free IgA-containing ileal supernatants from oral immunisation experiments were loaded onto the plates. The starting dilution for sera was 1:100-200 in 1 % BSA/PBS, ileal supernatants were loaded at 10-20 mg/ml faecal input (1:5-10 dilution

of frozen supernatants) in 1 % BSA/PBS. This initial dilution was titrated down the plate at a 1:4 ratio. The pooled serum/ileal supernatants of previously immunised mice served as positive controls, the serum/ileal supernatant of unimmunized mice as negative controls on each ELISA plate. The plates were incubated for 2 hours at room temperature and after another wash step the plates were incubated with 50 µl of polyclonal goat anti-mouse IgG1 HRP-conjugated antibodies (Abcam #ab97240; 1:10,000 in PBS) or polyclonal goat anti-mouse IgA HRP-conjugated antibodies (Bethyl #A90-103P; 1:25,000 in PBS) for 2 hours at room temperature. After a last wash step, the plates were developed with 100 µl/well TMB (Biolegend #421101) for up to 20 minutes, when the reaction was stopped with 50 µl/well 0.5M H_2SO_4. A PHERAstar FS microplate reader (BMG Labtech) was used to measure absorption at 450 nm. Absorbance values from serially diluted samples were plotted and values which fell into the linear range of the curve were selected to calculate endpoint titres.

2.6.2 Quantitation of total free IgA

ELISA plates (Thermo Fisher Scientific 96F Maxisorp #456537) were coated overnight at 4˚C with 1 µg/ml goat anti-mouse IgA (Bethyl Mouse IgA ELISA Quantitation Set #E90-103). The next day, plates were washed 4 times in wash buffer containing 0.05 % Tween 20 in PBS and blocked with 1 % BSA in PBS for 1 hour at room temperature. After an additional wash step, free IgA-containing faecal supernatants were loaded onto the plates in duplicates. The starting concentration was 0.1-0.5 mg/ml for ileal supernatants and 5-8.5 mg/ml for colonic supernatants. The plates were incubated for 2 hours at room temperature. After another wash step, the plates were incubated with 50 µl of polyclonal goat anti-mouse IgA HRP-conjugated antibodies (Bethyl #A90-103P) for 2 hours at room temperature. After a final wash step, the plates were developed with 100 µl/well TMB (Biolegend #421101) for up to 20 minutes, when the reaction was stopped with 50 µl/well 0.5 M H_2SO_4. A PHERAstar FS microplate reader (BMG Labtech) was used to measure absorbance at 450 nm. A standard dilution of mouse reference serum (Bethyl Mouse IgA ELISA Quantitation Set #E90-103) was used for the quantitation of free IgA in faecal supernatants using a 4-parameter-fitted curve within the MARS data analysis software (BMG Labtech).

2.7 Real-Time qPCR (RT-qPCR)

2.7.1 RNA isolation & cDNA synthesis from *in vitro* differentiated T cells and *ex vivo* cells

RNA isolation from *in vitro* differentiated Th17 cells and *ex vivo* isolated cells was performed using Qiagen's RNeasy Mini or Micro Kit (#74104 and #74004) following the manufacturer's instructions. Homogenisation of the samples achieved by vortexing for 1 minute or by using QIAshredders (Qiagen #79654). RNA concentrations obtained from the RNA isolation were measured using the NanoDrop system (Thermo Fisher Scientific). RNA samples were used for cDNA synthesis right away or stored at -80˚C. cDNA was synthesised from 100-1000 ng RNA using a combination of oligo-dT and random primers using Qiagen's cDNA synthesis kit containing Quantitect Reverse Transcriptase (#205311) following the manufacturer's instructions. cDNA samples were diluted 1:10 in DNase-free water for RT-qPCR and stored at -20˚C.

2.7.2 RNA isolation from lymph nodes

RNA isolation from whole inguinal LNs was achieved using Tri Reagent (Invitrogen #AM9738). Inguinal LNs were stored in RNAlater (Sigma #R0901) at -20˚C until RNA isolation, when they were transferred into 1 ml TRI Reagent and homogenised using a bounce homogeniser at full speed for 40 seconds. RNA precipitation in isopropanol was performed for 1 hour on ice to maximise RNA yields. An additional ethanol wash step was included in the protocol to improve RNA purity. RNA concentrations were determined using the NanoDrop system (Thermo Fisher Scientific). RNA samples were stored at -80°C until use.

2.7.3 RT-qPCR of *in vitro* differentiated T helper cells

RT-qPCR of cultured cells was performed using Life Technologies' TaqMan Gene Expression Assays (#4331182) combined with a TaqMan Universal PCR Master Mix (Applied Biosystems #4304437). PCR protocols and TaqMan Gene Expression Assays used are listed in Tables 2.4 and 2.5. All RT-qPCR reactions were assembled from 1 µl of a TaqMan Gene Expression Assay, 10 µl of the universal PCR master mix as well as 1 µl of PCR-grade water. 12 µl of the mix was transferred to each well of a PCR 96-well plate (Bio-Rad #MLL9601), then 8 µl of template cDNA, equivalent to 10-20ng input RNA per reaction, was added to the wells in duplicates. All plates were run on a BioRad CFX96 Real-Time System. Only duplicates with a standard deviation lower than 0.5 were considered for down-stream analysis.

The $2^{-\Delta\Delta Ct}$ -method - also known as comparative C_T method - was applied for relative quantification of mRNA levels. Using this $2^{-\Delta\Delta Ct}$ -method, the data are presented as the fold change in expression normalised to an internal control gene, relative to a control sample called calibrator (Livak & Schmittgen 2001). Expression levels were normalised to *Hprt* which was found to be stably expressed under all tested experimental conditions. When Th17 cells were sorted according to their FP expression, the FP^--fractions of c-Th17 cells were used as calibrators. Cq values were exported from the CFX Manager software (Bio-rad) and calculations were performed in Microsoft Excel. GraphPad Prism 6 was used to create graphics and perform statistical analysis.

RT-qPCR programme for TaqMan Universal PCR Master Mix

Step 1	50°C	2 min
Step 2	95°C	10 min
Step 3	95°C	15 sec
Step 4	60°C	1 min
repeat Steps 3 & 4 40-45 times		

RT-qPCR programme for TaqMan™ RNA-to-CT™ 1-Step Kit

Step 1	48°C	15 min
Step 2	95°C	10 min
Step 3	95°C	15 sec
Step 4	60°C	1 min
repeat Steps 3 & 4 48 times		

Table 2.4: Overview of the RT-qPCR programmes.

2.7.4 One-step RT-qPCR of LNs and *ex vivo* isolated cells

RT-qPCR was performed directly on RNA using Thermo Fisher Scientific's TaqMan™ RNA-to-CT™ 1-Step Kit (#4392656) combined with TaqMan Gene Expression Assays. The PCR protocol and TaqMan Gene Expression Assays used are listed in Tables 2.4 and 2.5. All RT-qPCR reactions were assembled in PCR 384-well plates (Bio-Rad #HSP3805), adding 2 µl of template RNA (10-20ng RNA per reaction) to 8 µl of a master mix containing the appropriate TaqMan Gene Expression Assay in duplicates or triplicates. All plates were run on a BioRad CFX384 Real-Time System. Only duplicates/triplicates with a standard deviation lower than 0.5 were considered for down-stream analysis. The $2^{-\Delta\Delta Ct}$-method was applied for relative quantification of mRNA levels. Expression levels were normalised to *Hprt* or *Gapdh* which were found to be stably expressed under all experimental conditions. Samples from young, unimmunised or immunised mice were used as

calibrators. As above, Cq values were exported from the CFX Manager software (Bio-rad) and calculations were performed in Microsoft Excel. GraphPad Prism 6 was used to create graphics and perform statistical analysis.

TaqMan Gene Expression Assays (Thermo Fisher Scientific #4331182)	
Ahr	Mm00478930 m1
Hif1a	Mm00468869_m1
Hprt	Mm03024075_m1
IFNg	Mm99999071 m1
Il10	Mm00439614 m1
Il17a	Mm00439618 m1
Il17f	Mm00521423 m1
Rora	Mm00443103 m1
Rorc	Mm01261019 g1
Tbx21	Mm00450960 m1
Tnf	Mm00443260 g1
Mx1	Mm00487796_m1
Ifit1	Mm00515153_m1
Gapdh	Mm99999915_g1
Ifnb1	Mm00439552_s1

Table 2.5: Overview of TaqMan Gene Expression Assays used for RT-qPCR.

2.8 RNA sequencing

2.8.1 Th17 cells: RNA library preparation and sequencing

Samples for RNA sequencing were obtained from FACS sorts of 5 different experiments. RNA isolation was performed using Qiagen's RNeasy Mini Plus Kit (#74104) following the manufacturer's instructions, using Qiagen's QIAshredders (#79654) to homogenise the samples. The RNA Integrity Number (RIN) was determined by the Babraham Sequencing facility using Agilent Bioanalyser RNA Pico Chips (#5067-1513). The RNA content was determined on a NanoDrop spectrometer and ranged from 0.9 – 11.1 µg RNA per sample. Two samples per experiment were chosen for sequencing based on their RIN (Table 2.6).

An input of 250 ng RNA per sample was used for the subsequent generation of non-directional RNA libraries using the NEBNext® Ultra™ RNA Library Prep Kit for Illumina (#E7530S), following the manufacturer's instructions. Succeeding an rRNA depletion step performed with the NEBNext® rRNA Depletion Kit (#E6310), we fragmented the RNA for 15 minutes at 94°C to obtain RNA fragments about 200 bp in size. After adapter ligation, we used NEBNext Multiplex

Oligos for Illumina (Set 1, NEB #E7335) to generate barcoded samples for multiplexing. PCR library enrichment was performed for 13 cycles. The quality of RNA libraries was assessed on Agilent Bioanalyser High Sensitivity DNA Chips (#5067-4626; Table 2.6 "% 200-1000 bp" and "RIN"). Library quantification was achieved using the KAPA Library Quantification Kits for NGS (#KK4824). All samples were pooled onto one NextSeq 500 sequencing lane and sequenced as 75 bp paired-end (PE) reads. This resulted in a total of more than 800 million reads, corresponding to 50 million reads per sample.

2.8.2 Th17 cells: RNA sequencing data analysis

The NextSeq 500 sequencer used the NextSeq Control Software 2.0.2. and Real Time Analysis software 2.4.11 for primary on-machine analysis, creating three *.bcl-output files: two files containing the PE reads and a separate files containing the barcode reads. These files were converted to *.fastq files with the Bcl2fastq2 software. FastQC was used for the initial assessment of read quality. Then, the barcodes were merged with the forward read using the bash command "paste" to concatenate the *.fastq files line by line. The resulting *.fastq file was imported into Qiagen's Genomics Workbench 9.5.2 (GxWB) together with the reverse read as PE data. The "Demultiplex" tool was used to split the reads according to their barcode sequence, followed by the removal of the 6 bp barcode and a 1 bp linker from the sequence. This gave rise to 8 separate read files, each of which contained 8-13 % of the total reads. Next, the demultiplexed reads were subjected to an adaptor and quality trimming step of reads which did not meet the quality limit of 0.05 and/or contained more than two ambiguous nucleotides. In addition, NEBNext adaptor sequences at the 3' ends were trimmed off. In the process, a total of 12 million reads were trimmed. After trimming, FastQC quality control was used to confirm the absence of adaptor contaminations from all reads. Demultiplexed raw reads are publicly available on ArrayExpress: E-MTAB-5692.

As a next step, all remaining 799 million reads were mapped to a reference genome using Qiagen's Biomedical Workbench 3.5.2 (BmWB). For this purpose, the "RNA-Seq Analysis" tool of the Advanced RNA-Seq Plugin was used. We used the mouse reference data library "GRCm38.p4" provided by the Genome Reference Consortium and mapped our reads against both the gene and mRNA tracks (Ashburner *et al.* 2000; The Gene Ontology Consortium 2019). In addition, we mapped them against inter-genic regions, applying the following alignment score: Mismatch cost = 2, Insertion cost = 3, Deletion cost = 3, Length fraction = 0.8, Similarity fraction = 0.8. The maximum number of hits per read was set to 10 and expression values were expressed as the number of total counts for downstream analysis. The expectation-maximization estimation algorithm was enabled to improve the estimation of expression levels in cases where reads map equally well to

several reference genes or transcripts. The quality of read mapping was assessed by inspecting the mapping report and the graphical output of the BmWB genome browser view. PE read distances were about 150 bp in average. 76.72 % of reads mapped to the reference in pairs, with a total of 65 % uniquely mapping to a specific reference sequence. 7.71 % of reads could not be mapped to the reference sequence, indicating a high overall mapping efficiency. 2.64 % of PE reads mapped to intergenic regions, indicating limited genomic DNA contamination.

Exp	Barcode	Name	Mouse ID	Gender	Age	Treatment	RIN	% 200-1000 bp
Exp 2	Index 3	TGF 1	IL-17A^{Cre} Rosa^{RFP} 1	Male	9	IL-6+TGFβ	10	99
Exp 2	Index 4	CPA 1				IL-6+CPA	10	98
Exp 3	Index 5	TGF 2	IL-17A^{Cre} Rosa^{RFP} 2	Male	20	IL-6+TGFβ	10	99
Exp 3	Index 6	CPA 2				IL-6+CPA	9.6	99
Exp 4	Index 7	TGF 3	IL-17A^{Cre} Rosa^{RFP} 3	Male	18	IL-6+TGFβ	10	97
Exp 4	Index 8	CPA 3				IL-6+CPA	9.3	90
Exp 5	Index 9	TGF 4	IL-17A^{Cre} Rosa^{RFP} 4	Male	22	IL-6+TGFβ	10	93
Exp 5	Index 12	CPA 4				IL-6+CPA	10	99

Table 2.6: Metadata table of RNA sequencing libraries used for sequencing. This table shows the metadata used for RNA sequencing data analysis. This includes the Experiment ID corresponding to each samples as well as sample names, RINs and the proportion of library fragments falling into the 200-1000 bp range as determined by the Agilent Bioanalyser. In addition, multiplexing barcodes associated with each sample are displayed. The table also includes information about mice such as their ID, gender and age in weeks.

Following the read mapping, inter-sample variation was assessed by principal component analysis (PCA) and box plot representations of each sample's expression level distribution using the "Quality Control" tool of the BmWB's "Advanced RNA-seq" plugin. Then differential gene expression (DGE) analysis was performed. The BmWB's "Differential Expression for RNA-Seq" tool was supplied with the metadata listed in Table 2.6 and set to compare all group pairs using the Wald test (Chen *et al.* 2011). Heat maps were calculated based on Euclidean distance and complete linkage, forming hierarchical trees by joining clusters of genes if the distance between the furthest genes in the clusters is smallest. Only genes with a minimal total count of 10 were included. The heat maps were set to display the 20 top hits. A gene expression browser listing all gene or transcript expression values as well as gene ontology annotations was created using MGI's *Mus musculus* gene ontology annotations "gene_association.mgi.gz" supplied online by the Gene Ontology Consortium (Ashburner *et al.* 2000; The Gene Ontology Consortium 2019). For functional analysis, we used the BmWB's "Ingenuity Pathway Analysis (IPA)" plugin. This software tool uses its richly annotated Ingenuity Knowledge Base to query the significance of sequencing data in the context of biological systems, predicting affected signalling pathways, regulatory networks as well as disease functions (QIAGEN Inc. 2016). To probe our data, we uploaded different subsets of our DGE data

to IPA using the settings described in Table 2.7. Briefly, only features with a FDR *p*-value ≤ 0.05 and a fold change of ≥ 1.0 or 1.5 were uploaded to IPA. In addition, features with a maximum group mean (MGM = maximum of the average reads per kilobase per million mapped reads) ≤ 3 or 10 were excluded from the analysis. In case of duplicates, only the entry with the maximal exponential log ratio was taken into account. IPA application preferences were changed to consider only molecules and/or relationships from mouse with a high confidence, either based on prediction or experimental observations. To restrict the analysis to networks and diseases relevant to T cell biology, the analysis was repeated with the settings changed to consider only genes and relationships related to murine T cells. The IPA results from all different settings were analysed and compared using the installed Ingenuity IPA version 28820210. Only pathways and networks consistently scoring high in all analyses are discussed in this report.

	Abs. Fold Change (≥)	FDR *p*-value (≤)	MGM (≥)	No. of uploaded genes
Set 0	1.0	0.05	3	3550
Set 1	1.5	0.05	3	1407
Set 2	1.0	0.05	10	1796
Set 3	1.5	0.05	10	724

Table 2.7: Subsets of differentially-expressed genes uploaded to IPA. Different subsets of our DGE data were created for IPA by adjusting the minimally-required absolute fold change and maximal group mean (MGM) values (all of which were obtained from the BmWB's DGE analysis). This resulted in gene sets of different sizes. Sets are ranked according to their statistical stringency.

2.8.3 cDC2 cells: RNA library preparation and sequencing

Samples for RNA sequencing were obtained from 16 mice in one FACS sort performed by Alexandre Bignon. cDNA was prepared by Danika Hill from sorted cells using the SMART-Seq v4 Ultra Low Input RNA Kit for Sequencing (Clontech # 634890) on the day of the sort following the manufacturer's protocol. cDNA enrichment was performed for 13 cycles. cDNA quality was assessed on Agilent Bioanalyser High Sensitivity DNA Chips (#5067-4626). 400 pg of cDNA per sample were used as input by Danika Hill for the preparation of sequencing libraries with the Illumina Nextera XT kit (#FC-131-1096) following the manufacturer's instructions. The quality of the libraries was again assessed using Agilent Bioanalyser High Sensitivity DNA Chips (#5067-4626). Library quantification was achieved using the Qubit dsDNA High Sensitivity Assay Kit (Invitrogen #Q32854) on a Qubit 4 Fluorometer (Invitrogen). Six samples from young mice and six samples from aged mice passed all quality controls, were pooled onto two HiSeq sequencing lanes and sequenced as 100 bp single-end reads.

2.8.4 cDC2 cells: RNA sequencing data analysis

RNA sequencing analysis was performed in SeqMonk by Edward Carr, Michelle Linterman and Christel Krueger using the SeqMonk software package (Babraham Institute, https://www.bioinformatics.babraham.ac.uk/projects/seqmonk/) after trimming (Trim Galore v0.4.2) and alignment of reads to the reference mouse genome GRCm38 using HISAT2 (Kim *et al.* 2015a) Reads were quantitated over exons and library size was standardized to 1 million reads, and then read counts were log2 transformed. Differentially expressed genes were determined by DESeq2 analysis using raw counts (adjusted p-value cut-off $p \leq 0.05$) (Love *et al.* 2014). Principal component analysis was performed using 1000 genes with the largest variances, after normalisation for batch effects with RUVSeq (Risso *et al.* 2014).

Pathway enrichment analysis was performed by Christel Krueger who filtered a publicly available list of gene sets for categories containing less than 20 or more than 500 genes (Bader Lab EM_Genesets, Mouse_GO_AllPathways_with_GO_iea_December_24_2014_symbol.gmt.txt) (Merico *et al.* 2010). Remaining gene sets were tested for differential expression between young and aged samples using Seqmonk Subgroup Statistics (t-test, $p<0.05$, average absolute z-score > 0.5, multiple testing correction). Genes in the Responsiveness to IFN-I pathway: *Stat1, Aim2, Pyhin1, Ifi204, Ifi203, Ifi202b, Ifi205, Gbp3, Gbp2, Ifnb1, Gbp6, Htra2, Ndufa13, Trex1, Pnpt1, Tgtp1, Irf1, Igtp, Ddx41, Irg1, Tmem173, Gm4951, Iigp1, Ifit3, Ifit1*. Principal component analysis was performed using the most variable genes.

2.9 16S rDNA sequencing of faecal bacteria

2.9.1 DNA isolation

Bacterial DNA isolation from faecal matter was performed using the QIAamp PowerFecal DNA Kit (Qiagen #12830-50) following the manufacturer's instructions. First, samples were homogenised by bead beating using a FastPrep24 (MP Biomedicals) machine at 5 m/s for 50 sec. Total genomic DNA was captured on a silica membrane and the QIAmp Inhibitor Removal Technology was used to remove common substances that can interfere with downstream applications. In the final step, purified DNA was eluted in 70 µl of Solution C6. DNA concentrations were determined using the Qubit dsDNA High Sensitivity Assay Kit (Invitrogen #Q32854) on a Qubit 4 Fluorometer (Invitrogen).

2.9.2 16S rDNA sequencing library preparation and sequencing

High-throughput sequencing of the V3-V4 hypervariable region of the bacterial 16S rRNA gene was performed by the Beijing Genomics Institute (ageing studies) or Eurofins (*Bcl6*$^{fl/fl}$*Cd4*$^{cre/+}$ analysis) on an Illumina MiSeq platform. The resulting sequencing reads were supplied as demultiplexed fasta files for downstream analysis.

At Eurofins, the V3-V4 region was PCR-amplified using universal primers that contained the adapter overhang nucleotide sequences for forward (TACGGGAGGCAGCAG) and reverse primers (CCAGGGTATCTAATCC). DNA was used at a concentration of 1-10 ng/ml. Amplicons were purified using AMPure XP beads (Beckman Coulter) and set up for index PCR with Nextera XT index primers (Illumina). The indexed samples were purified using AMPure XP beads (Beckman Coulter) and quantified using the Fragment Analyzer Standard Sensitivity NGS Fragment Analysis Kit (Advanced Analytical). Equal quantities from each sample were pooled. The pooled library was quantified using the Agilent DNA 7500 Kit (Agilent), and sequenced using v3 chemistry (2x300 bp paired-end reads, Illumina).

At the Beijing Genomics Institute, DNA integrity was assessed by agarose gel electrophoresis. After DNA quantification by Qubit Fluorometer, 30 ng DNA per sample were utilised to PCR-amplify the V3-V4 region using 341F forward (ACTCCTACGGGAGGCAGCAG) and 806R reverse fusion primers (GGACTACHVGGGTWTCTAAT). The PCR products were purified using Agencourt AMPure XP beads (Beckman Coulter) for library validation using an Agilent 2100 bioanalyzer instrument (Agilent DNA 1000 Reagents). All libraries passed the quality control and were sequenced on an Illumina MiSeq Platform using the MiSeq reagent kit (2x300 bp paired-end reads, Illumina). The demultiplexed raw reads are available on ArrayExpress upon request: E-MTAB-7750.

2.9.3 16S rDNA sequencing data analysis

16S rDNA sequencing analysis was performed using QIIME2 (Caporaso *et al.* 2010). Successfully merged reads were quality filtered in QIIME2 using default settings. Sequences were clustered into operational taxonomic units (OTUs) based on similarity to the annotated bacterial sequences provided by Silva (v132 SSU; https://www.arb-silva.de/ (Quast *et al.* 2012); 99 % sequence similarity cut-off). For this, classifiers were trained in QIIME2 based on the Silva database and the V3-V4 primers used for library preparation. Taxa bar plots were generated using QIIME2. Statistical analysis was performed with the Calypso software (v8.48-84; cgenome.net/calypso/ (Zakrzewski *et al.* 2017)) applying default parameters. Cumulative-sum scaling (CSS) was applied,

followed by log2 transformation to account for the non-normal distribution of taxonomic counts data. Calypso was also used to generate Bray-Curtis Principal Coordinates Analysis (PCoA) based on OTUs and KRONA plots (Ondov *et al.* 2011). Bacterial families whose abundance was statistically significantly different between groups were determined in Calypso by ANOVA, using FDR adjusted *p*-values ≤ 0.05 as the cut-off. Venn Diagrams were generated using the Metachart App (https://www.meta-chart.com/venn#/display).

2.10 Statistics

All experiments were repeated at least two times with 4-10 mice per group. Differences between experimental groups, as determined by flow cytometry, were assessed using the non-parametric Mann–Whitney or Kruskal-Wallis test (with Dunn's multiple testing correction) within the Prism 6 software (GraphPad). *P*-values ≤ 0.05 were considered statistically significant. Statistical differences between bacterial families based on 16S rDNA sequencing data were determined by ANOVA, using FDR adjusted *p*-values ≤ 0.05 as the cut-off. Statistical differences in gene expression based on RNA sequencing were determined by BmWB's DEG or DESeq2, with FDR *p*-values ≤ 0.05, fold changes ≥ 1.5 and, for Th17 cell RNA sequencing, MGM ≥ 3 as cut-offs. Statistical differences of clinical EAE scores between groups was performed using group comparisons by Mann-Whitney tests of the area under the curve (AUC) calculated for each mouse within the Prism 6 software (GraphPad) as suggested by Fleming *et al.* (Fleming *et al.* 2005). Significant differences between atypical EAE symptoms were assessed by Mantle-Cox tests in Prism 6 (GraphPad).

3 ER STRESS SUPPORTS TGFβ-INDEPENDENT T HELPER 17 DIFFERENTIATION

3.1 Abstract

T helper 17 (Th17) cells are important for immune protection at epithelial barrier sites, but they have also been implicated in the pathology of many autoimmune disorders. Sites of inflammation in autoimmune diseases are often characterised by low metabolite availability and/or hypoxia - conditions which are potent inducers of the endoplasmic reticulum (ER) stress response. Classically, Th17 cell differentiation has been thought to depend upon IL-6 and TGFβ. In this study, I demonstrate that sustained ER stress can drive mouse Th17 cell differentiation even in the absence of TGFβ. ER stress-generated Th17 cells exhibit increased Th1-associated features, express many genes associated with Th17 cell-mediated pathogenicity and cause atypical symptoms of experimental autoimmune encephalitis (EAE), a Th17 cell-mediated autoimmune disease, *in vivo*. The data presented here link the ER stress response with Th17 cell-mediated immune pathologies, which may inform the development of new therapies against autoimmune disorders.

3.2 Background

Th17 cells are a distinct T helper cell subset, which is most abundant at epithelial barrier sites, where they provide immunity against extracellular bacteria and fungi (Weaver *et al.* 2013). This is mediated by their production of IL-17A and IL-17F, pro-inflammatory cytokines which help to attract other immune cells to sites of infection. While they are crucial for immune protection, Th17 cells can also be involved in pathology (Stockinger & Omenetti 2017) and autoimmune diseases (Maddur *et al.* 2012). They are enriched at sites of inflammation and have been directly implicated in the immunopathology of rheumatoid arthritis, psoriasis, and multiple sclerosis (MS), an autoimmune disorder associated with axon demyelination in the central nervous system followed by progressive neurological deterioration (Bedoya *et al.* 2013; Jadidi-Niaragh & Mirshafiey 2011; Sie *et al.* 2014).

In mice, Th17 cell differentiation from naïve CD4 T cells is well characterised to be driven by IL-6 and TGFβ (Mangan *et al.* 2006; McGeachy *et al.* 2007; Veldhoen *et al.* 2006a). These cytokines induce the STAT3-mediated expression of the Th17 lineage-specific transcription factors RORγt and RORα of the retinoic acid receptor-related orphan receptors (ROR) family, as well as the activation of the transcription factors aryl hydrocarbon receptor (AhR), hypoxia-inducible factor 1 alpha (HIF1a), basic leucine zipper (bZIP) transcription factor ATF-like (BATF) and the interferon regulatory factor 4 (IRF4) (Brüstle *et al.* 2007; Dang *et al.* 2011; Huber *et al.* 2008; Schraml *et al.* 2009; Veldhoen *et al.* 2008a). While cytokines are important to guide immune cell differentiation, other environmental cues such as low local metabolite availability (Kominsky *et al.* 2010), high salt concentrations (Kleinewietfeld *et al.* 2013; Wu *et al.* 2013) and hypoxia (McNamee *et al.* 2013) can also influence Th cell differentiation. These conditions are potent inducers of the ER stress response pathway and often occur at sites of active immune responses and inflammation. These observations suggest that immune cell function and the ER stress response are functionally associated (Bettigole & Glimcher 2015).

The ER stress response, also known as unfolded protein response (UPR), is an essential cellular response to tissue stress and pathogen infection, but chronic ER stress can also contribute to the pathology of inflammatory diseases (Bettigole & Glimcher 2015). The ER stress response was found to be highly active in active lesions of MS patients (Mháille *et al.* 2008) as well as in EAE, the mouse model of this disease, and to promote astrocyte-dependent inflammation and pathology (Deslauriers *et al.* 2011; Meares *et al.* 2014; Mháille *et al.* 2008). EAE can be induced directly by immunisation with myelin oligodendrocyte glycoprotein (MOG) or by adoptive-transfers of MOG-specific T cells into wild-type mice (Stromnes & Goverman 2006a; 2006b). This leads to Th17 cell-mediated damage of the myelin sheath around neurons and brain inflammation, resulting in progressive neuronal loss typically manifesting itself in ascending paralysis (Cua *et al.* 2003; Rostami & Ciric 2013; Stromnes & Goverman 2006a). Excessive brain inflammation caused by pathogenic Th17 cells additionally triggers atypical forms of EAE characterised by a variety of other clinical symptoms, such as ataxia and unilateral paralysis (Domingues *et al.* 2010; Stromnes *et al.* 2008). Lin *et al.* demonstrated that the Protein Kinase RNA-like Endoplasmic Reticulum Kinase (PERK)-mediated ER stress response can be both protective or detrimental in EAE experiments, depending on the time of its activation (Lin *et al.* 2006; 2007). Furthermore, Kim *et al*. associated aggravated LPS-induced lung injury in mice treated with the ER stress-inducer Thapsigargin with increased levels of IL-17 (Kim *et al.* 2015b). These data suggest a link between ER stress and Th17-mediated pathology.

We hypothesised a potential role of ER stress in autoimmune disorders by driving Th17 cell differentiation and pathogenicity. To test this hypothesis, we treated murine CD4 T cells with IL-6 and the sarcoplasmic reticulum Calcium-ATPase (SERCA) inhibitor cyclopiazonic acid (CPA), which induces a strong ER stress response (Mason *et al.* 1991). This resulted in the robust generation of Th17 cells even in the absence of TGFβ. To determine whether these ER stress-generated Th17 cells (e-Th17 cells) differ in their pathogenic potential from conventional Th17 (c-Th17) cells generated by a combined treatment with IL-6 and TGFβ, I generated RNA sequencing data from sorted e- and c-Th17 cells. RNA sequencing analysis revealed that e-Th17 cells exhibit a unique gene expression profile characterised by a pronounced increase in "pathogenicity-associated" genes (Lee *et al.* 2012). This was linked with a high potential of these cells to trigger Th17 cell-mediated pathology in adoptive-transfer EAE experiments. This suggests that e-Th17 cells may play a role in the pathology associated with Th17-mediated autoimmune diseases.

3.3 Results

3.3.1 ER stress increases Th17 cell differentiation

To determine the impact of ER stress on the differentiation of different T helper subsets, I purified naïve $CD4^+$ T cells by magnetic cell separation (MACS) from the spleens of C57BL/6 mice and *in vitro* differentiated them into Th17, Th1 and Treg cells in the presence of increasing concentrations of two ER stress inducers: the SERCA inhibitor CPA (Figure 3.1A-C) and the pyruvate analogue 3-bromopyruvate (BrPA) (Figure 3.1D-F) (Ganapathy-Kanniappan *et al.* 2010; Mason *et al.* 1991). Both compounds specifically enhanced Th17 cell differentiation, with some negative effects on the differentiation of Th1 and Treg cells at high concentrations (Figure 3.1A-F). This reveals a general role for the ER stress response as a specific enhancer of *in vitro* Th17 cell differentiation.

To further characterise the impact of ER stress on Th17 cell differentiation, we generated Th17 cells with IL-6 and α-IFNγ antibodies in the additional presence or absence of CPA and/or TGFβ (Figure 3.2A). As expected, a combined treatment of naïve CD4 T cells with IL-6 and TGFβ induced conventional Th17 ("c-Th17") cell differentiation. The addition of the ER stress inducer CPA clearly increased Th17 cell differentiation efficiency by two-fold, albeit this was not detected as significant by the Kruskal-Wallis test due to the limitation of sample ranking. Even in the absence of TGFβ, a mix of CPA with IL-6 only ("e-Th17") induced Th17 cells in a dose-dependent manner (Figure 3.2A, C). To exclude an effect of endogenous TGFβ present in foetal bovine serum (FBS) (Oida & Weiner 2010)) on e-Th17 cell differentiation, "IL-6+CPA+α-TGFβ" samples were additionally treated with anti-TGFβ neutralising antibodies. This reduced the proportion of Th17

cells formed *in vitro*, confirming that, while TGFβ is not essential for Th17 cell differentiation, it enhances the generation of these cells under both conventional and ER stress conditions (Figure 3.2A). This demonstrates that ER stress induces the generation of Th17 cells even in the absence of an exogenous source of TGFβ.

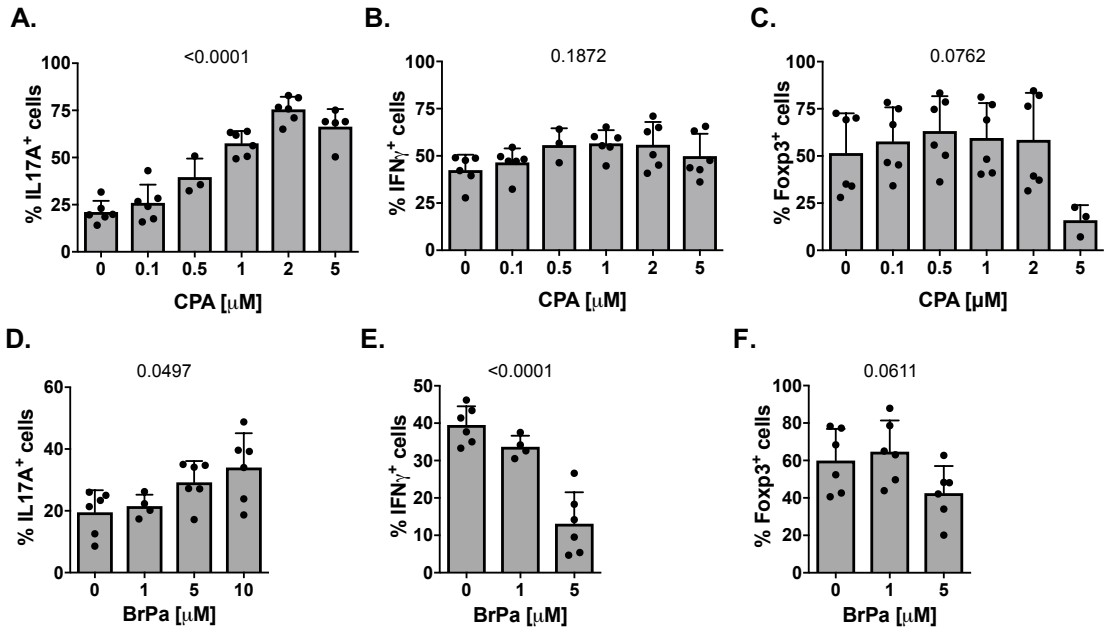

Figure 3.1: ER stress enhances the differentiation efficiency of Th17 cells, but not Th1 or Treg cells. Naïve $CD4^+CD62L^+$ T cells were isolated from the spleens of C57BL/6 mice and differentiated into Th17, Th1 and Treg cells. Cells were co-cultured with indicated concentrations of the ER stress inducers CPA or BrPa for three days. On day 3, cells were stimulated for 3 hours with 500 g/ml PdBU, 500 ng/ml ionomycin and 10 µg/ml brefeldin A, then the percentage of $IL17A^+$ cells (=Th17; **A, D**), IFN-γ^+ cells (=Th1; **B, E**), and $Foxp3^+$ cells (=Treg; **C, F**) was determined by flow cytometry. Data were collected in 2-3 independent experiments performed for biological duplicates or triplicates (n=4-6). Bar heights correspond to mean percentages with error bars representing standard deviations. Dots represent the proportion of IL-$17A^+$/ IFN-γ^+/$Foxp3^+$ cells generated from individual mice. *P*-values are based on Kruskal-Wallis tests without multiple testing in GraphPad Prism 6.

CPA titration experiments revealed a CPA dose-dependent increase in Th17 cell numbers up to a concentration of 2 µM CPA, where cell numbers plateaued in the presence or absence of TGFβ (Figure 3.1A, Figure 3.2B, C). In these experiments, *in vitro* Th17 cell differentiation efficiency was positively correlated with the duration of CPA treatment (Figure 3.2D, E): the number of IL-$17A^+$ Th17 cells increased with prolonged exposure to CPA. This demonstrates that extended periods of CPA treatment are required for enhanced Th17 cell differentiation. The UPR inhibitor TUDCA (tauroursodeoxycholic acid) reduced the frequency of Th17 cells formed *in vitro* under conventional Th17 cell culture conditions ("IL-6+TGFβ") (Figure 3.2A) (Xie *et al.* 2002). This suggests that the ER stress response is an integral part of the Th17 cell differentiation pathway, even in the absence of a dedicated ER stress inducer.

To characterise ER stress-generated Th17 (e-Th17) cells more thoroughly, I purified *in vitro*-generated Th17 cells to analyse their gene expression profile by RT-qPCR (Figure 3.3). I generated Th17 cells from *Rosa*$^{stop\text{-}tdRFP}$*Il17a*^{cre} or *Rosa*$^{stop\text{-}eYFP}$*Il17a*^{cre} reporter mice (both of which will from now on be referred to as "*Il17a*^{FP}" mice), which fate-map IL-17A-expressing cells by their fluorescent protein (FP) expression, and sorted them into FP$^-$ and FP$^+$ fractions by fluorescence-activated cell sorting (FACS) (gating strategy shown in Figure 3.3). This allowed us to compare the gene expression profiles of c-Th17 and e-Th17 cells by RT-qPCR, with the "non-Th17 cell" FP$^-$ fraction as an internal control. It is important to note that the FP$^+$ fraction also includes a fraction of FP$^+$IL-17A$^-$ ex-Th17 cells (Figure 3.3A-C). RT-qPCR revealed that the Th17 lineage-specific markers *Rora, Rorc, Il17a* and *Il17f* were expressed in the FP$^+$ fraction of all tested conditions (Figure 3.4A-D). RT-qPCR of e-Th17 cells generated in the presence of TGFβ blocking antibodies showed that, although fewer Th17 cells are formed under these conditions (Figure 3.2A, Figure 3.3C), the cells formed in the complete absence of TGFβ are *bona fide* Th17 cells which express all Th17 cell lineage markers (Figure 3.4A-D). This confirms that ER stress drives the formation of Th17 cells which express the relevant transcripts associated with this subset, even in the absence of TGFβ.

The FP$^-$ fraction also expressed some of the Th17 lineage markers. This may be due to the presence of early Th17 cells in the FP$^-$ fraction, which already express RORγt and IL-17A, but do not yet express the FP (Figure 3.3A-C). Consistent with this hypothesis, fewer FP-expressing cells were detected by flow cytometry than IL-17A$^+$ cells as determined by intracellular antibody staining (Figure 3.4E, F). This points towards the presence of a population of Th17 cells which express IL-17A but not the FP, consistent with observations by Hirota *et al.,* who also observed early commitment of Th17 cells to IL-17A production without FP expression upon PdBu/Ionomycin treatment using the same mice (Hirota *et al.* 2011).

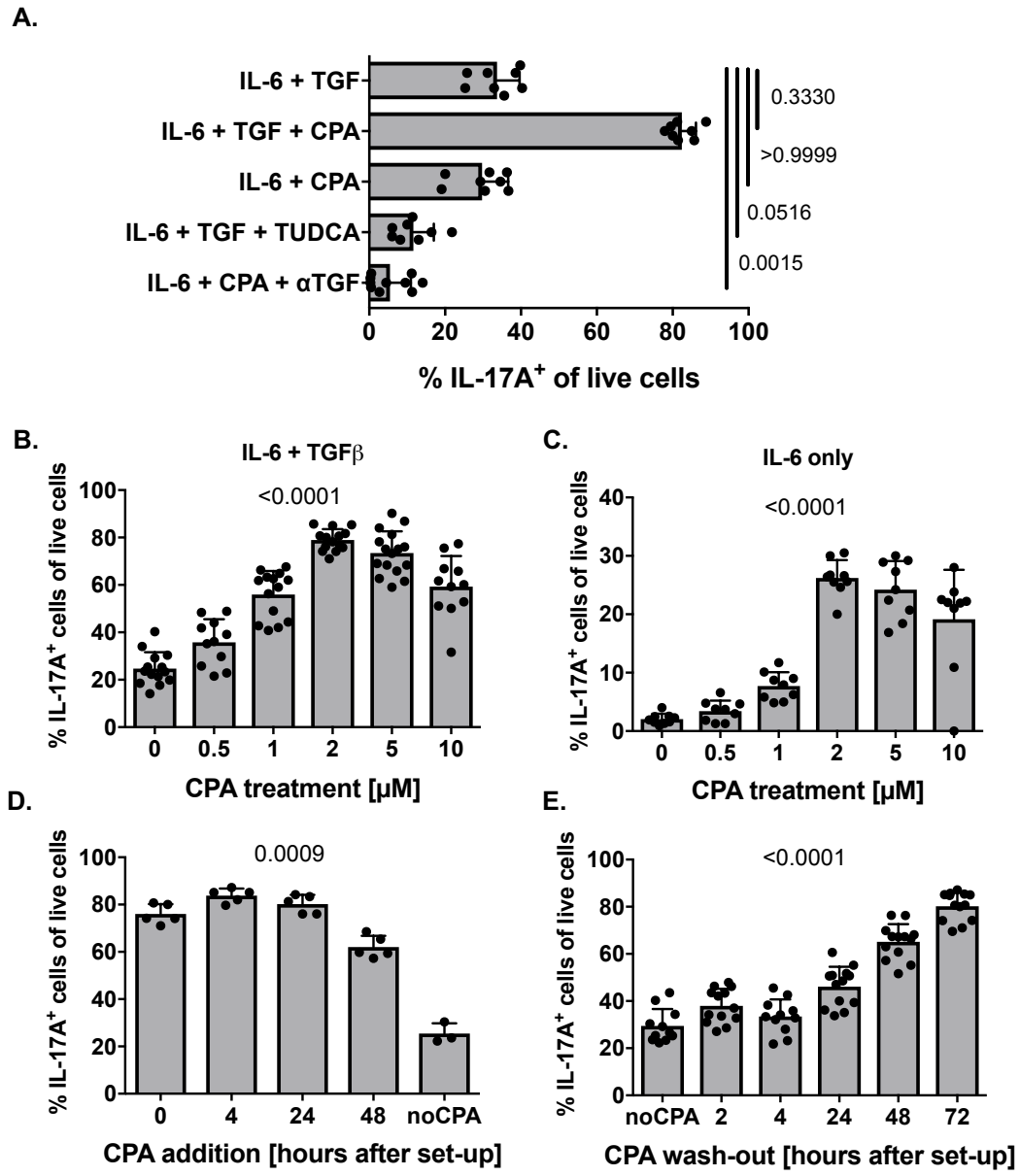

Figure 3.2: CPA enhances Th17 cell differentiation. (A-E) Naïve CD4$^+$ CD62L$^+$ T cells were MACS-purified from the spleens of *Rosa*$^{\text{stop-tdRFP}}$*Il17a*$^{\text{Cre}}$ or *Rosa*$^{\text{stop-eYFP}}$*Il17a*$^{\text{Cre}}$ reporter mice and differentiated into Th17 cells in the presence of TGFβ ("IL-6+TGFβ"; **A-B, D-E**) and/or 2 μM CPA ("IL-6+TGF+CPA" and "IL-6+CPA"; "IL-6 only"). In **A,** some cells were additionally treated with 10 μg/ml anti-TGFβ blocking antibodies ("IL-6+CPA+αTGF") or 0.5 mM TUDCA to block the UPR ("IL-6+TUDCA"). On day three, cells were stimulated for 3 hours with 500 g/ml PdBU, 500 ng/ml ionomycin and 10 μg/ml brefeldin A, then the percentage of IL-17A$^+$ cells was determined by flow cytometry. **(B, C)** In CPA titration experiments, cells were cultured with 0.5-10 μM CPA. Data in **A-C** were collected in 4-6 experiments performed for biological duplicates or triplicates (n=9-12). **(D)** For CPA time-courses, 2 μM CPA was added to the cultures 0 h, 4 h, 24 h or 48 h after cell culture set-up. **(E)** For washout experiments, cells were treated with 2 μM CPA at the start of the cell culture. At 2 h, 4 h, 24 h or 48 h CPA-containing media was removed and replaced by standard differentiation medium. Data were collected from 2 (time-course) or 6 (washout) experiments performed with biological duplicates or triplicates (n = 5-12). Bar heights correspond to mean percentages with error bars representing standard deviations. Dots represent the proportion of IL-17A$^+$ cells observed in individual samples. *P*-values are based on Kruskal-Wallis tests (in **A** with Dunn's correction for multiple testing) in GraphPad Prism 6.

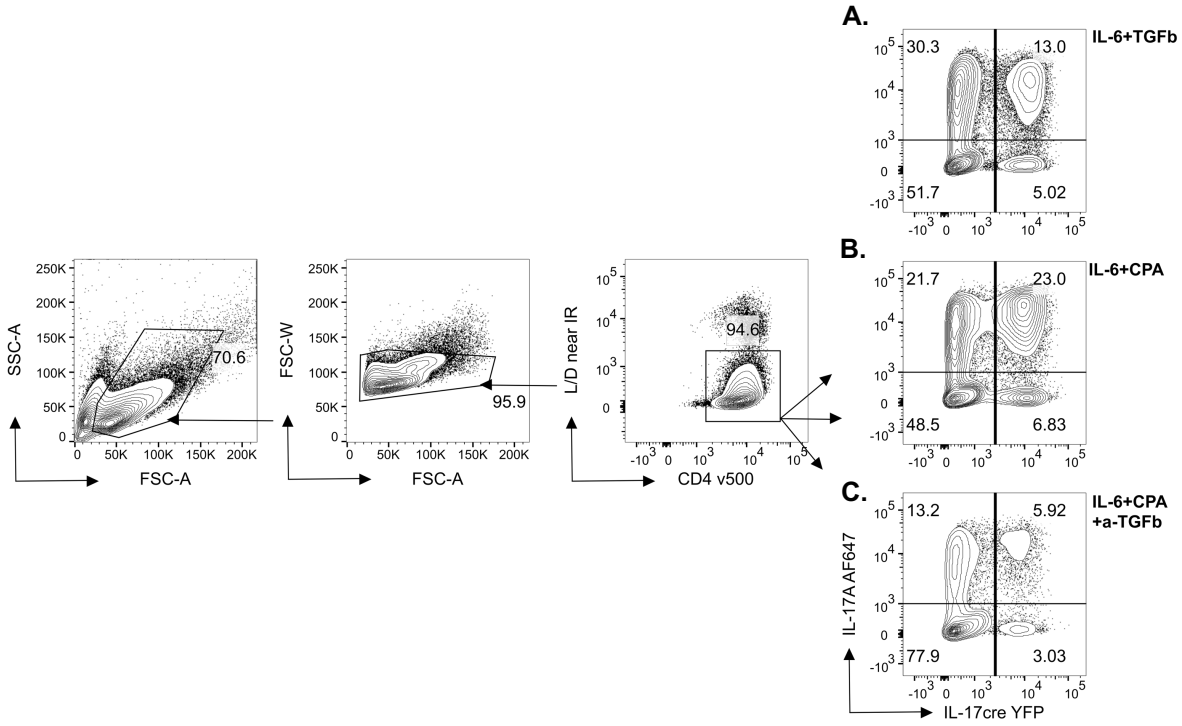

Figure 3.3: Gating strategy for sorting FP$^+$ and FP$^-$ T cells from *Il17a*^{FP} reporter mice. Naïve CD4$^+$ CD62L$^+$ T cells were isolated from the spleens of *Il17a*^{FP} reporter mice and differentiated into c-Th17 cells ("IL-6+TGFb"; **A**) and e-Th17 cells ("IL-6+CPA", **B**). Alternatively, they were treated with a combination of IL-6, CPA and α-TGFβ antibodies ("IL-6+CPA+αTGFb"; **C**). On day three, cells were optionally stimulated for 3 hours with 500 g/ml PdBU, 500 ng/ml ionomycin and 10 µg/ml brefeldin A for intracellular IL-17A staining, then cells were stained for flow cytometry and sorted into FP$^-$ (populations left of horizontal gate) and FP$^+$ (populations right of horizontal gate) fractions as shown above. **(A-C)** Representative flow plots for Th17 cells generated *in vitro* by treatment with IL-6+TGFβ, IL-6+CPA or IL-6+CPA+ αTGFβ.

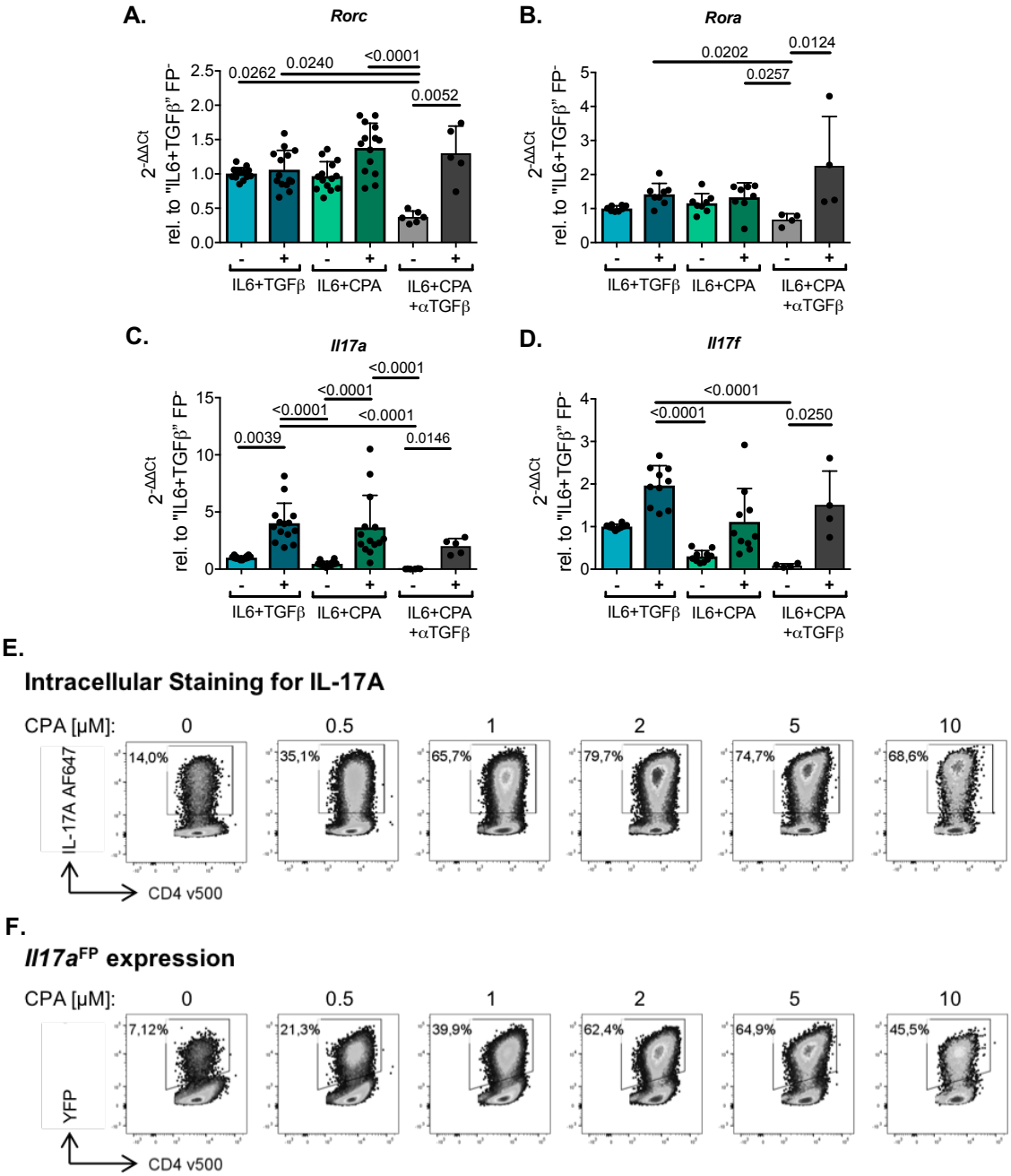

Figure 3.4: ER stress induces the expression of Th17 cell-associated genes in the absence of TGFβ. **(A-D)** Naïve CD4$^+$ CD62L$^+$ T cells were isolated from the spleens of *Il17a*^{FP} reporter mice and differentiated into c-Th17 cells ("IL-6+TGFβ") and e-Th17 cells ("IL-6+CPA"). Alternatively, they were treated with a combination of IL-6, CPA and α-TGFβ antibodies ("IL-6+CPA+αTGF"). On day three, cells were sorted into FP$^-$ ("-") and FP$^+$ ("+") fractions for RT-qPCR. Data were collected as biological duplicates in 2-7 independent experiments (n = 4-14). **(A-D)** RT-qPCR analysis of Th17 cell-associated gene expression in sorted cells. Dots represent relative gene expression levels of individual samples normalised to *Hprt* and relative to the c-Th17 FP$^-$ fraction as determined by the $2^{-\Delta\Delta Ct}$ method. Bar heights correspond to mean expression level with error bars representing standard deviations. *P*-values are based on Kruskal-Wallis tests with Dunn's multiple comparison corrections in GraphPad Prism 6. **(E, F)** Cells were cultured with a combination of IL-6, TGFβ and different concentration of CPA. The proportion of Th17 cells was assessed by flow cytometry after 3 hours of stimulation with 500 g/ml PdBU, 500 ng/ml ionomycin and 10 µg/ml brefeldin A, based on intracellular antibody staining for IL-17A **(E)** or their YFP expression **(F)** in 4 independent experimental repeats for biological duplicates (n = 8).

3.3.2 Increased expression of Th1 cell-associated genes in ER stress-generated Th17 cells

Next, I generated transcriptomic data from sorted c- and e-Th17 cells to investigate global gene expression differences between these cells. Principal component analysis and data clustering based on Euclidian distances revealed separate clustering of c-Th17 and e-Th17 cells, thus confirming global differences between these treatment groups (Figure 3.5A, B). Statistical comparison of e-Th17 and c-Th17 cells by differential gene expression (DGE) analysis in Qiagen's Biomedical Workbench (BmWB) generated a list of 3301 differentially-expressed genes with a false discovery rate (FDR) p-value ≤ 0.05 and absolute fold change ≥ 1.5. Many of these genes were involved in T cell development, activation and functions (Table 3.1). Notably, DGE revealed that the expression of *Tbx21* and *Ifng,* lineage marker genes associated with the T helper 1 (Th1) cell subset, was significantly upregulated in e-Th17 cells (Table 3.1, Figure 3.6A). The canonical Th17 transcripts *Il17f* and *Ahr* were reduced in e-Th17 cells, as was the expression of the anti-inflammatory cytokine *Il10*. These findings were confirmed by RT-qPCR (Figure 3.6B-H) and suggest there may be an increased Th17-to-Th1 plasticity of e-Th17 cells (Figure 3.6G, H). ex-Th17 Th1 cells have been described as potent drivers of EAE pathology, providing a potential link between ER stress and Th17 cell pathogenicity (Hirota *et al.* 2011; Stockinger & Omenetti 2017). The transcriptional signature of e-Th17 cells, characterised by high expression levels of *Tbx21* and low levels of *Ahr* and *Il10*, also highly resembles the pathogenic Th17 cell signature proposed by Lee *et al* (Lee *et al.* 2012). e-Th17 cells also express increased levels of secreted phosphoprotein 1 (*Spp1*), which has been implicated in the pathology of EAE (Chabas *et al.* 2001; Hur *et al.* 2007). This indicates that ER stress-generated Th17 cells exhibit increased EAE pathogenicity compared to c-Th17 cells.

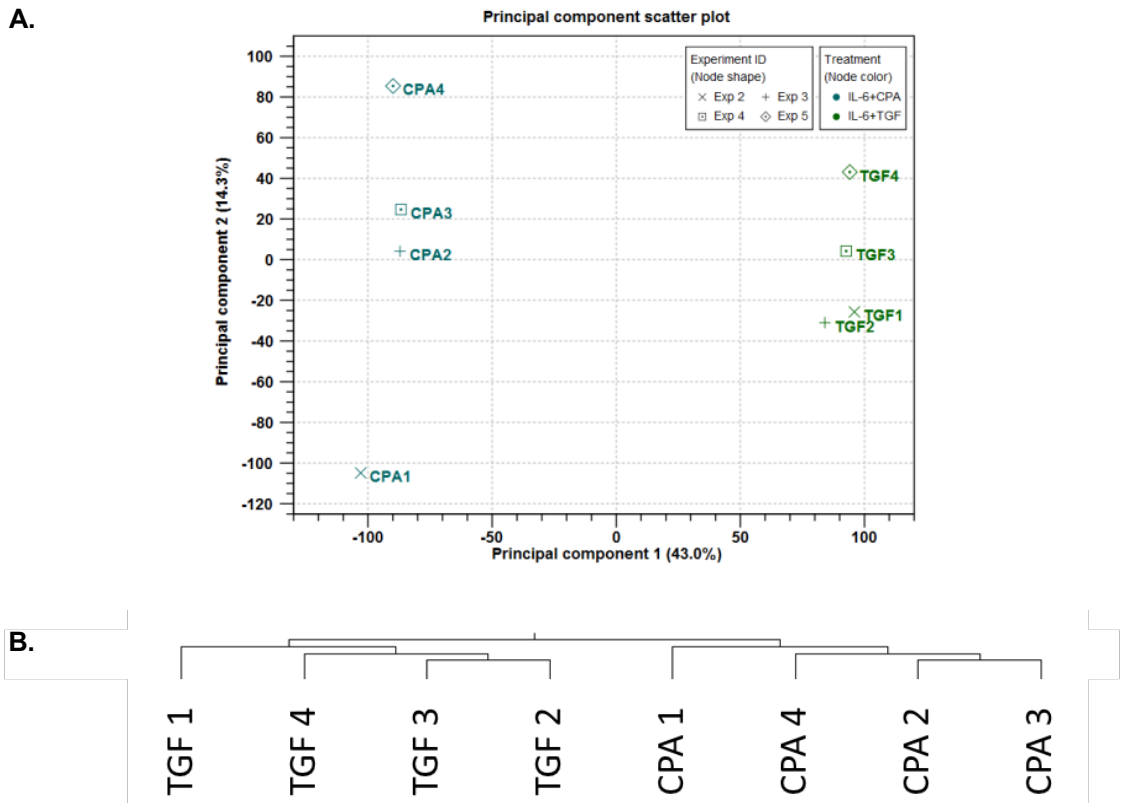

Figure 3.5: CPA treatment induces global gene expression changes in Th17 cells. (A) Principal component analysis reveals clustering of samples according to their respective treatment. c-Th17 (TGF) samples are coloured in green, CPA-treated e-Th17 cells in blue. Samples obtained from the same experiment share the same node shape. **(B)** This hierachical tree was generated using Qiagen's BmWB based on Euclidean distances and complete linkage, by joining clusters of genes if the distance between the furthest genes in the clusters is smallest. Only genes with a total count of 10 of greater were taken into account.

Rank	Symbol	Entrez Gene Name	Fold Change	Log_2 FC
1	NKG7	natural killer cell granule protein 7	304.10	8.24
2	GLP1R	glucagon-like peptide-1 receptor	291.25	8.19
3	SIGLEC-F	sialic acid binding Ig like lectin 8	278.59	8.12
4	ARL4D	ADP ribosylation factor like GTPase 4D	170.20	7.41
5	NRGN	neurogranin	142.83	7.16
6	MPZL2	myelin protein zero like 2	81.67	6.35
7	GPRIN2	G protein regulated inducer of neurite outgrowth 2	70.50	6.14
8	AJUBA	ajuba LIM protein	49.32	5.62
9	IFNG	Interferon gamma	45.27	5.50
10	TBX21	T-box protein 21	43.48	5.44
22	SPP1	secreted phosphoprotein 1	17.37	4.12
12	IL-22	interleukin 22	-19.44	-4.28
9	CRISPLD2	cysteine rich secretory protein 2	-34.27	-5.10
8	TNFRSF8	TNF receptor superfamily member 8	-34.50	-5.11
7	TIMP1	TIMP metallopeptidase inhibitor 1	-37.19	-5.22
6	GCNT2	N-acetyllactosaminide beta-1,6-N-acetylglucosaminyl-transferase	-47.33	-5.56
5	DNTT	DNA nucleotidylexotransferase	-49.41	-5.63
4	Ctla2a	cytotoxic T lymph-associated protein 2 α	-75.49	-6.24
3	Ctla2b	cytotoxic T lymph-associated protein 2 β	-101.38	-6.66
2	IL-24	interleukin 24	-474.82	-8.89
1	Ly6a	lymphocyte antigen 6 complex, locus A	-490.2	-8.94

Table 3.1: Top differentially-expressed genes between c-Th17 and e-Th17 cells. The list was obtained from a gene expression (DGE) analysis between treatment groups (CPA *versus* TGF) while controlling for variation between experimental repeats. It contains the top differentially-expressed genes with false-discovery rate (FDR) p-values ≤ 0.05 and maximal group means (MGMs) ≥ 3. The false-discovery rate (FDR) p-value accounts for the increased false-discovery rate in multiple testing, while the maximum group mean (MGM) describes the maximum average group RPKM (Reads Per Kilobase per Million mapped reads) values among all samples of a treatment group. Genes are ranked by their fold change, with rank 1 having the highest fold change, *i.e.* the highest or lowest expression in e-Th17 cells compared to c-Th17 cells. Genes upregulated in e-Th17 cells are marked in red, downregulated genes are highlighted in blue.

A.

Gene	RNA-seq		
	MGM	Fold change	FDR *p*-value
Ifng	3.3	45.27	0.00
Tbx21	21.8	43.48	0.00
Rorc	33.7	1.45	2.94E-08
Tnf	28.6	1.37	1.29E-05
Hif1a	152.5	1.15	0.15
Il17f	485.8	-1.92	0.00
Ahr	18.1	-2.84	1.57E-13
Il10	14.6	-5.94	0.00

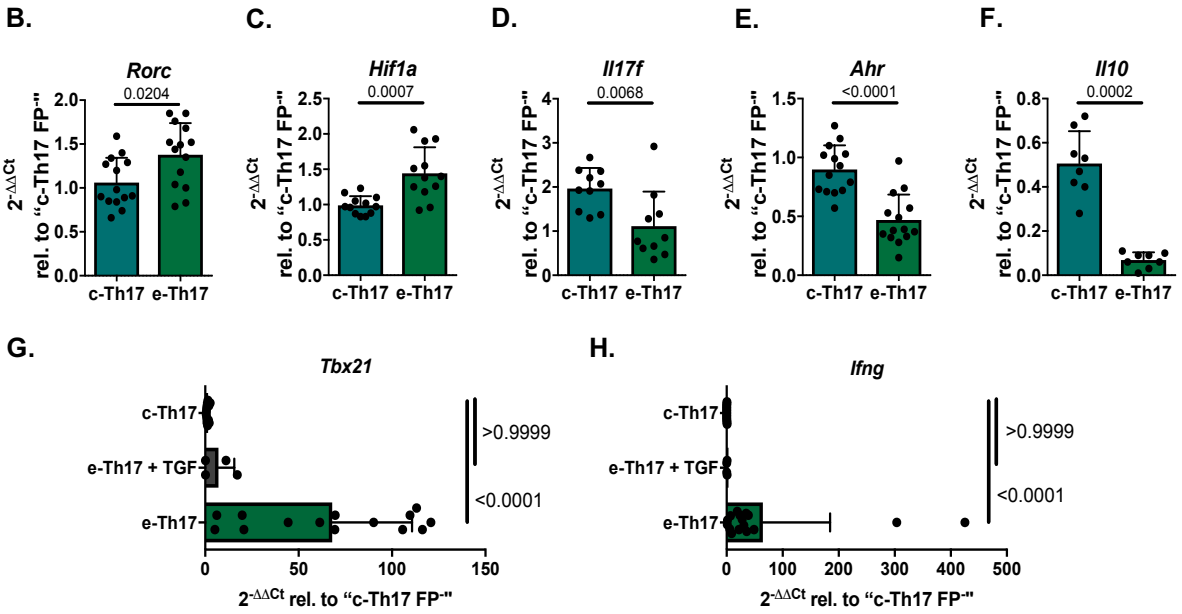

Figure 3.6: Distinct Th17 and Th1 cell type-specific mRNA expression by e-Th17 cells. (A) Table showing the fold change in gene expression of canonical Th17 and Th1 cell-associated genes as measured by DGE analysis of e-Th17 cells compared to c-Th17 cells. The false-discovery rate (FDR) *p*-value accounts for the increased false-discovery rate in multiple testing, while the maximum group mean (MGM) describes the maximum average group RPKM (Reads Per Kilobase per Million mapped reads) values among all samples of a treatment group. **(B-H)** Naïve $CD4^+$ $CD62L^+$ T cells were isolated from the spleens of *Il17a*^{FP} reporter mice and differentiated into c-Th17 cells (IL-6+TGFβ) and e-Th17 cells (IL-6+CPA). Alternatively, they were treated with a combination of IL-6, CPA and TGFβ ("e-Th17 + TGF"). On day three, cells were sorted into FP^- and FP^+ fractions and the FP^+ factions were subsequently analysed by RT-qPCR for *Il17f, Rorc, Ahr, Hif1a* or *Il10* **(C)**. Data were collected in 2-7 independent experiments performed for biological duplicates (n = 5-14). Dots represent gene expression levels of biological replicates normalised to *Hprt* and relative to the c-Th17 FP^- fraction as determined by the $2^{-\Delta\Delta Ct}$-method. Bar heights correspond to the mean expression level with error bars representing the standard deviation. *P*-values are based on Mann-Whitney **(B-F)** or Kruskal-Wallis tests with Dunn's multiple comparison corrections **(G, H)** calculated in GraphPad Prism v6.

3.3.3 Potential effects of ER stress on T cell receptor signalling in Th17 cells

Ingenuity Pathway Analysis (IPA; QIAGEN Inc. 2016) confirmed activation of the UPR in e-Th17 cells (Table 3.2) and revealed the reduced expression of EIF2 signalling pathway genes in e-Th17 cells, which is indicative of ER stress-induced translational repression by PERK. Another pathway identified as being underrepresented in e-Th17 cells compared to c-Th17 cells was mTOR signalling, a pathway often linked with ER stress (Appenzeller-Herzog & Hall 2012; Malhotra & Kaufman 2011). This confirms that the SERCA inhibitor CPA is indeed an inducer of the ER stress response.

IPA also confirmed differences in the expression of T cell differentiation-associated genes between e-Th17 and c-Th17 cells and revealed changes in gene expression associated with TCR-dependent T cell activation (Table 3.2, Figure 3.7, Figure 3.8): the genes encoding the TCR signalling-associated transmembrane receptors *Cd3*, *Cd28* and *Cd4* and the downstream signalling proteins *Zap70, Fyn* and *Lck* were found to be upregulated in e-Th17 compared to c-Th17 cells. This was associated with the increased expression of genes encoding *Erk, Nfatc1* and *Nfatc3* in these cells, while the expression of *Nfat2c* was decreased (Figure 3.8). This suggests that CPA treatment affects the signalling events downstream of the TCR, with possible implications for T cell activation and differentiation. Further experiments are required to determine whether this is due to downstream effects of the ER stress response or more directly caused by a CPA-induced increase in intracellular calcium signalling.

Rank	ER stress-linked Pathways	-log(*p*-value)	z score
1	EIF2 Signalling	57.6	-5.528
3	mTOR Signalling	22.7	-1
7	Mitochondrial Dysfunction	9.38	0
26	Unfolded protein response	6.1	0
2	Regulation of eIF4 and p70S6K Signalling	28.4	1.604
	T cell differentiation/activation Pathways		
4	T Cell Receptor Signalling	10.6	0
5	Regulation of IL-2 in Activated and Anergic T Cells	10.5	0
6	T Helper Cell Differentiation	10	0
10	Phospholipase C Signalling	7.63	0.209
8	Role of NFAT in Regulation of the Immune Response	8.02	1.859

Table 3.2: The top canonical IPA pathways are linked with ER stress or T cell differentiation and activation. This table lists the top IPA canonical pathways correlated with e-Th17 cell gene expression (abs. fold change ≥ 1.0, MGM ≥ 10). The pathways are ranked according to their IPA overlap *p*-values (shown as log-transformed values), which describe the correlation of the gene set with individual pathways. z-scores indicate whether the genes involved in a pathway are activated (z score > 0; orange), inhibited (z score < 0; blue) or neutral (z score ~ 0; grey). The top pathways can be loosely divided into two groups: ER stress-linked (upper section) as well as T cell differentiation and activation pathways (lower section).

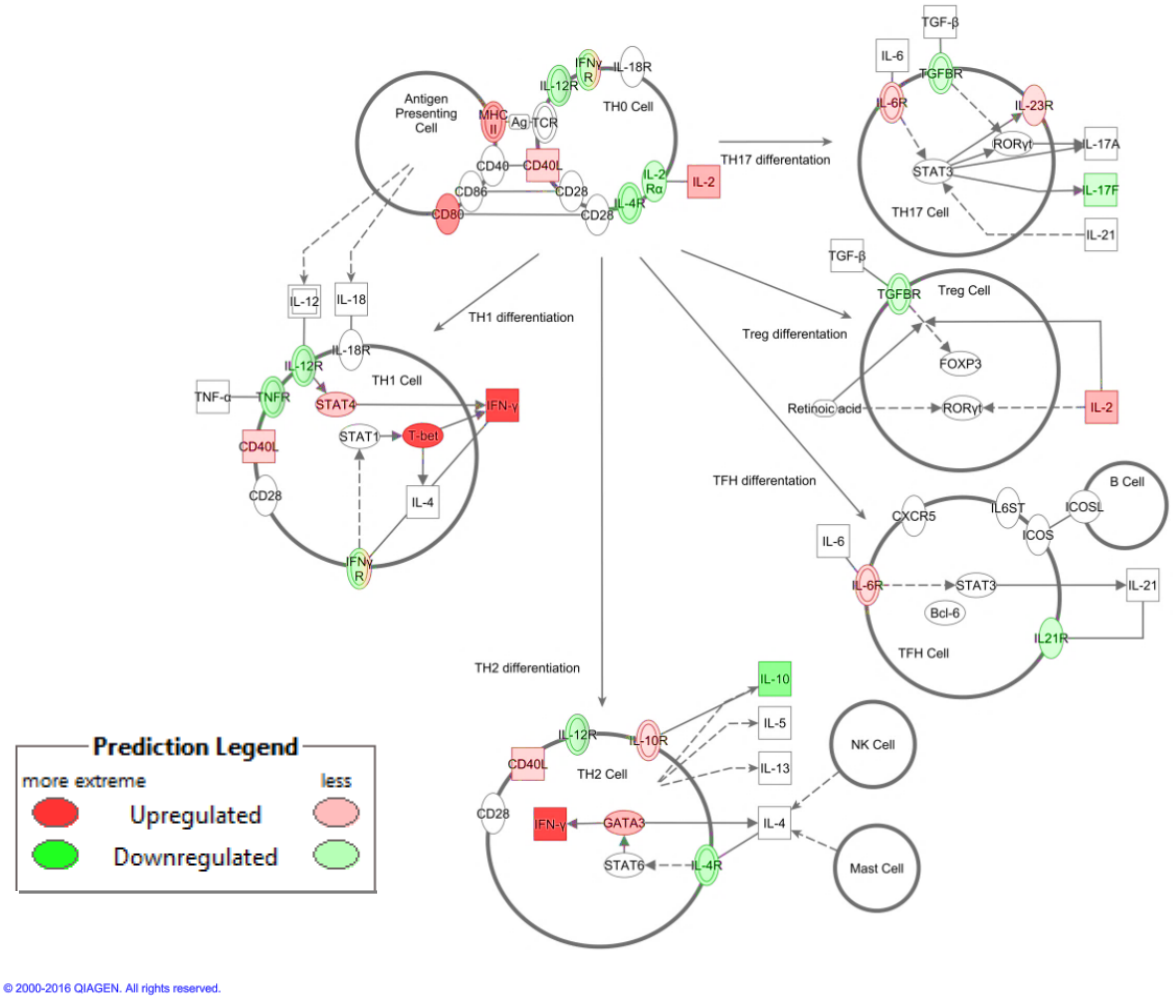

Figure 3.7: CPA treatment affects T cell differentiation. This graphical representation of the IPA "T cell differentiation" pathway depicts genes involved in Th subset differentiation and identity. The expression status of all involved genes in e-Th17 *versus* c-Th17 cells is colour-coded (upregulation=red; downregulation=green).

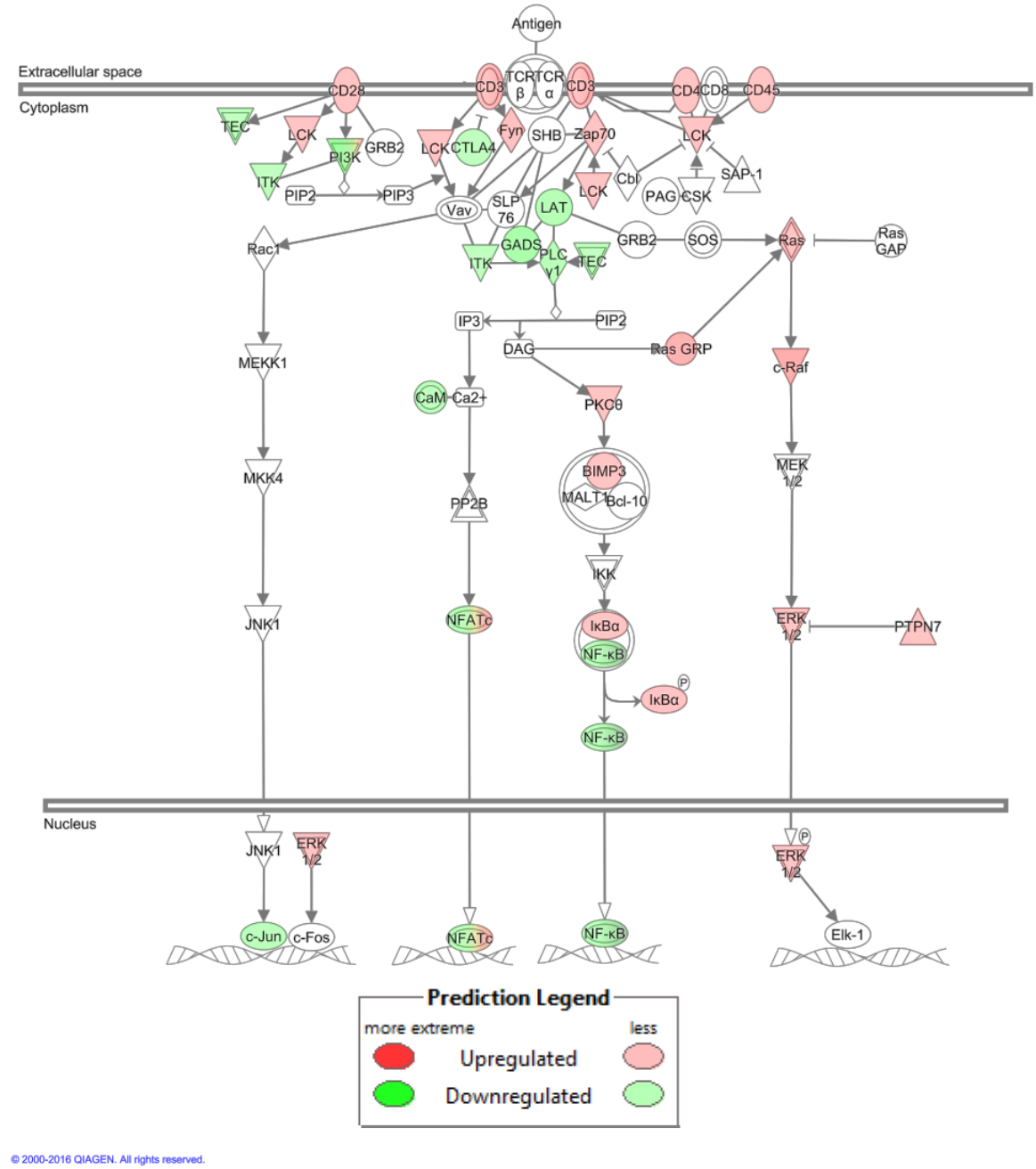

Figure 3.8: CPA treatment affects T cell activation. This graphical representation of the IPA "T cell receptor signalling" pathway shows the main genes involved in TCR signalling. The expression status of all involved genes in e-Th17 *versus* c-Th17 cells is colour-coded (upregulation=red; downregulation=green).

3.3.4 ER stress promotes EAE pathology

Downstream effects analysis (DEA) by IPA revealed that the gene expression pattern of e-Th17 cells was closely linked with several Th17-linked autoimmune disease pathways: DEA associated e-Th17 cells with systemic autoimmune syndrome (z score=1.45; log-transformed IPA overlap *p*-value=25), rheumatoid arthritis (z score=1.8; *p*=6.5) and EAE (z score=1.56; *p*=17.6).

To test whether these IPA predictions were correct, the impact of ER stress on Th17 cell-mediated EAE pathology *in vivo* was determined. For this, Verena Brucklacher-Waldert and Marc Veldhoen induced direct EAE in C57BL/6 mice by immunising them with myelin oligodendrocyte glycoprotein (MOG) in complete Freund's adjuvant (CFA). This triggers an immune response towards myelin, resulting in progressive neuronal loss and paralysis (Stromnes & Goverman 2006b). Daily dosing of MOG-immunised mice with the ER stress inhibitor TUDCA significantly delayed the onset of EAE compared to controls, strengthening the link between ER stress and EAE pathology (Figure 3.9A).

To determine whether TUDCA delayed the onset of EAE by blocking the ER stress response in T cells or other cell types, we made use of *Xbp1*$^{fl/fl}$*Rag1*$^{cre/+}$ mice. These mice delete *Xbp1* specifically from lymphocytes. The conditional excision of *Xbp1*, and its downstream ER stress response pathway, in lymphocytes again delayed the onset of EAE and reduced clinical EAE scores compared to wild-type and *Xbp1*$^{fl/fl}$*Rag1*$^{+/+}$ control mice (Figure 3.9B). This confirms that blockade of the ER stress response pathway in lymphocytes can ameliorate EAE pathology.

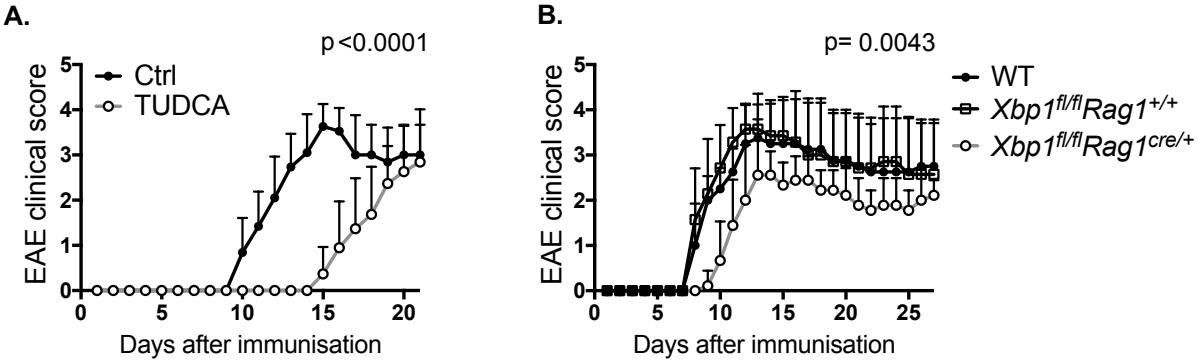

Figure 3.9: Blockade of the ER stress response ameliorates EAE disease severity. (A) Clinical scores of EAE induced by administration of MOG/CFA and daily dosing of PBS (Ctrl; closed circles) or 250 mg/kg TUDCA (open circles). *P*-values were calculated based on a Mann-Whitney test comparing the area under the curve (AUC) of each mouse as suggested by Fleming *et al.* (Fleming *et al.* 2005). **(B)** Clinical EAE scores from control C57BL/6 (closed circles), *Xbp1*$^{fl/fl}$*Rag*1$^{+/+}$ (open squares), and *Xbp1*$^{fl/fl}$*Rag1*$^{cre/+}$ (open circles) mice upon administration of MOG/CFA. *P*-values were calculated based on a Kruskal-Wallis test with Dunn's multiple testing correction comparing the AUC of *Xbp1*$^{fl/fl}$*Rag1*$^{cre/+}$ mice with the AUC of *Xbp1*$^{fl/fl}$*Rag*1$^{+/+}$ controls. Lines represent the mean, error bars the standard deviation of pooled data from 3 experiments with n = 19 mice per group **(A)** or two experiment with a total of n = 7-8 mice per group **(B)**. The data depicted here were generated by Verena Brucklacher-Waldert and Marc Veldhoen.

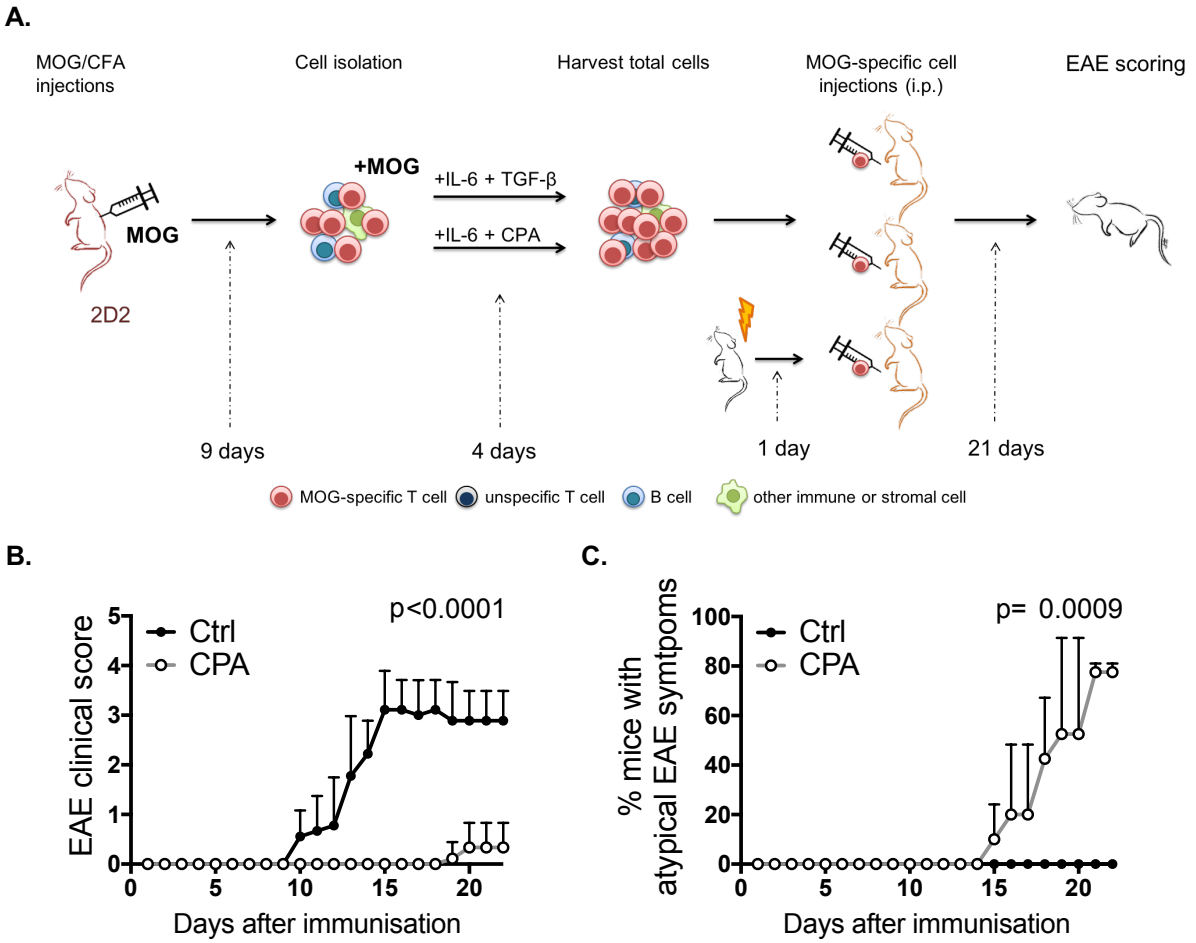

Figure 3.10: e-Th17 cells induce atypical symptoms in adoptive-transfer EAE experiments. **(A)** Schematic overview of the adoptive-transfer EAE protocol. **(B, C)** Adoptive-transfer EAE was induced by injecting mice with MOG-re-stimulated cell populations, which were isolated from MOG-immunised 2D2 mice and exposed to different Th17 cell differentiation conditions *in vitro* for 4 days. EAE progression was monitored over 22 days. Data were obtained from two experiments with a total of n = 9 mice per group. **(B)** Mean clinical EAE scores of mice injected with ER stress-generated e-Th17 (CPA) or c-Th17 (Ctrl) cells. Mean group scores of the "IL-6+CPA" treatment group are shown as open circles, the "IL-6+TGFβ" group as closed circles, error bars represent the standard deviation. *P*-values were calculated in GraphPad Prism6 and are based on Mann-Whitney tests comparing the area under the curve (AUC) of each mouse in the two different groups as suggested by Fleming *et al*. (Fleming *et al.* 2005). **(C)** Percentage of mice who developed atypical EAE symptoms during adoptive-transfer EAE experiments. The "CPA" treatment group is shown as open circles, the "Ctrl" group as closed circles. The lines represent the mean, error bars represent the standard deviation. The *p*-value is based on a Mantel-Cox curve comparison calculated in GraphPad Prism6. I performed the pilot experiment for this data set, but both repeats shown here were performed by Marc Veldhoen.

To further study the link between ER stress and T cell-mediated pathology of EAE, Marc Veldhoen and I conducted adoptive-transfer EAE experiments (Figure 3.10A). For this, we isolated total cells from the LNs and spleens of MOG-immunised 2D2 mice, whose T cells carry a transgenic TCR that is specific for a peptide of the MOG protein. These cells were expanded *in vitro* in the presence of MOG and a combination of either IL-6 plus TGFβ to generate c-Th17 cells, or a combination of IL-6 and CPA to promote the formation of e-Th17 cells. After four days, these cells were injected into sub-lethally irradiated C57BL/6 mice. These mice developed clinical signs of adoptive-transfer EAE within 8-18 days. While the "IL-6+TGFβ" group started showing clinical signs of EAE pathology on days 8-12 after T cell transfer, "IL-6+CPA" mice showed a delayed and reduced onset of classical EAE (Figure 3.10B). In contrast, they developed symptoms of atypical EAE such as ataxia (Figure 3.10C). This is indicative of Th17 cell-mediated brain inflammation as described by Stromnes *et al* (Stromnes *et al.* 2008). Taken together, these data provide evidence for a link between ER stress and EAE pathology and suggest that TUDCA, an FDA-approved drug, could potentially be used for the treatment of MS patients.

3.4 Discussion

It was long thought that the generation of Th17 cells requires a combination of both IL-6 and TGFβ signalling (Mangan *et al.* 2006; Veldhoen *et al.* 2006a). However, Ghoreschi *et al*. reported on the formation of Th17 cells in the absence of TGFβ when cultured with a combination of IL-6, IL-1β and IL-23 (Ghoreschi *et al.* 2010). The data presented here demonstrate that TGFβ-independent generation of Th17 cells can also occur in the presence of IL-6 and the ER stress inducers CPA and BrPA. This ER stress-generated Th17 cell population has a distinct gene expression profile, characterised by increased Th1 cell-associated gene expression and the expression of genes correlated with inflammation and autoimmune diseases such as rheumatoid arthritis and EAE. In line with this, we found that e-Th17 cells evoked Th17 cell-linked, atypical pathology in adoptive-transfer EAE experiments.

This study challenges the original theory that TGFβ is required for the formation of Th17 cells. TGFβ is thought to facilitate Th17 cell differentiation by relieving the SOCS3-dependent inhibition of STAT3 and repressing STAT4 and GATA3 expression (Das *et al.* 2009; Qin *et al.* 2009). Accordingly, mice with a dominant negative mutation in the TGFβ receptor II have reduced proportions of Th17 cells in their *lamina propria* and are protected from EAE (Ghoreschi *et al.* 2010; Qin *et al.* 2009; Veldhoen *et al.* 2006b). Ghoreschi *et al*. have recently described the TGFβ-independent generation of pathogenic Th17 cells under the influence of IL-6, IL-1β and IL-23 (Ghoreschi *et al.* 2010), however, and we have now established that a similar Th17 cell population

can be obtained under ER stress conditions *in vitro*. There is a high correlation between the gene expression changes we observed between c- and e-Th17 cells and the differentially expressed genes described by Ghoreschi *et al.* (Ghoreschi *et al.* 2010). Ghoreschi *et al.* compared microarray data from conventional Th17 cells (treated with IL-6 + IL-1β + TGFβ) with data obtained Th17 cells generated without TGFβ (Ghoreschi *et al.* 2010). Both in their, as well as in our transcriptomics data, the absence of TGFβ was correlated with the reduced expression of *Il10* and *Ahr* and increased expression levels of *Tbx21*. This indicates that, while TGFβ is not required for the generation of Th17 cells, it is important to shape the gene expression profile of Th17 cells. As a result, Th17 cells generated in the absence of TGFβ express higher levels of classical Th1 cell marker genes which has been linked with increased pathogenicity in autoimmune diseases (Lee *et al.* 2012).

In contrast to Ghoreschi *et al.*'s data, our transcriptomics data additionally revealed the CPA-associated upregulation of many genes associated with TCR signalling. Similar to CPA treatment, T cell activation culminates in the release of Ca^{2+} from the ER and drives NFAT-dependent transcription programmes, but can also induce the UPR (Feske 2007; Leitenberg & Bottomly 1999; Pino *et al.* 2008). Thus, the ER stress response and T helper cell activation are potentially closely associated. We cannot rule out, however, that the proposed ER stress-mediated effect on TCR signalling is caused by CPA-induced changes in calcium signalling rather than downstream effects of the UPR.

We observed potent Th17 cell differentiation not only under the influence of CPA, but also of the ER stress inducer BrPA. This indicates that CPA-driven Th17 cell differentiation is not due to CPA-specific effects on calcium signalling or unknown off-target effects, but that the generation of Th17 cells is promoted by a variety of conditions inducing ER stress. It would be interesting to perform RNA sequencing on Th17 cells differentiated under other stress conditions to further elucidate the molecular basis for stress-mediated Th17 cell differentiation.

Downstream analysis of our RNA sequencing data predicted an elevated potential of e-Th17 to cause pathology of EAE and arthritis. In accordance with this, mice dosed with the ER stress inhibitor TUDCA during active EAE induction exhibit a delayed onset of disease. As described above, e-Th17 cells have a lot in common with the Th17 cells generated by Ghoreschi *et al.*, which were also differentiated in the absence of TGFβ and were highly pathogenic in adoptive-transfer EAE experiments (Ghoreschi *et al.* 2010). Instead in our adoptive-transfer EAE model, mice injected with CPA-treated cells showed a delayed onset of classical disease symptoms. This could be linked with the increased expression of IFN-γ by e-Th17 cells, as IFN-γ-induced ER stress can have protective functions during EAE induction (Lin *et al.* 2007). While disease onset triggered by

e-Th17 cells was delayed, we did observe the emergence of atypical EAE symptoms in mice injected with CPA-treated cells. These symptoms had previously been associated with Th17 cell-mediated brain inflammation (Domingues *et al.* 2010; Stromnes *et al.* 2008). Further studies are required to confirm whether this phenotype is linked with an ER stress-related increase in Th17 cell numbers, or maybe an increase in Th17-to-Th1 plasticity of e-Th17 cells. It is important to note that in our adoptive-transfer EAE experiments, we injected recipient mice with a complex population of cells, all of which respond to ER stress and have the potential to influence disease progression. Unfortunately, MACS-sorted MOG-re-stimulated CD4 T cells did not induce adoptive-transfer EAE in our hands. Thus, it is not possible to rule out that non-Th17 cells are involved in directing EAE disease progression in this experimental system.

Nevertheless, our study provides compelling evidence for the ER stress response as a strong driver of Th17 cell differentiation into Th17 cells with a pathogenic gene expression signature. In adoptive-transfer EAE studies, these cells evoke atypical symptoms linked with Th17 cell-mediated brain inflammation. Thus, ER stress clearly affects the onset and progression of EAE. We do not yet fully understand the ER stress-mediated effect on e-Th17 cell pathogenicity, however. Additional T cell transfer and tracking studies could help to further dissect the plasticity, migration and pathogenic potential of e-Th17 cells. This would improve our understanding of the behaviour of ER stress-generated Th17 cells *in vivo* and could strengthen the novel link between ER stress and the pathology of Th17 cell-mediated autoimmune diseases proposed in this study.

Note:

This project was published in 2017 as part of a publication in Cell Reports: Brucklacher-Waldert V, Ferreira C, Stebegg M, Fesneau O, Innocentin S, Marie JC, Veldhoen M. 2017. Cellular Stress in the Context of an Inflammatory Environment Supports TGF-β-Independent T Helper-17 Differentiation, *Cell Reports* 19(11), 2357-2370 (Brucklacher-Waldert *et al.* 2017). No follow-up studies were performed, as I took on a new project in Michelle Linterman's group in January 2017. This was in consequence of Marc Veldhoen's move to Lisbon during the 1st year of my PhD and my wish to stay in Cambridge

4 HETEROCHRONIC FAECAL TRANSPLANTATION BOOSTS THE GUT GERMINAL CENTRE REACTION

4.1 Abstract

Ageing is a complex multifactorial process associated with a plethora of disorders which contribute to significant morbidity worldwide. One of the organs significantly affected by age is the gut. Age-dependent changes of the gut-associated microbiome have been linked to increased frailty and systemic inflammation. This change in microbial composition with age occurs in parallel with a decline in function of the gut immune system, however it is not clear if there is a causal link between the two. Here, we establish that the defective germinal centre (GC) reaction in Peyer's patches (PPs) of aged mice can be rescued by co-housing of adult and aged mice, and *via* faecal transfers from younger adults into aged mice. This demonstrates that the poor GC reaction in aged animals is not irreversible, and that it is possible to enhance this response in older individuals by replenishing the gut microbiome.

4.2 Background

One of the major achievements of human endeavour is the extension of lifespan through improvements in medical care, nutrition, sanitation and access to clean water. The consequent upward demographic shift in human age creates a challenge for medical science: how to enable people to age in good health. One of the organs that is significantly affected by age is the gastrointestinal tract and the gut-associated microbiome. The gut microbiota comprises hundreds of different commensal bacterial species, as well as fungi, protozoa and viruses. These commensal microorganisms are essential for health, affecting the functions of multiple bodily systems, such as host metabolism, brain functions and the immune response (Wang *et al.* 2017). Older individuals have age-related alterations in gut microbial composition (Buford 2017; Claesson *et al.* 2011; 2012; Maffei *et al.* 2017), which have been associated with increased frailty (Claesson *et al.* 2012; Maffei *et al.* 2017), reduced cognitive performance (Cattaneo *et al.* 2017) and an increased susceptibility to intestinal disorders (Kolling *et al.* 2012).

What drives these age-associated changes in the gut microflora remains unknown. The microbiome is shaped by many factors including host genetics, early life events, diet, and the gut immune system (Belkaid & Hand 2014; Kurilshikov *et al.* 2017; Power *et al.* 2014). While some of these factors remain relatively constant throughout life, the function of the immune system is known to deteriorate with age (Nikolich-Žugich 2018). This prompts the hypothesis that dysbiosis of the intestinal microbiome in older individuals may be driven by altered cross-talk between the host immune system and the microbiota. The gut immune system can regulate the composition of the microbiome by the production of IgA antibodies that coat commensal bacteria (Macpherson *et al.* 2018). Gut IgAs bind to a wide variety of bacteria in the gut lumen and alter the composition of the microbiome through several mechanisms, *e.g.* by blocking antigen interactions of gut microbes with the host, or trapping bacteria in the intestinal mucus (Macpherson *et al.* 2012). Animals that lack IgA production have aberrant expansion of anaerobic gut commensals and extensive immune hyperplasia (Fagarasan *et al.* 2002; Suzuki *et al.* 2004). In line with this, patients with selective IgA deficiency have an altered composition of the gut microbiome, associated with increased Th17 cell-associated inflammation (Fadlallah *et al.* 2018) and an increased susceptibility to recurrent infections, celiac disease and autoimmunity (Cunningham-Rundles 2001). This demonstrates an important role of IgA for gut health.

In the gastrointestinal tract, IgA antibodies are either produced by short-lived plasma cells in the *lamina propria* or from plasma cells that derive from GC reactions in PPs (Bunker & Bendelac 2018; Ost & Round 2018). In the *lamina propria*, plasma cells can be generated with or without T cell help, and typically secrete IgA antibodies that are encoded by germline immunoglobulin genes. In GCs, B cells proliferate and undergo somatic mutation of their immunoglobulin genes. GC B cells, which are able to bind antigen with improved affinity after somatic mutation, receive positive selection signals from T follicular helper (Tfh) cells and follicular dendritic cells (FDCs) that facilitate their differentiation into long-lived antibody secreting plasma cells that secrete high-affinity IgA (Bunker & Bendelac 2018; Mesin *et al.* 2016; Ost & Round 2018). Negative regulation of the GC reaction is mediated by suppressive T follicular regulatory (Tfr) cells that limit the output of the GC (Vanderleyden *et al.* 2014). Deregulation of Tfh or Tfr cell-mediated control or the absence of somatic hypermutation in GC B cells results in changes in the gut IgA repertoire which alter the composition of the gut microbiome (Kawamoto *et al.* 2012; 2014; Wei *et al.* 2011). This suggests that GC-derived IgA antibodies can regulate the commensal microbiome.

The studies described above have established the existence of a relationship between GC reactions and the microbiome and indicate clearly that the microbiome is causally influenced by the GC reaction. In the case of the gut-associated defects seen with advancing age in the GC reaction and

gut microbiota, however, the direction of causation is unclear. Here we report that the defective GC reaction in aged mice could be reversed by co-housing with younger animals or by direct faecal transplantation from adult donors. This demonstrates that the age-dependent defect in the gut GC reaction is not irreversible, but can be corrected by appropriate external stimuli.

4.3 Results

4.3.1 The GC reaction is diminished in aged PPs

To assess the impact of ageing on PPs, we compared the GC reaction at this site in 22-month-old "aged" mice with 3-month-old "adult" C57BL/6 and BALB/c mice by flow cytometry (gating strategy in Figure 4.1). Aged mice of both strains showed a reduction in frequency and number of $Bcl6^{+}Ki67^{+}B220^{+}$ GC B cells (Figure 4.2A-E). This was specific to the PPs, as there was no reduction in the proportion of GC B cells in the gut-draining mesenteric lymph nodes (LNs) in the same mice (Figure 4.3A-E). GC size depends on interactions with T cells: GC B cells receive positive signals from Tfh cells, while Tfr cells negatively regulate the response. The frequency of Tfh cells was not affected by age in the PPs (Figure 4.2F-J) in either strain, demonstrating that a reduction of Tfh cell number is not the cause of the diminished GC reaction in the PPs of aged mice. In mesenteric LNs, there was an increase in the number and frequency of Tfh cells in aged mice (Figure 4.3F-J). In the PPs of 22-month-old mice, Tfr cell frequency was not changed in BALB/c mice (Figure 4.2K-M) and was slightly decreased in C57BL/6 mice (Figure 4.2N, O), indicating that an increase in the proportion of Tfr cells does not contribute to the decreased magnitude of the GC reaction in the PPs of aged mice. There was an increase in Tfr cell numbers in mesenteric LNs from aged mice in both strains, consistent with previous observations (Sage *et al.* 2015) (Figure 4.3K-O). These data show that there is a decrease in the magnitude of the GC reaction in the PPs of aged mice, but that this is not obviously linked with age-associated changes in follicular T cell subset composition.

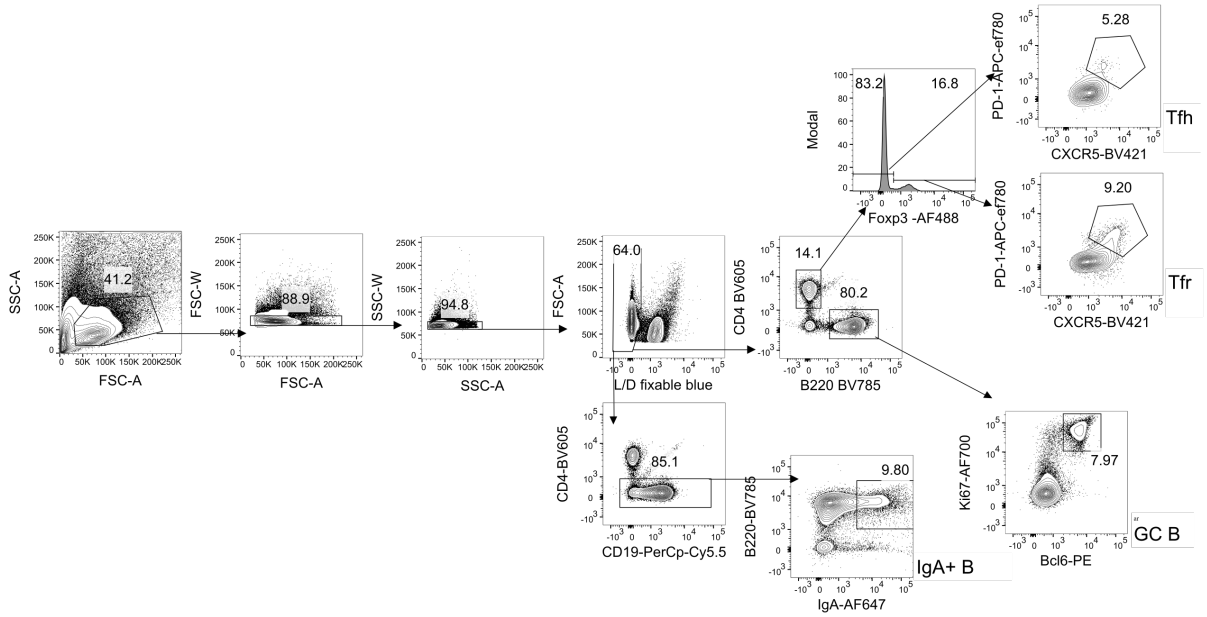

Figure 4.1: Gating strategy for germinal centre (GC) cell populations in Peyer's patches (PPs) or mesenteric lymph nodes (LNs). GC cell populations in PPs and mesenteric LNs were assessed by flow cytometry. IgA^+ B cells were defined as live $IgA^+B220^+CD4^-$ cells, GC B cells as live $Bcl6^+Ki67^+B220^+$ cells. T follicular helper (Tfh) cells were defined as live $CXCR5^{hi}PD\text{-}1^{hi}Foxp3^-CD4^+$ cells and T follicular regulatory (Tfr) cells as live $CXCR5^{hi}PD\text{-}1^{hi}Foxp3^+CD4^+$ cells.

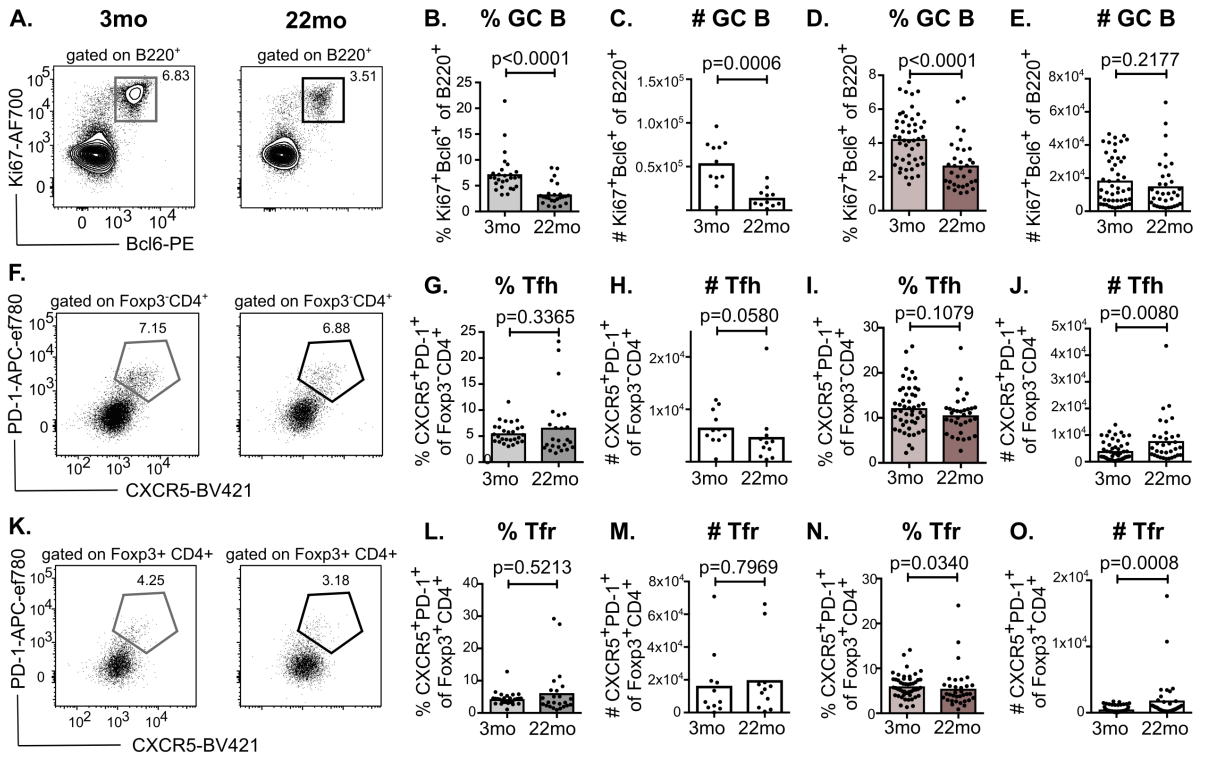

Figure 4.2: Germinal centre B cells are reduced in the Peyer's patches of aged BALB/c and C57BL/6 mice. Flow cytometric analysis of germinal centre (GC) cell populations in the Peyer's patches (PPs) of adult (3-month-old; 3mo) and aged (22-month-old; 22mo) BALB/c and C57BL/6 mice. **(A-C)** Representative flow cytometric plots **(A)** and quantitation of $B220^+Ki67^+Bcl6^+$ GC B cells **(B, C)** in the PPs of 3-month-old and 22-month-old BALB/c mice. **(D, E)** Quantitation of $B220^+Ki67^+Bcl6^+$ GC B cell percentage **(D)** and number **(E)** in C57BL/6 mice. **(F-H)** Representative flow plots **(F)** and quantitation of $CD4^+Foxp3^-CXCR5^+PD\text{-}1^+$ Tfh cells **(G, H)** in the PPs of BALB/c mice. **(I, J)** Quantitation of Tfh cell percentages **(I)** and numbers **(J)** in C57BL/6 mice. **(K-M)** Representative flow plots **(K)** and quantitation of $CD4^+Foxp3^+CXCR5^+PD\text{-}1^+$ Tfr cells **(L, M)** in BALB/c mice. **(N, O)** Quantitation of Tfr cell percentages **(N)** and numbers **(O)** in C57BL/6 mice. Bar graphs show the combined results of 3-6 independent experiments which were performed with female BALB/c mice and both male and female C57BL/6 mice with a total of n = 11-49 mice per group. Bar height corresponds to the mean, and each circle represents one biological replicate. *P*-values were determined using the Mann-Whitney test in GraphPad Prism6.

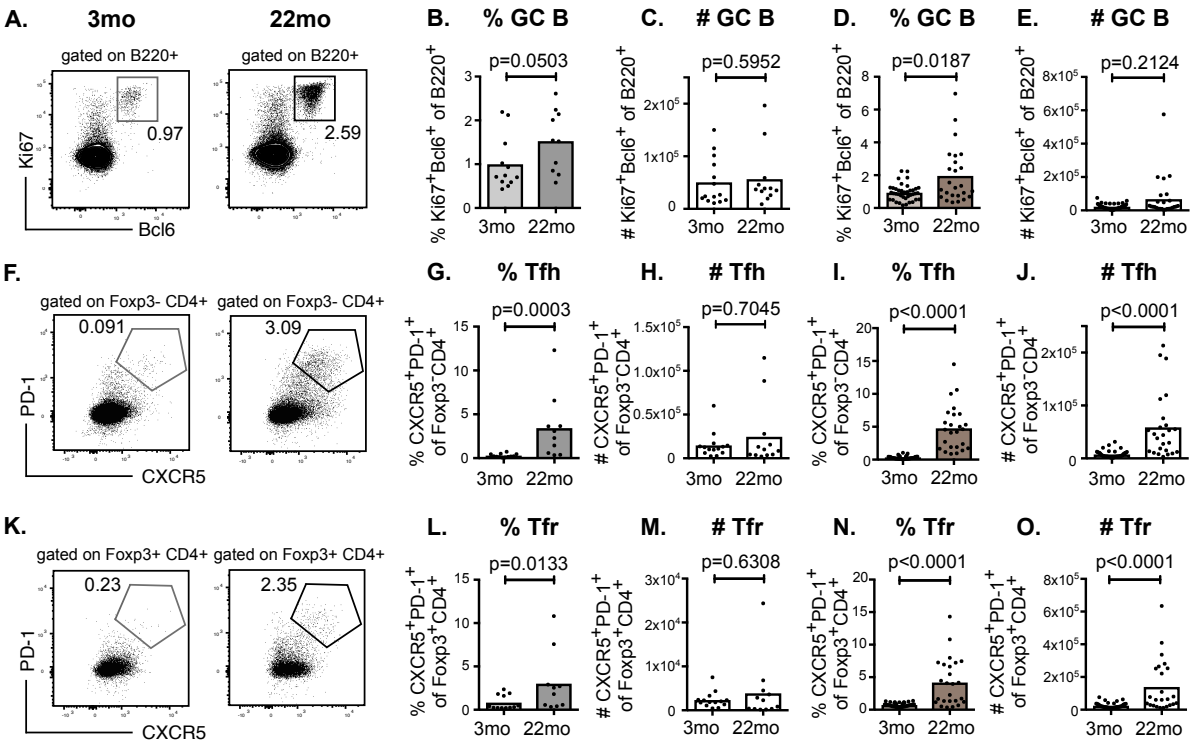

Figure 4.3: Germinal centre B cells are not reduced in the mesenteric lymph nodes (LNs) of aged BALB/c and C57BL/6 mice. Flow cytometric analysis of germinal centre (GC) cell populations in the mesenteric LNs of adult (3-month-old; 3mo) and aged (22-month-old; 22mo) BALBc and C57BL/6 mice. **(A-C)** Representative flow cytometric plots **(A)** and quantitation of B220+Ki67+Bcl6+ GC B cells (B, C) in the mesenteric LNs of 3-month-old and 22-month-old BALB/c mice. (D, E) Quantitation of $B220^{+}Ki67^{+}Bcl6^{+}$ GC B cell percentage **(D)** and number **(E)** in C57BL/6 mice. **(F-H)** Representative flow plots **(F)** and quantitation of $CD4^{+}Foxp3^{-}CXCR5^{+}PD\text{-}1^{+}$ Tfh cells **(G, H)** in BALB/c mice. **(I, J)** Quantitation of Tfh cell percentages **(I)** and numbers **(J)** in C57BL/6 mice. **(K-M)** Representative flow plots **(K)** and quantitation of $CD4^{+}Foxp3^{+}CXCR5^{+}PD\text{-}1^{+}$ Tfr cells **(L, M)** in BALB/c mice. **(N, O)** Quantitation of Tfr cell percentages **(N)** and numbers **(O)** in C57BL/6 mice. Bar graphs show the combined results of 3-6 independent repeats which were performed with female BALB/c mice and both male and female C57BL/6 mice with a total of 10-41 mice per group. Bar height corresponds to the mean, and each circle represents one biological replicate. *P*-values were determined using the Mann-Whitney test in GraphPad Prism6.

4.3.2 The composition of the gut microbiome changes with age

It is known that the output of the GC reaction can influence the composition of the gut microbiome (Ost & Round 2018). Therefore, we sought to understand whether the age-dependent change in the GC reaction of PPs was linked with changes in the microbiota. For this, I assessed the bacterial gut microbiome in C57BL/6 and BALB/c mice by 16S rDNA sequencing of DNA extracted from faecal pellets from 22-month-old "aged" and 3-month-old "adult" mice. Principal Coordinates Analysis (PCoA) showed that age impacts the composition of the microbiome and demonstrated that inter-individual variation of the microbiome increases in aged animals (Figure 4.4A, B; Figure 4.5A). In BALB/c mice, six classified bacterial families were reduced in aged mice, whilst two bacterial families increased in abundance with age (Figure 4.4C). This corresponded to reduced gut microbial diversity in aged BALB/c compared to adult mice (Figure 4.4D). Interestingly, *Bacteroides acidifaciens* and *Lactobacillus gasseri,* both of which have been shown to induce intestinal IgA production, were not detected in aged BALB/c mice (Table 4.1) (Sakai *et al.* 2014; Yanagibashi *et al.* 2013). Aged C57BL/6 males had increased bacterial diversity (Figure 4.4E), which was associated with the increased abundance of seven bacterial families in these mice (Figure 4.4F). Bacterial diversity was not changed in aged C57BL/6 females while two bacterial families were significantly decreased (Figure 4.5B, C). The abundance of *Bacteroides acidifaciens* and *Lactobacillus gasseri* was not affected in either female or male C57BL/6 aged mice (Table 4.1), suggesting that the age-associated immunological phenotype is not caused by a reduction of these particular species. Both aged BALB/c mice and C57BL/6 males had an expansion of *Firmicutes* at the expense of *Bacteroidetes* at the phylum level (Figure 4.4G, H; Figure 4.6). This analysis shows that the composition of the gut microbiome changes with age in mice and that these age-dependent changes are also shaped by the sex and genetics of the host.

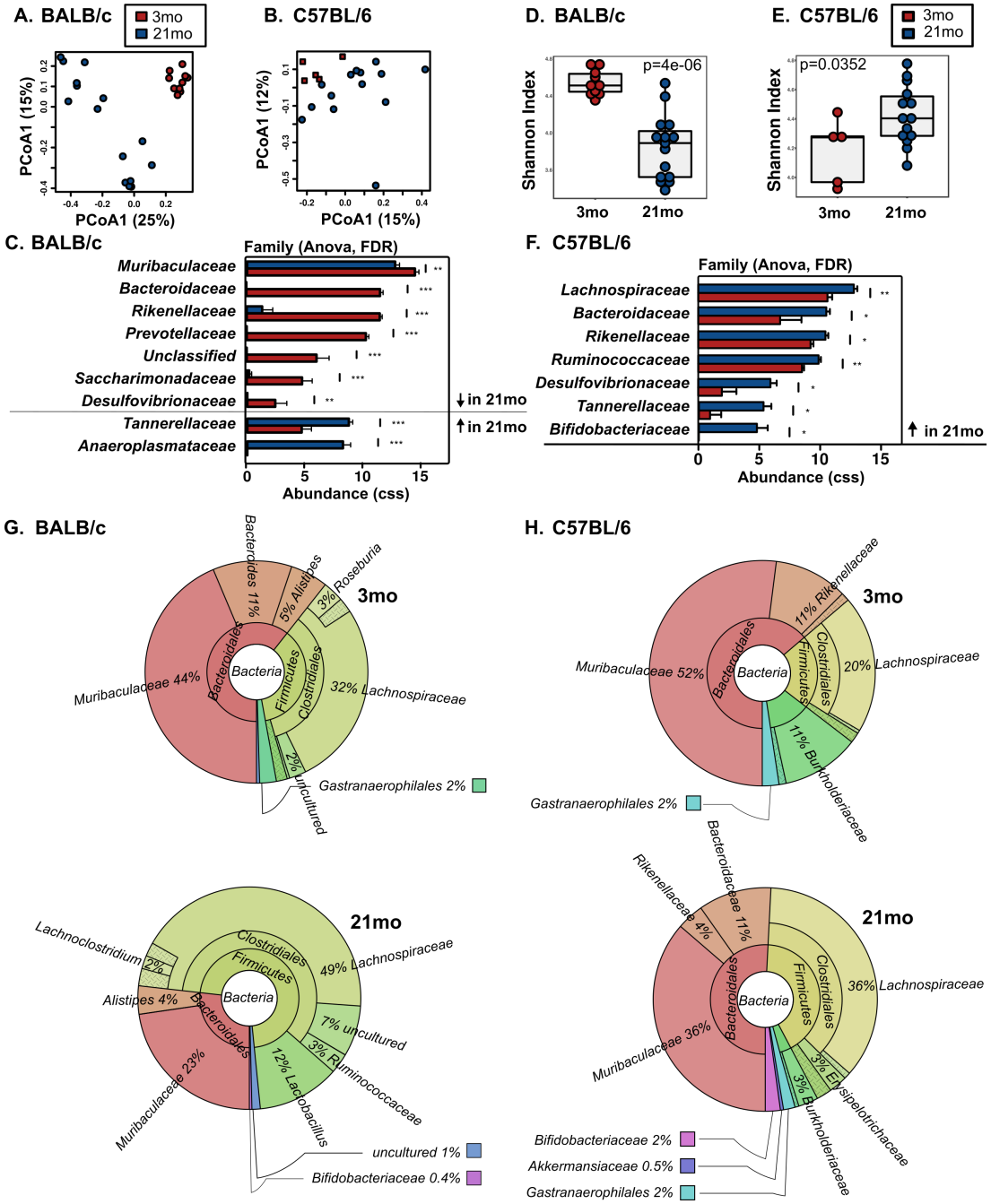

Figure 4.4: The gut microbiome changes during ageing. 16S rDNA sequencing data were generated from faecal pellets collected from adult (3-month-old; 3mo) and aged (21-month-old; 21mo) BALB/c females and C57BL/6 males. **(A, B)** Bray-Curtis PCoA and **(D, E)** bacterial diversities (measured by Shannon index) of samples collected from 3-month-old and 21-month-old BALB/c mice **(A, D)** and C57BL/6 mice **(B, E)**. The *p*-value was based on ANOVA tests. **(C, F)** Depiction of bacterial families whose abundance was significantly different between 3-month-old and 21-month-old BALB/c **(C)** and C57BL/6 **(F)** mice as determined by ANOVA analysis after cumulative-sum scaling (CSS). **(G, H)** Krona plots depicting the phylogenetic composition of the gut microbiome in 3-month-old (top) and 21-month-old (bottom) BALB/c **(G)** and C57BL/6 **(H)** mice. The percentages shown are averages of the samples in each age group. Samples were collected in 2 independent experiments for BALB/c mice and 3 independent experiments for C57BL/6 mice with a total of n = 5-14 mice per group. *P*-values are based on ANOVA tests *FDR ≤ 0.05, **FDR ≤ 0.01, ***FDR ≤ 0.001. This figure was published in Nature Communications (Stebegg *et al.* 2019).

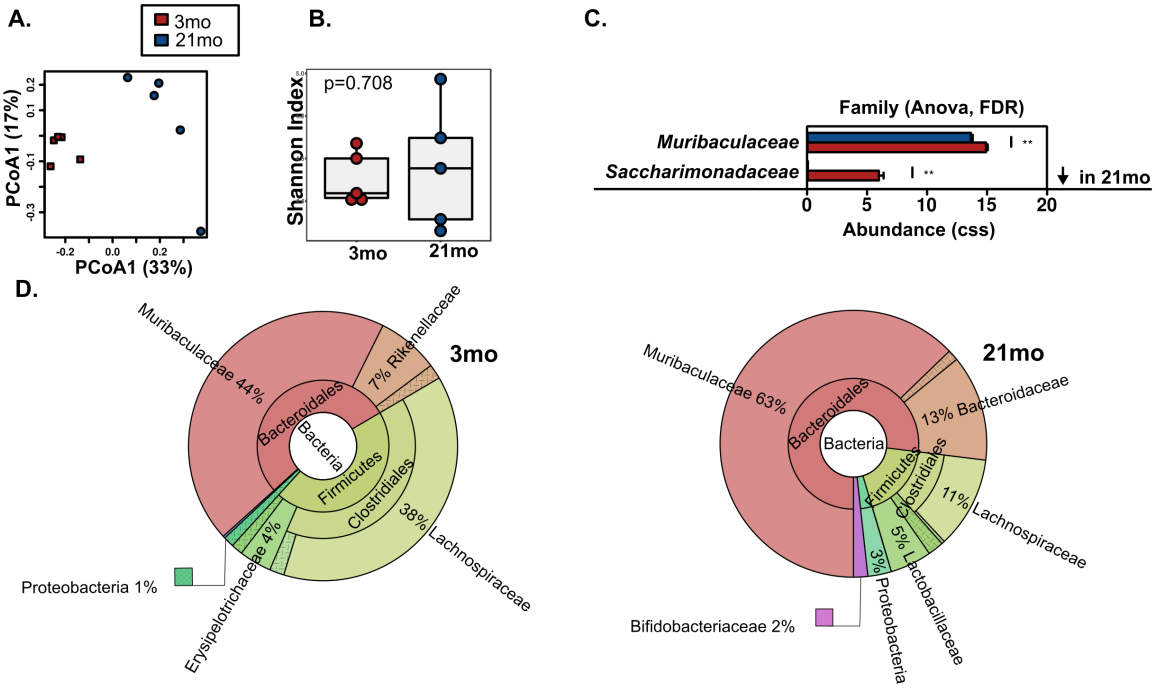

Figure 4.5: Age-associated changes of the gut microbiome in female C57BL/6 mice. 16S rDNA sequencing data were generated from faecal pellets collected from five adult (3-month-old; 3mo) and five aged (21-month-old; 21mo) female C57BL/6 mice. **(A)** Bray-Curtis PCoA of samples collected from female C57BL/6 mice. **(B)** Shannon diversities of samples collected from female C57BL/6 mice. The *p*-value was generated from an ANOVA test. **(C)** Depiction of bacterial families whose abundance was significantly different between adult and aged female C57BL/6 mice as determined by ANOVA analysis after cumulative-sum scaling (CSS). *FDR $\leq$ 0.05, **FDR $\leq$ 0.01, ***FDR $\leq$ 0.001. **(D)** Krona plots depicting the phylogenetic composition of the gut microbiome in 3-month-old (left) and 21-month-old (right) C57BL/6 females. The percentages shown are averages of the samples in each age group. This figure was adapted from Stebegg *et al.* (Stebegg *et al.* 2019).

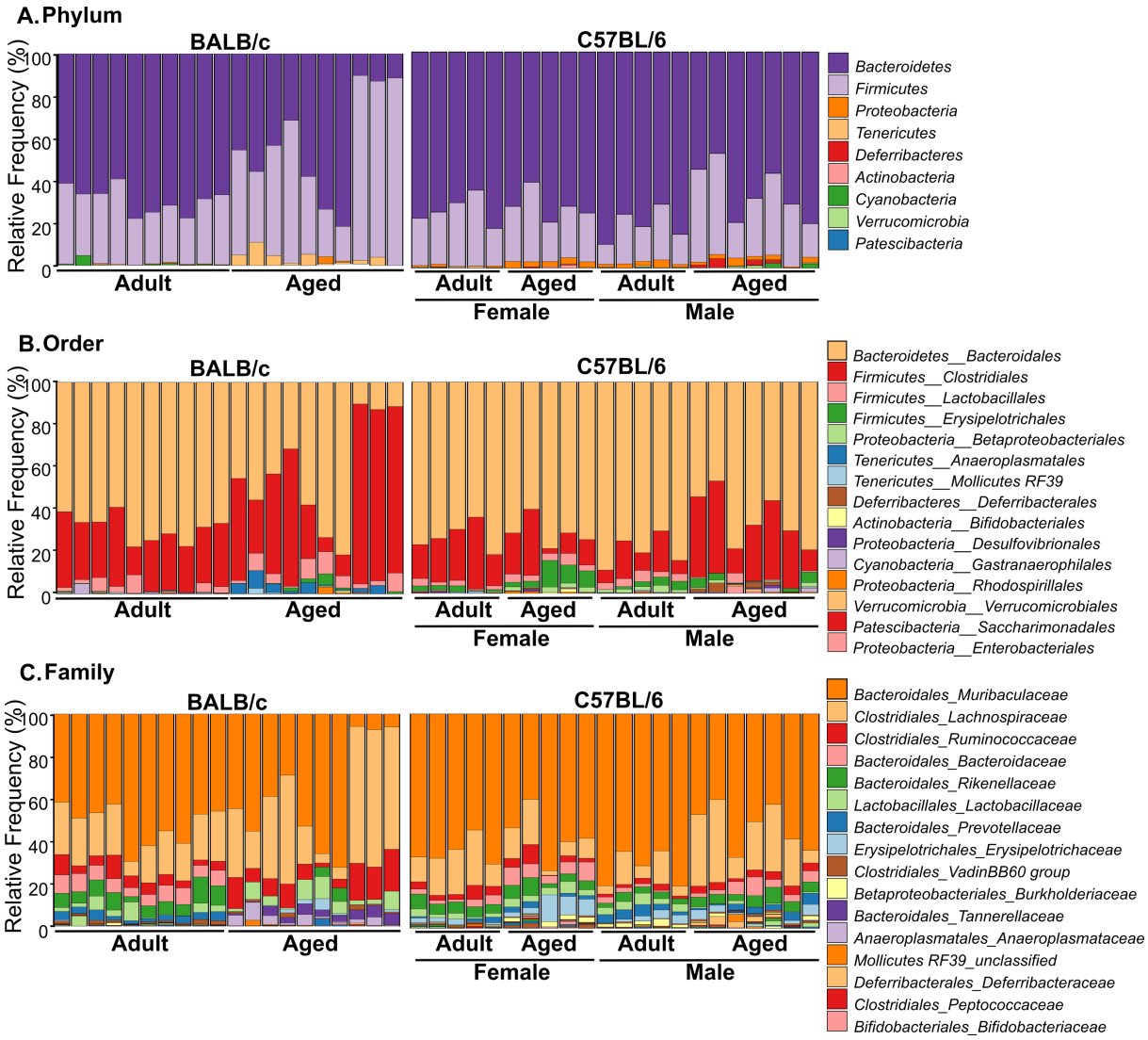

Figure 4.6: Age-associated changes in the taxa composition of the gut microbiome in C57BL/6 and BALB/c mice. 16S rDNA sequencing data were generated from faecal pellets collected from adult and aged female BALB/c mice as well as male and female C57BL/6 mice. Taxa plots of bacterial phyla **(A)**, orders **(B)** and families **(C)** detected in faecal samples from adult (3month-old) and aged (21-22month-old) BALB/c and C57BL/6 mice generated in QIIME2 with a total of n = 5-10 mice per group. In **(B)** and **(C)** only the 15 most abundant bacterial orders/families are listed in the legend. This figure was adapted from Stebegg *et al.* (Stebegg *et al.* 2019).

Taxa (Species level)	FDR	F	21mo	3mo
BALB/c mice: Aged (21mo) vs Adult (3mo)				
Bacteroides_Bacteroides_caecimuris	<1E-20	5600	0	7.43
Bacteroides_Bacteroides_acidifaciens	**<1E-20**	**2400**	**0**	**9.23**
Prevotellaceae_UCG001_uncultured_bacterium	<1E-20	2400	0	9.01
Rikenellaceae_RC9_gut_group_uncultured_organism	<1E-20	2300	0	8.06
Alistipes_uncultured_bacterium	<1E-20	1900	0	9.34
Anaeroplasma_uncultured_bacterium	4.8E-09	110	8.27	0
Parabacteroides_Parabacteroides_goldsteinii_CL02T12C30	9.1E-07	58	8.78	3.69
Lactobacillus_Lactobacillus_gasseri	**2.0E-05**	**39**	**0**	**5.92**
Lachnospiraceae_UCG001_uncultured_Clostridiales_bact.	0.0011	20	0	3.86
Turicibacter_Turicibacter_sp._LA61	0.0053	15	5	0.37
C57BL/6 mice: Aged (21mo) vs Adult (3mo)				
Bacteroides_Bacteroides_caecimuris	0.058	16	7.12	2.83
Parabacteroides_Parabacteroides_goldsteinii_CL02T12C30	0.11	11	4.81	0.98
Parasutterella_uncultured_organism	0.11	9.8	2.38	7.2
unclassified_bacterium_uncultured_bacterium	0.11	9.6	12.82	13.77
Bilophila_uncultured_bacterium	0.14	8.2	5.3	2.11
Rikenellaceae_RC9_gut_group_uncultured_organism	0.14	7.6	6.09	2.61
unclassified_uncultured_bacterium	0.15	7.2	8.11	5.17
Mucispirillum_Mucispirillum_schaedleri_ASF457	0.15	6.9	4.49	0
Lactobacillus_Lactobacillus_gasseri	**0.16**	**6.4**	**5.27**	**9.57**
Lachnospiraceae_FCS020_group_mouse_gut_metagenome	0.18	5.9	3.91	0
C57BL/6 mice: Aged (21mo) vs Adult (3mo)				
Parasutterella_Burkholderiales_bacterium_YL45	0.016	7.98	0	8.46
Odoribacter_uncultured_bacterium	1	6.24	0	7.88
Bacteroidales_Bacteroidales_bacterium	1	8.99	10.09	9.02
unclassified_bacterium_uncultured_bacterium	1	12.6	13.51	12.69
Ruminococcaceae_UCG014_uncultured_bacterium	1	2.56	7.19	0
Parasutterella_uncultured_organism	1	0	2.93	0
Lachnospiraceae_UCG006_uncultured_bacterium	1	0	4.46	0
Ruminiclostridium_5_Ruminiclostridium_sp._KB18	1	3.26	0	3.84
Ruminococcaceae_UCG010_uncultured_organism	1	2.92	0	3.61
Turicibacter_Turicibacter_sp._LA61	1	7.15	2.5	8.52

Table 4.1: Age-related changes on the species level in the gut microbiome of BALB/c and C57BL/6 mice. Top 9 species with the lowest false-discovery rate (FDR) *p*-value detected by 16S rDNA sequencing in 3-month-old compared to 23-month-old BALB/c and C57BL/6 mice. Significant changes in the abundance of bacterial species between adult and aged mice were determined by ANOVA analysis after cumulative-sum scaling (CSS). FDR-adjusted *p*-values and F value were calculated for each species. The table also lists the mean abundance of each species after CSS. This table was adapted from Stebegg *et al* (Stebegg *et al.* 2019).

4.3.3 Co-housing rescues the reduced PP GC reaction in aged mice

In our initial experiments, adult and aged mice were housed separately from each other, sharing cages with their respective littermates. Knowing that the gut microbiome can vary between cages (Goodrich *et al.* 2014) and that co-housed mice exchange faecal bacteria by coprophagy (Hildebrand *et al.* 2013), I decided to repeat these experiments, using 3-month-old adult and 21-month-old aged mice that were housed in the same cage for 30-40 days. To our surprise, the age-associated reduction of GC B cells in PPs of BALB/c mice was lost upon co-housing (Figure 4.7A, B). This correction of the GC reaction was accompanied by an increase in Tfh cells but Tfr cell numbers were unchanged (Figure 4.7C-F). This demonstrates that the age-dependent deficit in the magnitude of PP GCs is reversible.

To determine whether changes in the GC reaction upon co-housing were driven by the transfer of faecal microbiota between mice, bacterial 16S rDNA sequencing was performed on faecal pellets collected before and after co-housing. PCoA revealed that the microbiome of aged mice was more similar to that of 3-month-old adult mice after co-housing, while the microbiome of adult BALB/c mice was not significantly changed (Figure 4.7G). Co-housing also increased bacterial Shannon diversity in aged mice to levels similar to those in adult mice (Figure 4.7H). This was associated with the detection of bacterial species and families which were not identified in samples from aged mice prior to co-housing (Figure 4.7I, J), including the species *Bacteroides acidifaciens* and *Lactobacillus gasseri* (Table 4.2). This rescue of the diminished PP GC reaction in BALB/c mice was replicated in 22-month-old C57BL/6 mice upon co-housing with 3-month-old adult mice (Figure 4.8A-F). In C57BL/6 mice, co-housing led to reciprocal microbiota transfer between adult and aged mice, perhaps because there is no age-associated reduction in bacterial diversity in C57BL/6 mice (Figure 4.8G, H). Co-housing was associated with a trend for increased bacterial diversity in mice of both ages, although this was not significantly different (Figure 4.8H). Taken together, these data suggest that the poor PP GC reaction in aged mice can be rescued by the acquisition of the microbiota from younger animals. The rescue of the GC reaction in aged mice occurred independently of genetic background, and there was no overlap between the bacterial families significantly changed by age or co-housing between BALB/c and C57BL/6 mice (Figure 4.7J, Figure 4.8I, Table 4.2). This suggests that the co-housing-dependent increase of PP GC B cells in aged mice is not driven by a specific bacterial family, but is a response to a comprehensive change in the gut microbiome.

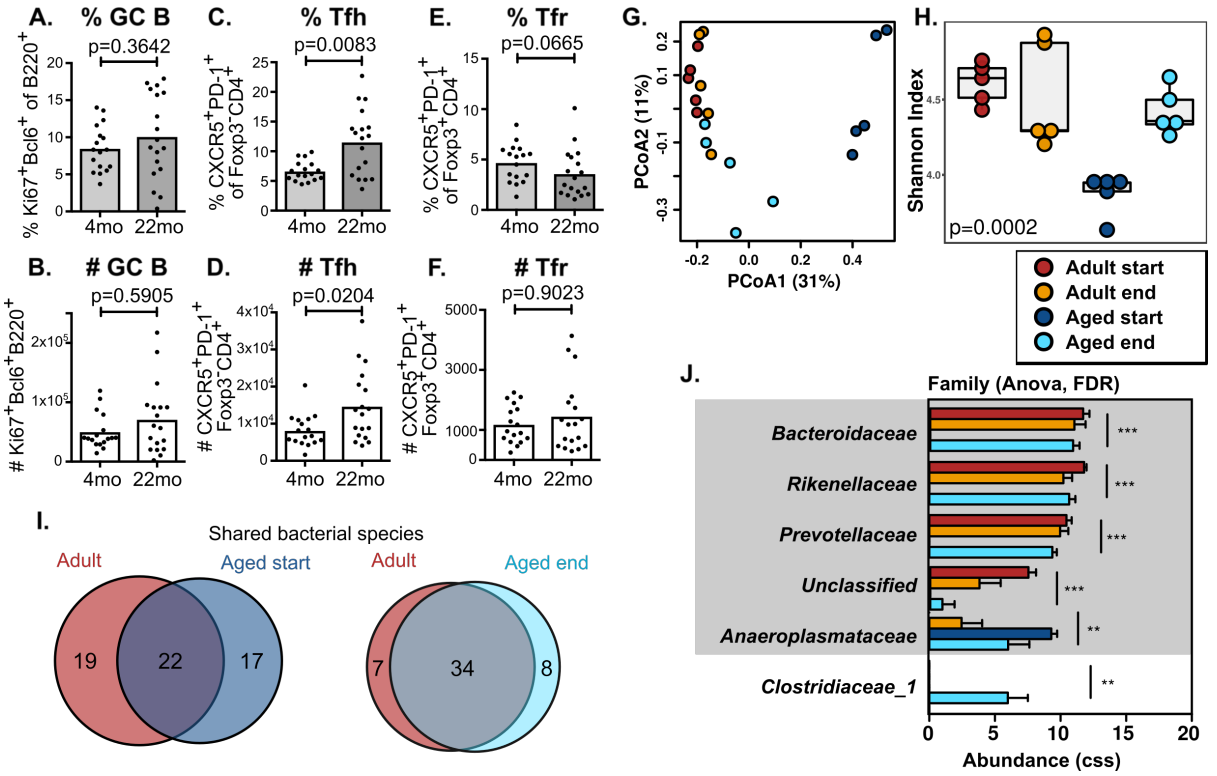

Figure 4.7: Co-housing boosts the germinal centre response in the Peyer's patches of aged BALB/c mice. Adult and aged female BALB/c mice were co-housed for 30-40 days, then Peyer's patch (PP) germinal centre (GC) cell populations were analysed by flow cytometry. The percentage and number of $B220^{+}Ki67^{+}Bcl6^{+}$ GC B cells **(A, B)**, $CD4^{+}Foxp3^{-}CXCR5^{+}PD\text{-}1^{+}$ Tfh cells **(C, D)** and $CD4^{+}Foxp3^{+}CXCR5^{+}PD\text{-}1^{+}$ Tfr cells **(E, F)** in Peyer's patches. **(G-J)** 16S rDNA sequencing data were generated from faecal pellets collected from 5 adult and 5 aged BALB/c mice at the start and end of co-housing (n=5 mice per group). Samples were clustered by Bray-Curtis PCoA **(G)** and bacterial diversities were measured by the Shannon index **(H)**. The overall *p*-value was based on ANOVA tests. **(I)** Venn diagrams showing the numbers of shared and unique bacterial species detected in both age groups of mice before co-housing and after co-housing. **(J)** Depiction of bacterial families whose abundance was significantly different between co-housed BALB/c mice as determined by ANOVA analysis after cumulative-sum scaling (CSS). *FD $\leq$ 0.05, **FDR $\leq$ 0.01, ***FDR $\leq$ 0.001. Families previously found to be significantly decreased in aged *versus* adult BALB/c mice before co-housing are marked in grey. In **(A-F)** bar plots show the combined results of 2 independent experiments with a total of n = 17-18 mice per group. Bar height corresponds to the mean, and each circle represents one biological replicate. *P*-values were determined using the Mann-Whitney test in GraphPad Prism6. This figure was published in Nature Communications (Stebegg *et al.* 2019).

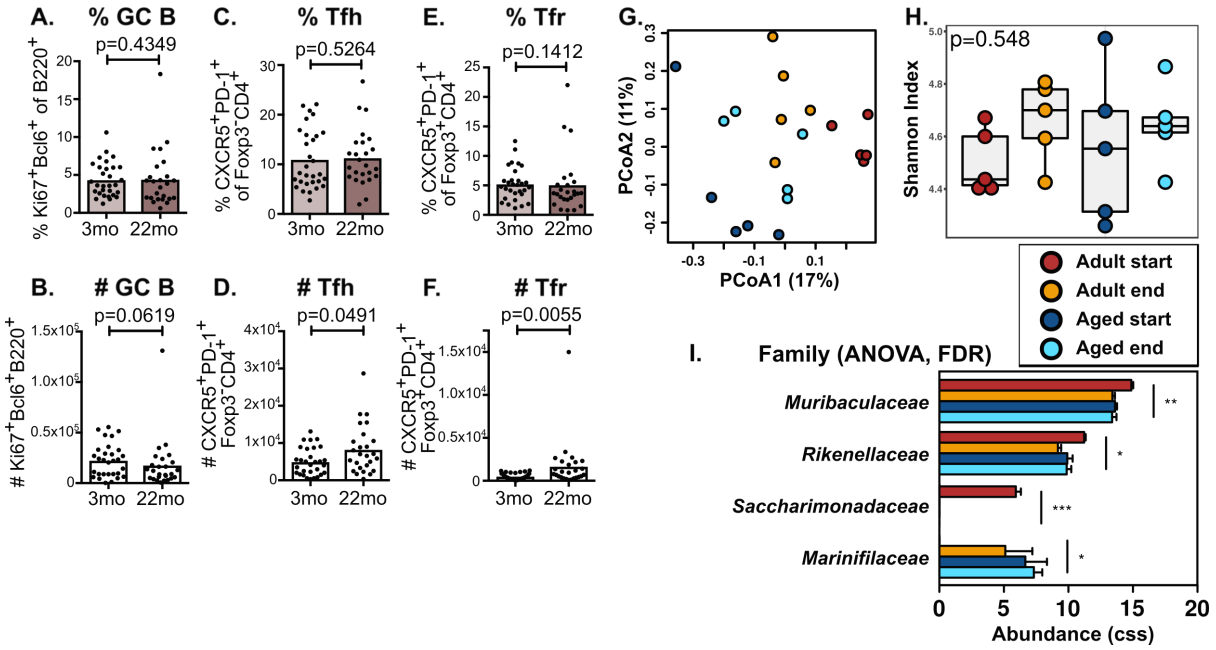

Figure 4.8: Co-housing boosts the germinal centre response in the Peyer's patches of aged C57BL/6 mice. (A-F) Adult and aged female C57BL/6 mice were co-housed for 30-40 days, then Peyer's patch (PP) germinal centre (GC) cell populations were analysed. The percentage and number of $B220^{+}Ki67^{+}Bcl6^{+}$ GC B cells **(A, B)**, $CD4^{+}Foxp3^{-}CXCR5^{+}PD\text{-}1^{+}$ Tfh cells **(C, D)** and $CD4^{+}Foxp3^{+}CXCR5^{+}PD\text{-}1^{+}$ Tfr cells **(E, F)** in Peyer's patches as quantified by flow cytometry. 16S rDNA sequencing data were generated from faecal pellets collected from 5 adult 3-month-old and 5 aged C57BL/6 mice before (start) and after (end) co-housing. Bray-Curtis PCoA **(G)** and Shannon diversities **(H)** of samples collected from adult and aged C57BL/6 mice. The overall *p*-value was based on ANOVA testing. **(I)** Depiction of bacterial families whose abundance was significantly different between co-housed C57BL/6 mice as determined by ANOVA analysis after cumulative-sum scaling (CSS). *FDR≤ 0.05, **FDR ≤ 0.01, ***FDR ≤ 0.001. In **(A-F)** bar plots show the combined results of 2 independent experiments with a total of n = 25-30 mice per group. Bar height corresponds to the mean, each circle represents one biological replicate. *P*-values were determined using the Mann-Whitney test in GraphPad Prism6. This figure was published in Nature Communications (Stebegg *et al.* 2019).

BALB/c: Cohousing group comparison			***P*-value (Tukey's test)**				**Mean Abundance**			
Taxa (Species)	**FDR**	**F**	**23mo start-23mo end**	**3mo start-23mo end**	**3mo start-23mo start**	**3mo start-3mo end**	**23mo start**	**23mo end**	**3mo**	**3mo end**
Alistipes_uncultured_bacterium	1.60E-13	410	3.30E-14	1	3.20E-14	0.43	0	9.6	9.6	9.13
Prevotellaceae_UCG001_uncultured_bacterium	2.70E-12	260	1.20E-12	0.97	9.10E-13	0.98	0	9.07	9.2	9.42
Bacteroides_Bacteroides_acidifaciens	**1.80E-10**	**140**	**3.70E-11**	**0.82**	**8.00E-11**	**1**	**0**	**10.07**	**9.5**	**9.48**
Lactobacillus_Lactobacillus_gasseri	**0.00012**	**21**	**0.000012**	**0.0039**	**0.034**	**0.029**	**0**	**10.01**	**4.2**	**8.62**
Bacteroides_Bacteroides_caecimuris	0.00064	16	0.00016	0.99	0.000097	0.49	0	7.25	7.5	5.75
Anaeroplasma_uncultured_bacterium	0.001	14	0.14	0.0091	0.000095	0.49	9.47	5.85	0	2.28
Lachnospiraceae_UCG001_uncultured_bacterium	0.0018	12	0.0085	0.29	0.00022	0.88	8.1	2.66	0	1.08
Rikenellaceae_RC9_gut_group_uncultured_organis	0.0025	11	0.025	0.087	0.00015	0.022	0	4.68	8.4	3.64
GCA900066575_uncultured_bacterium	0.014	7.8	0.12	0.00097	0.11	0.12	3.73	0	7.5	3.77
C57BL/6: Cohousing group comparison										
Parasutterella_Burkholderiales_bacterium_YL45	6.2E-08	78	0.53	1	1.1E-08	0.44	2.4E-09	1.4E-08	7.9	7.16
Ruminococcaceae_UCG014_uncultured_bacterium	0.006	12	0.24	0.94	0.00023	0.51	0.012	6.9E-04	2.5	0
Parasutterella_uncultured_organism	0.087	5.8	1	1	0.017	1	0.017	0.017	0	0
unclassified_bacterium_uncultured_bacterium	0.087	5.8	0.62	0.65	0.005	1	0.057	0.052	12.	12.2
Lachnospiraceae_UCG006_uncultured_bacterium	0.087	5.8	0.012	0.047	0.86	0.9	0.055	0.19	0	5.7
Odoribacter_uncultured_bacterium	0.087	5.7	0.99	0.74	0.0095	0.9	0.018	0.07	6.2	6.83
Mucispirillum_Mucispirillum_schaedleri_ASF457	0.18	4.5	0.29	0.88	0.11	0.085	0.94	0.028	2.3	5.81
Ruminiclostridium_5_Ruminiclostridium_sp._KB18	0.31	3.6	0.91	0.16	0.047	0.44	0.16	0.9	3.2	4.23
Bacteroidales_uncultured _Bacteroidales_bacterium	0.44	2.9	0.72	0.54	0.46	0.11	0.089	1	8.9	9.44

Table 4.2: Co-housing leads to species-level changes in the gut microbiome of BALB/c and C57BL/6 mice. 3-month-old and 23-month-old BALB/c and C57BL/6 mice were co-housed for 30-40 days, then the gut microbiome was analysed by 16S rDNA sequencing. The table generated in Calypso lists the overall false discovery rate (FDR)-adjusted *p*-values and F value for the top 9 species with the lowest FDR value. Tukey's tests were used to calculate *p*-values for group-to-group comparisons. The table also lists the mean abundance for each species in each group after cumulative-sum scaling (CSS). This table was adapted from Stebegg *et al.* (Stebegg *et al.* 2019).

4.3.4 Heterochronic FMT boosts the GC in PPs

To investigate whether the induction of the GC reaction during co-housing was solely dependent on direct transmission of gut microbiota, I conducted faecal microbiota transplantation (FMT) experiments in which recipient mice were given a suspension of faecal pellets from donor mice by oral gavage. The cages were also supplemented with fresh faecal pellets and dirty bedding from donor mice for three weeks (Figure 4.9A, H). First, I gavaged 22-month-old C57BL/6 mice with faecal pellets from 3-month-old adult mice (Figure 4.9A). Twenty-three days after this treatment, there was an increase in GC B cell numbers in aged mice (Figure 4.9B, C). I also observed a trend towards increased Tfh cells in aged mice (Figure 4.9D, E) and a significant increase in their Tfr cell numbers (Figure 4.9F, G). To determine whether the boost in the GC reaction by FMT is exclusive to aged mice, 3-month-old C57BL/6 mice were gavaged with faecal pellets from 22-month-old adult mice (Figure 4.9H). For this experiment C57BL/6 mice were used because I had evidence of reciprocal microbial transfer between adult and aged mice of this strain during co-housing: this result indicated that the gut microbiome of both adult and aged C57BL/6 mice is receptive to microbial transfer and presented us with a tool to assess whether the transfer of a new microbiome generally enhances the GC reaction irrespective of age, or if it constitutes a unique feature in aged mice. FMT of younger adult mice with faecal pellets from aged mice led to an increase in GC B as well as Tfh cells, while Tfr cell numbers were not affected (Figure 4.9I-N). This demonstrates that the GC reaction in PPs is highly sensitive to changes in the gut microbiome irrespective of age. Furthermore, the boost of the PP GC reaction appears to be independent of the transfer of a specific bacterial family or species, since FMT enhanced the response in both adult and aged recipients.

To determine whether FMT can rescue the PP GC reaction in aged mice of another strain, we performed FMT experiments in 22-month-old BALB/c mice (experimental set-up as in Figure 4.9A). GC B and Tfh cells had significantly expanded in 22-month-old mice 23 days after FMT compared to PBS-treated control mice (Figure 4.10A-D), but Tfr cells were not changed by FMT treatment (Figure 4.10E, F). Bacterial 16S rDNA sequencing confirmed the successful establishment of an “adult” microbiome in 22-month-old mice by FMT (Figure 4.10G), with a slight increase in gut microbial diversity in aged mice receiving FMT (Figure 4.10H). This included the presence of bacterial species that were originally not detected in aged mice (Figure 4.10I). Thus, microbial transfer is sufficient to restore the defective GC reaction in aged mice. Our data demonstrate that, even though the GCs in PPs diminish during ageing, this age-associated phenotype is not cell-intrinsic and can be rescued by stimulation from the gut microbiome.

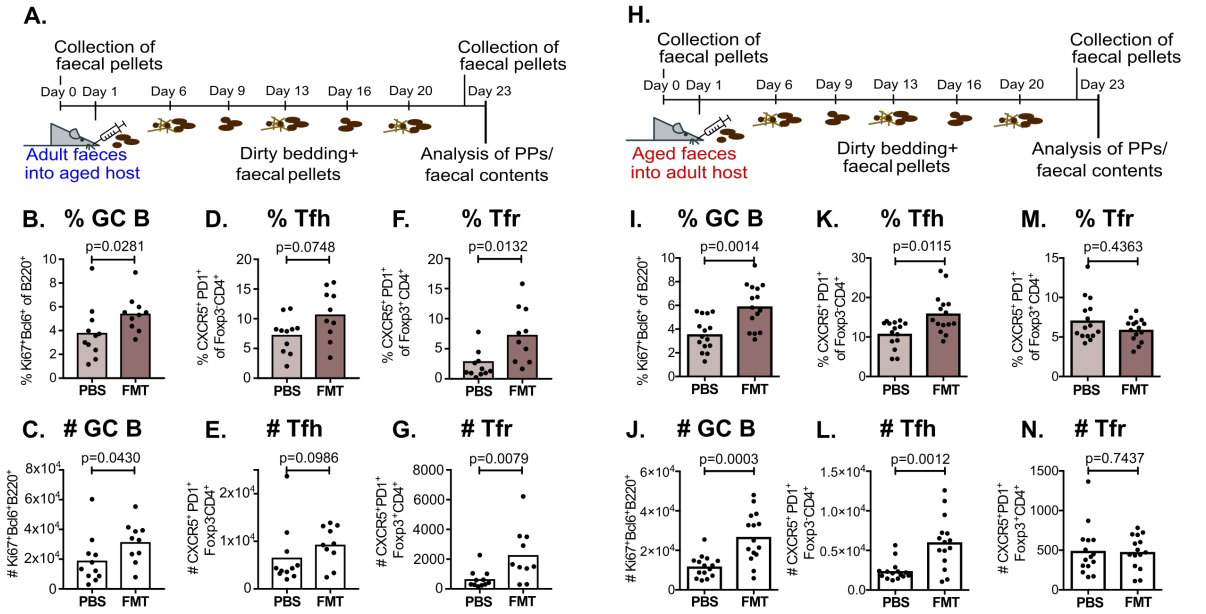

Figure 4.9: Faecal microbiota transplantation (FMT) boosts the germinal centre (GC) response in Peyer's patches irrespective of age. (A-G) 21-month-old C57BL/6 males were gavaged with faecal pellets from adult, 3-month-old mice. **(A)** Experimental outline of FMT where aged C57BL/6 males were given a suspension of faecal pellets from adult C57BL/6 donor mice by oral gavage. The cages of recipient mice were supplemented with fresh faecal pellets and dirty bedding from these donor mice once a week. The percentage and number of $B220^{+}Ki67^{+}Bcl6^{+}$ GC B cells **(B, C)**, $CD4^{+}Foxp3^{-}CXCR5^{+}PD\text{-}1^{+}$ Tfh cells **(D, E)** and $CD4^{+}Foxp3^{+}CXCR5^{+}PD\text{-}1^{+}$ Tfr cells **(F, G)** in Peyer's patches as quantified by flow cytometry. **(H-N)** 3-month-old C57BL/6 males were gavaged with faecal pellets from aged 21-month-old mice. **(H)** Experimental outline of FMT where adult C57BL/6 males were gavaged with faecal pellets from aged mice. The percentage and number of GC B **(I, J)**, Tfh **(K, L)** and Tfr **(M, N)** cells were quantified by flow cytometry. Bar height corresponds to the mean, each circle represents one biological replicate. Bar plots show the combined results of 2 independent experiments with a total of n = 10-15 mice per group. *P*-values were determined using the Mann-Whitney test in GraphPad Prism6. This figure was published in Nature Communications (Stebegg *et al.* 2019).

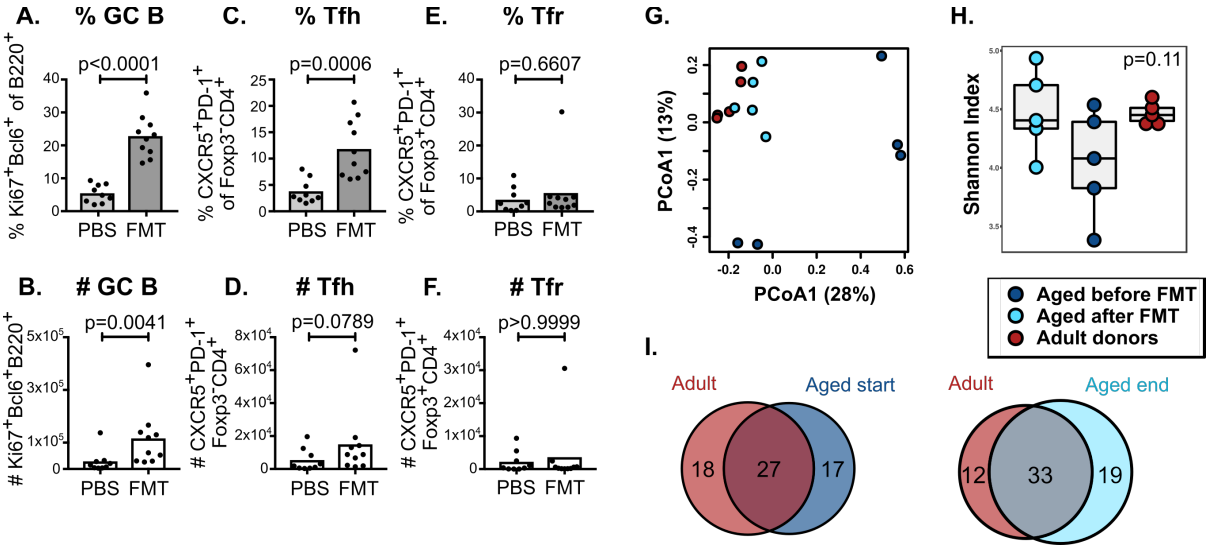

Figure 4.10: Faecal microbiota transplantation (FMT) boosts the germinal centre (GC) response in the Peyer's patches of aged BALB/c mice. 21-month-old BALB/c mice were given a suspension of faecal pellets taken from 3-month-old mice by oral gavage. The cages of aged recipients were supplemented with fresh faecal pellets and dirty bedding from these donors once a week. **(A-F)** Bar plots show the combined results of 2 independent experiments. The percentage and number of $B220^{+}Ki67^{+}Bcl6^{+}$ GC B cells **(A, B)**, $CD4^{+}Foxp3^{-}CXCR5^{+}PD\text{-}1^{+}$ Tfh cells **(C, D)** and $CD4^{+}Foxp3^{+}CXCR5^{+}PD\text{-}1^{+}$ Tfr cells **(E, F)** in Peyer's patches as quantified by flow cytometry. Bar height corresponds to the mean, each circle represents one biological replicate. Bar plots show the combined results of 2 independent experiments with a total of n = 9-10 mice per group. *P*-values were determined using the Mann-Whitney test in GraphPad Prism6. **(G-I)** 16S rDNA sequencing data were generated from faecal pellets collected from 5 adult donor mice and 5 aged BALB/c mice before and after FMT. **(G)** Bray-Curtis PCoA of FMT samples. **(H)** Shannon diversities with an overall *p*-value generated from ANOVA tests. **(I)** Venn diagrams showing the numbers of shared and unique bacterial species detected in adult donor mice and aged mice before FMT (start; left) or after FMT (end; right). This figure was published in Nature Communications (Stebegg *et al.* 2019).

4.3.5 Cross-strain FMT does not enhance the GC

The boost of the GC reaction by heterochronic faecal transplantation in both adult and aged mice suggests that alterations in the microbiome can enhance the GC reaction in PPs. To determine whether this occurs independently of an age mismatch between the donor and the recipient, I performed FMT from 3-month-old BALB/c mice into 3-month-old C57BL/6 mice (experimental set-up as in Figure 4.9A). This approach was chosen as there are differences in the microbiome between these two strains (Figure 4.11A), and adult BALB/c mice have a higher bacterial diversity than C57BL/6 mice (Figure 4.11B). Twenty-three days after FMT, there was no increase in the percentage or number of GC B cells, Tfh cells or Tfr cells in C57BL/6 mice that received FMT compared to the PBS-treated controls (Figure 4.11C-H). This suggests that the GC reaction in PPs responds specifically to heterochronic faecal transplantation.

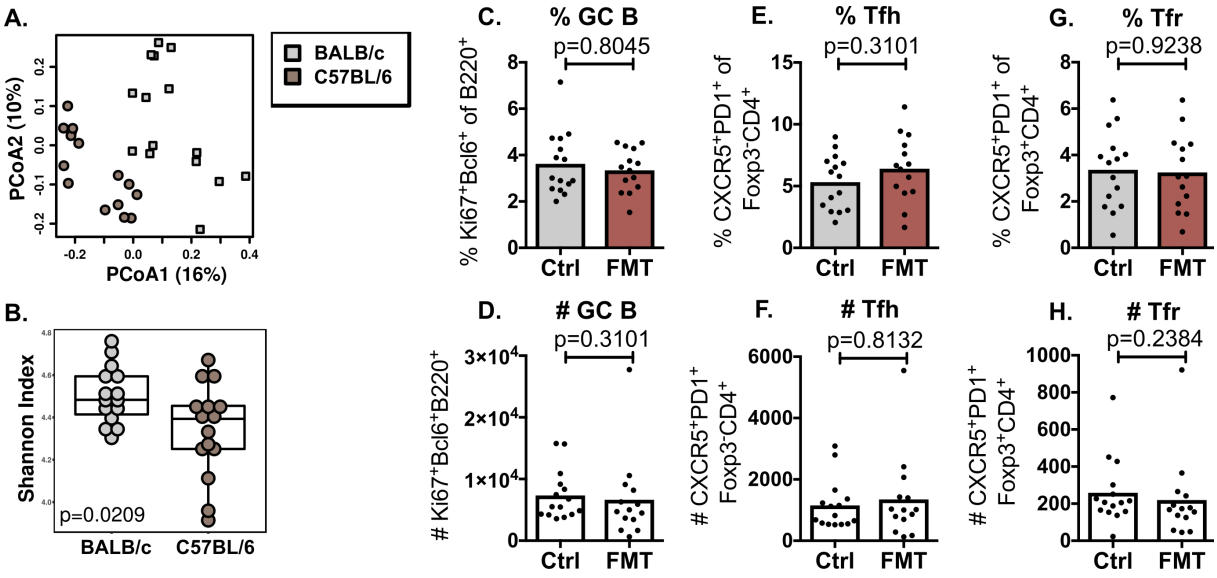

Figure 4.11: Faecal microbiota transplantation (FMT) between adult mice of different strains does not affect the germinal centre (GC) response in Peyer's patches. (A, B) 16S rDNA sequencing data generated from faecal pellets collected from adult 3-month-old C57BL/6 and BALB/c mice. **(A)** Bray-Curtis PCoA comparing samples from 3-month-old BALB/c and C57BL/6 mice. **(B)** Shannon diversities, with a *p*-value based on ANOVA tests. **(C-H)** Three-month-old C57BL/6 mice were given a suspension of faecal pellets taken from 3-month-old BALB/c mice by oral gavage to achieve FMT. In addition, the cages of C57BL/6 recipients were supplemented with fresh faecal pellets and dirty bedding from BALB/c mice once a week. Control mice were gavaged with PBS. The percentage and number of $B220^+Ki67^+Bcl6^+$ GC B cells **(C, D)**, $CD4^+Foxp3^-CXCR5^+PD\text{-}1^+$ Tfh cells **(E, F)** and $CD4^+Foxp3^+CXCR5^+PD\text{-}1^+$ Tfr cells **(G, H)** in Peyer's patches as quantified by flow cytometry. Bar plots show the combined results of two experiments with a total of n = 14-15 mice per group. Bar height corresponds to the mean, each circle represents one biological replicate. *P*-values were determined using the Mann-Whitney test in GraphPad Prism6. This figure was published in Nature Communications (Stebegg *et al.* 2019).

4.3.6 IgA-mediated control of the microbiome is not affected by ageing or FMT

Our data indicated that the composition of the gut microbiome has a dominant effect on the immune response in PPs. The question remained whether a diminished GC response in PPs would also affect the gut microbiome? PPs have been reported to control the gut microbiome by giving rise to plasma and memory B cells secreting IgA antibodies that bind to commensals with high affinity, but IgAs can also be produced in the *lamina propria* in a GC-independent manner (Reboldi & Cyster 2016). The reduction of GC B cells I observed in aged mice was not associated with reduced levels of commensal IgA-coating in the ileum or colon of BALB/c of C57BL/6 mice (Figure 4.12A-G). Both cohousing and FMT boosted the GC response, still there was no change in the levels of bacterial IgA-coating (Figure 4.12H-K, Figure 4.13J-M). FMT did not affect the levels of PP-resident IgA^+ B cells or free intestinal IgA in both mouse strain either (Figure 4.13A-I). This suggests that IgA-mediated control of the gut microbiome is not affected by changes in the GC response in aged mice and made us question whether GC-derived IgA antibodies are indeed a major contributor to the control of the commensal microbiota.

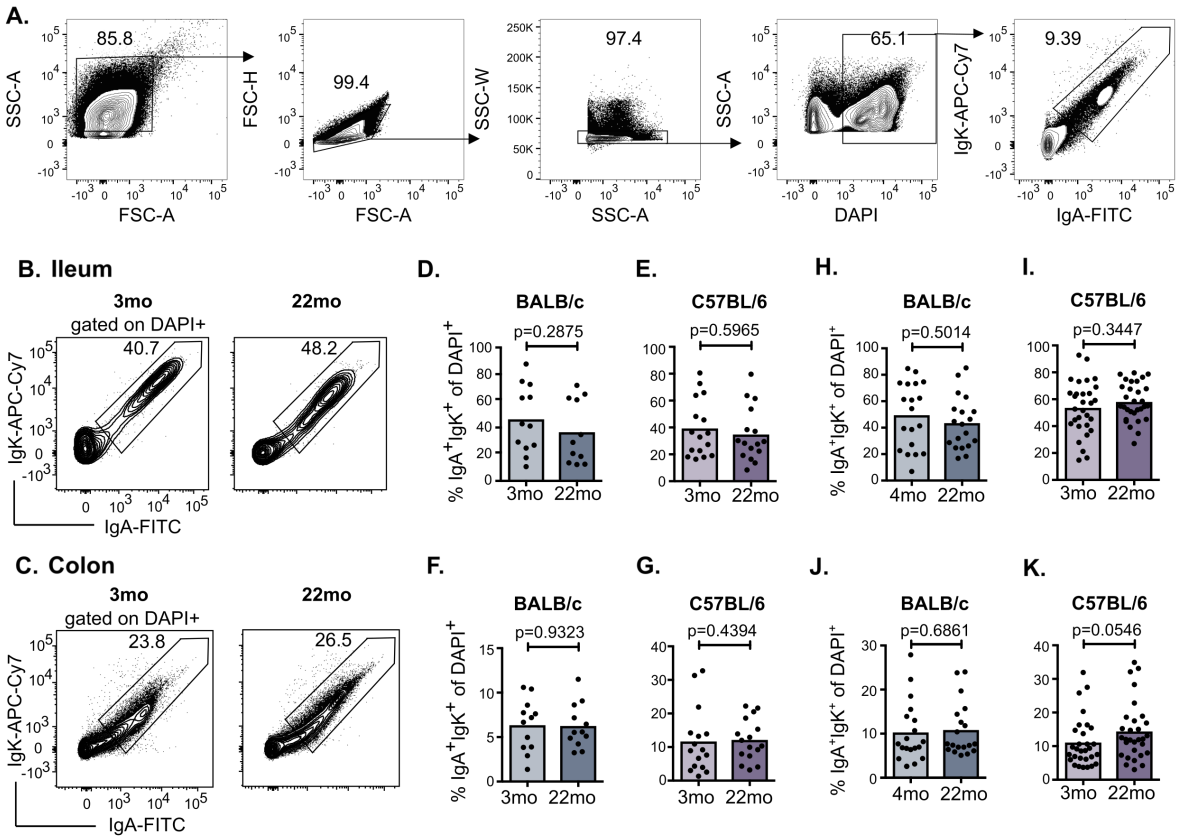

Figure 4.12: IgA-coating of faecal bacteria is not affected by ageing or cohousing. (A-G) Bacterial IgA-coating was assessed in adult (3-month-old; 3mo) and aged (22-month-old; 22mo) mice. **(A)** Gating strategy for IgA-coated bacteria. **(B, C)** Representative flow cytometric plots of IgA-coated faecal bacteria isolated from the ileum **(B)** and colon **(C)** of BALB/c mice. **(D-G)** Quantitation of IgA-coating of bacteria in faecal contents isolated from the ileum **(D, E)** and colon **(F, G)** of adult and aged BALB/c **(D, F)** and C57BL/6 **(E, G)** mice. Bar plots show the combined results of 2-4 independent experiments with a total of n = 11-16 mice per group. **(H-K)** Bacterial IgA-coating was assessed in adult (3-4-month-old; 3mo/4mo) and aged (22-month-old; 22mo) mice after co-housing for 40 days. Quantitation of IgA-coating of bacteria in faecal contents isolated from the ileum **(H, I)** and colon **(J, K)** of cohoused BALB/c **(H, J)** and C57BL/6 **(I, K)** mice. Bar plots show the combined results of 2-4 independent experiments with a total of n = 19-30 mice per group. Bar height corresponds to the mean, and each circle represents one biological replicate. *P*-values were determined using the Mann-Whitney test in GraphPad Prism6. This figure was adapted from Stebegg *et al.* (Stebegg *et al.* 2019).

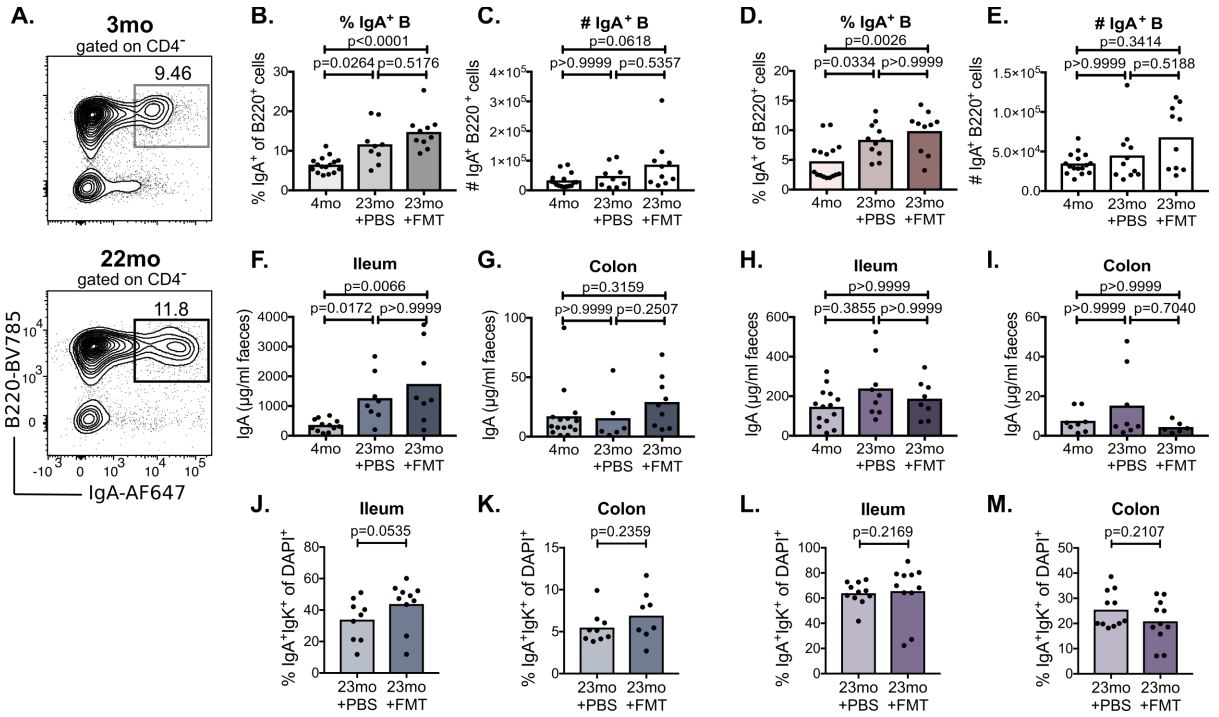

Figure 4.13: Faecal microbiota transplantation (FMT) does not affect gut IgA responses. 21-month-old mice were given a suspension of faecal pellets taken from 3-month-old mice by oral gavage. The cages of these aged recipients were supplemented with fresh faecal pellets and dirty bedding from adult donors once a week. A control group received PBS by oral gavage. After 3 weeks, intestinal IgA levels were assessed in adult donor mice (4mo), aged control mice (23mo+PBS) and aged mice receiving FMT (23mo+FMT). **(A)** Representative flow cytometric plots for IgA^+ B cells ($CD4^-B220^+IgA^+$) cells in the Peyer's patches (PPs) of adult (3-month-old; 3mo) and aged (22-month-old; 22mo) BALB/c mice. **(B-E)** Quantitation of IgA^+ B cells in percentage **(B, D)** and cell numbers **(C, E)** in BALB/c **(B, C)** and C57BL/6 **(D, E)** mice by flow cytometry. **(F-I)** Quantitation of free IgA in faecal contents isolated from the ileum **(F, H)** and colon **(G, I)** of BALB/c **(F, G)** and C57BL/6 **(H, I)** mice by ELISA. **(J-M)** Quantitation of IgA-coating of bacteria in faecal contents isolated from the ileum **(J, L)** and colon **(K, M)** of BALB/c **(J, K)** and C57BL/6 **(L, M)** mice. Bar plots show the combined results of two independent experiments with a total of n = 8-16 mice per group. Bar height corresponds to the mean, and each dot represents one biological replicate. *P*-values were determined using the Kruskal-Wallis test with Dunn's multiple testing correction in GraphPad Prism6. This figure was published in Nature Communications (Stebegg *et al.* 2019).

4.3.7 Reduction of PP GCs has a minimal impact on the gut microbiome

Previous studies described normal levels of intestinal IgA and commensal IgA-coating in T cell-deficient mice, suggesting that commensal-specific IgA can be produced in a GC-independent manner (Bergqvist *et al.* 2006; Bunker *et al.* 2015; Gärdby *et al.* 2003). To test this, I compared the microbiomes of *Bcl6*$^{fl/fl}$*Cd4*$^{cre/+}$ mice, which do not form GCs due to a failure of Tfh cell differentiation, with their *Bcl6*$^{fl/fl}$*Cd4*$^{+/+}$ littermates that were housed in the same cages (Hollister *et al.* 2013). PPs from *Bcl6*$^{fl/fl}$*Cd4*$^{cre/+}$ mice completely lacked Tfh and Tfr cells and had very few GC B cells (Figure 4.14A-F). This was associated with a significant reduction of IgA^{+} B cells in their PPs (Figure 4.14G-H). However, this did not affect commensal IgA-coating in the ileum (Figure 4.14I), suggesting that gut bacteria are primarily coated by IgA antibodies derived from the *lamina propria*. Unexpectedly, IgA-coating in the colon, where no PPs can be found, was increased in *Bcl6*$^{fl/fl}$*Cd4*$^{cre/+}$ mice (Figure 4.14J), possibly due to augmented IgA production in the *lamina propria* compensating for the loss of GC-derived IgA antibodies.

16S rDNA sequencing revealed only minor differences in microbial composition of the ileum and colon of *Bcl6*$^{fl/fl}$*Cd4*$^{cre/+}$ and their co-housed *Bcl6*$^{fl/fl}$*Cd4*$^{+/+}$ littermates (Figure 4.14K-Q). PCA of all 16S rDNA sequencing samples indicated that the source organ was the biggest driver of variation (Figure 4.14K). Separate analysis of the samples from the ileum and colon did not reveal clustering of samples by genotype (Figure 4.14L, M), and no differences in bacterial diversity between genotype groups was observed (Figure 4.14N, O). In our experiments, gender had a stronger effect on clustering in the PCA plots than the lack of GCs (Figure 4.14L, M). This indicates that GC-derived IgA is not required for the regulation of overall gut microbial composition. However, *Deltaproteobacteria* and *Bacteroidia* were significantly underrepresented in the ileum of *Bcl6*$^{fl/fl}$*Cd4*$^{cre/+}$ mice at the class level (Figure 4.14P). On the genus level, only one bacterial taxa was found to be significantly affected by the lack of GCs: *Candidatus Arthromitus*, a group of segmented filamentous bacteria (SFB) (Figure 4.14P) (Snel *et al.* 1995). This was also different between genotypes in the colon (Figure 4.14Q). Thus, the increase in bacterial IgA-coating observed in the colon of *Bcl6*$^{fl/fl}$*Cd4*$^{cre/+}$ mice does not result in global restructuring of the gut microbiome. Instead, the lack of GCs in PPs affects one species of SFBs. These data suggest that GC-derived IgA antibodies play a minor role in the control of the commensal microbiome. The microbiome, by contrast, is a potent regulator of the GC response in PPs.

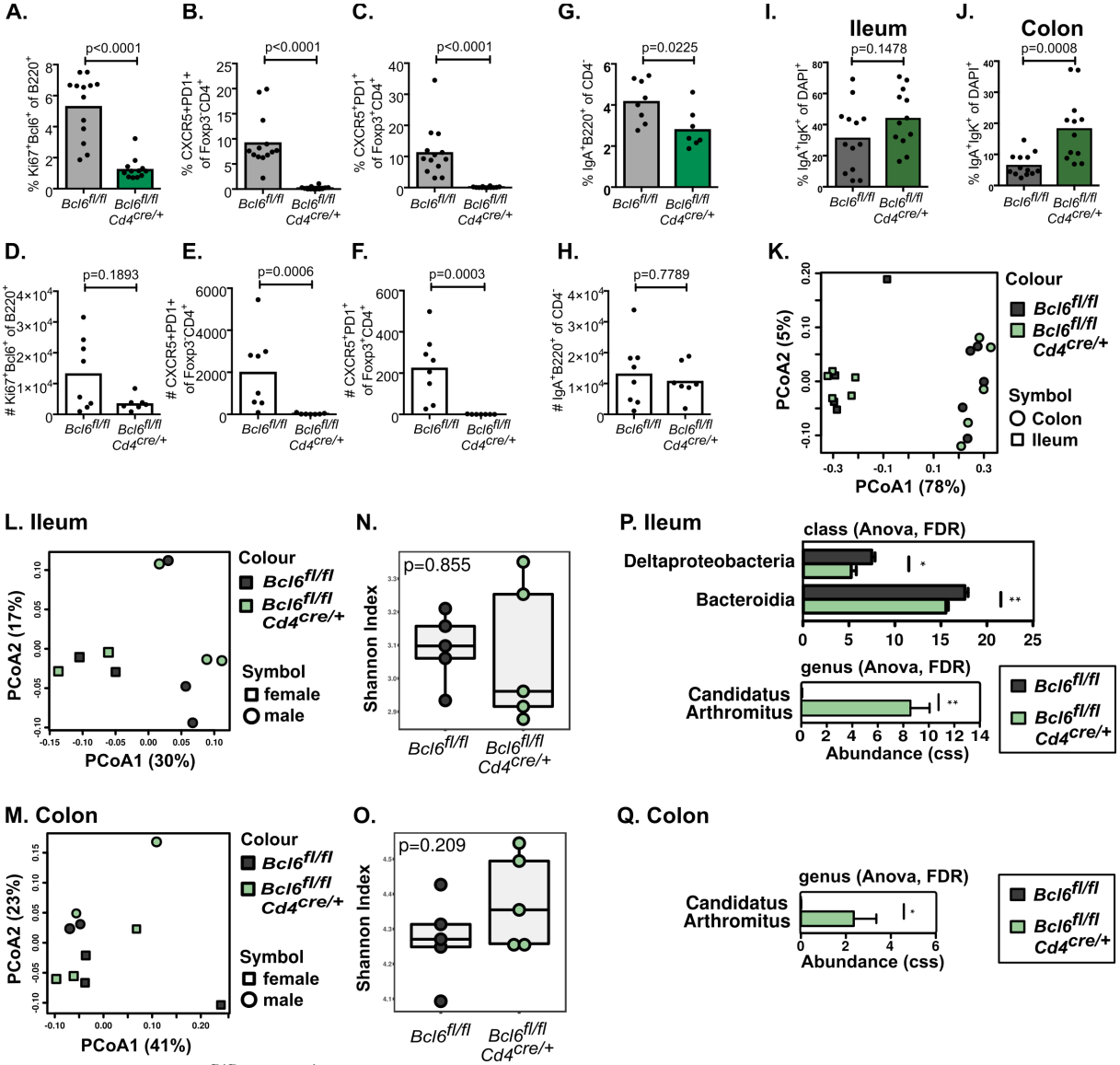

Figure 4.14: *Bcl6*$^{fl/fl}$*Cd4*$^{cre/+}$ mice have reduced germinal centre (GC) responses but a near-to-normal gut microbiome. (A-J) Characterisation of GC cell populations in the Peyer's patches (PPs) and IgA-coating of faecal bacteria in *Bcl6*$^{fl/fl}$*Cd4*$^{cre/+}$ mice and their littermate controls. The percentage and number of B220$^+$Ki67$^+$Bcl6$^+$ GC B cells **(A, B)**, CD4$^+$Foxp3$^-$CXCR5$^+$PD-1$^+$ Tfh cells **(C, D)** and CD4$^+$Foxp3$^+$CXCR5$^+$PD-1$^+$ Tfr cells **(E, F)** in Peyer's patches (PPs) as quantified by flow cytometry. **(G, H)** Quantitation of IgA$^+$ B cell percentages **(G)** and numbers **(H)** in the PPs of *Bcl6*$^{fl/fl}$*Cd4*$^{cre/+}$ mice. Quantitation of IgA-coating of bacteria in faecal contents isolated from the ileum **(I)** and colon **(J)**. Bar plots show the combined results of 2 independent experimental repeats with a total of n = 7-13 mice and each circle represents one biological replicate. Bar height corresponds to the mean, error bars to SD. *P*-values were determined using the Mann-Whitney test in GraphPad Prism6. **(K-Q)** 16S rDNA sequencing data were generated from the faecal contents of the colon and ileum collected from five *Cd4*$^{cre/+}$ *Bcl6*$^{fl/fl}$ mice and 5 littermate controls in two independent experiments. All samples **(K)**, or samples from the ileum **(L)** or colon **(M)** were clustered by Bray-Curtis PCoA. **(N, O)** Alpha diversities (measured by the Shannon index) of samples collected from the ileum **(N)** or colon **(O)** of *Bcl6*$^{fl/fl}$*Cd4*$^{cre/+}$ and *Bcl6*$^{fl/fl}$*Cd4*$^{+/+}$ mice. *P*-values are based on ANOVA tests. **(P, Q)** Depiction of bacterial clades whose abundance was found to be significantly different between genotypes in the ileum **(P)** and colon **(Q)** as determined by ANOVA analysis. *…FDR ≤ 0.05, **…FDR ≤ 0.01.

4.3.8 FMT does not enhance PP GC responses to cholera toxin

Even though GC-derived IgA antibodies might not be required to regulate commensal bacteria, they were shown to provide protection against intestinal pathogens (Hashizume *et al.* 2008) and oral tolerance (Fujihashi *et al.* 2001). To confirm a role of the GC response in PPs in the immune response to foreign antigen, I performed a pilot experiment, immunising *Bcl6*$^{fl/fl}$*Cd4*$^{cre/+}$ mice and their *Bcl6*$^{fl/fl}$*Cd4*$^{+/+}$ littermate controls with ovalbumin (OVA) in combination with cholera toxin (CTx), a strong mucosal immunogen, three times over the course of three weeks. PPs from CTx-treated *Bcl6*$^{fl/fl}$*Cd4*$^{cre/+}$ mice again had very few GC B cells, a decrease in the proportion of PP-resident IgA$^+$ B cells and a striking reduction in IgG1$^+$ B cells (Figure 4.15A-F). This was associated with the complete loss of OVA- and CTx-specific antibody responses in the serum and in the ileum, indicating that the GC response in PPs is indeed essential for mucosal antibody responses against foreign antigens (Figure 4.15G-J).

Kato *et al.* have previously linked the reduction of oral tolerance in aged mice with ageing-related changes in their PPs (Kato *et al.* 2003). Thus, the increase of intestinal infections in older individuals could be linked with an age-associated defect in their Peyer's patches (Kolling *et al.* 2012). To determine whether FMT can boost the immune response to foreign antigen in aged mice, I immunised 23-month-old C57BL/6 mice with CTx coupled to the hapten NP (NP-CTx) by oral gavage three times at weekly intervals, either with or without prior FMT from 3-month-old donors. Assessment of mucosal antibody responses in the faecal contents of the ileum showed that there was no difference in anti-CTx and anti-NP IgA titres between mice that received FMT and PBS controls (Figure 4.16A, B). Further, there was no difference in the titre of high-affinity anti-NP2 IgA or in the ratio of NP2/NP20 binding antibodies (Figure 4.16C, D), a measure of affinity maturation. Consistent with this, serum anti-CTx and anti-NP IgG1 antibody titres and affinity were not influenced by FMT in aged mice (Figure 4.16E-H). Assessment of the GC reaction in the PPs of these animals showed that immunisation with NP-CTx alone was sufficient to boost the GC response in 23-month-old animals independently of FMT, with no changes in Tfh or Tfr cell number (Figure 4.16I-N). This shows that FMT cannot enhance GC responses to immunisations with foreign antigen, but suggests the GC response in the PPs of aged mice can be induced by different immunological stimuli, such as microbial transfers or the strong immunogen CTx.

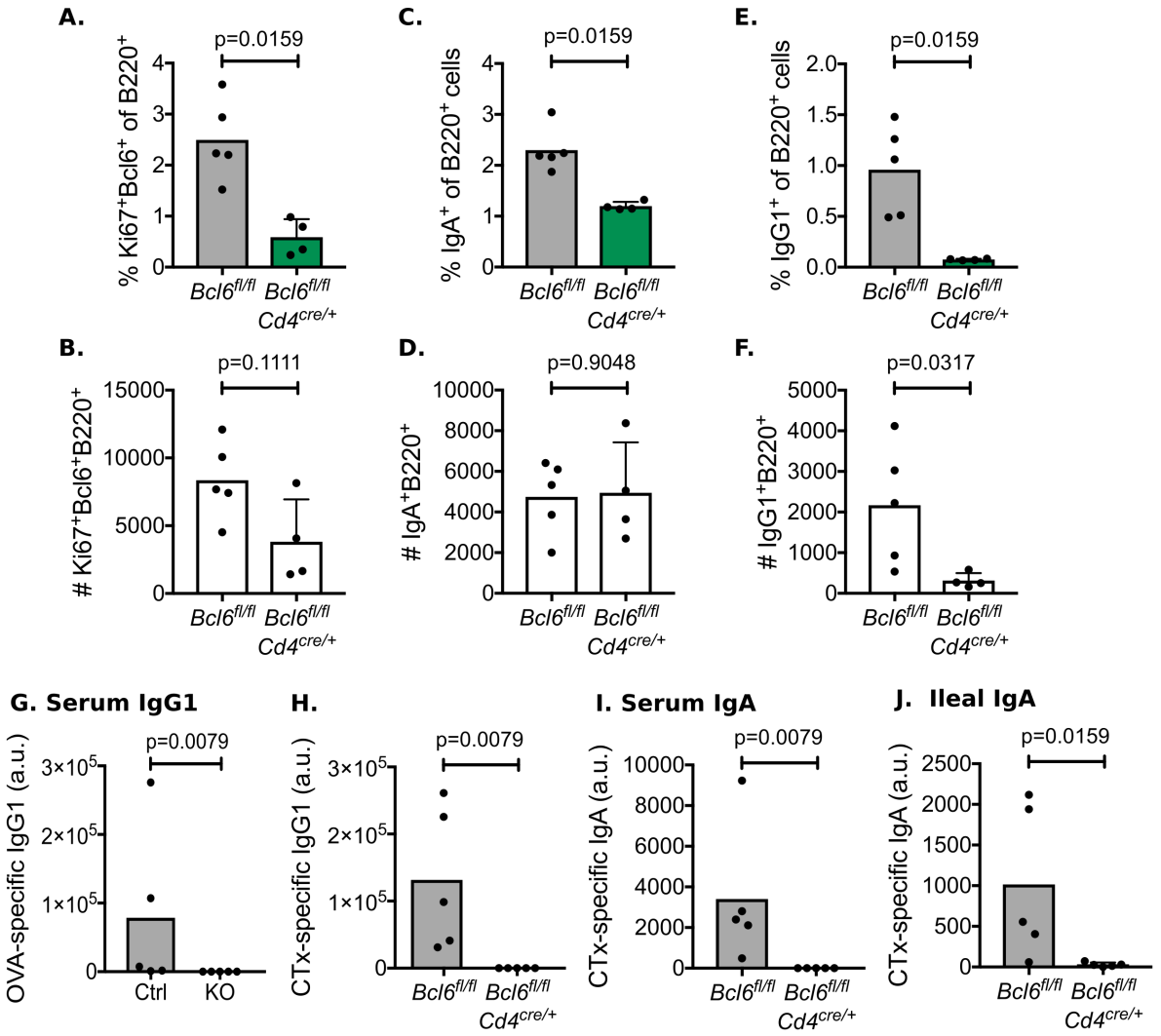

Figure 4.15: Tfh cells in Peyer's patches (PPs) are required for antibody responses to foreign antigen. *Bcl6*$^{fl/fl}$*Cd4*$^{cre/+}$ mice and their *Bcl6*$^{fl/fl}$*Cd4*$^{+/+}$ littermate controls were immunised with 1 mg OVA plus 50 µg CTx once a week for three weeks, then OVA- and CTx-specific antibody responses were assessed**. (A-F)** Quantitation of the percentage and number of B220^{+}Ki67^{+}Bcl6^{+} GC B cells **(A, B)**, IgA^{+} B cells **(C, D)** and IgG1^{+} B cells **(E, F)** in Peyer's patches (PPs) by flow cytometry. **(G-I)** OVA-specific **(G)** and CTx-specific **(H)** IgG1 as well as CTx-specific IgA levels were assessed in the serum by ELISAs. **(J)** CTx-specific IgA levels in faecal contents from the ileum were assessed by ELISA. No OVA-specific IgA antibodies could be detected in either *Bcl6*$^{fl/fl}$*Cd4*$^{cre/+}$ mice or *Bcl6*$^{fl/fl}$*Cd4*$^{+/+}$ littermate controls. Bar plots show the results of one experiment with n = 5 mice per group. Bar height corresponds to the mean, and each circle represents one biological replicate. *P*-values were determined using Mann-Whitney tests in GraphPad Prism6.

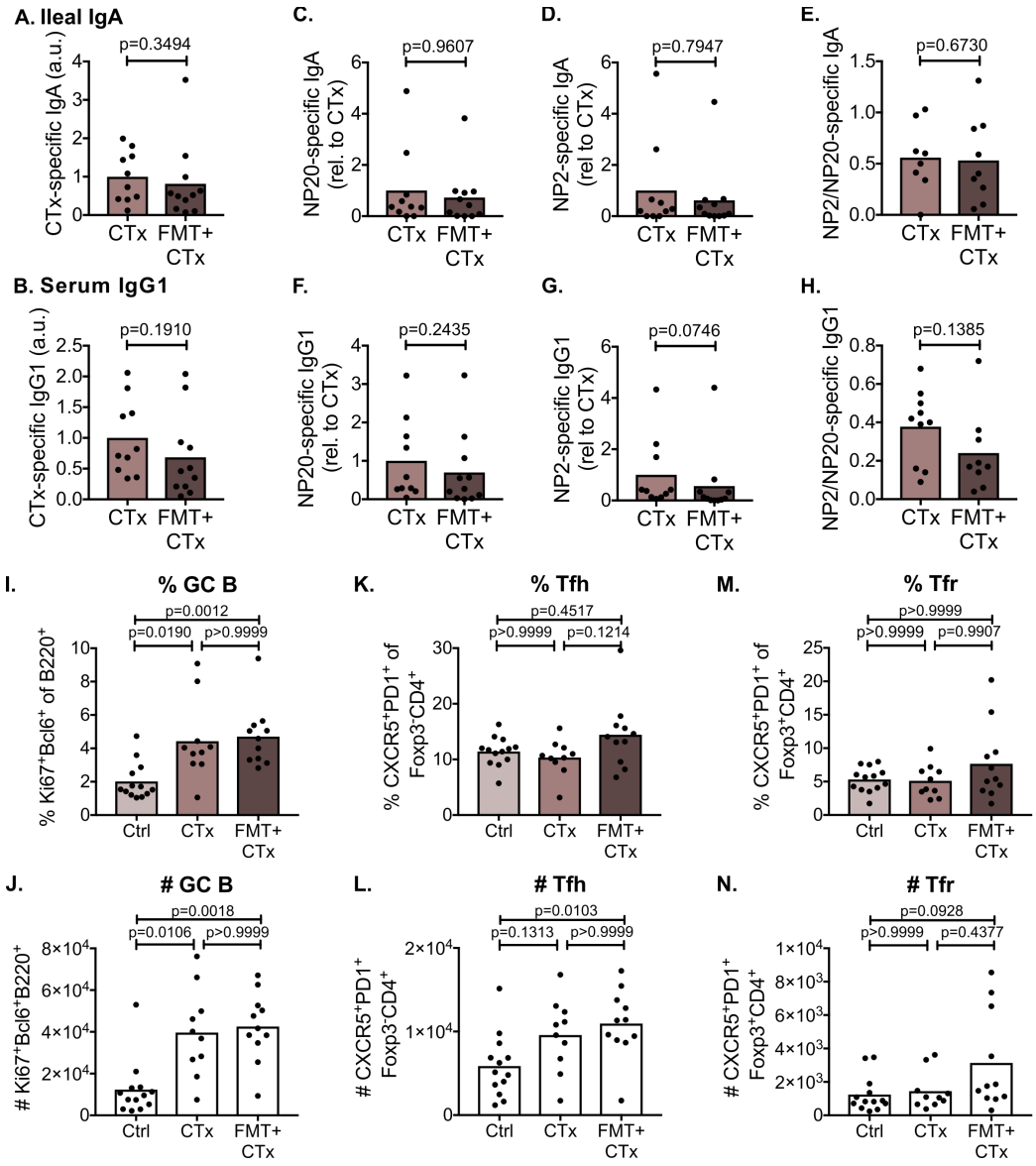

Figure 4.16: Faecal microbiota transplantation (FMT) does not enhance NP-CTx-specific immune responses in the gut. 21-month-old C57BL/6 mice received FMT or PBS by oral gavage as described above, followed by three oral immunisations with NP-CTx once a week**.** After three weeks, NP-CTx-specific antibody levels were analysed in PBS-gavaged, NP-CTx-immunised 23-months-old C57BL/6 mice (CTx) compared to aged mice receiving FMT plus NP-CTx (FMT+CTx). Peyer's patch (PP) germinal centre (GC) responses in these mice were compared to naïve, 23-month-old C57BL/6 mice (Ctrl). **(A-D)** Antigen-specific IgA levels against CTx **(A)** and NP **(B-D)** in faecal contents from the ileum were assessed by ELISA. NP20-specific IgA **(B),** high-affinity NP2-specific IgA **(C)** and the ratio of NP2-to-NP20-specific IgA antibodies **(D)** were used as a measure for affinity maturation. **(E-H)** Antigen-specific IgG1 levels against CTx **(E)** and NP **(F-H)** in the serum were assessed by ELISAs for CTx-specific IgG1 **(E),** NP20-specific IgG1 **(F),** high-affinity NP2-specific IgG1 **(G)** and the ratio of NP2-to-NP20-specific IgG1 antibodies **(H)**. **(I-N)** The percentage and number of $B220^+Ki67^+Bcl6^+$ GC B cells **(I, J)**, $CD4^+Foxp3^-CXCR5^+PD\text{-}1^+$ Tfh cells **(K, L)** and $CD4^+Foxp3^+CXCR5^+PD\text{-}1^+$ Tfr cells **(M, N)** in PPs were quantified by flow cytometry. Bar plots show the combined results of two independent experiments with a total of n = 10-13 mice per group. Bar height corresponds to the mean, and each circle represents one biological replicate. *P*-values were determined using Mann-Whitney tests **(A-H)** or the Kruskal-Wallis test with Dunn's multiple testing correction **(I-N)** in GraphPad Prism6. This figure was published in Nature Communications (Stebegg *et al.* 2019).

4.4 Discussion

The composition of the commensal gut flora changes with age. This linked with an increase in age-associated morbidities such as frailty (Claesson *et al.* 2012; Maffei *et al.* 2017) and intestinal disorders (Biagi *et al.* 2010), but the cause of this shift in the gut microbial composition is unknown. Here we sought to determine whether there is a causal link between age-dependent changes in the microbiome and the defective GC reaction in PPs of aged mice. I show that the diminished GC reaction in the PPs of aged mice can be rescued by co-housing with younger animals, as well as by transplantation of faecal microbiota from adult mice. These data demonstrate that the defective GC response in aged mice is not a cell-intrinsic feature of the ageing immune system and can be restored by replenishment of the microbiome or stimulation with CTx.

The ageing-related decline in the GC response in LNs has been linked to a decrease in the functions of multiple cell types, including antigen-presenting cells (APCs), T and B cells (Linterman 2014). However, it is not clear whether these age-associated defects are predominantly caused by accumulation of immune cell-intrinsic defects, or reduced stimulation of immune cells *via* their microenvironment (Weng 2006). Our data suggest that, in the PPs of aged mice, the capacity of GC B cells to respond to antigen is not impaired in a cell-intrinsic manner, but that they can respond to stimulation from the gut microbiota. Interestingly, the GC reaction in PPs was more strongly boosted following FMT than by co-housing. If the increase in magnitude of the GC response in aged mice is transient, this discrepancy could be explained by the duration of the different experiments, as we assessed the PPs GC reaction 23-days after FMT, and 30-40 days after the start of cohousing. The observation that not only microbial transfer, but also the potent mucosal immunogen CTx can stimulate the GC response in older animals indicates that the expansion of the GC reaction by FMT is not due to reactivation of commensal-specific memory B cells that persist in aged mice after their microbiome changes. Rather it suggests that strong immunogens, or potent adjuvants, can induce GC responses in the PPs of aged mice.

Despite smaller GCs in the PPs of aged mice, the levels of commensal IgA-coating are comparable between older mice and younger animals, indicating that sufficient IgA is produced by a compensatory mechanism. IgA antibodies can be generated in a T cell-independent fashion in the *lamina propria* or in a GC-dependent fashion in PPs (Pabst 2012). Elegant studies conducted by Fagarasan and co-workers suggested that GC-dependent IgA antibodies are essential for the maintenance of microbial homeostasis. They used mice lacking either Tfh- or Tfr-dependent control of their GCs (Kawamoto *et al.* 2012; 2014) or somatic hypermutation in GC B cells (Wei *et al.* 2011) to show that disruptions of the GC response in PPs leads to changes in the gut IgA repertoire

and in the gut microbial composition of these mice. What is more, Kubinak *et al.* suggested that Tfh cells in PPs are required to control the composition of the mucosa-resident gut microbiota in particular (Kubinak *et al.* 2015). However, other studies have shown that mice lacking T cell-dependent immune responses (CD28-deficient mice (Gärdby *et al.* 2003) and CD40-deficient mice(Bergqvist *et al.* 2006)) or Tfh cells ($Bcl6^{fl/fl}Cd4^{cre/+}$ (Bunker *et al.* 2015)) have high IgA antibody titres, near-to-normal levels of bacterial IgA-coating, and relatively normal microbial composition, despite the lack of a GC response. This suggests that GC-independent IgA is sufficient to control the gut microbiota. To investigate the role of the GC in controlling the microbiota, I studied mice that lack Tfh cells and therefore do not have a good GC response. I found that only the abundance of one species, a type of SFB, was altered in these mice, indicating that the GC is not required to control gut microbial homeostasis. This is consistent with the findings of Bunker *et al.,* who reported that IgA-coating of SFBs is T cell-dependent (Bunker *et al.* 2015). This indicates that GC-derived IgA antibodies only regulate a small subset of bacteria and that changes in the gut microbiome during ageing are not likely driven by the reduced PP GC response of aged mice.

It is well established that the gut microbiome is affected by ageing, but there is no consensus on how exactly the gut microbiome changes with age. This is probably due to the high variability detected in microbiomes from different geographical locations in both mice and humans (Ericsson *et al.* 2015; Mueller *et al.* 2006; Rausch *et al.* 2016). Several studies on the human microbiome reported of reduced bacterial diversity in aged individuals (Biagi *et al.* 2010; Maffei *et al.* 2017) and Claesson *et al.* observed larger inter-individual variability in older individuals compared to young controls (Claesson *et al.* 2011). Our study reports the same general trends – increased inter-individual variability of both aged BALB/c and C57BL/6 mice, and a reduced bacterial diversity in aged BALB/c mice. The differences in the microbiome observed between strains of mice and between the sexes of the same strain, all of which were aged in the same animal facility under the same environmental conditions, indicate that interactions between age, sex and genetics play a role in shaping age-associated alterations of the gut microbiome.

The change in gut microbial composition with age has been linked with many age-associated disorders (Fransen *et al.* 2017; Shin *et al.* 2018). Transfer of an aged microbiome into germ-free mice causes systemic inflammation (Fransen *et al.* 2017; Thevaranjan *et al.* 2017), suggesting that the aged microbiome itself may contribute to so-called inflammaging. Our results indicate that replenishing the microbiome of aged mice with that of a younger animal can boost the local GC reaction, which may have implications for the overall health of the organism. Consistent with this hypothesis, remodelling of the gut microbiome in *Drosophila melanogaster* has been shown to increase lifespan (Obata *et al.* 2018; Westfall *et al.* 2018). Similarly, middle-aged killifish colonised

with a young microbiome were found to live longer than untreated fish (Smith *et al.* 2017) and bacterial-derived indoles were shown to increase the lifespan of mice (Sonowal *et al.* 2017). These data suggest that there is a direct link between the phenotypes associated with ageing and age-associated changes in the gut microbiome. Previous studies showed that supplementation of older humans or mice with pre- and probiotics results in changes of gut microbial composition and can improve gut immunity in older individuals (Kaburagi *et al.* 2007; Landete *et al.* 2017). Further, the transfer of a young microbiome into aged mice increases protection against *C. difficile* infection (Shin *et al.* 2018), indicating that the microbiota of young animals can functionally boost intestinal immune protection. This makes the gut microbiome a possible target for the treatment of a range of age-associated symptoms. FMT (Gupta *et al.* 2016), probiotics (Landete *et al.* 2017), co-habitation (Song *et al.* 2013) and diet (Clements & R. Carding 2018) all have an impact on the composition of the gut microbiome and could prove to be innovative interventions to facilitate healthy ageing.

Note:

An adaption of this chapter was published in Nature Communications: Stebegg M, Silva-Cayetano A, Innocentin S, Jenkins TP, Cantacessi C, Gilbert C, Linterman MA. 2019. Heterochronic faecal transplantation boosts gut germinal centres in aged mice, *Nature Communications.* 10(1), 2443 (Stebegg *et al.* 2019).

5 TYPE I INTERFERON SIGNALLING BOOSTS T FOLLICULAR HELPER CELL DIFFERENTIATION IN AGED MICE

5.1 Abstract

Most vaccinations prevent infectious diseases by generating long-lasting humoral immunity. In older people, the efficacy of vaccinations is reduced, possibly due to an age-associated deterioration of vaccine-specific germinal centre (GC) responses. GCs are structures that form in secondary lymphoid organs (SLOs) such as lymph nodes (LNs). Here, antigen-specific B cells somatically mutate their antigen receptor in a process known as somatic hypermutation which, when coupled to affinity-based selection, can improve the affinity of the B cell receptor (BCR) for antigen. Within GCs, antigen-activated B cells interact with a specialised population of CD4 T cells, T follicular helper (Tfh) cells, whose differentiation is initiated by priming by dendritic cells (DCs). Previous studies by others have indicated that the impaired formation of GCs in aged mice is linked with defective T cell priming. Here, I demonstrate that T cell priming in aged animals is impaired due to defective interferon (IFN) signalling in type 2 conventional DCs (cDC2s). By enhancing type I IFN signalling at immunisation sites using the TLR7-agonist imiquimod, I was able to restore CD80/CD86 expression levels on cDC2s and improve the formation of Tfh cells in aged animals. This demonstrates that age-associated defects in the Tfh cell response are not irreversible and that DCs are a potential target to improve vaccine responses in the ageing population.

5.2 Background

Vaccinations are one of the most successful medical interventions for preventing infectious diseases, greatly contributing to the global extension of life expectancy in the 20th century. Most vaccines on the market provide protection by generating long-lived humoral immunity that derives from the GC responses as well as extrafollicular responses in the absence of an infection. Unfortunately, vaccinations are less effective in older people, which has been proposed to be driven by an age-associated impairment of their GC response (Aberle *et al.* 2013; Gustafson *et al.* 2018; Linterman 2014). GCs are specialised microstructures which form in SLOs such as LNs upon infection or vaccination. Here, antigen-specific GC B cells somatically hypermutate the genes encoding their

BCR, and this mutational process, coupled with subsequent affinity-based selection, results in the emergence of plasma cells and memory B cells that bind antigen with improved affinity (Stebegg, Kumar, Silva-Cayetano *et al.* 2018). Only B cells with high affinity for foreign antigen receive survival signals from Tfh cells and follicular dendritic cells (FDCs) in GCs, preventing the survival of B cells with self-reactive or non-functional antigen receptors from this random mutation process (Mesin *et al.* 2016).

Tfh cells are generated in SLOs by priming by antigen-presenting cells (APCs). APCs provide three signals to drive the differentiation of Tfh cells (Krishnaswamy *et al.* 2018): signal one is provided when APCs take up antigen, internalise it and present peptide-MHC-II complexes to T cells (Webb & Linterman 2017). Upon activation of pattern recognition receptors (PRRs) on APCs by pathogen-associated molecular patterns (PAMPs), they also provide signal two by upregulating their expression of co-stimulatory ligands such CD80 and CD86 which interact with CD28, a co-stimulatory receptor on the surface of T cells which, when bound by its ligands, enhances T cell receptor (TCR) signalling and boosts Tfh cell differentiation (Krishnaswamy *et al.* 2018). PAMP-dependent activation also triggers signal three – the production of cytokines implicated in Tfh cell priming such as IL-6, IL-12 and IL-27 (Eddahri *et al.* 2009; Webb & Linterman 2017). Several DC subtypes have been shown to activate T cells and to induce their migration to the T-B border, but migratory cDC2s have been proposed as the dominant Tfh cell-priming DC subset (Krishnaswamy *et al.* 2017; 2018). cDC2s have been shown to produce IL-6 and IL-27, cytokines known to favour Tfh cell differentiation in a type I IFN-dependent manner (Batten *et al.* 2010; Cucak *et al.* 2009; Gringhuis *et al.* 2014). Thus, cDC2 cells are potent inducers of Tfh cell differentiation and important to initiate GC responses.

Ageing is correlated with reductions in GC magnitude, somatic hypermutation (SHM) and high-affinity serum antibodies (Eaton *et al.* 2004; Kosco *et al.* 1989; Kraft *et al.* 1987; Linterman 2014; van Dijk-Härd *et al.* 1997; Yang *et al.* 1996). These defects in the output of the GC response have been linked with defects in the T cell compartment (Gustafson *et al.* 2018; Linterman 2014; Nikolich-Žugich 2018). Adoptive transfers of T cells from aged mice into young animals results in the formation of smaller GCs with reduced antibody output (Eaton *et al.* 2004). Increasing the naïve T cell output from the thymus, however, is not sufficient to rescue the ageing GC phenotype (Lefebvre *et al.* 2012). T cells from adult mice transferred into aged hosts prior to immunisation also form fewer Tfh cells than in adult hosts. This suggests that in addition to age-associated T-cell intrinsic defects, the aged microenvironment, which includes APCs, is also impaired in old age (Lefebvre *et al.* 2012).

In aged subjects, T cell priming by DCs has been reported to be impaired, linked with the reduced phagocytosis and migration of DCs in aged subjects (Agrawal *et al.* 2007). Furthermore, reduced expression of the costimulatory molecules CD80 and CD86, as well as MHC-II, on DCs has been observed in aged mice before and after infection (Moretto *et al.* 2008). This impairs the potential of these DCs for activating T cells *via* MHC-II-dependent antigen presentation. CD4 T cells from aged mice were also shown to be less responsive to IL-6 stimulation by DCs (Brahmakshatriya *et al.* 2017). Together, these data indicate that reduced T cell priming by DCs drives at least some of the age-associated defects in the GC response. What causes these defects is still unknown.

Our study investigated whether T cell priming by DCs could be improved to enhance GC responses. The results presented here show that impaired T cell priming in aged animals is associated with reduced expression levels of the co-stimulatory ligands CD80 and CD86 on migratory cDC2s. This is linked with defective type I IFN signalling in the same cells. By enhancing type I IFN signalling at immunisation sites, I was able to restore CD80 and CD86 expression levels on cDC2s. This enhanced the formation of antigen-specific Tfh cells in aged animals and demonstrates a link between impaired T cell priming in aged animals and reduced type I IFN signalling in cDC2s. This reveals that age-associated defects in Tfh cell priming are not irreversible and that cDC2s could be a target to improve vaccination efficacy in older individuals.

5.3 Results

5.3.1 GC responses are impaired in aged mice

The GC responses in aged, 22-24-month-old C57BL/6 mice after vaccination were compared to those in 2-3-month-old adult mice after subcutaneous immunisation with NP-1W1K in Alum. The use of a 1W1K peptide-conjugate allowed us to track antigen-specific T cell responses by flow cytometry using 1W1K-loaded MHC-II tetramers. In aged mice, there was a reduction in the proportion and number of $Ki67^{+}Bcl6^{+}B220^{+}$ GC B cells compared to adult mice 7 days after immunisation (gating strategy in Figure 5.1; Figure 5.2A-B). This was associated with a reduction in GC size as observed by confocal fluorescence microscopy on day 14 after immunisation (Figure 5.2C) and accompanied by reduced numbers of both total $CXCR5^{hi}PD\text{-}1^{hi}Foxp3^{-}CD4^{+}$ Tfh cells and antigen-specific Tfh cells in aged mice, as determined by 1W1K-coupled tetramer stains (Figure 5.2D-G). This confirms that GC responses in aged C57BL/6 mice are reduced in magnitude, which is associated with a defect in the Tfh cell compartment.

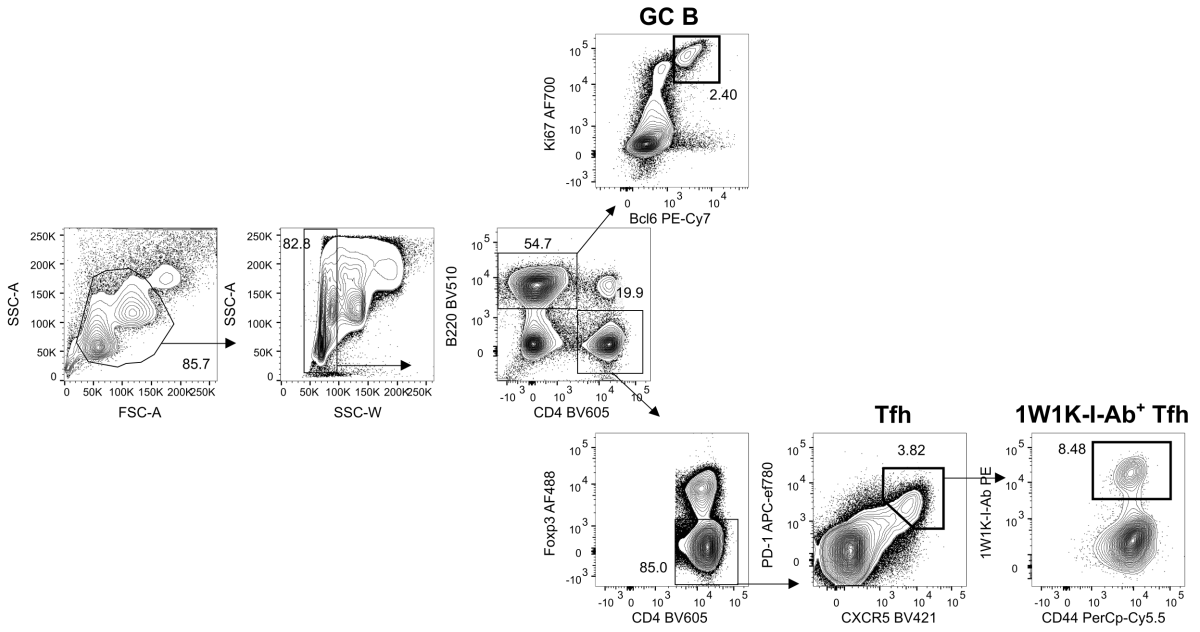

Figure 5.1: Gating strategy for germinal centre (GC) cell populations. 2-3-month-old adult and 22-24-month-old aged C57BL/6 mice were immunised subcutaneously with NP-1W1K in Alum. Their draining inguinal LNs were analysed by flow cytometry 7 days later. GC B cells were defined as $Bcl6^{+}Ki67^{+}B220^{+}$ cells, T follicular helper (Tfh) cells as $CXCR5^{hi}PD\text{-}1^{hi}Foxp3^{-}CD4^{+}$ cells and antigen-specific Tfh cells as $1W1K\text{-}I\text{-}Ab^{+}CXCR5^{hi}PD\text{-}1^{hi}Foxp3^{-}CD4^{+}$ cells.

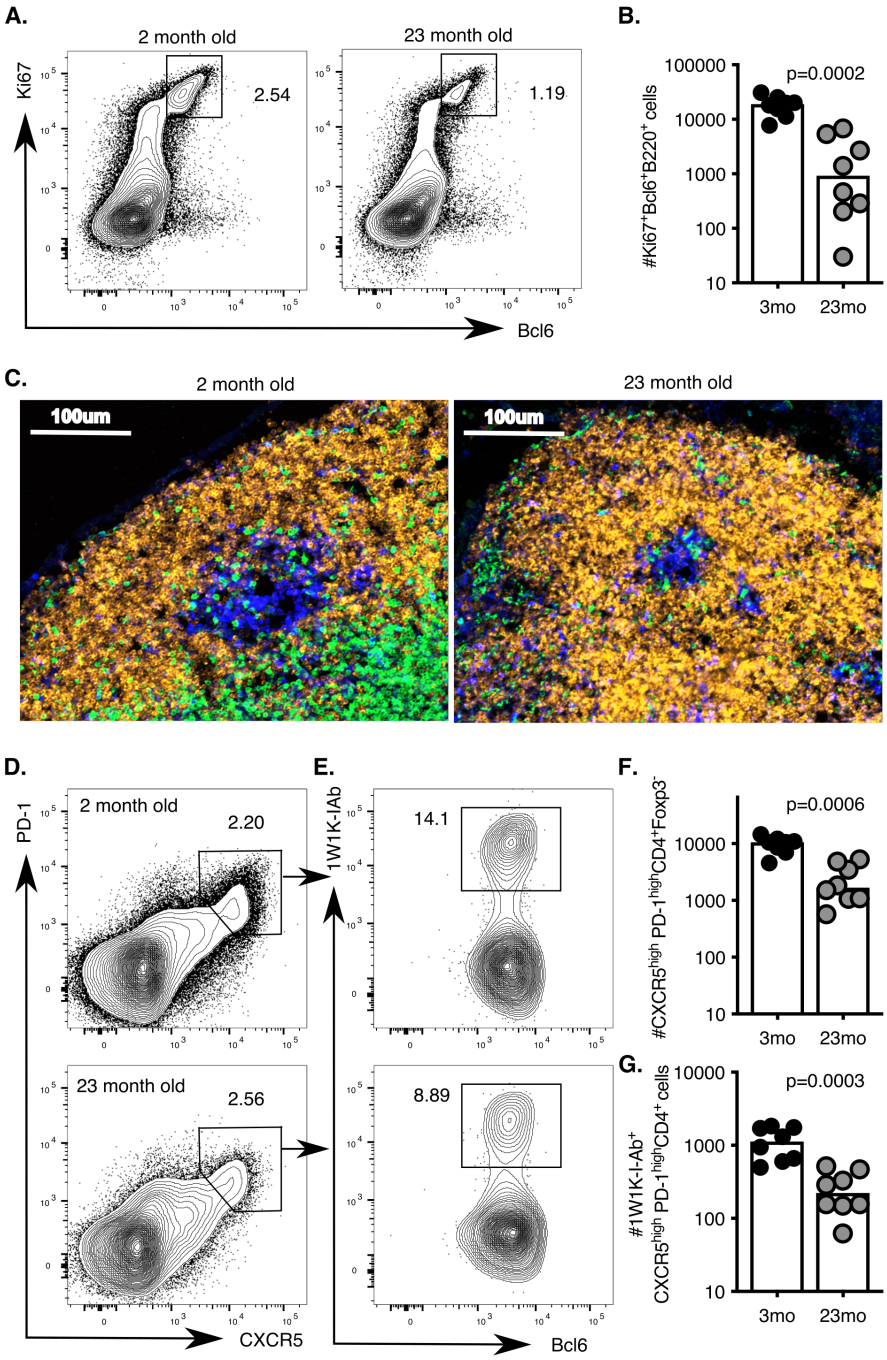

Figure 5.2: Germinal centre (GC) responses are impaired in aged mice. 2-month-old adult and 23-month-old aged C57BL/6 mice were subcutaneously immunised mice with NP-1W1K **(A, B, D-F)** or NP-KLH **(C)** in Alum. Their draining inguinal LNs were analysed 7 days later by flow cytometry **(A, B, D-F)** or after 14 days by confocal imaging **(C)**. **(A, B)** Representative flow cytometric plots **(A)** and quantitation **(B)** of $B220^{+}Ki67^{+}Bcl6^{+}$ GC B cells. **(C)** Confocal images generated by Ine Vanderleyden of draining LNs from 2-month-old and 23-month-old mice, taken 14 days after subcutaneous immunisation with NP-KLH. 10 µm LN sections were stained with anti-IgD (orange), anti-CD3 (green), anti-Ki67 (blue) and anti-Foxp3 (pink) antibodies. **(D-G)** Representative flow cytometric plots **(D, E)** and quantitation **(F, G)** of $CXCR5^{hi}PD\text{-}1^{hi}Foxp3^{-}CD4^{+}$ T follicular helper (Tfh) cells **(D, F)** and antigen-specific 1W1K-I-Ab^{+} Tfh cells **(E, G)**. Bar graphs show the results of one of two independent experiments performed by Alexandre Bignon. Bar height corresponds to the mean, and each circle represents one biological replicate. *P*-values were determined using the Mann-Whitney test in GraphPad Prism6.

5.3.2 Impaired T cell priming in aged animals

To test whether the reduced number of Tfh cells in aged mice was caused by a defect in early APC-dependent T cell activation and/or Tfh cell differentiation, TCRVβ3$^+$CD45.1$^+$ cells that are specific for a peptide of Hen Egg Lysozyme (HEL) were taken from 3-month-old adult TCR7 mice, CellTrace-labelled and then adoptively transferred into either adult or aged hosts. Three days after subcutaneous immunisation with HEL in Alum ~ 80 % of all CD45.1$^+$CD4$^+$ T cells had undergone one or more cell division in adult hosts (gating strategy in Figure 5.3A-B; Figure 5.3C-D). In aged hosts, fewer TCR7 T cells had entered the cell cycle (Figure 5.3C-D). Once T cells had entered the cell cycle, expression of the T cell co-stimulatory receptor ICOS was comparable between T cells in hosts of different ages (Figure 5.3E). This indicates that the aged microenvironment results in impaired T cell priming, and prompts the hypothesis that this impaired priming may underpin reduced antigen-specific Tfh cell numbers in aged mice.

Several DC subtypes, including LN-resident and type 1 conventional DCs (cDC1s), type 2 conventional DCs (cDC2s) and skin-resident Langerhans cells, have been implicated in T cell priming. Of these, migratory cDC2 subset have been suggested as the dominant Tfh-priming DC subset (Krishnaswamy *et al.* 2017; 2018), although the route of immunisation or infection influences which DC subtype plays the dominant role in Tfh cell priming . To test which cell type is the main APC in the draining LN in our experimental set-up, mice were immunised subcutaneously with Eα-coupled GFP in Incomplete Freund's Adjuvant (IFA) (Itano *et al.* 2003). This allowed us to track which cells had taken up antigen (GFP$^+$) and which cells were presenting a Eα-derived peptide on MHC-II using the Y-ae antibody (Itano *et al.* 2003). One day following subcutaneous immunisation in adult mice, the majority of GFP$^+$ APCs were migratory CD11b$^+$ cDC2s (gating strategy based on Guilliams *et al.* 2016) in Figure 5.4A; Figure 5.4B). The number of antigen-bearing GFP$^+$ CD11b$^+$ cDC2s were reduced in the draining LNs of aged compared to adult mice (Figure 5.4C). Of the cDC2 cells that had taken up antigen, there was less presentation of peptide-MHC-II in aged mice even though levels of total MHC-II expression on the cell surface was unchanged (Figure 5.4D, H, I). Expression of the costimulatory ligands CD86, CD80 and the receptor CD40 was reduced on the surface of GFP$^+$ CD11b$^+$ cDC2s from aged mice (Figure 5.4E-G, J-L). This observation is consistent with previous reports on reduced co-stimulation by DCs from aged mice and suggests a link between impaired T cell priming in draining LNs of aged mice and defects in the CD11b$^+$ cDC2 subset (Moretto *et al.* 2008).

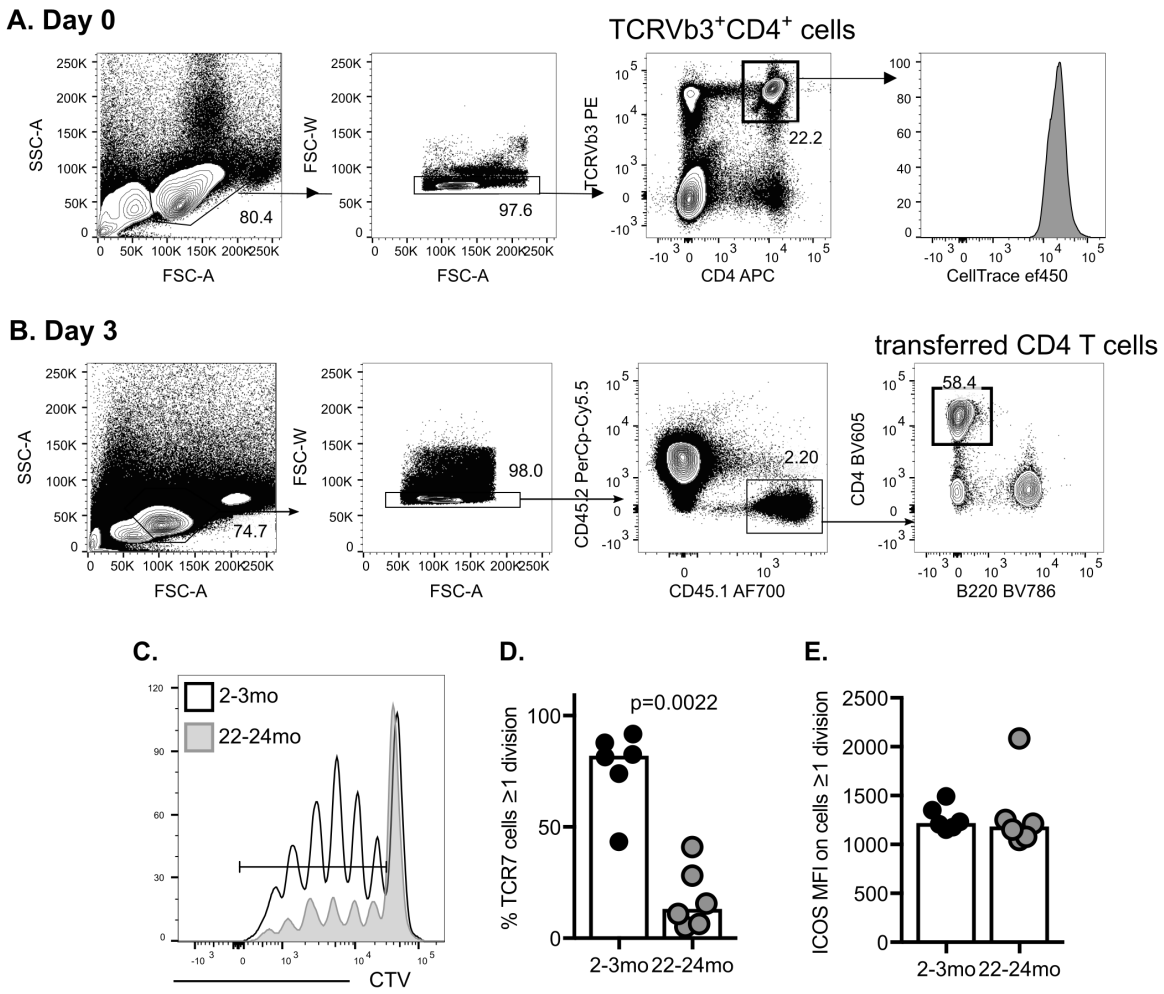

Figure 5.3: T cell proliferation is impaired in aged hosts. (A) 3-5 × 10^6 CellTrace violet (CTV)-labelled Hen Egg Lysozyme (HEL)-specific TCRVβ3$^+$CD4$^+$ cells from TCR7 mice were adoptively transferred into recipient mice by intravenous injections followed by subcutaneous immunisations with HEL in Alum. **(B)** On day three, cell proliferation was assessed by flow cytometry as defined by the serial dilution of CellTrace median fluorescence intensity (MFI) with each division. Transferred cells were defined by CD4 expression and the CD45.1 or CD45.2 congenic markers. **(C-E)** CellTrace-labelled HEL-specific (CTV$^+$TCRVβ3$^+$CD4$^+$) TCR7 cells were adoptively transferred into 2-3month-old and 22-24-month-old C57BL/6 recipients, which were subsequently immunised with HEL in Alum subcutaneously in the hind flank. Three days after immunisation, proliferation of CD45.1$^+$CD4$^+$ T cells was analysed by flow cytometry. **(C)** Representative flow cytometric plot of divided CD45.1$^+$CD4$^+$ cells in 2-3-month-old (white) and 22-24-month-old (grey) C57BL/6 recipients. **(D-E)** Quantitation of the proportion of divided CTV$^+$CD45.1$^+$CD4$^+$ cells **(D)** and their ICOS expression **(E)** in 2-3-month-old and 22-24-month-old C57BL/6 recipients. Bar graphs show the results of one of two independent experiments performed by Alexandre Bignon. Bar height corresponds to the mean, and each circle represents one biological replicate. *P*-values were determined using the Mann-Whitney test in GraphPad Prism6. Only p-values ≤ 0.05 are shown.

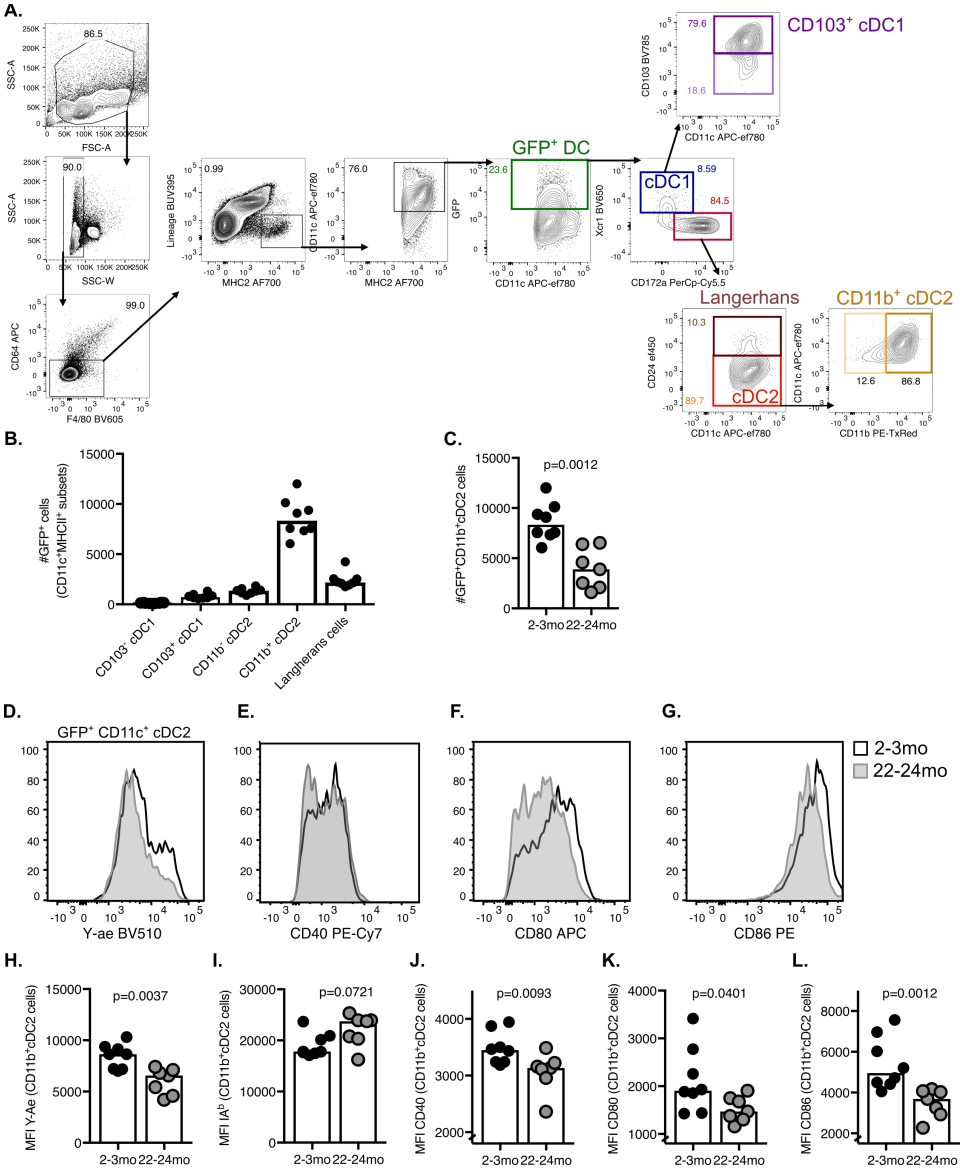

Figure 5.4: cDC2s from aged mice have an impaired activation phenotype. 2-3-month-old mice were immunised subcutaneously with Eα-GFP in IFA. Antigen-bearing GFP$^+$ and antigen-presenting Y-Ae$^+$ dendritic cells (DCs) in draining inguinal lymph nodes (LNs) were analysed 24 hours after immunisation. **(A)** Gating strategy for DC subsets. All antigen-carrying DCs were defined as GFP$^+$CD11c^{hi}MHC-II^{hi}Lineage$^-$(CD3$^-$B220$^-$CD19$^-$)CD64$^-$F4/80$^-$ events. Type 1 conventional DCs (cDC1s) were defined as Xcr1$^+$CD172a$^-$ DCs and were subdivided into CD103$^+$ and CD103$^-$ cDC1s. Langerhans cells were defined as CD24$^+$CD172a$^+$Xcr1$^-$ DCs. Type 2 conventional DCs (cDC2s) were defined as CD24$^-$CD172a$^+$Xcr1$^-$ DCs and were subdivided into CD11b$^+$ and CD11b$^-$ cDC2s. **(B)** Quantitation of GFP$^+$ cells from different DC subsets in the draining LNs of 2-3-month-old mice. **(C)** Quantitation of GFP$^+$CD11b$^+$ cDC2s in the draining LNs of 2-3-month-old and 22-24-month-old mice 24 hours after immunisation with Eα-GFP in IFA. **(D-G)** Representative histograms for median fluorescence intensity (MFI) levels of Y-Ae **(D)**, CD40 **(E)**, CD80 **(F)** and CD86 **(G)** on the surface of GFP$^+$ CD11b$^+$ cDC2s from 2-month-old and 23-month-old mice. **(H-L)** Quantitation of median fluorescence intensity (MFI) levels of Y-Ae **(H)**, I-A^b (C57BL/6 MHC-II) **(I)**, CD40 **(J)**, CD80 **(K)** and CD86 **(L)** on the surface of GFP$^+$CD11b$^+$ cDC2s in adult and aged mice. Bar graphs show the results of one of two independent experiments performed by Alexandre Bignon. Bar height corresponds to the mean, and each circle represents one biological replicate. *P*-values were determined using the Mann-Whitney test in GraphPad Prism6.

5.3.3 Interferon signalling is reduced in cDC2 cells from aged mice

To test a possible link between impaired T cell priming and reduced antigen presentation by cDC2s in aged mice, we utilised $H2^{+/-}$ mice that carry only one allele encoding MHC-II. cDC2s from $H2^{+/-}$ mice present less antigen on their surface 24 hours after immunisation with Eα-GFP in IFA than cDC2s from $H2^{+/+}$ control mice (Figure 5.5A), which recapitulates the phenotype observed in aged mice (Figure 5.4H). Despite reduced antigen-presentation, T cell proliferation of CellTrace-labelled TCR7 T cells adoptively transferred into HEL-immunised $H2^{+/-}$ and $H2^{+/+}$ hosts was comparable (Figure 5.5B, C). This indicates that reduced early T cell priming in aged mice is not due to reduced antigen presentation. To assess whether impaired T cell priming in aged mice was instead caused by reduced CD80/CD86 co-stimulation by cDC2s, I performed adoptive T cell transfers into 2-month-old C57BL/6 mice treated intraperitoneally with 500µg Abatacept, an FDA-approved CTLA4-IgG1 fusion protein which binds to CD80/86 with high affinity and blocks CD28 co-stimulation. Abatacept completely blocked $CD45.1^{+}CD4^{+}$ T cell proliferation, confirming a strong dependency of T cell priming on CD80/CD86 co-stimulation (Figure 5.5D, E) (Platt *et al.* 2010). This suggests a possible link between the age-associated reduction in CD80/CD86 expression on cDC2s and reduced T cell priming in aged mice.

Next, we decided to investigate the underlying cause for age-associated changes in cDC2s. For this, Alexandre Bignon and Danika Hill generated RNA sequencing data from sorted GFP^{+} $CD11b^{+}$ cDC2s isolated from 2-month-old and 23-month-old mice 24 hours after immunisation with Eα-GFP in IFA (gating strategy shown in Figure 5.4A). RNA sequencing analysis by Christel Krueger revealed 700 genes that were differentially expressed between cDC2s from young and aged mice. Principal component analysis demonstrated distinct clustering of samples from 2-month-old compared to 23-month-old mice (Figure 5.6A). Pathway enrichment analysis revealed that the cellular response to IFNβ, a pathway which had previously been linked with DC-dependent T cell priming, was one of the cellular pathways most affected by age (Figure 5.6B) (Cucak *et al.* 2009). Of the genes that make up the "cellular response to IFNβ" signature, the average expression of most genes was reduced in cDC2s from aged mice in the RNA sequencing data set (Figure 5.6C). I confirmed that *Ifnb1* was expressed early after Eα-GFP in IFA immunisation in the draining LN by RT-qPCR, peaking 6 hours after immunisation in adult mice (Figure 5.6D). This early wave of *Ifnb1* was followed by induction of the interferon-inducible myxovirus resistance gene *Mx1*, a canonical type I interferon-stimulated gene (ISG), which peaked at 14-24 hours after immunisation (Figure 5.6E). RT-qPCR of GFP^{+} $CD11b^{+}$ cDC2 cells sorted from an independent cohort confirmed reduced *Mx1* mRNA levels in cDC2 from 23-month-old mice compared to 3-month-old mice, demonstrating that type I IFN signalling is reduced in cDC2s of aged mice 24 hours after Eα-GFP

in IFA immunisation (Figure 5.6F). This reduction in ISG expression in aged mice could be recapitulated in whole LNs mRNA (Figure 5.6G), suggesting that the age-associated reduction in type I IFN signalling is not specific to cDC2s in aged mice.

Cucak *et al.* have previously reported that type I IFN signalling in DCs is essential for Tfh cell priming and type I IFNs have been shown to enhance protective immune responses upon influenza vaccination in mice (Cucak *et al.* 2009; Proietti *et al.* 2002). The type I IFN family of proteins is comprised of up to 20 members which are divided into IFNα and IFNβ subtypes (Rauch *et al.* 2013). IFNβ can be produced by almost all cell types when their PRRs are exposed to PAMPs, while IFNα is predominantly produced by immune cells such as plasmacytoid dendritic cells (pDCs) (Ivashkiv & Donlin 2014). Both forms of type I IFNs bind the interferon alpha receptor (IFNαR), a heterodimeric complex of IFNAR1 and IFNAR2 chains. The intracellular domain of this receptor is associated with JAK1 and Tyk2 kinases which phosphorylate STAT1 and STAT2 molecules upon IFN-induced activation. These form part of the transcriptional complex ISGF3 (interferon-stimulated gene factor 3) which regulates the expression of several hundred interferon-stimulated genes (ISGs), including Mx1 and Ifit1 (Interferon-induced protein with tetratricopeptide repeats 1) (Hoffmann *et al.* 2015). In DCs, type I IFN signalling has been shown to enhance the expression of the co-stimulatory molecules CD80 and CD86 as well as the Tfh cell differentiation-inducing cytokine IL-6 (Hassanzadeh-Kiabi *et al.* 2017; Luft *et al.* 1998). Hence, we hypothesised that reduced type I IFN signalling in cDC2s of aged mice could be linked with defective T cell priming and impaired GC responses in these mice.

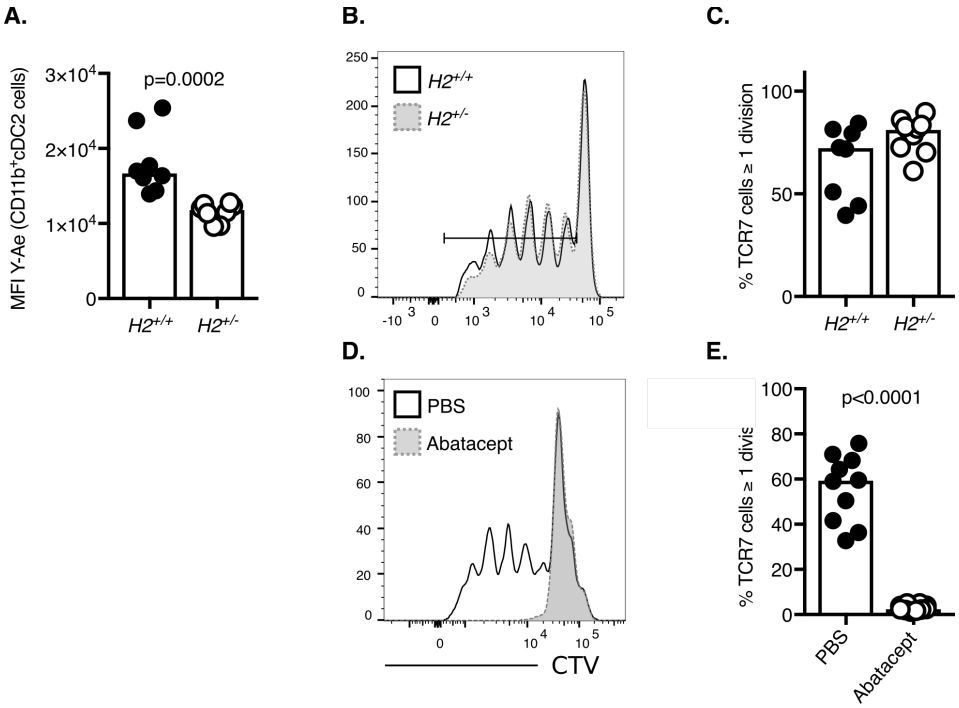

Figure 5.5: T cell priming is abrogated upon blockade of CD80/86 co-stimulation. (A-C) CellTrace violet (CTV)-labelled HEL-specific TCRVβ3$^+$CD45.1$^+$CD4$^+$ cells were adoptively transferred into *H2*$^{+/+}$ and *H2*$^{+/-}$ mice, followed by subcutaneous immunisations with HEL in Alum. On day 3, proliferation of CD45.1$^+$CD4$^+$ T cells was analysed by flow cytometry. These experiments were performed by Michelle Linterman. **(A)** Quantitation of Eα-peptide presentation on CD11b$^+$ cDC2s as determined by Y-Ae surface staining. **(B-C)** Representative flow cytometric plot **(B)** and quantitation **(C)** of divided CTV$^+$CD45.1$^+$CD4$^+$ cells in *H2*$^{+/-}$ and *H2*$^{+/+}$ recipients. **(D-E)** CellTrace(CTV)-labelled HEL-specific TCRVβ3$^+$CD45.1$^+$CD4$^+$ cells were adoptively transferred into C57BL/6 mice, directly followed by subcutaneous immunisations with HEL in Alum and intraperitoneal injections with 500 µg Abatacept or PBS. On day 3, proliferation of CD45.1$^+$CD4$^+$ T cells was analysed by flow cytometry. Representative flow cytometric plot **(D)** and quantitation **(E)** of divided CTV$^+$CD45.1$^+$CD4$^+$ cells in mice treated with Abatacept or PBS. Bar graphs show the results of one of two independent experiments. Bar height corresponds to the mean, and each circle represents one biological replicate. *P*-values were determined using the Mann-Whitney test in GraphPad Prism6. Only significant *p*-values ≤ 0.05 are shown.

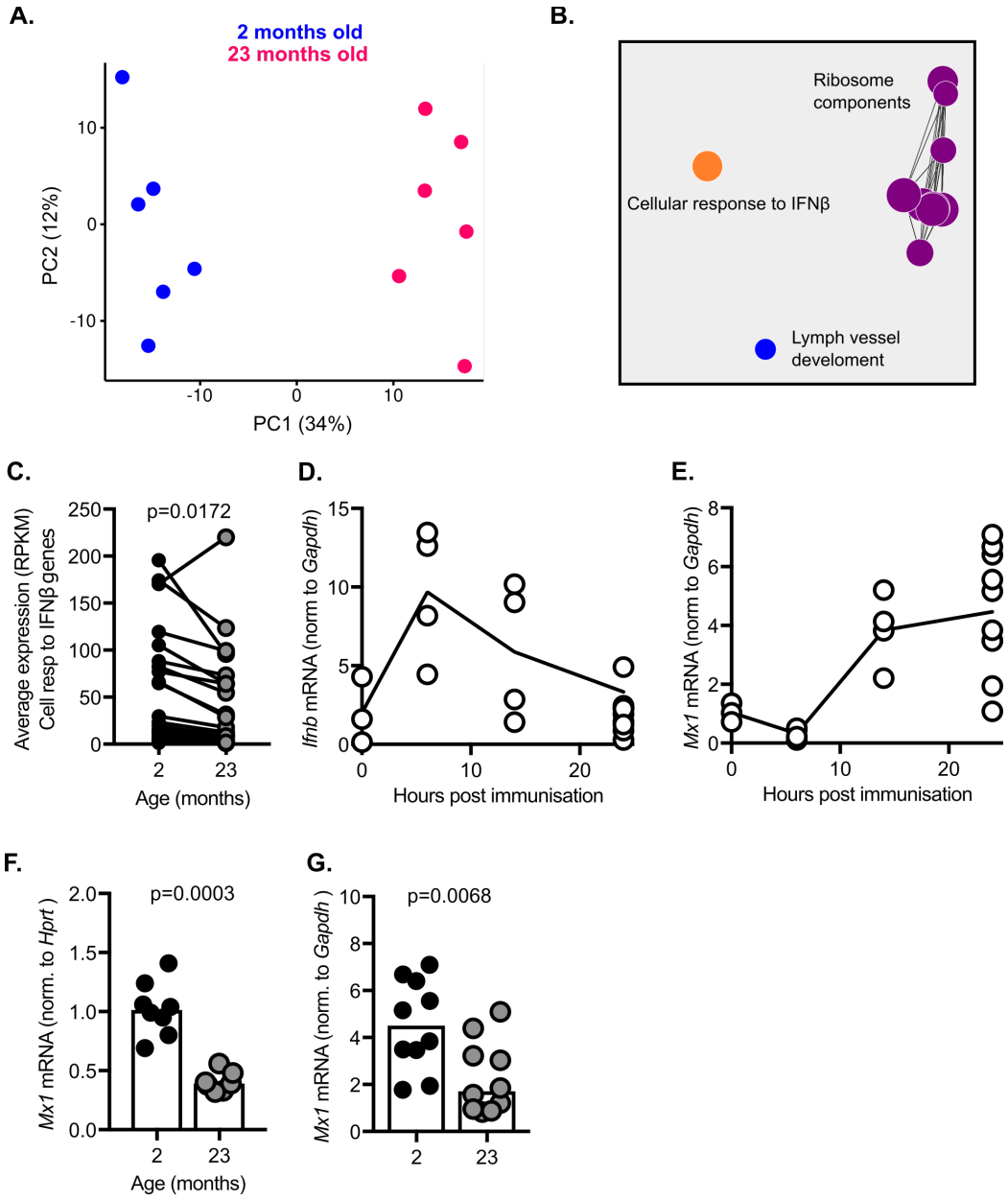

Figure 5.6: Reduced type I interferon (IFN) signalling in cDC2s from aged mice. (A-C) RNA sequencing data were generated by Danika Hill and Alexandre Bignon from sorted GFP$^+$ CD11b$^+$ cDC2s isolated from 2-month-old and 23-month-old C57BL/6 mice 24 hours after subcutaneous immunisation with Eα-GFP in IFA. **(A)** Principal component analysis of the most variable genes in samples from young 2-month-old (blue) and aged 23-month-old (pink) mice. **(B)** Cellular pathways significantly affected by age as determined by Christel Krueger by Pathway Enrichment Analysis. **(C)** Average RPKM (read per kilobase million) expression of IFNβ-responsive genes in GFP$^+$ CD11b$^+$ cDC2s as determined by RNA sequencing. **(D-E)** *Ifnb1* **(D)** and *Mx1* **(E)** mRNA expression in whole LN mRNA taken 0, 6, 14 and 24 hours after subcutaneous immunisation of 2-month-old mice with Eα-GFP in IFA **(F-G)** 2-month-old and 23-month-old C57BL/6 mice were subcutaneously immunised with Eα-GFP in IFA. 24 hours later, *Mx1* mRNA levels were determined in sorted GFP$^+$ CD11b$^+$ cDC2s **(F)** or extracts of whole draining LNs **(G)** by RT-qPCR. Bar graphs show the results of one of two independent experiments **(D, E)** or the combined results of two experiments **(F, G)**. Bar height corresponds to the mean, and each circle represents one biological replicate. *P*-values were determined using the Mann-Whitney test in GraphPad Prism6.

5.3.4 Lack of type I IFN signalling in DCs is linked with impaired Tfh cell formation

To test this hypothesis, I first examined whether a loss of type I IFN signalling recapitulates the phenotype of cDC2s from aged mice. Adult C57BL/6 mice were treated with an anti-IFNAR1 blocking antibody followed by subcutaneous immunisation with Eα-GFP in IFA 20 hours later. One day after immunisation, blockade of type I IFN signalling did not affect antigen presentation or CD40 expression by GFP^+ $CD11b^+$ cDC2s (gating strategy shown in Figure 5.7; Figure 5.8A, B), but the expression of the co-stimulatory ligands CD80 and CD86 was significantly reduced (Figure 5.8C, D). This indicates that a blockade of type I IFN signalling can partly recapitulate the ageing cDC2 phenotype.

To determine whether loss of IFNαR signalling also impacts T cell priming, I adoptively transferred IFNαR-sufficient HEL-specific TCR7 into *Ifnar1*$^{-/-}$ or WT control mice immunised with HEL in Alum. Fewer T cells entered the cell cycle in *Ifnar1*$^{-/-}$ hosts (Figure 5.8E, F), recapitulating the defect in T cell priming seen in aged mice. When this experiment was repeated using ovalbumin (OVA)-specific OTII cells transferred into recipient mice immunised with OVA in Alum, the same effect was seen (Figure 5.8G, H). To test whether Tfh cell formation after immunisation is also affected in mice lacking type I IFN signalling only in DCs, *Ifnar1*$^{fl/f}$*Cd11c*$^{cre/+}$ mice, and their *Ifnar1*$^{fl/fl}$*Cd11c*$^{+/+}$ littermate controls were inoculated subcutaneously with NP-1W1K in Alum. Fewer Tfh cells formed in *Cd11c*$^{cre/+}$*Ifnar1*$^{fl/fl}$ mice seven days after immunisation compared to their littermates (Figure 5.8I, J). This shows that the lack of type I IFN signalling can mimic age-associated defects both in T cell priming and their subsequent differentiation into Tfh cells. This could be due to reduced CD28-dependent T cell co-stimulation, as both ageing as well as IFNAR1 blockade were associated with reduced expression levels of CD80 and CD86, the costimulatory ligands for CD28, on antigen-presenting cDC2s.

Reduced type I IFN signalling in DCs could be driven to two factors: decreased levels of type I IFNs in their microenvironment or a reduction in the IFN responsiveness of DCs in aged animals. As described above, I observed that *Mx1* mRNA levels were not only reduced in sorted cDC2 cells, but also in whole LN extracts of immunised mice. This suggests a reduced production of type I IFNs in the draining LNs of aged mice. Upon infection, pDCs quickly produce large amounts of type I IFN in the LNs of both humans and mice, and this response has been reported to be impaired in aged mice and humans (Agrawal 2013; Agrawal *et al.* 2017; Panda *et al.* 2010; Sridharan *et al.* 2011; Stout-Delgado *et al.* 2008). I observed reduced proportions and numbers of pDCs in the LNs of aged 23-month-old mice compared to adult controls both at the steady-state and 24 hours after

immunisation with Eα-GFP in IFA (Figure 5.9A-D). This suggests that the reduction in type I IFN signalling in cDC2s is due to a loss of IFN-producing pDCs in the LNs of aged mice.

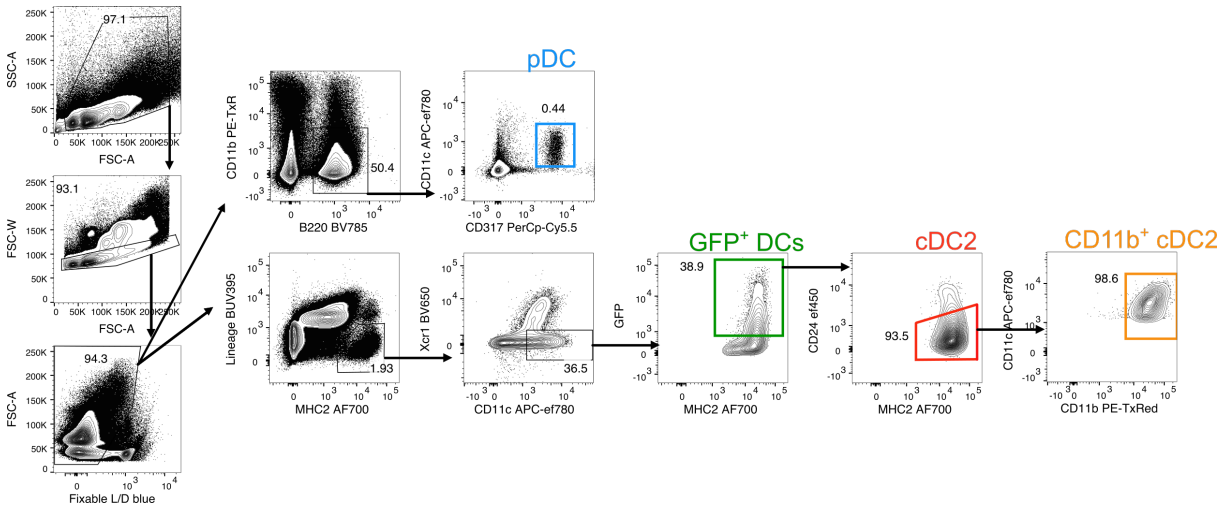

Figure 5.7: Gating strategy for the quantitation of GFP$^+$ CD11b$^+$ cDC2s and plasmacytoid dendritic cells (pDCs). Mice were immunised subcutaneously with Eα-GFP in Alum. 24 hours later, pDCs and antigen-bearing GFP$^+$ CD11b$^+$ cDC2s were analysed by flow cytometry or - in the case of cDC2s - sorted for RT-qPCR. GFP$^+$ CD11b$^+$ cDC2s were defined as live CD11b$^+$CD24$^-$ GFP$^+$CD11c^{hi}MHC-II^{hi}Lineage$^-$(CD3$^-$CD19$^-$) events. pDCs were defined as live CD317(=PDCA-1)$^+$CD11c$^+$CD11b$^-$B220$^+$ events.

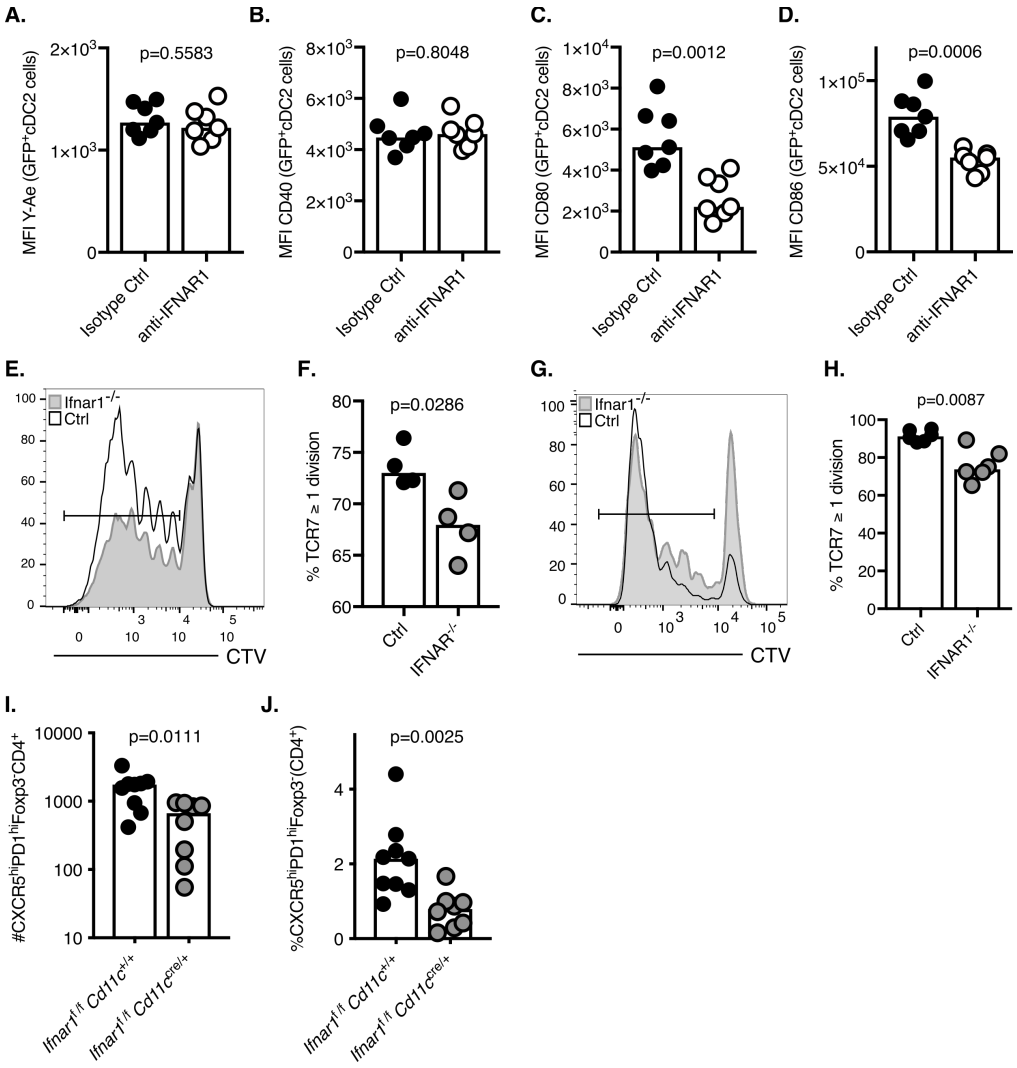

Figure 5.8: Lack of type I interferon (IFN) signalling in DCs impairs Tfh cell differentiation. **(A-D)** Flow cytometric analysis of CD11b$^+$ cDC2s isolated from mice intraperitoneally injected with anti-IFNAR1 blocking or isotype control antibodies 20 hours prior to subcutaneous immunisation with Eα-GFP in IFA. **(A)** Quantitation of Eα-peptide presentation on GFP$^+$ CD11b$^+$ cDC2s as determined by Y-Ae stains 24 hours after immunisation with Eα-GFP in IFA. **(B-D)** Quantitation of median fluorescence intensity (MFI) levels of CD40, CD80 and CD86 on the surface of GFP$^+$ CD11b$^+$ cDC2s in mice treated with anti-IFNAR1 blocking or isotype control antibodies. (**E-F)** CellTrace(CTV)-labelled Hen Egg Lysozyme (HEL)-specific TCRVβ3$^+$CD45.1$^+$CD4$^+$ cells from TCR7 mice were adoptively transferred into *Ifnar1*$^{-/-}$ and control mice, which were subsequently immunised with HEL in Alum. On day three, proliferation of CD45.1$^+$CD4$^+$ T cells was analysed by flow cytometry. **(E-F)** Representative flow cytometric plot **(E)** and quantitation **(F)** of divided CTV$^+$CD45.1$^+$CD4$^+$ cells. (**G-H)** CellTrace(CTV)-labelled ovalbumin (OVA)-specific TCRVα2$^+$CD45.1$^+$CD4$^+$ cells from OTII mice were adoptively transferred into *Ifnar1*$^{-/-}$ and control mice, which were subsequently immunised with OVA in Alum. On day three, proliferation of CD45.1$^+$CD4$^+$ T cells was analysed by flow cytometry. **(G-H)** Representative flow cytometric plot **(G)** and quantitation **(H)** of divided CTV$^+$CD45.1$^+$CD4$^+$ cells. **(I-J)** Flow cytometric analysis of CXCR5^{hi}PD-1^{hi}Foxp3$^-$CD4$^+$ T follicular helper (Tfh) cells isolated from *Ifnar1*$^{fl/fl}$*Cd11c*$^{cre/+}$ or *Ifnar1*$^{fl/fl}$*Cd11c*$^{+/+}$ control mice 7 days after immunisation with NP-1W1K in Alum. Quantitation of Tfh cell numbers **(I)** and proportion of CD4$^+$ T cells **(J)** on day 7. Bar graphs show the results of one **(E-H)** or one of two **(A-D, I-J)** independent experiments. Bar height corresponds to the mean, and each circle represents one biological replicate. *P*-values were determined using the Mann-Whitney test in GraphPad Prism6.

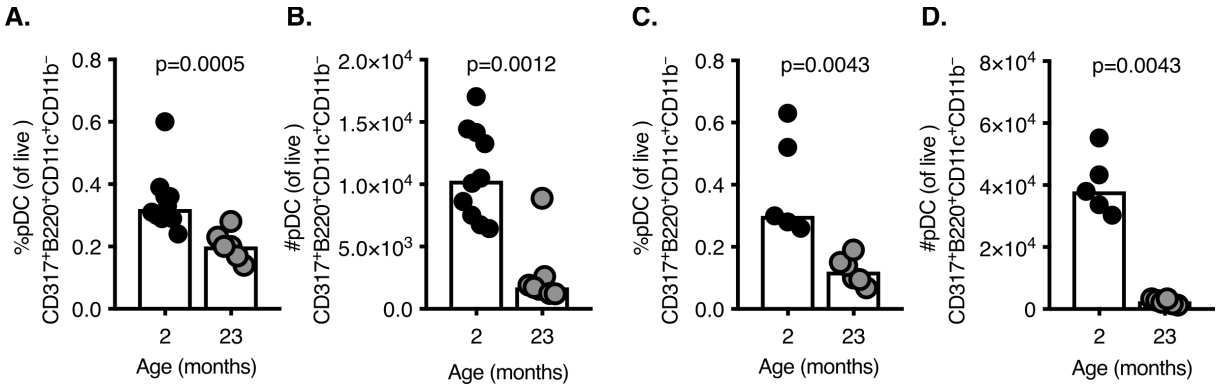

Figure 5.9: Numbers of plasmacytoid DCs (pDCs) are reduced in the lymph nodes (LNs) of aged mice. (A-B) Flow cytometric quantitation of the proportion **(A)** and number **(B)** of pDCs in the inguinal LNs of unimmunised 2-month-old and 23-month-old C57BL/6 mice. **(C-D)** Flow cytometric quantitation of the proportion **(C)** and number **(D)** of pDCs in the inguinal LNs of 2-month-old and 23-month-old C57BL/6 mice 24 hours after immunisation with Eα-GFP in IFA. Bar graphs show the results of one of three independent experiments. Bar height corresponds to the mean, and each circle represents one biological replicate. *P*-values were determined using the Mann-Whitney test in GraphPad Prism6.

5.3.5 Imiquimod-induced type I IFN signalling rejuvenates cDC2s in aged mice

Next, I investigated whether artificially boosting the production of type I IFN could rejuvenate the cDC2 phenotype in aged mice. For this, 23-month-old C57BL/6 mice were topically administered Aldara, a cream containing 5 % of the TLR7-agonist imiquimod, a strong inducer of type I IFN responses (Moore *et al.* 2001; Reiter *et al.* 1994). This cream was applied on top of the injection sites directly after subcutaneous immunisations with Eα-GFP in IFA (experimental set-up shown in Figure 5.10A). 24 hours later, I observed increased expression of the ISGs *Ifit1* and *Mx1* in sorted GFP^+ $CD11b^+$ cDC2s isolated from imiquimod-treated 23-month-old mice compared to aged controls that were immunised but did not receive imiquimod (Figure 5.10B, C). This was associated with an increase in the proportions and total numbers of both total and GFP-positive $CD11b^+$ cDC2s in draining LNs (Figure 5.10D-G). Further, these cells expressed higher levels of CD80 and CD86, while antigen-presentation and CD40 expression was not affected (Figure 5.10H-O). This demonstrates that promoting type I IFN signalling in DCs can rescue the age-dependent co-stimulatory defects observed in cDC2s from aged mice. This mirrors the results from IFNAR1 blocking experiments, where blockade of type I IFN signalling in cDC2s resulted in reduced expression levels of CD80 and CD86, while antigen-presentation and CD40 expression were not affected. This shows that the topical application of imiquimod onto immunisation sites induces type I IFN signalling and potently enhances the activation and recruitment of cDC2s into the draining LNs of aged mice.

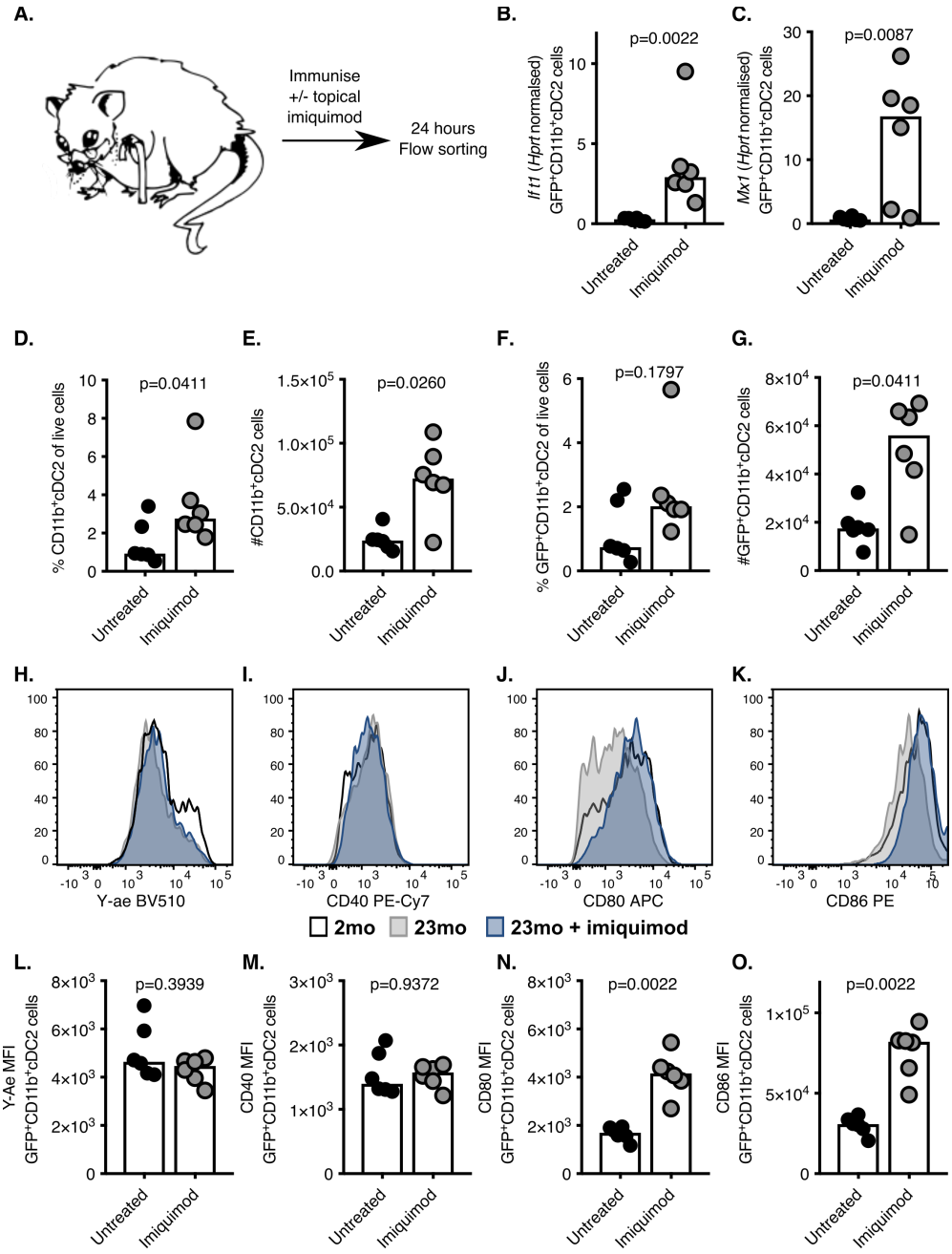

Figure 5.10: Imiquimod rejuvenates cDC2s in aged mice. (A) Schematic representation of the experimental set-up. 23-month-old mice were subcutaneously immunised with Eα-GFP in IFA. Half of the mice were topically treated with imiquimod cream on top of their immunisation sites. 24 hours later, GFP^+ $CD11b^+$ cDC2 cells were sorted by FACS for RT-qPCR **(B-C)** or analysed by flow cytometry **(D-K)**. **(B-C)** *Ifit1* **(B)** and *Mx1* **(C)** mRNA expression in sorted GFP^+ $CD11b^+$ cDC2s were analysed by RT-qPCR. **(D-G)** Flow cytometric quantitation of the proportions **(D, F)** and numbers **(E, G)** of total **(D, E)** and GFP^+ **(F, G)** $CD11b^+$ cDC2 cells. **(H-K)** Representative histograms for median fluorescence intensity (MFI) levels of Y-Ae **(H)**, CD40 **(I)**, CD80 **(J)** and CD86 **(K)** on the surface of GFP^+ $CD11b^+$ cDC2s in 23-month-old mice with or without imiquimod treatment compared to 2-month-old control mice. **(L-O)** Quantitation of MFI levels of Y-Ae **(L)**, CD40 **(M)**, CD80 **(N)** and CD86 **(O)** on the surface of GFP^+ $CD11b^+$ cDC2s in 23-month-old mice with or without imiquimod treatment. Bar graphs show the results of one of two independent experiments. Bar height corresponds to the mean, and each circle represents one biological replicate. *P*-values were determined using the Mann-Whitney test in GraphPad Prism6. The mouse artwork was kindly provided by Alice Denton.

5.3.6 Imiquimod enhances Tfh cell priming in aged mice

These findings raised the question of whether imiquimod treatment could ultimately boost the defective Tfh cell responses in aged animals. To test this, I analysed GC responses on day 7 in 23-month-old mice which were, or were not, treated topically with imiquimod after subcutaneous immunisation with NP-1W1K in Alum (experimental set-up shown in Figure 5.11A). In these experiments, imiquimod potently induced the expansion of both total and antigen-specific Tfh cell numbers (Figure 5.11B-E). This was linked with a small, but significant, increase in the number of GC B cells in imiquimod-treated mice compared to aged control mice (Figure 5.11F-G). Together, these results show that restoration of type I IFN signalling in aged mice after vaccination rescues defective Tfh cell differentiation, likely due to improved T cell activation by cDC2s with adequate levels of type I IFN signalling, but is not sufficient to completely rejuvenate GC B cells responses.

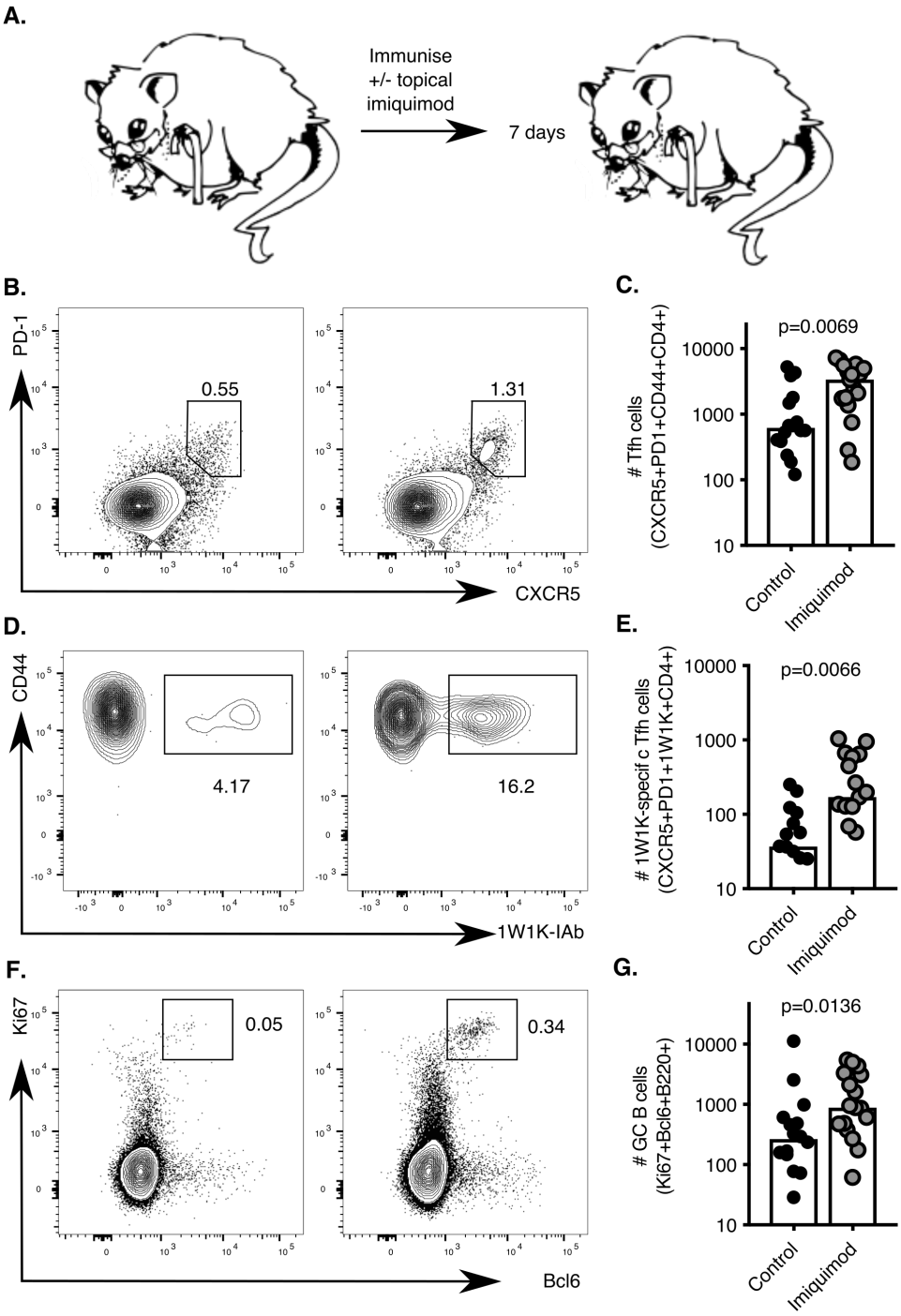

Figure 5.11: Imiquimod boosts antigen-specific Tfh cell differentiation in aged mice. (A) Schematic representation of the experimental set-up. 23-month-old mice were subcutaneously immunised with NP-1W1K in Alum. Half of the mice were topically treated with imiquimod cream on top of their immunisation sites. 7 days later, draining LNs were analysed by flow cytometry. **(B-E)** Representative flow cytometric plots **(B, D)** and quantitation **(C, E)** of $CXCR5^{hi}PD\text{-}1^{hi}CD4^{+}$ T follicular helper (Tfh) cells **(B, C)** as well as antigen-specific 1W1K-I-Ab^{+} Tfh cells **(D, E)**. **(F-G)** Representative flow cytometric plots **(F)** and quantitation **(G)** of $B220^{+}Ki67^{+}Bcl6^{+}$ GC B cells. Bar graphs show the combined results of three independent experiments. Bar height corresponds to the mean, and each circle represents one biological replicate. *P*-values were determined using the Mann-Whitney test in GraphPad Prism6. The mouse artwork was kindly provided by Alice Denton.

5.4 Discussion

Vaccination responses in older individuals are reduced, at least in part due to age-associated defects in the GC response and the subsequent reduction in the generation of high-affinity antigen-specific antibodies (Gustafson *et al.* 2018; Linterman 2014). A potent GC response is dependent on the formation of Tfh cells for Tfh cell-mediated B cell help (Vinuesa *et al.* 2016). Here, we show that the development of antigen-specific Tfh cells is impaired in aged mice, and that this is associated with an altered phenotype of cDC2s, the main antigen-presenting cell type in the LN after subcutaneous protein immunisation. RNA-sequencing of cDC2s from aged mice revealed a defective type I IFN response, resulting in the reduced expression of the co-stimulatory ligands CD80 and CD86. Based on this finding, we decided to treat aged mice with the type I IFN-inducing TLR7 agonist imiquimod, to increase levels of IFN signalling in cDC2s. This ultimately increased formation of Tfh and GC B cells in aged mice upon immunisation. Taken together, this highlights cDC2s as an exciting therapeutic target for the improvement of vaccine efficacy in the ageing population, potentially by using imiquimod or other adjuvants that promote of type I IFN signalling.

Recently, type I IFNs have emerged as potent vaccine adjuvants (Bracci *et al.* 2008; Proietti *et al.* 2002). They were found to boost humoral antibody responses in mice by exerting direct effects on B cells (Le Bon *et al.* 2006), as well as T cells (Le Bon *et al.* 2006; Nakayamada *et al.* 2014; Riteau *et al.* 2016) and DC cells (Cucak *et al.* 2009; Le Bon *et al.* 2001). In DCs, type I IFN was shown to promote the expression of co-stimulatory molecules and pro-inflammatory cytokines (Moretto *et al.* 2008). Signalling downstream of IFNαR additionally promotes the secretion of IL-6 and IL-1β by DCs, which were shown to enhance the expression of Bcl6, CXCR5 and ICOS by Tfh cells (Barbet *et al.* 2018; Cucak *et al.* 2009). Taken together, these studies demonstrate a clear link between type I IFN signalling in DCs and their potential for T cell priming. Here, we describe a link between defective T cell priming in aged mice and reduced type I IFN signalling in cDC2s. Consistent with data from Moretto *et al.*, we observed reduced expression levels of the co-stimulatory ligands CD80 and CD86 on DCs from aged mice (Moretto *et al.* 2008). Moretto *et al.* have shown that IL-15 treatment can rescue the expression of CD86 on DCs from one-year-old mice (Moretto *et al.* 2008). I found that imiquimod-boosted type I IFN signalling can also potently increase CD80 and CD86 expression on cDC2s in aged mice. This is associated with the improved generation of antigen-specific Tfh cells in these mice, providing novel mechanistic insights into the drivers of age-associated defects in GCs.

Several strategies are currently being used to enhance the GC response of aged individuals to infections and vaccinations. Modifications of the vaccine adjuvant (Frech *et al.* 2005) or

administration of increased antigen doses (Remarque *et al.* 1993) can improve vaccination responses in older subjects. Hung *et al.* have previously shown that topical imiquimod treatment at the time of vaccination potently enhances immune responses to influenza vaccination in both young and older individuals (Hung *et al.* 2014; 2016). This is exciting, as it suggests - together with the data presented here - that the age-related defect in the GC response is not irreversible, and can be targeted therapeutically to improve immune protection in older individuals. Our study provides novel mechanistic insights into how imiquimod might enhance vaccination responses *in vivo*. In mice, the beneficial effect of imiquimod has previously been linked with direct effects of imiquimod on B cells *in vitro* as well as improved IL-6 cytokine production by and CD80/CD86 expression on DCs in young mice (Fehres *et al.* 2014; Li *et al.* 2018; Thomsen *et al.* 2004). My data confirm that imiquimod boosts GC responses in aged animals by enhancing cDC2-dependent T cell priming and Tfh cell differentiation. This highlights cDC2s as an important target for improved vaccination strategies in older individuals and suggests possible applications for imiquimod in promoting vaccine responses in the ageing population.

Note:

This project was started by Alexandre Bignon, who generated all data depicted in Figures 5.1, 5.2, 5.3, 5.4, 5.6A-C. He performed initial GC and DC phenotyping experiments, generated the DC RNA sequencing data together with Danika Hill, Edward Carr, Michelle Linterman and Christel Krueger and also started validating the RNA sequencing results. When he left the lab, I followed up on the role of type I IFN signalling in cDC2s from aged mice and performed all imiquimod experiments under the supervision of Michelle Linterman (Figures 5.5D-E, 5.6D-G, 5.7, 5.8, 5.9, 5.10, 5.11).

6 DISCUSSION

The immune system has evolved to respond to its environment, to sense tissue damage, infections and changes in normal homeostasis. As a result, immune cells and their functions are dynamically regulated by changes in their microenvironment. In this thesis, I demonstrate that stress and ageing have key roles in CD4 T cell differentiation and in the formation of the GC response. My results further demonstrate that changes in the environment are able to stimulate the aged immune system and can be used to potentiate immune responses in older individuals.

6.1 ER stress: a novel driver of Th17 cell pathogenicity?

In this thesis, a link between ER stress and Th17 cell differentiation and pathogenicity is described. This could provide an explanation why Th17 cells have been implicated in both protective and pathogenic immunity: while they are crucial for barrier immunity, they have also been implicated in the pathogenesis of autoimmune disease, such as rheumatoid arthritis and multiple sclerosis (Stockinger & Omenetti 2017). Work from both *in vitro* and *in vivo* settings identified that Th17 cell pathogenicity is linked with their propensity to adopt a Th1-like cell phenotype and produce GM-CSF and IFNγ under the influence of IL-23 (El-Behi *et al.* 2011; Ghoreschi *et al.* 2010; Hirota *et al.* 2011; Jain *et al.* 2016; McGeachy *et al.* 2007). After the initial implication of IL-23 in Th17-driven pathology, it has become clear that other environmental factors, such as high salt concentrations or the presence of different AhR ligands, can also influence Th cell differentiation and pathogenicity (Quintana *et al.* 2008; Veldhoen *et al.* 2008a; Wu *et al.* 2013). The data presented here reveal that the ER stress-inducer CPA drives the generation of Th17 cells with a pathogenic gene expression signature. This suggests that ER stress, a common feature of inflammatory sites, could be a driver of Th17 cell pathogenicity in autoimmune disorders. To test whether there is a broad role for stress in the differentiation of pathogenic Th17 cells, it would be interesting to investigate whether other stress conditions, such as BrPA or nutrient deprivation, can also induce the formation of pathogenic Th17 cells. To determine whether my findings have implications for human autoimmune diseases, it would be important to determine whether there is a link between stress and Th17 cell-driven pathology in humans.

The ER stress response was found to be highly active in inflammatory lesions of MS patients (Mháille *et al.* 2008) as well as in EAE, where it was described to promote inflammation and

pathology (Deslauriers *et al.* 2011; Meares *et al.* 2014; Mháille *et al.* 2008). This prompts the hypothesis that ER stress in the CNS promotes EAE pathology by driving the local generation of pathogenic Th17 cells. ER stress is induced by inflammation, and, when triggered, enhances the secretion of pro-inflammatory cytokines such as IL-23, IL-6, TNF-α and type I IFNs (Bettigole & Glimcher 2015; Hu *et al.* 2011; Martinon *et al.* 2010; Smith *et al.* 2008), creating a feed-forward-loop in which the inflammatory microenvironment might potentiate the development of autoimmune disorders (Sprenkle *et al.* 2017). In our adoptive-transfer EAE experiments, ER stress-generated Th17 cells caused the delayed onset of typical EAE clinical symptoms, but triggered atypical symptoms of Th17-mediated brain inflammation. This could point to an increased pathogenic potential of ER stress-generated Th17 cells in the brain *in vivo*. To test this, e-Th17 cells need to be characterised further: ER stress-induced changes in Th17-to-Th1 plasticity, a common feature of EAE as measured by the IFNγ production of ex-Th17 cells (Hirota *et al.* 2011), could be tested *in vivo* using adoptive transfers of $Rosa^{\text{stop-tdRFP}}Il17a^{\text{Cre}}$ cells. In these experiments, it would also be important to study the potential of e-Th17 cells to infiltrate the CNS, a hallmark of EAE pathology (Rostami & Ciric 2013). Furthermore, it would be interesting to assess the pathogenic potential of e-Th17 cells in other Th17-cell mediated diseases. To determine whether e-Th17 cells have a broad role in Th17-driven pathology, arthritis or *Helicobacter pylori*-induced inflammation could be induced and studied in $Xbp1^{fl/fl}Cd4^{cre/+}$ mice, which lack Xbp1-mediated ER stress responses in T cells. These experiments would further test the hypothesis that there is a link between Th17 cell-mediated disorders and ER stress.

Another open question is whether physiological levels of ER stress can drive Th17 cell differentiation *in vivo*? We observed the delayed onset of EAE symptoms in TUDCA-treated or $Xbp1^{fl/fl}Rag1^{cre/+}$ mice with repressed ER stress responses, suggesting that suppression of ER stress response pathways lessens EAE pathology *in vivo*. To determine whether ER stress drives EAE by directly acting on T cells, these experiments could be repeated using $Xbp1^{fl/fl}Cd4^{cre/+}$ or $Xbp1^{fl/fl}Il17a^{cre/+}$ mice that lack an ER stress response in all T cells or Th17 cells specifically, or by inducing adoptive-transfer EAE using MOG-specific T cells from 2D2 mice with a specific deletion in *Xbp1*. ER stress levels in T cells could be measured in different disease settings using the Xbp1-luciferase mouse model generated by Spiotto *et al.* (Spiotto *et al.* 2010), to test whether the generation of pathogenic Th17 cells is indeed associated with ER stress conditions *in vivo*. Together, these experiments would build on the work presented here to further understand the contribution of ER stress to *in vivo* pathogenesis.

Elevated ER stress responses are a common feature of neuroinflammation and other inflammatory disorders (Sprenkle *et al.* 2017). In this study, treatment of mice with the ER stress inhibitor

TUDCA delayed the onset of EAE in mice suggesting that this FDA-approved drug could be used to slow disease progression in MS patients. However, there are concerns about the potential side-effects of ER stress inhibitors when systemically administered to patients, as the ER stress response is an essential pathway important for normal homeostasis in all cells (Hetz *et al.* 2013). Instead of targeting the ER stress response pathway, our data suggest that therapeutic efforts could also more directly target ER stress-generated Th17 cells. The gene signature of ER stress-generated Th17 cells reported here, together with the pathogenic Th17 cell gene signature proposed by Lee *et al.* (Lee *et al.* 2012), might help to guide the development of novel therapies which specifically target pathogenic Th17 cells at sites of inflammation without affecting protective Th17 cells at barrier sites.

6.2 The GC response in ageing

Ageing results in a plethora of biological changes which can influence immune cells in a cell-intrinsic manner and in a cell-extrinsic way by changes in their microenvironment (López-Otín *et al.* 2013; Nikolich-Žugich 2018). The relative contribution of these effects to age-associated immune defects is difficult to disentangle, though. On a molecular level, all human cells experience age-related telomere shortening, the accumulation of genetic mutations, epigenetic changes, defective mitochondria and an increased burden of unfolded proteins which is associated with alterations in the ER stress response and protein degradation (Brown & Naidoo 2012; López-Otín *et al.* 2013). On the cellular level, ageing affects the communication between cells, tissue regeneration is reduced and senescent cells, that secrete pro-inflammatory mediators, accumulate over time (Linterman 2014; López-Otín *et al.* 2013; Tchkonia *et al.* 2013). In lymphocytes specifically, the reduced production of lymphoid precursors in the bone marrow and the prolonged exposure to antigens over the life-time additionally leads to an age-related increase in memory cells and a reduction in the pool of naïve T and B cells (Nikolich-Žugich 2018). The GC response has also been described to be impaired in aged mice and humans, resulting in the reduced formation of high-affinity plasma cells and serum antibody levels (Eaton *et al.* 2004; Kosco *et al.* 1989; Kraft *et al.* 1987; Linterman 2014; van Dijk-Härd *et al.* 1997; Yang *et al.* 1996). This is associated with an increased susceptibility to infections and decreased vaccination efficacy in older individuals (Linterman 2014).

GCs are complex structures consisting of multiple cell types including stromal cells, GC B cells, Tfh cells and Tfr cells. Age-associated defects in the output of the GC response have been linked with changes in all of these cell types (Gustafson *et al.* 2018; Linterman 2014; Nikolich-Žugich 2018). This makes it difficult to dissect the contributions of ageing-related changes in individual

cell types to changes in the GC output. What is more, ageing seems to affect GCs in PPs differently from GCs in the spleen and LNs. In this thesis, I describe distinct age-associated changes in environmental stimuli which shape GC responses in the PPs and draining LNs of aged mice: the gut microbiome and type I IFN signalling, respectively.

6.2.1 Cross-talk between the gut microbiome and GC responses in the PPs of aged mice

6.2.1.1 Ageing differentially affects GC responses in PPs and LNs

PPs are unique SLOs in that they take up antigens directly from the gut lumen and always contain GCs due to constant antigenic stimulation from the gut microbiota and exposure to food antigens (Kawamoto *et al.* 2014; Reboldi & Cyster 2016; Stebegg, Kumar, Silva-Cayetano *et al.* 2018). PPs are also differently affected by ageing compared to other lymphoid tissues: like LNs, PPs show an age-associated reduction in the proportion of GC B cells, however there is an increase in somatically mutated antibodies in the gut of aged mice, while in LNs SHM is reduced with advancing age (Banerjee *et al.* 2002; González-Fernández *et al.* 1994). What is more, both BALB/c and C57BL/6 mice exhibit reduced antigen-specific antibody responses in the gut (Kato *et al.* 2003; Kawanishi & Kiely 1989; Koga *et al.* 2000), but the levels of total secreted IgA in the intestine are not negatively affected (Senda *et al.* 1988; Thoreux *et al.* 2000). The data presented here confirm that the GC response in the PPs of aged mice is diminished, but that they age differently from GCs in mLNs and other peripheral LNs, where not only GC B cells, but also Tfh and Tfr cell numbers are affected by age. This demonstrates the unique effect of ageing on PPs compared to other SLOs. Unlike peripheral lymphoid tissues, the gut is constantly exposed to antigenic stimulation from the commensal microbiome. There are also specialised mechanisms of immune regulation in GCs in PPs, potentially to favour the generation of a highly diverse IgA pool in response to the constant exposure to microbial antigens (Reboldi & Cyster 2016; Stebegg, Kumar, Silva-Cayetano *et al.* 2018). This has been linked with unique properties of DCs, Tfh cells and Tfr cells in PPs compared to LNs (Stebegg, Kumar, Silva-Cayetano *et al.* 2018), which may impact how ageing affects these cell types and the PP GC response.

6.2.1.2 The IgA-mediated control of the gut microbiome is largely GC independent

Fagarasan and co-workers have implicated IgA antibodies produced in a GC-dependent manner in PPs in the control of gut microbial homeostasis (Kawamoto *et al.* 2012; 2014; Wei *et al.* 2011). There is conflicting evidence, however, from mice lacking either T-dependent immune responses

(CD28-deficient mice (Gärdby *et al.* 2003) and CD40-deficient mice (Bergqvist *et al.* 2006)) or Tfh cells (*Bcl6*$^{fl/fl}$*Cd4*$^{cre/+}$ (Bunker *et al.* 2015)). These animals, all of which lack functional GC responses, have high mucosal IgA antibody titres and near-to-normal levels of bacterial IgA-coating were reported in *Bcl6*$^{fl/fl}$*Cd4*$^{cre/+}$ mice, suggesting that GC-independent IgA is the main regulator of the gut microbiome. Despite smaller GCs in the PPs of aged mice, I did not observe any defects in the total levels of mucosal IgA or commensal IgA-coating in older mice. This suggests that sufficient IgA is produced by a compensatory mechanism in a GC-independent manner and that changes in the gut microbiome during ageing are not likely driven by the reduced PP GC response of aged mice.

To test this hypothesis and rule out a role of the GC in controlling the gut microbiota, we studied *Bcl6*$^{fl/fl}$*Cd4*$^{cre/+}$ mice that lack Tfh cells and therefore do not have good GC responses. I found that only the abundance of one species, a type of SFB, was affected in the gut of these mice, indicating that PP GCs are not required to control the composition of the gut microbiome as a whole, but may have a role in controlling particular bacterial species. This addresses a controversial topic in the field and suggests that GCs contribute little to the overall IgA-mediated control of the gut microbiota. I hypothesise that current discrepancies in the literature could be linked with disparities in the composition of the gut microbiome in different animal facilities. Several mouse disease phenotypes have been shown to be affected by the presence or absence of SFB in the gut and my 16S rDNA sequencing data suggest that these bacteria are amongst the few whose abundance is regulated by GC-dependent IgA antibodies (Ericsson *et al.* 2015; Ivanov *et al.* 2009; Lee *et al.* 2011; Wu *et al.* 2010). Thus, changes in the PP GC response are expected to have a more pronounced effect in animals carrying SFB than in animals lacking this taxa. *Bcl6*$^{fl/fl}$*Cd4*$^{cre/+}$ mice housed at the Babraham Institute harbour only low levels of SFBs and do not exhibit changes in their gut microbiome compared to littermate controls, while SFBs constitute a large proportion of the gut commensals detected in mice used by Fagarasan and co-workers, which experience large differences in their gut microbiota composition upon changes in GC-dependent IgA production (Kawamoto *et al.* 2014; Suzuki *et al.* 2004). These differences could explain how the GC-dependent control of only a very limited set of bacterial taxa can have global effects on gut microbial composition in some mice. This also highlights that vendor- and facility-specific differences in the composition of the gut microbiome cannot be neglected when studying the cross-talk between the gut microbiome and the gut immune system.

6.2.1.3 No obvious effects of FMT on antigen-specific GC responses in the PPs of aged mice

Even though the importance of GC-derived IgA antibodies for controlling the gut microbiome is under debate, they have a clear role in the protection against intestinal pathogens (Hashizume *et al.* 2008) and oral tolerance (Fujihashi *et al.* 2001). Kato *et al*. linked impaired oral tolerance in aged mice with impaired PP GCs (Kato *et al.* 2003), associated with defective M cell maturation in the PPs of aged mice (Kobayashi *et al.* 2013). Thus, the increase in intestinal infections in the elderly could be linked with an age-associated defect in their Peyer's patches (Kolling *et al.* 2012). In this thesis, I describe an age-associated reduction in PP GC B cells, which is reverted by the acquisition of the microbiome of a younger animal. This demonstrates that the poor GC reaction in aged animals is not irreversible, and can be boosted by changes in the gut microbiome.

Shin *et al*. demonstrated that the microbial transfer of a young microbiome into aged hosts increases protection against *C. difficile* infections in these mice (Shin *et al.* 2018). Also in humans, FMT has proven to be an effective treatment against *C. difficile* infections in both young and older individuals (Friedman-Korn *et al.* 2018; Mamo *et al.* 2018). Two mechanisms for how FMT enhances protection against *C. difficile* infections have been proposed: the induction of protective mucosal immune responses or restoration of microbiota-dependent protection (Khoruts & Sadowsky 2016). In the experiments reported here, FMT did not improve local or systemic immune responses to NP-CTx in aged mice, suggesting that FMT does not enhance immune responses to this antigen under the conditions used. Before completely excluding any beneficial effects of FMT on antigen-specific PP GC responses, however, some open questions should be addressed: is the effect of FMT and co-housing on the composition of the gut microbiome transient or stable? Similarly, is the boost in GC B cells in the PPs of aged mice upon microbial transfer transient or stable? Prolonged co-housing experiments and an extension of the observation period after FMT could help to answer these questions. Maybe FMT could enhance antigen-specific immune responses if NP-CTx immunisations are performed at a later time point, when the gut microbiome and the effects of FMT on the PP GC reaction have stabilised?

Another unanswered question is whether microbial transfers boost the PP GC reaction by antigenic stimulation, by acting as an adjuvant for existing GCs, or a combination of the two. Both FMT and the administration of the strong immunogen CTx were found to boost GC B cell numbers in the PPs of aged mice. This indicates that the expansion of the GC reaction by FMT is not due to reactivation of commensal-specific memory B cells. Rather, it suggests that both FMT and CTx boost PP GC reactions in an antigen- or adjuvant-like manner. Sequencing analysis of the B cell repertoires in aged mice which received FMT and PBS-treated control mice could help to

distinguish between these two mechanisms. If FMT acted as an adjuvant, this should lead to the numerical expansion of pre-existing GC B cell clones, while antigenic stimulation would result in the emergence of new clones, which would potentially be shared amongst FMT recipients. Answering the questions above could help to reveal or refute any potential beneficial effects of FMT on antigen-specific GC responses in the gut.

6.2.1.4 Rejuvenation of the gut microbiome as a potential intervention to improve healthy ageing

Age-associated changes in the composition of the gut microbiome have been linked with increased frailty and systemic inflammation (Claesson *et al.* 2012; Fransen *et al.* 2017; Maffei *et al.* 2017). Germ-free mice were found to live longer than their SPF counterparts (Thevaranjan *et al.* 2017) and short-lived Killifish colonised with a young microbiome were found to live longer than untreated fish (Smith *et al.* 2017). The supplementation of older individuals and aged mice with pre- and probiotics was also found to improve gut immunity in the elderly (Kaburagi *et al.* 2007; Landete *et al.* 2017). This suggests a direct effect of the rejuvenation of the gut microbiome in aged individuals on intestinal health as well as lifespan.

We were able to demonstrate that cohousing is very effective in altering the composition of the microbiome of aged mice and that one single FMT, even without previous antibiotic treatment, is sufficient to achieve the same effect. This raises the question whether FMT from young donors or cohabitation with young individuals could also improve healthspan in older individuals? FMT is already in routine use for the treatment of *C. difficile* infections in aged patients in the UK (NICE guidelines, 2014). A long-term follow-up study of patients who received FMT from a younger donor as a successful treatment of their *C. difficile* infection could reveal potential beneficial effects of FMT on other age-associated disorders. These studies might also uncover associations of any FMT-associated health benefits with the transfer of certain bacterial species. However, I detected no conservation of the bacterial species transferred from adult into aged mice during co-housing or FMT between C57BL/6 and BALB/c mice. This could indicate that rejuvenation of the gut microbiome exerts its effects by reintroducing bacterial functions shared between taxa, such as the generation of short-chain fatty acids or other bacterial metabolites, or by the simple transfer of antigen back into aged mice, rather than the transfer of specific bacterial species with immunogenic properties. Metagenomics studies could reveal such shared bacterial functions, which are missing in the gut microbiome of aged animals and are replenished by microbial transfers from adult mice (Alves *et al.* 2018).

Cohabitation has also been described to have strong effects on both the gut microbiome and the cellular composition of the immune system, with people living together sharing more bacterial species and having more similar immunoprofiles than individuals from different households (Carr *et al.* 2016; Song *et al.* 2013). What is more, Claesson *et al.* observed a significant decrease in gut bacterial diversity in aged individuals living in long-stay care compared to community dwellers and this was associated with increased age-associated frailty (Claesson *et al.* 2012). This suggests a possible link between environmental factors, gut microbiota composition and the immune system not only in mice and fish, but also in humans. In addition to cohabitation and FMT (Gupta *et al.* 2016), probiotics (Landete *et al.* 2017) and diet (Clements & R. Carding 2018) also have a strong impact on the composition of the gut microbiome. Separately or in combination, they could prove to be effective interventions to promote intestinal health and healthy ageing.

6.2.2 T cell priming in aged mice is improved by enhanced type I IFN signalling in cDC2s

Immune responses of older individuals to infections or vaccinations are reduced, at least in part due to defects in the GC response and a subsequent reduction in the generation of antigen-specific antibodies (Gustafson *et al.* 2018; Linterman 2014). This is associated with increased infection-related morbidity and mortality in the elderly (Linterman 2014) and creates a burden for public healthcare in ageing societies (WHO 2011). Therefore, there are many efforts to enhance GC-dependent vaccination responses in older individuals, *e.g.* to influenza vaccinations. Injections of increased antigen doses (Remarque *et al.* 1993) and modifications of the vaccine adjuvant (Frech *et al.* 2005) were found to improve vaccination responses in older subjects. Recently, type I IFNs have also emerged as potent vaccine adjuvants (Bracci *et al.* 2008; Proietti *et al.* 2002). The TLR7-agonist imiquimod induces the production of type I IFNs *in vivo* and potently enhances influenza vaccine responses in older individuals (Hung *et al.* 2014; 2016). This demonstrates that age-related defects in vaccine responses are not irreversible, and can be targeted therapeutically to improve immune protection in older individuals. Our study provides novel mechanistic insights into how imiquimod might enhance vaccination responses *in vivo*.

6.2.2.1 The age-associated reduction of the GC response is linked with defects in several GC cell types

By boosting type I IFN signalling in DCs at the time of immunisation using imiquimod, Tfh cell differentiation was improved in aged mice. This restoration of Tfh cell responses corresponded to a significant, but small, increase in the formation of GC B cells, indicating that impaired GC

responses in aged mice are only partly driven by a reduction in Tfh cells, and are also linked with age-associated defects in other GC components (Linterman 2014). B cells from aged mice, when transferred into young hosts, were found to have reduced rates of SHM, but were otherwise fully capable of forming GCs in a young environment (Yang *et al.* 1996). This suggests that the impaired expansion of GC B cells in aged mice is primarily due to B cell-extrinsic defects. Sage *et al.* reported on reduced B cell help by Tfh cells in aged mice, which was not linked with a reduction in Tfh cells, but with the reduced expression of the important co-stimulatory molecules ICOS and CD40L on the surface of aged T cells, combined with increased levels of co-inhibitory PD-1 (Sage *et al.* 2015). Also in humans, B cell help from memory Tfh cells during recall responses was found to be impaired (Yu *et al.* 2012). In this thesis, I demonstrated that administration of imiquimod at the time of immunisation potently enhances the generation of Tfh cells in aged mice, but I didn't test the ability of these Tfh cells to provide B cell help. B cell co-cultures with Tfh cells as well as flow cytometric analysis of CD40, ICOS, IL-21 and IL-4 expression by Tfh cells after immunisation with or without imiquimod could reveal potential beneficial effects of imiquimod not only on Tfh cell formation, but also Tfh cell-dependent B cell help.

In addition to defects in the T cell (and DC) compartment, FDCs in aged mice form smaller networks and retain fewer antigen-immune complexes 24 hours after immunisation compared to adult mice (Turner & Mabbott 2017). Sage *et al*. also reported on an increase of suppressive Tfr cells in the LNs of aged BALB/c mice (Sage *et al.* 2015), which we confirmed in our lab. Taken together, this suggests that the defect in GC B cell expansion observed in aged mice is not only linked with a defect in T cell priming, but possibly also with reduced B cell help from Tfh cells, reduced antigen retention on FDCs and increased suppression by Tfr cells. Thus, in addition to imiquimod, further therapeutic routes targeting FDCs, Tfr cells and Tfh cell-mediated B cell help need to be explored for full restoration of GC B cell formation and antibody production in aged mice.

6.2.2.2 Imiquimod: a potential vaccine adjuvant in humans

In humans the topical application of imiquimod on injection sites can potently enhance antibody production in response to vaccination (Hung *et al.* 2014; 2016). This suggests that in humans, imiquimod might be sufficient to not only boost T cell priming but also B cell responses. So, does imiquimod act *via* a similar mechanism in both mice and humans? Using human skin explants, Fehres *et al.* demonstrated that imiquimod also enhances migration and CD80/86 expression of human DCs from young donors (Fehres *et al.* 2014). To confirm that this action mode of imiquimod is retained in older individuals, *in vitro* experiments with DCs isolated from the blood or skin

biopsies of older compared to younger individuals are required. Circulating peripheral blood Tfh cells can be used as biomarker for Tfh cell responses in SLOs and could be analysed by flow cytometry to assess the effect of imiquimod treatment on Tfh cell differentiation and overall GC responses *in vivo* (Heit *et al.* 2017; Linterman & Hill 2016). What is more, fine needle aspirates of lymph nodes coupled with flow cytometry have recently emerged as a promising method to quantitatively monitor germinal centre activity in primates and humans where lymph nodes are not easily obtained (Havenar-Daughton *et al.* 2016; Silowash *et al.* 2016). These fine needle aspirates could provide additional insights into the effect of imiquimod on DCs, Tfh cell formation and GC B cell responses in aged humans *in vivo*. This could help the design of novel type I IFN-based adjuvants or other DC-targeted adjuvants with enhanced efficacy in the elderly, based on the novel link between defective type I IFN signalling in DCs with age-associated defects in the GC response reported in this thesis.

In conclusion, the work reported here revealed that adaptive immunity is strongly influenced by environmental changes. Both cellular stress as well as ageing have previously been reported to exert global effects on immune cell functions (Bettigole & Glimcher 2015; Montecino-Rodriguez *et al.* 2013). The data presented here reveal a previously unknown role for the ER stress response in inducing Th17 differentiation, potentially associated with Th17 cell pathogenicity in autoimmune disorders. The studies of GC responses in aged mice presented here further revealed that not only the gut microbiome, but also DCs are exciting targets to improve GC responses in ageing. Taken together, this demonstrates that environmental stimuli shape adaptive immunity by enhancing T helper cell differentiation and the germinal centre response.

7 REFERENCES

Aberle, J.H., K. Stiasny, M. Kundi & F.X. Heinz, 2013. Mechanistic insights into the impairment of memory B cells and antibody production in the elderly, *AGE* 35(2), 371–81.

Adamu, A., F. Aliyu, A.H. Aminu & B.S. Mienda, 2017. Phenotypic and functional features of CD4 + T helper cells subsets, *Life Science Press* 1(1), 19–24.

Agrawal, A., 2013. Mechanisms and implications of age-associated impaired innate interferon secretion by dendritic cells: a mini-review., *Gerontology* 59(5), 421–26.

Agrawal, A., S. Agrawal, J.-N. Cao, H. Su, K. Osann & S. Gupta, 2007. Altered innate immune functioning of dendritic cells in elderly humans: a role of phosphoinositide 3-kinase-signaling pathway., *Journal of immunology* 178(11), 6912–22.

Agrawal, A., S. Agrawal & S. Gupta, 2017. Role of Dendritic Cells in Inflammation and Loss of Tolerance in the Elderly, *Frontiers in Immunology* 8, 896.

Alberts, B., A. Johnson, J. Lewis, M. Raff, K. Roberts & P. Walter, 2002a. Lymphocytes and the Cellular Basis of Adaptive Immunity, in *Molecular Biology of the Cell*. , 4th edition. New York: Garland Science.

Alberts, B., A. Johnson, J. Lewis, M. Raff, K. Roberts & P. Walter, 2002b. The Generation of Antibody Diversity, in *Molecular Biology of the Cell*. , 4th edition. New York: Garland Science.

Allen, C.D.C., K.M. Ansel, C. Low, R. Lesley, H. Tamamura, N. Fujii & J.G. Cyster, 2004. Germinal center dark and light zone organization is mediated by CXCR4 and CXCR5., *Nature immunology* 5(9), 943–52.

Aloulou, M., E.J. Carr, M. Gador, A. Bignon, R.S. Liblau, N. Fazilleau & M.A. Linterman, 2016. Follicular regulatory T cells can be specific for the immunizing antigen and derive from naive T cells, *Nature Communications* 7(1), 10579.

Alves, L. de F., C.A. Westmann, G.L. Lovate, G.M.V. de Siqueira, T.C. Borelli & M.-E. Guazzaroni, 2018. Metagenomic Approaches for Understanding New Concepts in Microbial Science, *International Journal of Genomics* 2018, 1–15.

Appenzeller-Herzog, C. & M.N. Hall, 2012. Bidirectional crosstalk between endoplasmic reticulum stress and mTOR signaling., *Trends in cell biology* 22(5), 274–82.

Ashburner, M., C.A. Ball, J.A. Blake, D. Botstein, H. Butler, J.M. Cherry, A.P. Davis, K. Dolinski, S.S. Dwight, J.T. Eppig, M.A. Harris, D.P. Hill, L. Issel-Tarver, A. Kasarskis, S. Lewis, J.C. Matese, J.E. Richardson, M. Ringwald, G.M. Rubin & G. Sherlock, 2000. Gene Ontology: tool for the unification of biology, *Nature Genetics* 25(1), 25–29.

Bailey, S.R., M.H. Nelson, R.A. Himes, Z. Li, S. Mehrotra & C.M. Paulos, 2014. Th17 cells in cancer: the ultimate identity crisis., *Frontiers in immunology* 5, 276.

Balato, A., D. Unutmaz & A.A. Gaspari, 2009. Natural Killer T Cells: An Unconventional T-Cell Subset with Diverse Effector and Regulatory Functions, *Journal of Investigative Dermatology* 129(7), 1628–42.

Banerjee, M., R. Mehr, A. Belelovsky, J. Spencer & D.K. Dunn-Walters, 2002. Age- and tissue-specific differences in human germinal center B cell selection revealed by analysis of IgVH gene hypermutation and lineage trees, *European Journal of Immunology* 32(7), 1947–57.

Bannard, O., R.M. Horton, C.D.C. Allen, J. An, T. Nagasawa & J.G. Cyster, 2013. Germinal center centroblasts transition to a centrocyte phenotype according to a timed program and depend on the dark zone for effective selection, *Immunity* 39(5), 912–24.

Barbet, G., L.E. Sander, M. Geswell, I. Leonardi, A. Cerutti, I. Iliev & J.M. Blander, 2018. Sensing Microbial Viability through Bacterial RNA Augments T Follicular Helper Cell and Antibody Responses, *Immunity* 48(3), 584–98.

Barnden, M.J., J. Allison, W.R. Heath & F.R. Carbone, 1998. Defective TCR expression in transgenic mice constructed using cDNA-based α- and β-chain genes under the control of heterologous regulatory elements, *Immunology and Cell Biology* 76(1), 34–40.

Bassing, C.H., W. Swat & F.W. Alt, 2002. The Mechanism and Regulation of Chromosomal V(D)J Recombination, *Cell* 109(2), S45–55.

Batista, F.D. & N.E. Harwood, 2009. The who, how and where of antigen presentation to B cells, *Nature Reviews Immunology* 9(1), 15–27.

Batten, M., N. Ramamoorthi, N.M. Kljavin, C.S. Ma, J.H. Cox, H.S. Dengler, D.M. Danilenko, P. Caplazi, M. Wong, D.A. Fulcher, M.C. Cook, C. King, S.G. Tangye, F.J. de Sauvage & N. Ghilardi, 2010. IL-27 supports germinal center function by enhancing IL-21 production and the function of T follicular helper cells, *The Journal of Experimental Medicine* 207(13), 2895–2906.

Baumgarth, N., 2011. The double life of a B-1 cell: self-reactivity selects for protective effector functions, *Nature Reviews Immunology* 11(1), 34–46.

Bedoya, S.K., B. Lam, K. Lau & J. Larkin, 2013. Th17 cells in immunity and autoimmunity., *Clinical & Developmental Immunology* 2013, 986789.

Belkaid, Y. & T.W.W. Hand, 2014. Role of the Microbiota in Immunity and Inflammation, *Cell* 157(1), 121–41.

Bennett, C.L., J. Christie, F. Ramsdell, M.E. Brunkow, P.J. Ferguson, L. Whitesell, T.E. Kelly, F.T. Saulsbury, P.F. Chance & H.D. Ochs, 2001. The immune dysregulation, polyendocrinopathy, enteropathy, X-linked syndrome (IPEX) is caused by mutations of FOXP3, *Nature Genetics* 27(1), 20–21.

Bennstein, S.B., 2017. Unraveling Natural Killer T-Cells Development., *Frontiers in immunology* 8, 1950.

Bergqvist, P., E. Gärdby, A. Stensson, M. Bemark & N.Y. Lycke, 2006. Gut IgA class switch recombination in the absence of CD40 does not occur in the lamina propria and is independent of germinal centers., *Journal of immunology* 177(11), 7772–83.

Bergqvist, P., A. Stensson, L. Hazanov, A. Holmberg, J. Mattsson, R. Mehr, M. Bemark & N.Y. Lycke, 2013. Re-utilization of germinal centers in multiple Peyer's patches results in highly synchronized, oligoclonal and affinity-matured gut IgA responses, *Mucosal Immunology* 6(1), 122–35.

Bettelli, E., M. Pagany, H.L. Weiner, C. Linington, R.A. Sobel & V.K. Kuchroo, 2003. Myelin Oligodendrocyte Glycoprotein–specific T Cell Receptor Transgenic Mice Develop Spontaneous Autoimmune Optic Neuritis, *The Journal of Experimental Medicine* 197(9), 1073–81.

Bettigole, S.E. & L.H. Glimcher, 2015. Endoplasmic Reticulum Stress in Immunity, *Annu. Rev. Immunol* 33, 107–38.

Biagi, E., L. Nylund, M. Candela, R. Ostan, L. Bucci, E. Pini, J. Nikkïla, D. Monti, R. Satokari, C. Franceschi, P. Brigidi & W. De Vos, 2010. Through Ageing, and Beyond: Gut Microbiota and Inflammatory Status in Seniors and Centenarians, *PLoS ONE* 5(5), .

Blank, U. & S. Karlsson, 2015. TGF-β signaling in the control of hematopoietic stem cells., *Blood* 125(23), 3542–50.

Blum, J.S., P.A. Wearsch & P. Cresswell, 2013. Pathways of antigen processing., *Annu. Rev. Immunol* 31(1), 443–73.

Bonilla, F.A. & H.C. Oettgen, 2010. Adaptive immunity, *Journal of Allergy and Clinical Immunology* 125(2), S33–40.

Bortnick, A. & D. Allman, 2013. What is and what should always have been: long-lived plasma cells induced by T cell-independent antigens., *Journal of immunology* 190(12), 5913–18.

Bracci, L., V. La Sorsa, F. Belardelli & E. Proietti, 2008. Type I interferons as vaccine adjuvants against infectious diseases and cancer, *Expert Review of Vaccines* 7(3), 373–81.

Brahmakshatriya, V., Y. Kuang, P. Devarajan, J. Xia, W. Zhang, A.M. Vong & S.L. Swain, 2017. IL-6 Production by TLR-Activated APC Broadly Enhances Aged Cognate CD4 Helper and B Cell Antibody Responses In Vivo., *Journal of immunology* 198(7), 2819–33.

Brown, M.K. & N. Naidoo, 2012. The endoplasmic reticulum stress response in aging and age-related diseases, *Frontiers in Physiology* 3, 263.

Brucklacher-Waldert, V., C. Ferreira, M. Stebegg, O. Fesneau, S. Innocentin, J.C. Marie & M. Veldhoen, 2017. Cellular Stress in the Context of an Inflammatory Environment Supports TGF-β-Independent T Helper-17 Differentiation, *Cell Reports* 19(11), .

Brunkow, M.E., E.W. Jeffery, K.A. Hjerrild, B. Paeper, L.B. Clark, S.-A. Yasayko, J.E. Wilkinson, D. Galas, S.F. Ziegler & F. Ramsdell, 2001. Disruption of a new forkhead/winged-helix protein, scurfin, results in the fatal lymphoproliferative disorder of the scurfy mouse., *Nature Genetics* 27(1), 68–73.

Brüstle, A., S. Heink, M. Huber, C. Rosenplänter, C. Stadelmann, P. Yu, E. Arpaia, T.W. Mak, T. Kamradt & M. Lohoff, 2007. The development of inflammatory TH-17 cells requires interferon-regulatory factor 4, *Nature Immunology* 8(9), 958–66.

Buchbinder, E.I. & A. Desai, 2016. CTLA-4 and PD-1 Pathways: Similarities, Differences, and Implications of Their Inhibition., *American journal of clinical oncology* 39(1), 98–106.

Buford, T.W., 2017. (Dis)Trust your gut: the gut microbiome in age-related inflammation, health, and disease, *Microbiome* 5(1), 80.

Bunker, J.J. & A. Bendelac, 2018. IgA Responses to Microbiota, *Immunity* 49(2), 211–24.

Bunker, J.J., T.M. Flynn, J.C. Koval, D.G. Shaw, M. Meisel, B.D. McDonald, I.E. Ishizuka, A.L. Dent, P.C. Wilson, B. Jabri, D.A. Antonopoulos & A. Bendelac, 2015. Innate and Adaptive Humoral Responses Coat Distinct Commensal Bacteria with Immunoglobulin A, *Immunity* 43(3), 541–53.

Cantrell, D., 2015. Signaling in Lymphocyte Activation, *Cold Spring Harbor Perspectives in Biology* 7(6), .

Caporaso, J.G., J. Kuczynski, J. Stombaugh, K. Bittinger, F.D. Bushman, E.K. Costello, N. Fierer, A.G. Peña, J.K. Goodrich, J.I. Gordon, G.A. Huttley, S.T. Kelley, D. Knights, J.E. Koenig, R.E. Ley, C.A. Lozupone, D. McDonald, B.D. Muegge, M. Pirrung, J. Reeder, J.R. Sevinsky, P.J. Turnbaugh, W.A. Walters, J. Widmann, T. Yatsunenko, J. Zaneveld & R. Knight, 2010. QIIME allows analysis of high-throughput community sequencing data, *Nature Methods* 7(5), 335–36.

Carr, E.J., J. Dooley, J.E. Garcia-Perez, V. Lagou, J.C. Lee, C. Wouters, I. Meyts, A. Goris, G. Boeckxstaens, M.A. Linterman & A. Liston, 2016. The cellular composition of the human immune system is shaped by age and cohabitation., *Nature immunology* 17(4), 461–68.

Casamayor-Palleja, M., J. Feuillard, J. Ball, M. Drew & I.C. MacLennan, 1996. Centrocytes rapidly adopt a memory B cell phenotype on co-culture with autologous germinal centre T cell-enriched preparations., *International immunology* 8(5), 737–44.

Casteleyn, C., A. Rekecki, A. Van Der Aa, P. Simoens & W. Van Den Broeck, 2010. Surface area assessment of the murine intestinal tract as a prerequisite for oral dose translation from mouse to man, *Laboratory Animals* 44(3), 176–83.

Caton, M.L., M.R. Smith-Raska & B. Reizis, 2007. Notch–RBP-J signaling controls the homeostasis of CD8 ⁻ dendritic cells in the spleen, *The Journal of Experimental Medicine* 204(7), 1653–64.

Cattaneo, A., N. Cattane, S. Galluzzi, S. Provasi, N. Lopizzo, C. Festari, C. Ferrari, U.P. Guerra, B. Paghera, C. Muscio, A. Bianchetti, G.D. Volta, M. Turla, M.S. Cotelli, M. Gennuso, A. Prelle, O. Zanetti, G. Lussignoli, D. Mirabile, D. Bellandi, S. Gentile, G. Belotti, D. Villani, T. Harach, T. Bolmont, A. Padovani, M. Boccardi & G.B. Frisoni, 2017. Association of brain amyloidosis with pro-inflammatory gut bacterial taxa and peripheral inflammation markers in cognitively impaired elderly, *Neurobiology of Aging* 49, 60–68.

Caza, T. & S. Landas, 2015. Functional and Phenotypic Plasticity of CD4(+) T Cell Subsets., *BioMed research international* 2015, 521957.

Chabas, D., S. Baranzini, D. Mitchell, C. Bernard, S. Rittling, D. Denhardt, R. Sobel, C. Lock, M. Karpuj, R. Pedotti, R. Heller, J. Oksenberg & L. Steinman, 2001. The Influence of the Proinflammatory Cytokine, Osteopontin, on Autoimmune Demyelinating Disease, *Science* 294(5547), 1731–35.

Chan, T.D., D. Gatto, K. Wood, T. Camidge, A. Basten & R. Brink, 2009. Antigen affinity controls rapid T-dependent antibody production by driving the expansion rather than the differentiation or extrafollicular migration of early plasmablasts., *Journal of immunology* 183(5), 3139–49.

Chang, J.E. & S.J. Turley, 2015. Stromal infrastructure of the lymph node and coordination of immunity, *Trends in Immunology* 36(1), 30–39.

Chaplin, D.D., 2010. Overview of the immune response., *The Journal of allergy and clinical immunology* 125(2 Suppl 2), S3-23.

Chen, L. & D.B. Flies, 2013. Molecular mechanisms of T cell co-stimulation and co-inhibition., *Nature Reviews Immunology* 13(4), 227–42.

Chen, Z., J. Liu, H. Ng, S. Nadarajah, H.L. Kaufman, J.Y. Yang & Y. Deng, 2011. Statistical methods on detecting differentially expressed genes for RNA-seq data, *BMC Systems Biology* 5, S1.

Chien, Y., C. Meyer & M. Bonneville, 2014. γδ T Cells: First Line of Defense and Beyond, *Annual Review of Immunology* 32(1), 121–55.

Ciofani, M. & J.C. Zúñiga-Pflücker, 2007. The Thymus as an Inductive Site for T Lymphopoiesis, *Annual Review of Cell and Developmental Biology* 23, 463–93.

Claesson, M.J., S. Cusack, O. O'Sullivan, R. Greene-Diniz, H. de Weerd, E. Flannery, J.R. Marchesi, D. Falush, T. Dinan, G. Fitzgerald, C. Stanton, D. van Sinderen, M. O'Connor, N. Harnedy, K. O'Connor, C. Henry, D. O'Mahony, A.P. Fitzgerald, F. Shanahan, C. Twomey, C. Hill, R.P. Ross & P.W. O'Toole, 2011. Composition, variability, and temporal stability of the intestinal microbiota of the elderly, *Proceedings of the National Academy of Sciences* 108, 4586–91.

Claesson, M.J., I.B. Jeffery, S. Conde, S.E. Power, E.M. O'Connor, S. Cusack, H.M.B. Harris, M. Coakley, B. Lakshminarayanan, O. O'Sullivan, G.F. Fitzgerald, J. Deane, M. O'Connor, N. Harnedy, K. O'Connor, D. O'Mahony, D. van Sinderen, M. Wallace, L. Brennan, C. Stanton, J.R. Marchesi, A.P. Fitzgerald, F. Shanahan, C. Hill, R.P. Ross & P.W. O'Toole, 2012. Gut microbiota composition correlates with diet and health in the elderly, *Nature* 488(7410), 178–84.

Clavel, T., I. Lagkouvardos, M. Blaut & B. Stecher, 2016. The mouse gut microbiome revisited: From complex diversity to model ecosystems, *International Journal of Medical Microbiology* 306(5), 316–27.

Clements, S.J. & S. R. Carding, 2018. Diet, the intestinal microbiota, and immune health in aging, *Critical Reviews in Food Science and Nutrition* 58(4), 651–61.

Cong, Y., T. Feng, K. Fujihashi, T.R. Schoeb & C.O. Elson, 2009. A dominant, coordinated T regulatory cell-IgA response to the intestinal microbiota., *Proceedings of the National Academy of Sciences of the United States of America* 106(46), 19256–61.

Craig, S.W. & J.J. Cebra, 1971. Peyer's patches: an enriched source of precursors for IgA-producing immunocytes in the rabbit., *The Journal of experimental medicine* 134(1), 188–200.

Cua, D.J., J. Sherlock, Y. Chen, C.A. Murphy, B. Joyce, B. Seymour, L. Lucian, W. To, S. Kwan, T. Churakova, S. Zurawski, M. Wiekowski, S.A. Lira, D. Gorman, R.A. Kastelein & J.D. Sedgwick, 2003. Interleukin-23 rather than interleukin-12 is the critical cytokine for autoimmune inflammation of the brain, *Nature* 421(6924), 744–48.

Cucak, H., U. Yrlid, B. Reizis, U. Kalinke & B. Johansson-Lindbom, 2009. Type I Interferon Signaling in Dendritic Cells Stimulates the Development of Lymph-Node-Resident T Follicular Helper Cells, *Immunity* 31(3), 491–501.

Cunningham-Rundles, C., 2001. Physiology of IgA and IgA Deficiency, *Journal of Clinical Immunology* 21(5), 303–9.

Cunningham, A.F., K. Serre, K.-M. Toellner, M. Khan, J. Alexander, F. Brombacher & I.C.M. MacLennan, 2004. Pinpointing IL-4-independent acquisition and IL-4-influenced maintenance of Th2 activity by CD4 T cells, *European Journal of Immunology* 34(3), 686–94.

Dang, E. V, J. Barbi, H.-Y. Yang, D. Jinasena, H. Yu, Y. Zheng, Z. Bordman, J. Fu, Y. Kim, H.-R. Yen, W. Luo, K. Zeller, L. Shimoda, S.L. Topalian, G.L. Semenza, C. V Dang, D.M. Pardoll & F. Pan, 2011. Control of T(H)17/T(reg) balance by hypoxia-inducible factor 1., *Cell* 146(5), 772–84.

Dardalhon, V., A. Awasthi, H. Kwon, G. Galileos, W. Gao, R.A. Sobel, M. Mitsdoerffer, T.B. Strom, W. Elyaman, I.-C. Ho, S. Khoury, M. Oukka & V.K. Kuchroo, 2008. IL-4 inhibits TGF-β-induced Foxp3+ T cells and, together with TGF-β, generates IL-9+ IL-10+ Foxp3− effector T cells, *Nature Immunology* 9(12), 1347–55.

Das, J., G. Ren, L. Zhang, A.I. Roberts, X. Zhao, A.L.M. Bothwell, L. Van Kaer, Y. Shi & G. Das, 2009. Transforming growth factor β is dispensable for the molecular orchestration of Th17 cell differentiation, *Journal of Experimental Medicine* 206(11), 2407–16.

Davis, M.M. & P.J. Bjorkman, 1988. T-cell antigen receptor genes and T-cell recognition, *Nature* 334(6181), 395–402.

Deslauriers, A.M., A. Afkhami-Goli, A.M. Paul, R.K. Bhat, S. Acharjee, K.K. Ellestad, F. Noorbakhsh, M. Michalak & C. Power, 2011. Neuroinflammation and Endoplasmic Reticulum Stress Are Coregulated by Crocin To Prevent Demyelination and Neurodegeneration, *Journal of immunology* 187(9), 4788–99.

Doebel, T., B. Voisin & K. Nagao, 2017. Langerhans Cells - The Macrophage in Dendritic Cell Clothing., *Trends in immunology* 38(11), 817–28.

Domingues, H.S., M. Mues, H. Lassmann, H. Wekerle & G. Krishnamoorthy, 2010. Functional and Pathogenic Differences of Th1 and Th17 Cells in Experimental Autoimmune Encephalomyelitis, *PLoS ONE* 5(11), .

Domínguez, P.M. & C. Ardavín, 2010. Differentiation and function of mouse monocyte-derived dendritic cells in steady state and inflammation, *Immunological Reviews* 234(1), 90–104.

Eaton, S.M., E.M. Burns, K. Kusser, T.D. Randall & L. Haynes, 2004. Age-related defects in CD4 T cell cognate helper function lead to reductions in humoral responses., *The Journal of experimental medicine* 200(12), 1613–22.

Eddahri, F., S. Denanglaire, F. Bureau, R. Spolski, W.J. Leonard, O. Leo & F. Andris, 2009. Interleukin-6/STAT3 signaling regulates the ability of naive T cells to acquire B-cell help capacities, *Blood* 113(11), 2426–33.

El-Behi, M., B. Ciric, H. Dai, Y. Yan, M. Cullimore, F. Safavi, G.X. Zhang, B.N. Dittel & A. Rostami, 2011. The encephalitogenicity of T(H)17 cells is dependent on IL-1- and IL-23-induced production of the cytokine GM-CSF, *Nat Immunol* 12(6), 568–75.

Ericsson, A.C., J.W. Davis, W. Spollen, N. Bivens, S. Givan, C.E. Hagan, M. McIntosh & C.L. Franklin, 2015. Effects of Vendor and Genetic Background on the Composition of the Fecal Microbiota of Inbred Mice, *PLOS ONE* 10(2), .

Fadlallah, J., H. El Kafsi, D. Sterlin, C. Juste, C. Parizot, K. Dorgham, G. Autaa, D. Gouas, M. Almeida, P. Lepage, N. Pons, E. Le Chatelier, F. Levenez, S. Kennedy, N. Galleron, J.-P.P. de Barros, M. Malphettes, L. Galicier, D. Boutboul, A. Mathian, M. Miyara, E. Oksenhendler, Z. Amoura, J. Doré, C. Fieschi, S.D. Ehrlich, M. Larsen & G. Gorochov, 2018. Microbial ecology perturbation in human IgA deficiency., *Science translational medicine* 10(439), .

Fagarasan, S., S. Kawamoto, O. Kanagawa & K. Suzuki, 2010. Adaptive Immune Regulation in the Gut: T Cell–Dependent and T Cell–Independent IgA Synthesis, *Annual Review of Immunology* 28(1), 243–73.

Fagarasan, S., M. Muramatsu, K. Suzuki, H. Nagaoka, H. Hiai & T. Honjo, 2002. Critical roles of activation-induced cytidine deaminase in the homeostasis of gut flora., *Science* 298(5597), 1424–27.

Fagundes, C., F. Amaral, A. Vieira, A. Soares, V. Pinho, J. Nicoli, L. Vieira, M. Teixeira & D. Souza, 2012. Transient TLR Activation Restores Inflammatory Response and Ability To Control Pulmonary Bacterial Infection in Germfree Mice, *Journal of immunology* 188, 1411–20.

Fehres, C.M., S.C.M. Bruijns, A.J. van Beelen, H. Kalay, M. Ambrosini, E. Hooijberg, W.W.J. Unger, T.D. de Gruijl & Y. van Kooyk, 2014. Topical rather than intradermal application of the TLR7 ligand imiquimod leads to human dermal dendritic cell maturation and CD8 $^{+}$ T-cell cross-priming, *European Journal of Immunology* 44(8), 2415–24.

Fei Teng, A., C.N. Klinger, K.M. Felix, C. Bradley, E. Wu, N.L. Tran, Y. Umesaki & H.-J.J. Wu, 2016. Gut Microbiota Drive Autoimmune Arthritis by Promoting Differentiation and Migration of Peyer's Patch T Follicular Helper Cells, *Immunity* 44(4), 875–88.

FELASA working group, M. Mähler Convenor, M. Berard, R. Feinstein, A. Gallagher, B. Illgen-Wilcke, K. Pritchett-Corning & M. Raspa, 2014. FELASA recommendations for the health monitoring of mouse, rat, hamster, guinea pig and rabbit colonies in breeding and experimental units, *Laboratory Animals* 48(3), 178–92.

Feske, S., 2007. Calcium signalling in lymphocyte activation and disease, *Nature Reviews Immunology* 7(9), 690–702.

Fleming, K.K., J.A. Bovaird, M.C. Mosier, M.R. Emerson, S.M. LeVine & J.G. Marquis, 2005. Statistical analysis of data from studies on experimental autoimmune encephalomyelitis, *Journal of Neuroimmunology* 170(1–2), 71–84.

Fontenot, J.D., M.A. Gavin & A.Y. Rudensky, 2003. Foxp3 programs the development and function of CD4+CD25+ regulatory T cells, *Nature Immunology* 4(4), 330–36.

Foy, T.M., D.M. Shepherd, F.H. Durie, A. Aruffo, J.A. Ledbetter & R.J. Noelle, 1993. In vivo CD40-gp39 interactions are essential for thymus-dependent humoral immunity. II. Prolonged suppression of the humoral immune response by an antibody to the ligand for CD40, gp39., *The Journal of experimental medicine* 178(5), 1567–75.

Fransen, F., A.A. van Beek, T. Borghuis, S. El Aidy, F. Hugenholtz, C. van der Gaast – de Jongh, H.F.J. Savelkoul, M.I. De Jonge, M. V. Boekschoten, H. Smidt, M.M. Faas & P. de Vos, 2017. Aged Gut Microbiota Contributes to Systemical Inflammaging after Transfer to Germ-Free Mice., *Frontiers in immunology* 8, 1385.

Frech, S.A., R.T. Kenney, C.A. Spyr, H. Lazar, J.-F. Viret, C. Herzog, R. Glück & G.M. Glenn, 2005. Improved immune responses to influenza vaccination in the elderly using an immunostimulant patch, *Vaccine* 23(7), 946–50.

Friedman-Korn, T., D.M. Livovsky, N. Maharshak, N. Aviv Cohen, K. Paz, A. Bar-Gil Shitrit, E. Goldin & B. Koslowsky, 2018. Fecal Transplantation for Treatment of Clostridium Difficile Infection in Elderly and Debilitated Patients, *Digestive Diseases and Sciences* 63(1), 198–203.

Fu, W., X. Liu, X. Lin, H. Feng, L. Sun, S. Li, H. Chen, H. Tang, L. Lu, W. Jin & C. Dong, 2018. Deficiency in T follicular regulatory cells promotes autoimmunity., *The Journal of experimental medicine* 215(3), 815–25.

Fujihashi, K., T. Dohi, P.D. Rennert, M. Yamamoto, T. Koga, H. Kiyono & J.R. McGhee, 2001. Peyer's patches are required for oral tolerance to proteins, *Proceedings of the National Academy of Sciences* 98(6), 3310–15.

Gagliani, N. & S. Huber, 2017. Basic Aspects of T Helper Cell Differentiation, *Methods in Molecular Biology* 1514, 19–30.

Ganapathy-Kanniappan, S., J.-F.H. Geschwind, R. Kunjithapatham, M. Buijs, L.H. Syed, P.P. Rao, S. Ota, B.K. Kwak, R. Loffroy & M. Vali, 2010. 3-Bromopyruvate induces endoplasmic reticulum stress, overcomes autophagy and causes apoptosis in human HCC cell lines., *Anticancer research* 30(3), 923–35.

Gärdby, E., J. Wrammert, K. Schön, L. Ekman, T. Leanderson & N. Lycke, 2003. Strong Differential Regulation of Serum and Mucosal IgA Responses as Revealed in CD28-Deficient Mice Using Cholera Toxin Adjuvant, *The Journal of Immunology* 170(1), 55–63.

Garg, A.D., A. Kaczmarek, O. Krysko, P. Vandenabeele, D. V. Krysko & P. Agostinis, 2012. ER stress-induced inflammation: does it aid or impede disease progression?, *Trends in Molecular Medicine* 18(10), 589–98.

Georgiev, H., I. Ravens, G. Papadogianni, S. Halle, B. Malissen, G.G. Loots, R. Förster & G. Bernhardt, 2018. Shared and Unique Features Distinguishing Follicular T Helper and Regulatory Cells of Peripheral Lymph Node and Peyer's Patches, *Frontiers in Immunology* 9, 714.

Ghoreschi, K., A. Laurence, X.-P. Yang, C.M. Tato, M.J. McGeachy, J.E. Konkel, H.L. Ramos, L. Wei, T.S. Davidson, N. Bouladoux, J.R. Grainger, Q. Chen, Y. Kanno, W.T. Watford, H.-W. Sun, G. Eberl, E.M. Shevach, Y. Belkaid, D.J. Cua, W. Chen & J.J. O'Shea, 2010. Generation of pathogenic T(H)17 cells in the absence of TGF-β signalling., *Nature* 467(7318), 967–71.

Ghosh, S., 2004. *T Cell Receptor Signaling Pathway | Cell Signaling Technology*. T cell Receptor Signaling Pathway 2004 . https://www.cellsignal.com/contents/science-pathway-research-immunology-and-inflammation/t-cell-receptor-signaling-pathway/pathways-tcell [Accessed 24 Nov 2016].

Gitlin, A.D., Z. Shulman & M.C. Nussenzweig, 2014. Clonal selection in the germinal centre by regulated proliferation and hypermutation, *Nature* 509(7502), 637–40.

Glusman, G., L. Rowen, I. Lee, C. Boysen, J.C. Roach, A.F.A. Smit, K. Wang, B.F. Koop & L. Hood, 2001. Comparative Genomics of the Human and Mouse T Cell Receptor Loci, *Immunity* 15(3), 337–49.

González-Fernández, A., D. Gilmore & C. Milstein, 1994. Age-related decrease in the proportion of germinal center B cells from mouse Peyer's patches is accompanied by an accumulation of somatic mutations in their immunoglobulin genes, *European Journal of Immunology* 24(11), 2918–21.

González, D., M. van der Burg, R. García-Sanz, J.A. Fenton, A.W. Langerak, M. González, J.J. van Dongen, J.F. San Miguel & G.J. Morgan, 2007. Immunoglobulin gene rearrangements and the pathogenesis of multiple myeloma., *Blood* 110(9), 3112–21.

Goodrich, J.K., S.C. Di Rienzi, A.C. Poole, O. Koren, W.A. Walters, J.G. Caporaso, R. Knight & R.E. Ley, 2014. Conducting a Microbiome Study, *Cell* 158(2), 250–62.

Gringhuis, S.I., T.M. Kaptein, B.A. Wevers, M. van der Vlist, E.J. Klaver, I. van Die, L.E.M. Vriend, M.A.W.P. de Jong & T.B.H. Geijtenbeek, 2014. Fucose-based PAMPs prime dendritic cells for follicular T helper cell polarization via DC-SIGN-dependent IL-27 production, *Nature Communications* 5(1), 5074.

Guilliams, M., C.-A. Dutertre, C.L. Scott, N. McGovern, D. Sichien, S. Chakarov, S. Van Gassen, J. Chen, M. Poidinger, S. De Prijck, S.J. Tavernier, I. Low, S.E. Irac, C.N. Mattar, H.R. Sumatoh, G.H.L. Low, T.J.K. Chung, D.K.H. Chan, K.K. Tan, T.L.K. Hon, E. Fossum, B. Bogen, M. Choolani, J.K.Y. Chan, A. Larbi, H. Luche, S. Henri, Y. Saeys, E.W. Newell, B.N. Lambrecht, B. Malissen & F. Ginhoux, 2016. Unsupervised High-Dimensional Analysis Aligns Dendritic Cells across Tissues and Species., *Immunity* 45(3), 669–84.

Gupta, S., E. Allen-Vercoe & E.O. Petrof, 2016. Fecal microbiota transplantation: in perspective., *Therapeutic advances in gastroenterology* 9(2), 229–39.

Gurkan, U.A. & O. Akkus, 2008. The Mechanical Environment of Bone Marrow: A Review, *Annals of Biomedical Engineering* 36(12), 1978–91.

Gustafson, C.E., C.M. Weyand & J.J. Goronzy, 2018. T follicular helper cell development and functionality in immune ageing., *Clinical science (London, England : 1979)* 132(17), 1925–35.

Harding, F.A., J.G. McArthur, J.A. Gross, D.H. Raulet & J.P. Allison, 1992. CD28-mediated signalling co-stimulates murine T cells and prevents induction of anergy in T-cell clones, *Nature* 356(6370), 607–9.

Hardy, R.R. & K. Hayakawa, 2001. B cell development pathways, *Annual Review of Immunology* 19(1), 595–621.

Harris, T.J., J.F. Grosso, H.-R. Yen, H. Xin, M. Kortylewski, E. Albesiano, E.L. Hipkiss, D. Getnet, M. V. Goldberg, C.H. Maris, F. Housseau, H. Yu, D.M. Pardoll & C.G. Drake, 2007. Cutting Edge: An In Vivo Requirement for STAT3 Signaling in TH17 Development and TH17-Dependent Autoimmunity, *The Journal of Immunology* 179(7), 4313–17.

Hashizume, T., A. Togawa, T. Nochi, O. Igarashi, M.-N. Kweon, H. Kiyono & M. Yamamoto, 2008. Peyer's patches are required for intestinal immunoglobulin A responses to Salmonella spp., *Infection and immunity* 76(3), 927–34.

Hassanzadeh-Kiabi, N., A. Yáñez, I. Dang, G.A. Martins, D.M. Underhill & H.S. Goodridge, 2017. Autocrine Type I IFN Signaling in Dendritic Cells Stimulated with Fungal β-Glucans or Lipopolysaccharide Promotes CD8 T Cell Activation., *Journal of immunology* 198(1), 375–82.

Havenar-Daughton, C., D.G. Carnathan, A. Torrents de la Peña, M. Pauthner, B. Briney, S.M. Reiss, J.S. Wood, K. Kaushik, M.J. van Gils, S.L. Rosales, P. van der Woude, M. Locci, K.M. Le, S.W. de Taeye, D. Sok, A.U.R. Mohammed, J. Huang, S. Gumber, A. Garcia, S.P. Kasturi, B. Pulendran, J.P. Moore, R. Ahmed, G. Seumois, D.R. Burton, R.W. Sanders, G. Silvestri & S. Crotty, 2016. Direct Probing of Germinal Center Responses Reveals Immunological Features and Bottlenecks for Neutralizing Antibody Responses to HIV Env Trimer., *Cell reports* 17(9), 2195–2209.

Heit, A., F. Schmitz, S. Gerdts, B. Flach, M.S. Moore, J.A. Perkins, H.S. Robins, A. Aderem, P. Spearman, G.D. Tomaras, S.C. De Rosa & M.J. McElrath, 2017. Vaccination establishes clonal relatives of germinal center T cells in the blood of humans, *The Journal of Experimental Medicine* 214(7), 2139–52.

Hetz, C., E. Chevet & H.P. Harding, 2013. Targeting the unfolded protein response in disease, *Nature Reviews Drug Discovery* 12(9), 703–19.

Hetz, C., A.-H. Lee, D. Gonzalez-Romero, P. Thielen, J. Castilla, C. Soto & L.H. Glimcher, 2008. Unfolded protein response transcription factor XBP-1 does not influence prion replication or pathogenesis, *Proceedings of the National Academy of Sciences* 105(2), 757–62.

Hildebrand, F., T.L.A. Nguyen, B. Brinkman, R. Yunta, B. Cauwe, P. Vandenabeele, A. Liston & J. Raes, 2013. Inflammation-associated enterotypes, host genotype, cage and inter-individual effects drive gut microbiota variation in common laboratory mice, *Genome Biology* 14(1), R4.

Hirota, K., J.H. Duarte, M. Veldhoen, E. Hornsby, Y. Li, D.J. Cua, H. Ahlfors, C. Wilhelm, M. Tolaini, U. Menzel, A. Garefalaki, A.J. Potocnik & B. Stockinger, 2011. Fate mapping of IL-17-producing T cells in inflammatory responses, *Nature Immunology* 12(3), 255–63.

Hirota, K., J.-E. Turner, M. Villa, J.H. Duarte, J. Demengeot, O.M. Steinmetz & B. Stockinger, 2013. Plasticity of Th17 cells in Peyer's patches is responsible for the induction of T cell-dependent IgA responses., *Nature immunology* 14(4), 372–79.

Hoffman, W., F.G. Lakkis & G. Chalasani, 2016. B Cells, Antibodies, and More., *Clinical journal of the American Society of Nephrology : CJASN* 11(1), 137–54.

Hoffmann, H.-H., W.M. Schneider & C.M. Rice, 2015. Interferons and viruses: an evolutionary arms race of molecular interactions., *Trends in immunology* 36(3), 124–38.

Hollister, K., S. Kusam, H. Wu, N. Clegg, A. Mondal, D. V. Sawant & A.L. Dent, 2013. Insights into the Role of Bcl6 in Follicular Th Cells Using a New Conditional Mutant Mouse Model, *Journal of immunology* 191(7), 3705–11.

Hori, S., T. Nomura & S. Sakaguchi, 2003. Control of Regulatory T Cell Development by the Transcription Factor Foxp3, *Science* 299(5609), 1057–61.

Hotamisligil, G.S., 2010. Endoplasmic Reticulum Stress and the Inflammatory Basis of Metabolic Disease, *Cell* 140(6), 900–917.

Hsieh, C.-S., H.-M. Lee & C.-W.J. Lio, 2012. Selection of regulatory T cells in the thymus, *Nature Reviews Immunology* 12(3), 157–67.

Hu, F., X. Yu, H. Wang, D. Zuo, C. Guo, H. Yi, B. Tirosh, J.R. Subjeck, X. Qiu & X.-Y. Wang, 2011. ER stress and its regulator X-box-binding protein-1 enhance polyIC-induced innate immune response in dendritic cells, *European Journal of Immunology* 41(4), 1086–97.

Huber, M., A. Brüstle, K. Reinhard, A. Guralnik, G. Walter, A. Mahiny, E. von Löw & M. Lohoff, 2008. IRF4 is essential for IL-21-mediated induction, amplification, and stabilization of the Th17 phenotype., *Proceedings of the National Academy of Sciences of the United States of America* 105(52), 20846–51.

Hung, I.F.-N., A.J. Zhang, K.K.-W. To, J.F.-W. Chan, P. Li, T.-L. Wong, R. Zhang, T.-C. Chan, B.C.-Y. Chan, H.H. Wai, L.-W. Chan, H.P.-Y. Fong, R.K.-C. Hui, K.-L. Kong, A.C.-F. Leung, A.H.-T. Ngan, L.W.-K. Tsang, A.P.-C. Yeung, G.C.-N. Yiu, W. Yung, J.Y.-N. Lau, H. Chen, K.-H. Chan & K.-Y. Yuen, 2016. Topical imiquimod before intradermal trivalent influenza vaccine for protection against heterologous non-vaccine and antigenically drifted viruses: a single-centre, double-blind, randomised, controlled phase 2b/3 trial, *The Lancet Infectious Diseases* 16(2), 209–18.

Hung, I.F.N., A.J. Zhang, K.K.W. To, J.F.W. Chan, C. Li, H.-S. Zhu, P. Li, C. Li, T.-C. Chan, V.C.C. Cheng, K.-H. Chan & K.-Y. Yuen, 2014. Immunogenicity of Intradermal Trivalent Influenza Vaccine With Topical Imiquimod: A Double Blind Randomized Controlled Trial, *Clinical Infectious Diseases* 59(9), 1246–55.

Hur, E.M., S. Youssef, M.E. Haws, S.Y. Zhang, R.A. Sobel & L. Steinman, 2007. Osteopontin-induced relapse and progression of autoimmune brain disease through enhanced survival of activated T cells, *Nature Immunology* 8(1), 74–83.

Itano, A.A., S.J. McSorley, R.L. Reinhardt, B.D. Ehst, E. Ingulli, A.Y. Rudensky & M.K. Jenkins, 2003. Distinct Dendritic Cell Populations Sequentially Present Antigen to CD4 T Cells and Stimulate Different Aspects of Cell-Mediated Immunity, *Immunity* 19(1), 47–57.

Ivanov, I.I., K. Atarashi, N. Manel, E.L. Brodie, T. Shima, U. Karaoz, D. Wei, K.C. Goldfarb, C.A. Santee, S. V Lynch, T. Tanoue, A. Imaoka, K. Itoh, K. Takeda, Y. Umesaki, K. Honda & D.R. Littman, 2009. Induction of intestinal Th17 cells by segmented filamentous bacteria., *Cell* 139(3), 485–98.

Ivashkiv, L.B. & L.T. Donlin, 2014. Regulation of type I interferon responses., *Nature reviews. Immunology* 14(1), 36–49.

Iwakoshi, N.N., M. Pypaert & L.H. Glimcher, 2007. The transcription factor XBP-1 is essential for the development and survival of dendritic cells, *The Journal of Experimental Medicine* 204(10), 2267–75.

Jadidi-Niaragh, F. & A. Mirshafiey, 2011. Th17 Cell, the New Player of Neuroinflammatory Process in Multiple Sclerosis, *Scandinavian Journal of Immunology* 74(1), 1–13.

Jain, R., Y. Chen, Y. Kanno, B. Joyce-Shaikh, G. Vahedi, K. Hirahara, W.M. Blumenschein, S. Sukumar, C.J. Haines, S. Sadekova, T.K. McClanahan, M.J. McGeachy, J.J. O'Shea & D.J. Cua, 2016. Interleukin-23-Induced Transcription Factor Blimp-1 Promotes Pathogenicity of T Helper 17 Cells, *Immunity* 44(1), 131–42.

Janeway, C.A. & R. Medzhitov, 2002. Innate immune recognition, *Annual Review of Immunology* 20(1), 197–216.

Janeway, C., P. Travers, M. Walport & M. Shlomchik, 2001. The generation of diversity in immunoglobulins, in *Immunobiology: The Immune System in Health and Disease.* , 5th edition. : Garland Science.

Johnston, C.M., A.L. Wood, D.J. Bolland & A.E. Corcoran, 2006. Complete sequence assembly and characterization of the C57BL/6 mouse Ig heavy chain V region., *Journal of immunology* 176(7), 4221–34.

Jovel, J., J. Patterson, W. Wang, N. Hotte, S. O'Keefe, T. Mitchel, T. Perry, D. Kao, A.L. Mason, K.L. Madsen & G.K.-S. Wong, 2016. Characterization of the Gut Microbiome Using 16S or Shotgun Metagenomics., *Frontiers in microbiology* 7, 459.

Kaburagi, T., T. Yamano, Y. Fukushima, H. Yoshino, N. Mito & K. Sato, 2007. Effect of Lactobacillus johnsonii La1 on immune function and serum albumin in aged and malnourished aged mice, *Nutrition* 23(4), 342–50.

Kamimura, D. & M.J. Bevan, 2008. Endoplasmic reticulum stress regulator XBP-1 contributes to effector CD8+ T cell differentiation during acute infection., *Journal of immunology* 181(8), 5433–41.

Kato, H., K. Fujihashi, R. Kato, T. Dohi, K. Fujihashi, Y. Hagiwara, K. Kataoka, R. Kobayashi & J.R. McGhee, 2003. Lack of oral tolerance in aging is due to sequential loss of Peyer's patch cell interactions, *International Immunology* 15(2), 145–58.

Kato, L.M., S. Kawamoto, M. Maruya & S. Fagarasan, 2014. Gut TFH and IgA: key players for regulation of bacterial communities and immune homeostasis, *Immunology and Cell Biology* 92(1), 49–56.

Kawamoto, S., M. Maruya, L.M. Kato, W. Suda, K. Atarashi, Y. Doi, Y. Tsutsui, H. Qin, K. Honda, T. Okada, M. Hattori & S. Fagarasan, 2014. Foxp3+ T Cells Regulate Immunoglobulin A Selection and Facilitate Diversification of Bacterial Species Responsible for Immune Homeostasis, *Immunity* 41(1), 152–65.

Kawamoto, S., T.H. Tran, M. Maruya, K. Suzuki, Y. Doi, Y. Tsutsui, L.M. Kato & S. Fagarasan, 2012. The inhibitory receptor PD-1 regulates IgA selection and bacterial composition in the gut., *Science* 336(6080), 485–89.

Kawanishi, H. & J. Kiely, 1989. Immune-related alterations in aged gut-associated lymphoid tissues in mice, *Digestive Diseases and Sciences* 34(2), 175–84.

Khattri, R., T. Cox, S.-A. Yasayko & F. Ramsdell, 2003. An essential role for Scurfin in CD4+CD25+ T regulatory cells, *Nature Immunology* 4(4), 337–42.

Khoruts, A. & M.J. Sadowsky, 2016. Understanding the mechanisms of faecal microbiota transplantation, *Nature Reviews Gastroenterology & Hepatology* 13(9), 508–16.

Khosravi, A., A. Yáñez, J.G. Price, A. Chow, M. Merad, H.S. Goodridge & S.K. Mazmanian, 2014. Gut Microbiota Promote Hematopoiesis to Control Bacterial Infection, *Cell host & microbe* 15(3), 374–81.

Kim, D., B. Langmead & S.L. Salzberg, 2015a. HISAT: a fast spliced aligner with low memory requirements, *Nature Methods* 12(4), 357–60.

Kim, M., Y. Qie, J. Park & C.H. Kim, 2016. Gut Microbial Metabolites Fuel Host Antibody Responses, *Cell Host & Microbe* 20(2), 202–14.

Kim, S.R., H.J. Kim, D.I. Kim, K.B. Lee, H.J. Park, J.S. Jeong, S.H. Cho & Y.C. Lee, 2015b. Blockade of Interplay between IL-17A and Endoplasmic Reticulum Stress Attenuates LPS-Induced Lung Injury, *Theranostics* 5(12), 1343–62.

Kleinewietfeld, M., A. Manzel, J. Titze, H. Kvakan, N. Yosef, R.A. Linker, D.N. Muller & D.A. Hafler, 2013. Sodium chloride drives autoimmune disease by the induction of pathogenic TH17 cells., *Nature* 496(7446), 518–22.

Kline, K.A. & D.M. Bowdish, 2016. Infection in an aging population, *Current Opinion in Microbiology* 29, 63–67.

Kobayashi, A., D.S. Donaldson, C. Erridge, T. Kanaya, I.R. Williams, H. Ohno, A. Mahajan & N.A. Mabbott, 2013. The functional maturation of M cells is dramatically reduced in the Peyer's patches of aged mice, *Mucosal Immunology* 6(5), 1027–37.

Koch, U. & F. Radtke, 2011. Mechanisms of T Cell Development and Transformation, *Annual Review of Cell and Developmental Biology* 27, 539–62.

Koga, T., J.R. McGhee, H. Kato, R. Kato, H. Kiyono & K. Fujihashi, 2000. Evidence for early aging in the mucosal immune system., *Journal of immunology* 165(9), 5352–59.

Kolling, G., M. Wu & R.L. Guerrant, 2012. Enteric pathogens through life stages., *Frontiers in cellular and infection microbiology* 2, 114.

Kominsky, D.J., E.L. Campbell & S.P. Colgan, 2010. Metabolic Shifts in Immunity and Inflammation, *Journal of immunology* 184(8), 4062–68.

Korn, T., E. Bettelli, M. Oukka & V.K. Kuchroo, 2009. IL-17 and Th17 Cells., *Annual review of immunology* 27, 485–517.

Kosco, M.H., G.F. Burton, Z.F. Kapasi, A.K. Szakal & J.G. Tew, 1989. Antibody-forming cell induction during an early phase of germinal centre development and its delay with ageing., *Immunology* 68(3), 312–18.

Kostic, A.D., M.R. Howitt & W.S. Garrett, 2013. Exploring host-microbiota interactions in animal models and humans., *Genes & development* 27(7), 701–18.

Kraft, R., M. Bachmann, K. Bachmann, H. Buerki, M.W. Hess, H. Cottier & R.D. Stoner, 1987. Satisfactory primary tetanus antitoxin responses but markedly reduced germinal centre formation in first draining lymph nodes of ageing mice., *Clinical and experimental immunology* 67(2), 447–53.

Krangel, M.S., 2009. Mechanics of T cell receptor gene rearrangement., *Current opinion in immunology* 21(2), 133–39.

Krishnaswamy, J.K., S. Alsén, U. Yrlid, S.C. Eisenbarth & A. Williams, 2018. Determination of T Follicular Helper Cell Fate by Dendritic Cells, *Frontiers in Immunology* 9, 2169.

Krishnaswamy, J.K., U. Gowthaman, B. Zhang, J. Mattsson, L. Szeponik, D. Liu, R. Wu, T. White, S. Calabro, L. Xu, M.A. Collet, M. Yurieva, S. Alsén, P. Fogelstrand, A. Walter, W.R. Heath, S.N. Mueller, U. Yrlid, A. Williams & S.C. Eisenbarth, 2017. Migratory CD11b+ conventional dendritic cells induce T follicular helper cell-dependent antibody responses., *Science immunology* 2(18), .

Kubinak, J.L., C. Petersen, W.Z. Stephens, R. Soto, E. Bake, R.M. O'Connell & J.L. Round, 2015. MyD88 Signaling in T Cells Directs IgA-Mediated Control of the Microbiota to Promote Health, *Cell Host & Microbe* 17(2), 153–63.

Kurilshikov, A., C. Wijmenga, J. Fu & A. Zhernakova, 2017. Host Genetics and Gut Microbiome: Challenges and Perspectives, *Trends in Immunology* 38(9), 633–47.

Landete, J.M., P. Gaya, E. Rodríguez, S. Langa, Á. Peirotén, M. Medina & J.L. Arqués, 2017. Probiotic Bacteria for Healthier Aging: Immunomodulation and Metabolism of Phytoestrogens., *BioMed research international* 2017, 5939818.

Le Bon, A., G. Schiavoni, G. D'Agostino, I. Gresser, F. Belardelli & D.F. Tough, 2001. Type i interferons potently enhance humoral immunity and can promote isotype switching by stimulating dendritic cells in vivo., *Immunity* 14(4), 461–70.

Le Bon, A., C. Thompson, E. Kamphuis, V. Durand, C. Rossmann, U. Kalinke & D.F. Tough, 2006. Cutting Edge: Enhancement of Antibody Responses Through Direct Stimulation of B and T Cells by Type I IFN, *Journal of immunology* 176(4), 2074–78.

LeBien, T.W. & T.F. Tedder, 2008. B lymphocytes: how they develop and function., *Blood* 112(5), 1570–80.

Lee, P.P., D.R. Fitzpatrick, C. Beard, H.K. Jessup, S. Lehar, K.W. Makar, M. Pérez-Melgosa, M.T. Sweetser, M.S. Schlissel, S. Nguyen, S.R. Cherry, J.H. Tsai, S.M. Tucker, W.M. Weaver, A. Kelso, R. Jaenisch & C.B. Wilson, 2001. A Critical Role for Dnmt1 and DNA Methylation in T Cell Development, Function, and Survival, *Immunity* 15(5), 763–74.

Lee, Y., A. Awasthi, N. Yosef, F.J. Quintana, S. Xiao, A. Peters, C. Wu, M. Kleinewietfeld, S. Kunder, D.A. Hafler, R.A. Sobel, A. Regev & V.K. Kuchroo, 2012. Induction and molecular signature of pathogenic TH17 cells., *Nature immunology* 13(10), 991–99.

Lee, Y.K., J.S. Menezes, Y. Umesaki & S.K. Mazmanian, 2011. Proinflammatory T-cell responses to gut microbiota promote experimental autoimmune encephalomyelitis., *Proceedings of the National Academy of Sciences of the United States of America* 108, 4615–22.

Lefebvre, J.S., A.C. Maue, S.M. Eaton, P.A. Lanthier, M. Tighe & L. Haynes, 2012. The aged microenvironment contributes to the age-related functional defects of CD4 T cells in mice, *Aging Cell* 11(5), 732–40.

Leitenberg, D. & K. Bottomly, 1999. Regulation of naive T cell differentiation by varying the potency of TCR signal transduction, *Seminars in Immunology* 11(4), 283–92.

Li, C., K.K.W. To, A.J.X. Zhang, A.C.Y. Lee, H. Zhu, W.W.N. Mak, I.F.N. Hung & K.-Y. Yuen, 2018. Co-stimulation With TLR7 Agonist Imiquimod and Inactivated Influenza Virus Particles Promotes Mouse B Cell Activation, Differentiation, and Accelerated Antigen Specific Antibody Production., *Frontiers in immunology* 9, 2370.

Li, J., E. Lu, T. Yi & J.G. Cyster, 2016. EBI2 augments Tfh cell fate by promoting interaction with IL-2-quenching dendritic cells, *Nature* 533(7601), 110–14.

Lin, W., S.L. Bailey, H. Ho, H.P. Harding, D. Ron, S.D. Miller & B. Popko, 2007. The integrated stress response prevents demyelination by protecting oligodendrocytes against immune-mediated damage., *The Journal of clinical investigation* 117(2), 448–56.

Lin, W., A. Kemper, J.L. Dupree, H.P. Harding, D. Ron & B. Popko, 2006. Interferon-γ inhibits central nervous system remyelination through a process modulated by endoplasmic reticulum stress, *Brain* 129(5), 1306–18.

Linterman, M.A., 2014. How T follicular helper cells and the germinal centre response change with age, *Immunology and Cell Biology* 92(1), 72–79.

Linterman, M.A., L. Beaton, D. Yu, R.R. Ramiscal, M. Srivastava, J.J. Hogan, N.K. Verma, M.J. Smyth, R.J. Rigby & C.G. Vinuesa, 2010. IL-21 acts directly on B cells to regulate Bcl-6 expression and germinal center responses., *The Journal of experimental medicine* 207(2), 353–63.

Linterman, M.A. & D.L. Hill, 2016. Can follicular helper T cells be targeted to improve vaccine efficacy?, *F1000Research* 5, .

Linterman, M.A., W. Pierson, S.K. Lee, A. Kallies, S. Kawamoto, T.F. Rayner, M. Srivastava, D.P. Divekar, L. Beaton, J.J. Hogan, S. Fagarasan, A. Liston, K.G.C. Smith & C.G. Vinuesa, 2011. Foxp3+ follicular regulatory T cells control the germinal center response, *Nature Medicine* 17(8), 975–82.

Linterman, M.A., R.J. Rigby, R.K. Wong, D. Yu, R. Brink, J.L. Cannons, P.L. Schwartzberg, M.C. Cook, G.D. Walters & C.G. Vinuesa, 2009. Follicular helper T cells are required for systemic autoimmunity., *The Journal of experimental medicine* 206(3), 561–76.

Livak, K.J. & T.D. Schmittgen, 2001. Analysis of relative gene expression data using real-time quantitative PCR and the 2(-Delta Delta C(T)) Method., *Methods* 25(4), 402–8.

López-Otín, C., M.A. Blasco, L. Partridge, M. Serrano & G. Kroemer, 2013. The Hallmarks of Aging, *Cell* 153(6), 1194–1217.

Love, M.I., W. Huber & S. Anders, 2014. Moderated estimation of fold change and dispersion for RNA-seq data with DESeq2, *Genome Biology* 15(12), 550.

Lu, L.L., T.J. Suscovich, S.M. Fortune & G. Alter, 2017. Beyond binding: antibody effector functions in infectious diseases, *Nature Reviews Immunology* 18(1), 46–61.

Luche, H., O. Weber, T. Nageswara Rao, C. Blum & H.J. Fehling, 2007. Faithful activation of an extra-bright red fluorescent protein in 'knock-in' Cre-reporter mice ideally suited for lineage tracing studies, *European Journal of Immunology* 37(1), 43–53.

Luckheeram, R.V., R. Zhou, A.D. Verma & B. Xia, 2012. $CD4^+$T cells: differentiation and functions., *Clinical & Developmental Immunology* 2012, 925135.

Luft, T., K.C. Pang, E. Thomas, P. Hertzog, D.N. Hart, J. Trapani & J. Cebon, 1998. Type I IFNs enhance the terminal differentiation of dendritic cells., *Journal of immunology* 161(4), 1947–53.

MacLennan, I.C.M., K.-M. Toellner, A.F. Cunningham, K. Serre, D.M.-Y. Sze, E. Zúñiga, M.C. Cook & C.G. Vinuesa, 2003. Extrafollicular antibody responses., *Immunological reviews* 194, 8–18.

Macpherson, A.J., M.B. Geuking, E. Slack, S. Hapfelmeier & K.D. McCoy, 2012. The habitat, double life, citizenship, and forgetfulness of IgA, *Immunological Reviews* 245(1), 132–46.

Macpherson, A.J., K.D. McCoy, F.-E. Johansen & P. Brandtzaeg, 2008. The immune geography of IgA induction and function, *Mucosal Immunology* 1(1), 11–22.

Macpherson, A.J., B. Yilmaz, J.P. Limenitakis & S.C. Ganal-Vonarburg, 2018. IgA Function in Relation to the Intestinal Microbiota, *Annual Review of Immunology* 36, 359–81.

Maddur, M.S., P. Miossec, S. V. Kaveri & J. Bayry, 2012. Th17 Cells: Biology, Pathogenesis of Autoimmune and Inflammatory Diseases, and Therapeutic Strategies, *The American Journal of Pathology* 181(1), 8–18.

Madsen, L., N. Labrecque, J. Engberg, A. Dierich, A. Svejgaard, C. Benoist, D. Mathis & L. Fugger, 1999. Mice lacking all conventional MHC class II genes., *Proceedings of the National Academy of Sciences of the United States of America* 96(18), 10338–43.

Maffei, V.J., S. Kim, E. Blanchard, M. Luo, S.M. Jazwinski, C.M. Taylor & D.A. Welsh, 2017. Biological Aging and the Human Gut Microbiota, *The Journals of Gerontology: Series A* 72(11), 1474–82.

Malhotra, J.D. & R.J. Kaufman, 2011. ER stress and its functional link to mitochondria: role in cell survival and death., *Cold Spring Harbor perspectives in biology* 3(9), .

Mamo, Y., M.H. Woodworth, T. Wang, T. Dhere & C.S. Kraft, 2018. Durability and Long-term Clinical Outcomes of Fecal Microbiota Transplant Treatment in Patients With Recurrent Clostridium difficile Infection, *Clinical Infectious Diseases* 66(11), 1705–11.

Mangan, P.R., L.E. Harrington, D.B. O'Quinn, W.S. Helms, D.C. Bullard, C.O. Elson, R.D. Hatton, S.M. Wahl, T.R. Schoeb & C.T. Weaver, 2006. Transforming growth factor-β induces development of the TH17 lineage, *Nature* 441(7090), 231–34.

Manjarrez-Orduño, N., T.D. Quách & I. Sanz, 2009. B cells and immunological tolerance., *The Journal of investigative dermatology* 129(2), 278–88.

Martinon, F., X. Chen, A.-H. Lee & L.H. Glimcher, 2010. TLR activation of the transcription factor XBP1 regulates innate immune responses in macrophages, *Nature Immunology* 11(5), 411–18.

Mason, M.J., C. Garcia-Rodriguez & S. Grinstein, 1991. Coupling between intracellular Ca2+ stores and the Ca2+ permeability of the plasma membrane. Comparison of the effects of thapsigargin, 2,5-di-(tert-butyl)-1,4-hydroquinone, and cyclopiazonic acid in rat thymic lymphocytes., *The Journal of biological chemistry* 266(31), 20856–62.

Matsuno, K., H. Ueta, Z. Shu, X. Xue-Dong, Y. Sawanobori, Y. Kitazawa, Y. Bin, M. Yamashita & C. Shi, 2010. The microstructure of secondary lymphoid organs that support immune cell trafficking, *Archives of Histology and Cytology* 73(1), 1–21.

Matthews, S.A. & D.A. Cantrell, 2009. New insights into the regulation and function of serine/threonine kinases in T lymphocytes, *Immunological Reviews* 228(1), 241–52.

McComb, S., A. Thiriot, L. Krishnan & F. Stark, 2013. Introduction to the Immune System, *Methods in Molecular Biology* (1061), 1–20.

McCormack, M.P., A. Forster, L. Drynan, R. Pannell & T.H. Rabbitts, 2003. The LMO2 T-cell oncogene is activated via chromosomal translocations or retroviral insertion during gene therapy but has no mandatory role in normal T-cell development., *Molecular and cellular biology* 23(24), 9003–13.

McGeachy, M.J., K.S. Bak-Jensen, Y. Chen, C.M. Tato, W. Blumenschein, T. McClanahan & D.J. Cua, 2007. TGF-β and IL-6 drive the production of IL-17 and IL-10 by T cells and restrain TH-17 cell–mediated pathology, *Nature Immunology* 8(12), 1390–97.

McNamee, E.N., D. Korns Johnson, D. Homann & E.T. Clambey, 2013. Hypoxia and hypoxia-inducible factors as regulators of T cell development, differentiation, and function, *Immunologic Research* 55, 58–70.

Meares, G.P., Y. Liu, R. Rajbhandari, H. Qin, S.E. Nozell, J.A. Mobley, J.A. Corbett & E.N. Benveniste, 2014. PERK-dependent activation of JAK1 and STAT3 contributes to endoplasmic reticulum stress-induced inflammation., *Molecular and cellular biology* 34(20), 3911–25.

Merad, M., P. Sathe, J. Helft, J. Miller & A. Mortha, 2013. The dendritic cell lineage: ontogeny and function of dendritic cells and their subsets in the steady state and the inflamed setting., *Annual review of immunology* 31, 563–604.

Merico, D., R. Isserlin, O. Stueker, A. Emili & G.D. Bader, 2010. Enrichment Map: A Network-Based Method for Gene-Set Enrichment Visualization and Interpretation,Ravasi, T. (ed.) *PLoS ONE* 5(11), e13984.

Mesin, L., J. Ersching & G.D. Victora, 2016. Germinal Center B Cell Dynamics, *Immunity* 45(3), 471–82.

Mháille, A.N., S. McQuaid, A. Windebank, P. Cunnea, J. McMahon, A. Samali & U. FitzGerald, 2008. Increased Expression of Endoplasmic Reticulum Stress-Related Signaling Pathway Molecules in Multiple Sclerosis Lesions, *Journal of Neuropathology & Experimental Neurology* 67(3), 200–211.

Michalek, R.D. & J.C. Rathmell, 2010. The metabolic life and times of a T-cell., *Immunological reviews* 236, 190–202.

Migalska, M., A. Sebastian & J. Radwan, 2018. Profiling of the TCRβ repertoire in non-model species using high-throughput sequencing, *Scientific Reports* 8(1), 11613.

Moens, E. & M. Veldhoen, 2012. Epithelial barrier biology: Good fences make good neighbours, *Immunology* 135(1), 1–8.

Montecino-Rodriguez, E., B. Berent-Maoz & K. Dorshkind, 2013. Causes, consequences, and reversal of immune system aging, *Journal of Clinical Investigation* 123(3), 958–65.

Moore, R.A., J.E. Edwards, J. Hopwood & D. Hicks, 2001. Imiquimod for the treatment of genital warts: a quantitative systematic review, *BMC Infectious Diseases* 1(1), 3.

Moretto, M.M., E.M. Lawlor & I.A. Khan, 2008. Aging mice exhibit a functional defect in mucosal dendritic cell response against an intracellular pathogen., *Journal of immunology* 181(11), 7977–84.

Morito, D. & K. Nagata, 2012. ER Stress Proteins in Autoimmune and Inflammatory Diseases, *Frontiers in Immunology* 3, 48.

Mosmann, T.R., H. Cherwinski, M.W. Bond, M.A. Giedlin & R.L. Coffman, 1986. Two types of murine helper T cell clone. I. Definition according to profiles of lymphokine activities and secreted proteins., *Journal of immunology (Baltimore, Md. : 1950)* 136(7), 2348–57.

Mowat, A.M. & W.W. Agace, 2014. Regional specialization within the intestinal immune system, *Nature Reviews Immunology* 14(10), 667–85.

Mueller, C.G. & M.C. Coles, 2014. Emerging immune functions of non-hematopoietic stromal cells., *Frontiers in immunology* 5, 437.

Mueller, S., K. Saunier, C. Hanisch, E. Norin, L. Alm, T. Midtvedt, A. Cresci, S. Silvi, C. Orpianesi, M.C. Verdenelli, T. Clavel, C. Koebnick, H.-J.F. Zunft, J. Doré & M. Blaut, 2006. Differences in fecal microbiota in different European study populations in relation to age, gender, and country: a cross-sectional study., *Applied and environmental microbiology* 72(2), 1027–33.

Muranski, P., A. Boni, P.A. Antony, L. Cassard, K.R. Irvine, A. Kaiser, C.M. Paulos, D.C. Palmer, C.E. Touloukian, K. Ptak, L. Gattinoni, C. Wrzesinski, C.S. Hinrichs, K.W. Kerstann, L. Feigenbaum, C.-C. Chan & N.P. Restifo, 2008. Tumor-specific Th17-polarized cells eradicate large established melanoma, *Blood* 112(2), 362–73.

Nakayamada, S., A.C. Poholek, K.T. Lu, H. Takahashi, M. Kato, S. Iwata, K. Hirahara, J.L. Cannons, P.L. Schwartzberg, G. Vahedi, H. -w. Sun, Y. Kanno & J.J. O'Shea, 2014. Type I IFN Induces Binding of STAT1 to Bcl6: Divergent Roles of STAT Family Transcription Factors in the T Follicular Helper Cell Genetic Program, *Journal of immunology* 192(5), 2156–66.

Naradikian, M.S., J.L. Scholz, M.A. Oropallo & M.P. Cancro, 2014. Understanding B Cell Biology, in *Drugs Targeting B-Cells in Autoimmune Diseases*. : Springer, Basel, 11–35.

Neighbors, M., S.B. Hartley, X. Xu, A.G. Castro, D.M. Bouley & A. O'Garra, 2006. Breakpoints in immunoregulation required for Th1 cells to induce diabetes, *European Journal of Immunology* 36(9), 2315–23.

NICE, 2014. Faecal microbiota transplant for recurrent Clostridium difficile infection [IPG485], in *National Institute for Health and Care Excellence (NICE) Guidelines*.

Nikolich-Žugich, J., 2018. The twilight of immunity: emerging concepts in aging of the immune system, *Nature Immunology* 19(1), 10–19.

Obata, F., C.O. Fons & A.P. Gould, 2018. Early-life exposure to low-dose oxidants can increase longevity via microbiome remodelling in Drosophila, *Nature Communications* 9(1), 975.

Oida, T. & H.L. Weiner, 2010. Depletion of TGF-β from fetal bovine serum., *Journal of immunological methods* 362(1–2), 195–98.

Okada, T., M.J. Miller, I. Parker, M.F. Krummel, M. Neighbors, S.B. Hartley, A. O'Garra, M.D. Cahalan & J.G. Cyster, 2005. Antigen-engaged B cells undergo chemotaxis toward the T zone and form motile conjugates with helper T cells, *PLOS Biology* 3(6), e150.

Ondov, B.D., N.H. Bergman & A.M. Phillippy, 2011. Interactive metagenomic visualization in a Web browser, *BMC Bioinformatics* 12(1), 385.

Ost, K.S. & J.L. Round, 2018. Communication Between the Microbiota and Mammalian Immunity, *Annual Review of Microbiology* 72(1), 399–422.

Pabst, O., 2012. New concepts in the generation and functions of IgA, *Nature Reviews Immunology* 12(12), 821–32.

Palmer, D.B., 2013. The effect of age on thymic function., *Frontiers in immunology* 4, 316.

Panda, A., F. Qian, S. Mohanty, D. van Duin, F.K. Newman, L. Zhang, S. Chen, V. Towle, R.B. Belshe, E. Fikrig, H.G. Allore, R.R. Montgomery & A.C. Shaw, 2010. Age-Associated Decrease in TLR Function in Primary Human Dendritic Cells Predicts Influenza Vaccine Response, *Journal of immunology* 184(5), 2518–27.

Pearse, G., 2006. Normal Structure, Function and Histology of the Thymus, *Toxicologic Pathology* 34(5), 504–14.

Peled, J.U., F.L. Kuang, M.D. Iglesias-Ussel, S. Roa, S.L. Kalis, M.F. Goodman & M.D. Scharff, 2008. The Biochemistry of Somatic Hypermutation, *Annual Review of Immunology* 26, 481–511.

Pennock, N.D., J.T. White, E.W. Cross, E.E. Cheney, B.A. Tamburini & R.M. Kedl, 2013. T cell responses: naive to memory and everything in between., *Advances in physiology education* 37(4), 273–83.

Pereira, J.P., L.M. Kelly, Y. Xu & J.G. Cyster, 2009. EBI2 mediates B cell segregation between the outer and centre follicle, *Nature* 460(7259), 1122–26.

Phan, T.G., S. Gardam, A. Basten & R. Brink, 2005. Altered Migration, Recruitment, and Somatic Hypermutation in the Early Response of Marginal Zone B Cells to T Cell-Dependent Antigen, *Journal of immunology* 174(8), 4567–78.

Pino, S.C., B. O'Sullivan-Murphy, E.A. Lidstone, T.B. Thornley, A. Jurczyk, F. Urano, D.L. Greiner, J.P. Mordes, A.A. Rossini & R. Bortell, 2008. Protein kinase C signaling during T cell activation induces the endoplasmic reticulum stress response., *Cell stress & chaperones* 13(4), 421–34.

Platt, A.M., V.B. Gibson, A. Patakas, R.A. Benson, S.G. Nadler, J.M. Brewer, I.B. McInnes & P. Garside, 2010. Abatacept Limits Breach of Self-Tolerance in a Murine Model of Arthritis via Effects on the Generation of T Follicular Helper Cells, *Journal of immunology* 185(3), 1558–67.

Power, S.E., P.W. O'Toole, C. Stanton, R.P. Ross & G.F. Fitzgerald, 2014. Intestinal microbiota, diet and health, *British Journal of Nutrition* 111(3), 387–402.

Proietti, E., L. Bracci, S. Puzelli, T. Di Pucchio, P. Sestili, E. De Vincenzi, M. Venditti, I. Capone, I. Seif, E. De Maeyer, D. Tough, I. Donatelli & F. Belardelli, 2002. Type I IFN as a natural adjuvant for a protective immune response: lessons from the influenza vaccine model., *Journal of immunology* 169(1), 375–83.

Proietti, M., V. Cornacchione, T. Rezzonico Jost, A. Romagnani, C.E. Faliti, L. Perruzza, R. Rigoni, E. Radaelli, F. Caprioli, S. Preziuso, B. Brannetti, M. Thelen, K.D. McCoy, E. Slack, E. Traggiai & F. Grassi, 2014. ATP-Gated Ionotropic P2X7 Receptor Controls Follicular T Helper Cell Numbers in Peyer's Patches to Promote Host-Microbiota Mutualism, *Immunity* 41(5), 789–801.

Qi, H., J.L. Cannons, F. Klauschen, P.L. Schwartzberg & R.N. Germain, 2008. SAP-controlled T-B cell interactions underlie germinal centre formation., *Nature* 455(7214), 764–69.

QIAGEN Inc., 2016. *Ingenuity Pathway Analysis (IPA)*. 2016 . https://www.qiagenbioinformatics.com/products/ingenuity-pathway-analysis [Accessed 29 Nov 2016].

Qin, H., L. Wang, T. Feng, C.O. Elson, S.A. Niyongere, S.J. Lee, S.L. Reynolds, C.T. Weaver, K. Roarty, R. Serra, E.N. Benveniste & Y. Cong, 2009. TGF-beta promotes Th17 cell development through inhibition of SOCS3., *Journal of immunology* 183(1), 97–105.

Quast, C., E. Pruesse, P. Yilmaz, J. Gerken, T. Schweer, P. Yarza, J. Peplies & F.O. Glöckner, 2012. The SILVA ribosomal RNA gene database project: improved data processing and web-based tools, *Nucleic Acids Research* 41(D1), D590–96.

Quintana, F.J., A.S. Basso, A.H. Iglesias, T. Korn, M.F. Farez, E. Bettelli, M. Caccamo, M. Oukka & H.L. Weiner, 2008. Control of T(reg) and T(H)17 cell differentiation by the aryl hydrocarbon receptor., *Nature* 453(7191), 65–71.

Ramiscal, R.R. & C.G. Vinuesa, 2013. T-cell subsets in the germinal center, *Immunological Reviews* 252(1), 146–55.

Rauch, I., M. Müller & T. Decker, 2013. The regulation of inflammation by interferons and their STATs., *JAK-STAT* 2(1), e23820.

Rausch, P., M. Basic, A. Batra, S.C. Bischoff, M. Blaut, T. Clavel, J. Gläsner, S. Gopalakrishnan, G.A. Grassl, C. Günther, D. Haller, M. Hirose, S. Ibrahim, G. Loh, J. Mattner, S. Nagel, O. Pabst, F. Schmidt, B. Siegmund, T. Strowig, V. Volynets, S. Wirtz, S. Zeissig, Y. Zeissig, A. Bleich & J.F. Baines, 2016. Analysis of factors contributing to variation in the C57BL/6J fecal microbiota across German animal facilities, *International Journal of Medical Microbiology* 306(5), 343–55.

Reboldi, A. & J.G. Cyster, 2016. Peyer's patches: organizing B-cell responses at the intestinal frontier, *Immunological Reviews* 271(1), 230–45.

Reiter, M.J., T.L. Testerman, R.L. Miller, C.E. Weeks & M.A. Tomai, 1994. Cytokine induction in mice by the immunomodulator imiquimod, *Journal of Leukocyte Biology* 55(2), 234–40.

Remarque, E.J., W.C. van Beek, G.J. Ligthart, R.J. Borst, L. Nagelkerken, A.M. Palache, M.J. Sprenger & N. Masurel, 1993. Improvement of the immunoglobulin subclass response to influenza vaccine in elderly nursing-home residents by the use of high-dose vaccines., *Vaccine* 11(6), 649–54.

Rey, J., N. Garin, F. Spertini & B. Corthésy, 2004. Targeting of secretory IgA to Peyer's patch dendritic and T cells after transport by intestinal M cells., *Journal of immunology* 172(5), 3026–33.

Risso, D., J. Ngai, T.P. Speed & S. Dudoit, 2014. Normalization of RNA-seq data using factor analysis of control genes or samples, *Nature Biotechnology* 32(9), 896–902.

Riteau, N., A.J. Radtke, K. Shenderov, L. Mittereder, S.D. Oland, S. Hieny, D. Jankovic & A. Sher, 2016. Water-in-Oil–Only Adjuvants Selectively Promote T Follicular Helper Cell Polarization through a Type I IFN and IL-6–Dependent Pathway, *Journal of immunology* 197(10), 3884–93.

Rogerson, B.J., D.P. Harris, S.L. Swain & D.O. Burgess, 2003. Germinal center B cells in Peyer's patches of aged mice exhibit a normal activation phenotype and highly mutated IgM genes, *Mechanisms of Ageing and Development* 124(2), 155–65.

Rosselli, R., O. Romoli, N. Vitulo, A. Vezzi, S. Campanaro, F. de Pascale, R. Schiavon, M. Tiarca, F. Poletto, G. Concheri, G. Valle & A. Squartini, 2016. Direct 16S rRNA-seq from bacterial communities: a PCR-independent approach to simultaneously assess microbial diversity and functional activity potential of each taxon, *Scientific Reports* 6(1), 32165.

Rosser, E.C. & C. Mauri, 2015. Regulatory B Cells: Origin, Phenotype, and Function, *Immunity* 42(4), 607–12.

Rostami, A. & B. Ciric, 2013. Role of Th17 cells in the pathogenesis of CNS inflammatory demyelination, *Journal of the Neurological Sciences* 333(1–2), 76–87.

Round, J. & S. Mazmanian, 2009. The gut microbiota shapes intestinal immune responses during health and disease, *Nature Reviews Immunology* 9(5), 313–23.

Ruddle, N.H. & E.M. Akirav, 2009. Secondary lymphoid organs: responding to genetic and environmental cues in ontogeny and the immune response, *Journal of immunology* 183(4), 2205–12.

Rush, C.M. & J.M. Brewer, 2010. Tracking Dendritic Cells In Vivo, in *Methods in Molecular Biology (Clifton, N.J.)*, 169–85.

Sage, P.T., A.M. Paterson, S.B. Lovitch & A.H. Sharpe, 2014. The Coinhibitory Receptor CTLA-4 Controls B Cell Responses by Modulating T Follicular Helper, T Follicular Regulatory, and T Regulatory Cells, *Immunity* 41(6), 1026–39.

Sage, P.T., N. Ron-Harel, V.R. Juneja, D.R. Sen, S. Maleri, W. Sungnak, V.K. Kuchroo, W.N. Haining, N. Chevrier, M. Haigis & A.H. Sharpe, 2016. Suppression by TFR cells leads to durable and selective inhibition of B cell effector function, *Nature Immunology* 17(12), 1436–46.

Sage, P.T., C.L. Tan, G.J. Freeman, M. Haigis & A.H. Sharpe, 2015. Defective TFH Cell Function and Increased TFR Cells Contribute to Defective Antibody Production in Aging., *Cell reports* 12(2), 163–71.

Sakaguchi, S., N. Sakaguchi, M. Asano, M. Itoh & M. Toda, 1995. Immunologic self-tolerance maintained by activated T cells expressing IL-2 receptor alpha-chains (CD25). Breakdown of a single mechanism of self-tolerance causes various autoimmune diseases., *Journal of immunology* 155(3), 1151–64.

Sakai, F., T. Hosoya, A. Ono-Ohmachi, K. Ukibe, A. Ogawa, T. Moriya, Y. Kadooka, T. Shiozaki, H. Nakagawa, Y. Nakayama & T. Miyazaki, 2014. Lactobacillus gasseri SBT2055 induces TGF-β expression in dendritic cells and activates TLR2 signal to produce IgA in the small intestine., *PloS one* 9(8), e105370.

Schaefer, B.C., M.L. Schaefer, J.W. Kappler, P. Marrack & R.M. Kedl, 2001. Observation of Antigen-Dependent CD8+ T-Cell/ Dendritic Cell Interactions in Vivo, *Cellular Immunology* 214(2), 110–22.

Scheu, S., D.B. Stetson, R.L. Reinhardt, J.H. Leber, M. Mohrs & R.M. Locksley, 2006. Activation of the integrated stress response during T helper cell differentiation, *Nature Immunology* 7(6), 644–51.

Schraml, B.U., K. Hildner, W. Ise, W.-L. Lee, W.A.-E. Smith, B. Solomon, G. Sahota, J. Sim, R. Mukasa, S. Cemerski, R.D. Hatton, G.D. Stormo, C.T. Weaver, J.H. Russell, T.L. Murphy & K.M. Murphy, 2009. The AP-1 transcription factor Batf controls T(H)17 differentiation., *Nature* 460(7253), 405–9.

Schroeder, H.W. & L. Cavacini, 2010. Structure and function of immunoglobulins., *The Journal of allergy and clinical immunology* 125(2 Suppl 2), S41-52.

Segura, E., 2016. Review of Mouse and Human Dendritic Cell Subsets, *Methods in Molecular Biology* 1423, 3–15.

Senda, S., E. Cheng & H. Kawanishi, 1988. Aging-associated changes in murine intestinal immunoglobulin A and M secretions., *Scandinavian journal of immunology* 27(2), 157–64.

Sender, R., S. Fuchs & R. Milo, 2016. Revised Estimates for the Number of Human and Bacteria Cells in the Body, *PLOS Biology* 14(8), .

Shaffer, A.., M. Shapiro-Shelef, N.N. Iwakoshi, A.-H. Lee, S.-B. Qian, H. Zhao, X. Yu, L. Yang, B.K. Tan, A. Rosenwald, E.M. Hurt, E. Petroulakis, N. Sonenberg, J.W. Yewdell, K. Calame, L.H. Glimcher & L.M. Staudt, 2004. XBP1, Downstream of Blimp-1, Expands the Secretory Apparatus and Other Organelles, and Increases Protein Synthesis in Plasma Cell Differentiation, *Immunity* 21(1), 81–93.

Shimizu, A., N. Takahashi, Y. Yaoita & T. Honjo, 1982. Organization of the constant-region gene family of the mouse immunoglobulin heavy chain, *Cell* 28(3), 499–506.

Shin, J.H., Y. Gao, J.H. Moore, D.T. Bolick, G.L. Kolling, M. Wu & C.A. Warren, 2018. Innate Immune Response and Outcome of Clostridium difficile Infection Are Dependent on Fecal Bacterial Composition in the Aged Host, *The Journal of Infectious Diseases* 217(2), 188–97.

Shulman, Z., A.D. Gitlin, J.S. Weinstein, B. Lainez, E. Esplugues, R.A. Flavell, J.E. Craft & M.C. Nussenzweig, 2014. Dynamic signaling by T follicular helper cells during germinal center B cell selection, *Science* 345(6200), 1058–62.

Sie, C., T. Korn & M. Mitsdoerffer, 2014. Th17 cells in central nervous system autoimmunity, *Experimental Neurology* 262, 18–27.

Silowash, R., L. Pantanowitz, F.E. Craig, J.P. Simons & S.E. Monaco, 2016. Utilization of Flow Cytometry in Pediatric Fine-Needle Aspiration Biopsy Specimens, *Acta Cytologica* 60(4), 344–53.

Skarnes, W.C., B. Rosen, A.P. West, M. Koutsourakis, W. Bushell, V. Iyer, A.O. Mujica, M. Thomas, J. Harrow, T. Cox, D. Jackson, J. Severin, P. Biggs, J. Fu, M. Nefedov, P.J. de Jong, A.F. Stewart & A. Bradley, 2011. A conditional knockout resource for the genome-wide study of mouse gene function, *Nature* 474(7351), 337–42.

Smith, J.A., M.J. Turner, M.L. DeLay, E.I. Klenk, D.P. Sowders & R.A. Colbert, 2008. Endoplasmic reticulum stress and the unfolded protein response are linked to synergistic IFN-β inductionvia X-box binding protein 1, *European Journal of Immunology* 38(5), 1194–1203.

Smith, P., D. Willemsen, M. Popkes, F. Metge, E. Gandiwa, M. Reichard & D.R. Valenzano, 2017. Regulation of life span by the gut microbiota in the short-lived African turquoise killifish, *eLife* 6, .

Snel, J., P.P. Heinen, H.J. Blok, R.J. Carman, A.J. Duncan, P.C. Allen & M.D. Collins, 1995. Comparison of 16S rRNA Sequences of Segmented Filamentous Bacteria Isolated from Mice, Rats, and Chickens and Proposal of Candidatus Arthromitus;, *International Journal of Systematic Bacteriology* 45(4), 780–82.

So, J.-S., 2018. Roles of Endoplasmic Reticulum Stress in Immune Responses., *Molecules and cells* 41(8), 705–16.

Song, H. & J. Cerny, 2003. Functional heterogeneity of marginal zone B cells revealed by their ability to generate both early antibody-forming cells and germinal centers with hypermutation and memory in response to a T-dependent antigen., *The Journal of experimental medicine* 198(12), 1923–35.

Song, S.J., C. Lauber, E.K. Costello, C.A. Lozupone, G. Humphrey, D. Berg-Lyons, J.G. Caporaso, D. Knights, J.C. Clemente, S. Nakielny, J.I. Gordon, N. Fierer & R. Knight, 2013. Cohabiting family members share microbiota with one another and with their dogs., *eLife* 2, e00458.

Sonowal, R., A. Swimm, A. Sahoo, L. Luo, Y. Matsunaga, Z. Wu, J.A. Bhingarde, E.A. Ejzak, A. Ranawade, H. Qadota, D.N. Powell, C.T. Capaldo, J.M. Flacker, R.M. Jones, G.M. Benian & D. Kalman, 2017. Indoles from commensal bacteria extend healthspan., *Proceedings of the National Academy of Sciences of the United States of America* 114(36), E7506–15.

Spiotto, M.T., A. Banh, I. Papandreou, H. Cao, M.G. Galvez, G.C. Gurtner, N.C. Denko, Q.T. Le & A.C. Koong, 2010. Imaging the unfolded protein response in primary tumors reveals microenvironments with metabolic variations that predict tumor growth., *Cancer research* 70(1), 78–88.

Sprenkle, N.T., S.G. Sims, C.L. Sánchez & G.P. Meares, 2017. Endoplasmic reticulum stress and inflammation in the central nervous system., *Molecular neurodegeneration* 12(1), 42.

Sridharan, A., M. Esposo, K. Kaushal, J. Tay, K. Osann, S. Agrawal, S. Gupta & A. Agrawal, 2011. Age-associated impaired plasmacytoid dendritic cell functions lead to decreased CD4 and CD8 T cell immunity, *AGE* 33(3), 363–76.

Srinivas, S., T. Watanabe, C.S. Lin, C.M. William, Y. Tanabe, T.M. Jessell & F. Costantini, 2001. Cre reporter strains produced by targeted insertion of EYFP and ECFP into the ROSA26 locus., *BMC developmental biology* 1, 4.

Stavnezer, J. & C.E. Schrader, 2014. IgH chain class switch recombination: mechanism and regulation., *Journal of immunology* 193(11), 5370–78.

Stebegg, M., S.D. Kumar, A. Silva-Cayetano, V.R. Fonseca, M.A. Linterman & L. Graca, 2018. Regulation of the Germinal Center Response, *Frontiers in Immunology* 9, 2469.

Stebegg, M., A. Silva-Cayetano, S. Innocentin, T.P. Jenkins, C. Cantacessi, C. Gilbert & M.A. Linterman, 2019. Heterochronic faecal transplantation boosts gut germinal centres in aged mice, *Nature Communications* 10(1), 2443.

Stockinger, B. & S. Omenetti, 2017. The dichotomous nature of T helper 17 cells, *Nature Reviews Immunology* 17(9), 535–44.

Stout-Delgado, H.W., X. Yang, W.E. Walker, B.M. Tesar & D.R. Goldstein, 2008. Aging impairs IFN regulatory factor 7 up-regulation in plasmacytoid dendritic cells during TLR9 activation., *Journal of immunology* 181(10), 6747–56.

Stromnes, I.M., L.M. Cerretti, D. Liggitt, R.A. Harris & J.M. Goverman, 2008. Differential regulation of central nervous system autoimmunity by TH1 and TH17 cells, *Nature Medicine* 14(3), 337–42.

Stromnes, I.M. & J.M. Goverman, 2006a. Passive induction of experimental allergic encephalomyelitis, *Nature Protocols* 1(4), 1952–60.

Stromnes, I.M. & J.M. Goverman, 2006b. Active induction of experimental allergic encephalomyelitis, *Nature Protocols* 1(4), 1810–19.

Suzuki, K., I. Grigorova, T.G. Phan, L.M. Kelly & J.G. Cyster, 2009. Visualizing B cell capture of cognate antigen from follicular dendritic cells, *J Exp Med* 206(7), 1485–93.

Suzuki, K., B. Meek, Y. Doi, M. Muramatsu, T. Chiba, T. Honjo & S. Fagarasan, 2004. Aberrant expansion of segmented filamentous bacteria in IgA-deficient gut., *Proceedings of the National Academy of Sciences of the United States of America* 101(7), 1981–86.

Swiecki, M. & M. Colonna, 2015. The multifaceted biology of plasmacytoid dendritic cells, *Nature Reviews Immunology* 15(8), 471–85.

Takahashi, Y., P.R. Dutta, D.M. Cerasoli & G. Kelsoe, 1998. In situ studies of the primary immune response to (4-hydroxy-3-nitrophenyl)acetyl. V. Affinity maturation develops in two stages of clonal selection., *The Journal of experimental medicine* 187(6), 885–95.

Takemori, T., T. Kaji, Y. Takahashi, M. Shimoda & K. Rajewsky, 2014. Generation of memory B cells inside and outside germinal centers, *European Journal of Immunology* 44(5), 1258–64.

Tchkonia, T., Y. Zhu, J. van Deursen, J. Campisi & J.L. Kirkland, 2013. Cellular senescence and the senescent secretory phenotype: therapeutic opportunities, *The Journal of Clinical Investigation* 123(3), 966–72.

Tesmer, L.A., S.K. Lundy, S. Sarkar & D.A. Fox, 2008. Th17 cells in human disease., *Immunological reviews* 223, 87–113.

Thaxton, J.E., C. Wallace, B. Riesenberg, Y. Zhang, C.M. Paulos, C.C. Beeson, B. Liu & Z. Li, 2017. Modulation of Endoplasmic Reticulum Stress Controls CD4 $^{+}$ T-cell Activation and Antitumor Function, *Cancer Immunology Research* 5(8), 666–75.

The Gene Ontology Consortium, 2019. The Gene Ontology Resource: 20 years and still GOing strong, *Nucleic Acids Research* 47(D1), D330–38.

Thevaranjan, N., A. Puchta, C. Schulz, A. Naidoo, J.C. Szamosi, C.P. Verschoor, D. Loukov, L.P. Schenck, J. Jury, K.P. Foley, J.D. Schertzer, M.J. Larché, D.J. Davidson, E.F. Verdú, M.G. Surette & D.M.E. Bowdish, 2017. Age-Associated Microbial Dysbiosis Promotes Intestinal Permeability, Systemic Inflammation, and Macrophage Dysfunction., *Cell host & microbe* 21(4), 455–66.

Thomsen, L.L., P. Topley, M.G. Daly, S.J. Brett & J.P. Tite, 2004. Imiquimod and resiquimod in a mouse model: adjuvants for DNA vaccination by particle-mediated immunotherapeutic delivery, *Vaccine* 22(13–14), 1799–1809.

Thoreux, K., R.L. Owen & D.L. Schmucker, 2000. Intestinal lymphocyte number, migration and antibody secretion in young and old rats, *Immunology* 101(1), 161–67.

Todd, D.J., A.-H. Lee & L.H. Glimcher, 2008. The endoplasmic reticulum stress response in immunity and autoimmunity, *Nature Reviews Immunology* 8(9), 663–74.

Tsuji, M., N. Komatsu, S. Kawamoto, K. Suzuki, O. Kanagawa, T. Honjo, S. Hori & S. Fagarasan, 2009. Preferential Generation of Follicular B Helper T Cells from Foxp3+ T Cells in Gut Peyer's Patches, *Science* 323(5920), 1488–92.

Turner, V.M. & N.A. Mabbott, 2017. Structural and functional changes to lymph nodes in ageing mice., *Immunology* 151(2), 239–47.

Valenta, R., I. Mittermann, T. Werfel, H. Garn & H. Renz, 2009. Linking allergy to autoimmune disease, *Trends in Immunology* 30(3), 109–16.

van Dijk-Härd, I., I. Söderström, S. Feld, D. Holmberg & I. Lundkvist, 1997. Age-related impaired affinity maturation and differential D-JH gene usage in human VH6-expressing B lymphocytes from healthy individuals, *European Journal of Immunology* 27(6), 1381–86.

Vanderleyden, I., M.A. Linterman & K.G.C. Smith, 2014. Regulatory T cells and control of the germinal centre response., *Arthritis research & therapy* 16(5), 471.

Vantourout, P. & A. Hayday, 2013. Six-of-the-best: unique contributions of γδ T cells to immunology, *Nature Reviews Immunology* 13(2), 88–100.

Veldhoen, M., K. Hirota, A.M. Westendorf, J. Buer, L. Dumoutier, J.-C. Renauld & B. Stockinger, 2008a. The aryl hydrocarbon receptor links TH17-cell-mediated autoimmunity to environmental toxins., *Nature* 453(7191), 106–9.

Veldhoen, M., R.J. Hocking, C.J. Atkins, R.M. Locksley & B. Stockinger, 2006a. TGFbeta in the context of an inflammatory cytokine milieu supports de novo differentiation of IL-17-producing T cells., *Immunity* 24(2), 179–89.

Veldhoen, M., R.J. Hocking, R.A. Flavell & B. Stockinger, 2006b. Signals mediated by transforming growth factor-β initiate autoimmune encephalomyelitis, but chronic inflammation is needed to sustain disease, *Nature Immunology* 7(11), 1151–56.

Veldhoen, M., C. Uyttenhove, J. van Snick, H. Helmby, A. Westendorf, J. Buer, B. Martin, C. Wilhelm & B. Stockinger, 2008b. Transforming growth factor-β 'reprograms' the differentiation of T helper 2 cells and promotes an interleukin 9–producing subset, *Nature Immunology* 9(12), 1341–46.

Victora, G.D. & M.C. Nussenzweig, 2012. Germinal centers., *Annual review of immunology* 30, 429–57.

Vinuesa, C.G., M.C. Cook, C. Angelucci, V. Athanasopoulos, L. Rui, K.M. Hill, D. Yu, H. Domaschenz, B. Whittle, T. Lambe, I.S. Roberts, R.R. Copley, J.I. Bell, R.J. Cornall & C.C. Goodnow, 2005. A RING-type ubiquitin ligase family member required to repress follicular helper T cells and autoimmunity, *Nature* 435(7041), 452–58.

Vinuesa, C.G., M.A. Linterman, D. Yu & I.C.M. MacLennan, 2016. Follicular Helper T Cells., *Annual Review of Immunology* 34, 335–68.

Wang, B., M. Yao, L. Lv, Z. Ling & L. Li, 2017. The Human Microbiota in Health and Disease, *Engineering* 3(1), 71–82.

Wang, L., T. Yi, M. Kortylewski, D.M. Pardoll, D. Zeng & H. Yu, 2009. IL-17 can promote tumor growth through an IL-6–Stat3 signaling pathway, *The Journal of Experimental Medicine* 206(7), 1457–64.

Wardemann, H., S. Yurasov, A. Schaefer, J.W. Young, E. Meffre & M.C. Nussenzweig, 2003. Predominant Autoantibody Production by Early Human B Cell Precursors, *Science* 301(5638), 1374–77.

Weaver, C.T., C.O. Elson, L.A. Fouser & J.K. Kolls, 2013. The Th17 Pathway and Inflammatory Diseases of the Intestines, Lungs, and Skin, *Annual Review of Pathology: Mechanisms of Disease* 8, 477–512.

Webb, L.M.C. & M.A. Linterman, 2017. Signals that drive T follicular helper cell formation, *Immunology* 152(2), 185–94.

Wei, M., R. Shinkura, Y. Doi, M. Maruya, S. Fagarasan & T. Honjo, 2011. Mice carrying a knock-in mutation of Aicda resulting in a defect in somatic hypermutation have impaired gut homeostasis and compromised mucosal defense, *Nature Immunology* 12(3), 264–70.

Weng, N., 2006. Aging of the Immune System: How Much Can the Adaptive Immune System Adapt?, *Immunity* 24(5), 495–99.

Westfall, S., N. Lomis & S. Prakash, 2018. Longevity extension in Drosophila through gut-brain communication, *Scientific Reports* 8(1), 8362.

Wheeler, M.C., M. Rizzi, R. Sasik, G. Almanza, G. Hardiman & M. Zanetti, 2008. KDEL-retained antigen in B lymphocytes induces a proinflammatory response: a possible role for endoplasmic reticulum stress in adaptive T cell immunity., *Journal of immunology* 181(1), 256–64.

WHO, 2011. *What are the public health implications of global ageing?* World Health Organisation 2011 . https://www.who.int/features/qa/42/en/ [Accessed 10 Mar 2019].

Wildin, R.S., F. Ramsdell, J. Peake, F. Faravelli, J.L. Casanova, N. Buist, E. Levy-Lahad, M. Mazzella, O. Goulet, L. Perroni, F.D. Bricarelli, G. Byrne, M. McEuen, S. Proll, M. Appleby & M.E. Brunkow, 2001. X-linked neonatal diabetes mellitus, enteropathy and endocrinopathy syndrome is the human equivalent of mouse scurfy., *Nature genetics* 27(1), 18–20.

Wing, J.B., W. Ise, T. Kurosaki & S. Sakaguchi, 2014. Regulatory T Cells Control Antigen-Specific Expansion of Tfh Cell Number and Humoral Immune Responses via the Coreceptor CTLA-4, *Immunity* 41(6), 1013–25.

Wollenberg, I., A. Agua-Doce, A. Hernández, C. Almeida, V.G. Oliveira, J. Faro & L. Graca, 2011. Regulation of the germinal center reaction by Foxp3+ follicular regulatory T cells., *Journal of immunology* 187(9), 4553–60.

Wu, C., N. Yosef, T. Thalhamer, C. Zhu, S. Xiao, Y. Kishi, A. Regev & V.K. Kuchroo, 2013. Induction of pathogenic TH17 cells by inducible salt-sensing kinase SGK1., *Nature* 496(7446), 513–17.

Wu, H.-J., I.I. Ivanov, J. Darce, K. Hattori, T. Shima, Y. Umesaki, D.R. Littman, C. Benoist & D. Mathis, 2010. Gut-residing segmented filamentous bacteria drive autoimmune arthritis via T helper 17 cells., *Immunity* 32(6), 815–27.

Wu, H., M.M. Xie, H. Liu & A.L. Dent, 2016. Stat3 Is Important for Follicular Regulatory T Cell Differentiation, *PLOS ONE* 11(5), .

Wu, S., K.-J. Rhee, E. Albesiano, S. Rabizadeh, X. Wu, H.-R. Yen, D.L. Huso, F.L. Brancati, E. Wick, F. McAllister, F. Housseau, D.M. Pardoll & C.L. Sears, 2009. A human colonic commensal promotes colon tumorigenesis via activation of T helper type 17 T cell responses., *Nature medicine* 15(9), 1016–22.

Wu, W., M. Sun, F. Chen, A.T. Cao, H. Liu, Y. Zhao, X. Huang, Y. Xiao, S. Yao, Q. Zhao, Z. Liu & Y. Cong, 2017. Microbiota metabolite short-chain fatty acid acetate promotes intestinal IgA response to microbiota which is mediated by GPR43, *Mucosal Immunology* 10(4), 946–56.

Xie, Q., V.I. Khaoustov, C.C. Chung, J. Sohn, B. Krishnan, D.E. Lewis & B. Yoffe, 2002. Effect of tauroursodeoxycholic acid on endoplasmic reticulum stress–induced caspase-12 activation, *Hepatology* 36(3), 592–601.

Yam-Puc, J.C., L. Zhang, Y. Zhang & K.-M. Toellner, 2018. Role of B-cell receptors for B-cell development and antigen-induced differentiation, *F1000Research* 7, 429.

Yanagibashi, T., A. Hosono, A. Oyama, M. Tsuda, A. Suzuki, S. Hachimura, Y. Takahashi, Y. Momose, K. Itoh, K. Hirayama, K. Takahashi & S. Kaminogawa, 2013. IgA production in the large intestine is modulated by a different mechanism than in the small intestine: Bacteroides acidifaciens promotes IgA production in the large intestine by inducing germinal center formation and increasing the number of IgA+ B cells, *Immunobiology* 218(4), 645–51.

Yang, X., J. Stedra & J. Cerny, 1996. Relative contribution of T and B cells to hypermutation and selection of the antibody repertoire in germinal centers of aged mice., *The Journal of experimental medicine* 183(3), 959–70.

Ye, J., 2004. The immunoglobulin IGHD gene locus in C57BL/6 mice, *Immunogenetics* 56(6), 399–404.

Yu, M., G. Li, W.-W. Lee, M. Yuan, D. Cui, C.M. Weyand & J.J. Goronzy, 2012. Signal inhibition by the dual-specific phosphatase 4 impairs T cell-dependent B-cell responses with age, *Proceedings of the National Academy of Sciences* 109(15), E879–88.

Zakrzewski, M., C. Proietti, J.J. Ellis, S. Hasan, M.-J. Brion, B. Berger & L. Krause, 2017. Calypso: a user-friendly web-server for mining and visualizing microbiome-environment interactions., *Bioinformatics* 33(5), 782–83.

Zhang, K. & R.J. Kaufman, 2008. From endoplasmic-reticulum stress to the inflammatory response., *Nature* 454(7203), 455–62.

Zhang, N. & M.J. Bevan, 2011. CD8(+) T cells: foot soldiers of the immune system., *Immunity* 35(2), 161–68.